SPECTROPHOTOMETRIC, MASS SPECTROMETERIC, AND STRUCTURAL STUDIES OF THE PROTOTYPICAL G PROTEIN COUPLED RECEPTOR RHODOPSIN

by

Thomas Emil Angel

A dissertation submitted in partial fulfillment
of the requirements for the degree

of

Doctor of Philosophy

in

Microbiology

MONTANA STATE UNIVERSITY
Bozeman, Montana

April 2007

© COPYRIGHT

By

Thomas Emil Angel

2007

All rights reserved

APPROVAL

of a dissertation submitted by

Thomas Emil Angel

This dissertation has been read by each member of the dissertation committee and has been found to be satisfactory regarding content, English usage, format, citations, bibliographic style, and consistency, and is ready for submission to the Division of Graduate Education.

Dr. Algirdas J. Jesaitis

Dr. Edward A. Dratz

Approved for the Department of Microbiology

Dr. Tim Ford

Approved for the Division of Graduate Education

Dr. Carl A. Fox

STATEMENT OF PERMISSION TO USE

In presenting this dissertation in partial fulfillment of the requirements for a doctoral degree at Montana State University, I agree that the Library shall make it available to borrowers under rules of the Library. I further agree that copying of this dissertation is allowable only for scholarly purposes, consistent with "fair use" as prescribed in the U.S. Copyright Law. Requests for extensive copying or reproduction of this dissertation should be referred to ProQuest Information and Learning, 300 North Zeeb Road, Ann Arbor, Michigan 48106, to whom I have granted "the exclusive right to reproduce and distribute my dissertation in and from microform along with the non-exclusive right to reproduce and distribute my abstract in any format in whole or in part."

Thomas Emil Angel

April, 2007

ACKNOWLEDGEMENTS

My graduate experience has been multidisciplinary by design as a participant in the NSF Integrated Graduate Education and Research Training (IGERT) program and has involved collaboration with many people and usage of a wide range of technologies. I would like to thank all of the members of the Dratz, Jesaitis, Lawrence, and Teintze labs for their assistance over the years. I would not have been able to consider graduate school without the support of my extended family, to them I am greatly in indebted. The support given by my wife Susan, and my children Oscar, Finn, and Peter has been critical for my successful completion of my graduate studies, my achievements are truly their achievements alike.

TABLE OF CONTENTS

1. INTRODUCTION AND REVIEW OF RHODOPSIN 1

History and Biology of Rhodopsin 1
GPCR Super Family Classification Schemes 2
Biological Source and Features of Rhodopsin in Rod Cells 8
Structural and Functional Features of Rhodopsin 13
Conformational Changes Upon Receptor Activation 19
Spectral Features of Rhodopsin 20
Metarhodopsin I-II Equilibrium 27
Transducin Interactions with Metarhodopsin II 31

2. BINDING KINETICS OF PEPTIDE ANALOGS OF THE C TERMINAL TAIL OF TRANSDUCIN 33

Introduction 33
Results 40
Discussion 48
Material and Methods 53
Rod Outer Segment Preparation 53
Peptide Synthesis 54
Light Titration 55
Equilibrium Binding and Kinetic Analysis of Synthetic Gtα C-terminal Tail Analog 56

3. MASS SPECTROMETRIC ANAYLSIS OF G PROTEIN COUPLED RECEPTORS RHODOPSIN AND CCR5 57

Introduction 57
Electrospray Ionization 57
Results and Discussion 62
Material and Methods 93
Rhodopsin sample preparation 93
CCR5 Expression and Purification 95
Capillary HPLC-QIT 95
MicroTOF 96
Nanospray –QIT 96
FT-MS 97
Mass Spectral Analysis of Intact Rhodopsin 97

TABLE OF CONTENTS-CONTINUED

4. METARHODOPSIN-II STABILIZATION BY CROSSLINKED Gαt C-TERMINAL PEPTIDES....98

Introduction....98
Results....101
Discussion....111
Materials and Methods....120
Rod Outer Segment Preparation....120
Peptide Synthesis....120
Chemical Coupling of Peptides to Rhodopsin....121
Light Titration Experiments....122
Difference Absorbance Spectral Measurement and Analysis....122
Mass Spectrometry....123

5. ANTIBODY IMPRINTING OF RHODOPSIN....125

Introduction to Antibody Imprinting....125
Single Chain Fv Selection....128
Monoclonal Antibody Screening....135
Structural characterization of antibody K42-41L with mimetope bound....139
Conformational States of Rhodopsin and the Activity of K42-41L....141
Effect of K42-41L on the Metarhodopsin-I ↔Metarhodopsin-II Equilibrium....143
The Structure of K42-41L and the Epitope Mimetic, TGALQERSK....148
Material and Methods....160
Rod Outer Segment Preparation....160
Light Titration Experiments....160
Difference Absorbance Spectra....161
Enzyme Linked Immunosorbant Assay....162
DNA Sequencing of Antibody K42-41L....163
Single Chain Fv Selection....163
ScFv Screening by ELISA....164
Screening of Anti-rhodopsin Monoclonal Antibodies....165

TABLE OF CONTENTS-CONTINUED

6. VALIDATION OF EPIALIGN EMPLOYING
MODEL SYSTEMS, LYSOZYME AND INTERLUKEN 10.....167

Introduction.....167
Phage Display.....168
Computational Methods for Epitope Mapping.....171
FINDMAP and EpiAlign.....173
Substitution Matrices.....175
Epitope mapping of anti-lysozyme antibodies.....183
Epitope mapping of anti-Interleukin 10 antibody 9D7.....193
Discussion and Conclusion.....201

Material and Methods.....204
Biopanning and Mimetic Peptide Selection.....204
DNA Sequencing of Phage.....205
Plaque Lift Assay.....206
Enzyme Linked Immunosorbant Assay.....206

REFERENCES.....208

LIST OF TABLES

Table Page

2.1 Kinetics of Interaction of Peptides with Metarhodopsin-I 47

2.2 Gα C-terminal Tail Sequences 51

3.1 Theoretical Cyanogen Bromide Digest Products 65

3.2 LC/MS Analysis of Rhodopsin Fragments on a Bruker microTOF 69

3.3 Cyanogen Bromide Fragments of CCR5 88

4.1 Gαt C-terminal Peptide Analogs 101

5.1 Analayis of a Panel of Mouse Anti-rhodopsin Antibodies 135

6.1 Atlas of Amino Acid Side Chain Interactions Substitution Matrix 179

6.2 Identity Amino Acid Substitution Matrix 180

6.3 Argos and Bordo Derived Substitution Matrix 181

6.4 Peptide Selected with Three Different Anti-lysozyme Antibodies 187

6.5 Phage sequences from second and third rounds of affinity selection for IL 10 mimetic peptides 198

LIST OF FIGURES

Figure Page

1.1 Phylogenetic tree of G protein coupled receptors 4

1.2 Stereo view of bovine rhodopsin with conserved residues in the rhodopsin GPCR family highlighted 5

1.3 Snake diagram showing conserved residues in the rhodopsin GPCR family 6

1.4 Diagram of the retinal rod cell and disk membrane of rhodopsin 9

1.5 Schematic of Visual signal transduction 10

1.6 Crystal structure of the unactivated state of bovine rhodopsin 14

1.7 Comparison of 5 high resolution crystal structures of rhodopsin 15

1.8 View of interaction network of highly conserved ERY motif on rhodopsin 17

1.9 Bound water molecules extending the hydrogen bonding network 18

1.10 Photoactivated rhodopsin relaxation intermediates 22

1.11 Energetics of rhodopsin and photointermediates 24

1.12 Comparison of retinal conformation in different photoexcited and ground state rhodopsin crystal structures 26

1.13 Spectral features of meta stable species of rhodopsin 28

LIST OF FIGURES-CONTINUED

Figure Page

1.14 The temperature and pH dependence of the equilibrium between metarhodopsin-I and metarhodopsin II 30

2.1 Rhodopsin extra-MII reaction scheme....41

2.2 Light titration of rhodopsin measuring the effects of addition of varied amounts of peptide analogs of the c terminal tail of Gαt 42

2.3 Light titration of peptide analogs of the C-terminal tail of Gαt 43

2.4 Simplex C analysis of light titration for peptide analogs 45

2.5 Peptide analog of the C-terminal tail of transducin interact with rhodopsin with different observed kinetic rates....46

2.6 Rigid body docking of a analog of the C-terminal 11 residues of transducin alpha subunit onto structure of unactivated rhodopsin 49

3.1 Chemical cleavage at methionine residues with Cyanogen Bromide 63

3.2 Snake diagram of bovine rhodopsin with methionine residue highlighted....64

3.3 Base peak chromatogram of bovine rhodopsin CNBr digest analyzed on the microTOF 68

3.4 Detection of the phosphorylated C-terminal tail of rhodopsin....71

3.5 Glycosylated amino terminal fragment of rhodopsin detected on the microTOF....73

LIST OF FIGURES-CONTINUED

Figure Page

3.6 Example maximum entropy deconvolution of rhodopsin fragment 74

3.7 Base peak chromatogram and extracted ion chromatograms of rhodopsin CNBr digest peptide fragments detected on a FT-MS 76

3.8 Base peak chromatogram and extracted ion chromatograms of rhodopsin CNBr digest peptide fragments detected on a microTOF 77

3.9 Comparison in the observed resolution between the FT-MS and microTOF 78

3.10 Maximum entropy deconvolution of the larger CNBr digest peptide fragments of rhodopsin detected on the microTOF 79

3.11 Maximum entropy deconvolution of the larger CNBr digest peptide fragments of rhodopsin detected on the FT-MS 80

3.12 Esquire 3000 ESI ion trap base peak chromatogram of bovine rhodopsin CNBr digest derived peptides 82

3.13 Base peak chromatogram of a CNBr digest of bovine rhodopsin separated on the XCT Ultra II with Chip LC front end 83

3.14 MS/MS spectrum of fragment #7 of rhodopsin from analysis with the esquire 3000 QIT 84

3.15 MS/MS spectrum of fragment #7 of rhodopsin from analysis with the XCT nanospray 84

3.16 MS/MS spectrum of fragment #14 from bovine rhodopsin detected on the XCT ultra II 85

LIST OF FIGURES-CONTINUED

Figure Page

3.17 Direct infusion of Opsin and ESI TOF detection....86

3.18 Snake diagram of CCR5 88

3.19 Model of CCR5....89

3.20 Base peak chromatogram of CNBr digest of CCR5 90

3.21 Mass spectra of CCR5 CNBr digest fragments detected in the microTOF 91

4.1 Endogenous cysteines present in rhodopsin 102

4.2 Cytoplasmic face of rhodopsin showing the location of C140 and C316 104

4.3 MALDI-TOF of intact modified and unmodified rhodopsin 105

4.4 Rhodopsin difference absorbance spectra....107

4.5 Extracted ion chromatogram mass spectra of rhodopsin C140 unmodified and modified....109

4.6 Crosslinking peptide B23S-IA to C316 on rhodopsin leads to the stabilization of metarhodopsin-II....110

4.7 Model of metarhodopsin II showing changes in distance between C140 and C316 in this model of the activated receptor....117

4.8 Model of interaction of heterotrimeric G-protein with a rhodopsin dimer....118

5.1 Positions on the single chain Fv randomized in generation of the library....130

5.2 Scheme for scFv selection 131

LIST OF FIGURES-CONTINUED

Figure Page

5.3 Schematic of scFv selection against immobilized bovine rhodopsin 132

5.4 ELISA of selected anti rhodopsin scFv 133

5.5 Extra MII assay of several anti-rhodopsin antibodies....137

5.6 Antibody 541-27 shows discrimination between MIIa and MIIb 138

5.7 Schematic diagram of the light excitation pathway of rhodopsin and ELISA assay of K4241L binding to opsin and rhodopsin 142

5.8 Extra MII assay showing that K42-41L inhibits formation of metarhodopsin-II 145

5.9 Effect of antibody K42-41L on the UV-Vis absorbance spectra 147

5.10 Figure 5.10. Co-crystal structure of Fab fragment derived from the monoclonal antibody K42-41L and epitope mimetic peptide TGALQERSK....150

5.11 Interpretation of the epitope mapping of antibody K4241L with respect to the co-crystal complex of mimetope and K42-41L....152

5.12 Crystal structure of antibody K42-41L docked onto a model of the extended conformation of the CIII loop of rhodopsin....153

5.13 Models for the stabilization of metarhodopsin-I by antibody K42-41L 156

6.1 M13 phage schematic representation....169

6.2 Display of the electrostatic potential of the N1 domain of the pIII protein....170

LIST OF FIGURES-CONTINUED

Figure Page

6.3 Schematic for alignment of peptide probe to antigen primary sequence with FINDMAP and EpiAlign 174

6.4 Cluster analysis of the Pearson correlation coefficients derived from the amino acid side chain interactions 181

6.5 Venn diagram showing "typical" grouping of similar amino acids 182

6.6 Crystal structures of lysozyme with three different antibodies, F9.13.7, D1.3, and D11.15 displayed 184

6.7 Epitope mapping results from EpiAlign for antibody f9.13.7 188

6.8 Epitope mapping results from EpiAlign for antibody D1.3 189

6.9 Epitope mapping results from EpiAlign for antibody D11.15 190

6.10 Comparison of D1.3 epitope on lysozyme and anti-idotope antibody E5.2 192

6.11 Epitope of antibody 9D7 rendered in yellow on the structure of IL-10 and displayed on the primary sequence of IL-10 194

6.12 Plaque lift of phage clones present in the sub library derived from three rounds of affinity selection and enrichment 195

6.13 ELISA assay demonstrating that the phage displaying sequence GIRNDPIRW is capable of binding to antibody 9D7 with specificity 196

LIST OF FIGURES-CONTINUED

Figure Page

6.14 Binding of phage displaying peptide GIRNDPIRW to antibody 9D7 relative to an irrelevant antibody 198

6.15 Competitive binding assayed between clone displaying peptide GIRNDPIRW and recombinant IL10 for 9D7 binding 198

6.16 EpiAlign results for the mapping 9D7 epitope on IL-10 199

6.17 Conservative amino acid substitution for residues that make up the epitope for antibody 9D7 allow for mimetope sequence recovery 199

ABSTRACT

Rhodopsin is the integral membrane protein responsible for black and white vision in low light conditions and is found at high concentration in the mammalian retina. Rhodopsin is a prototypical member of the G protein coupled receptor super family that control much of physiology. Improved understanding of rhodopsin signal transduction and amplification via coupling to the heterotrimeric G protein transducin may reveal conserved activation mechanisms that are relevant to other members of the GPCR super family.

Described here are several studies that examine the molecular determinants responsible for heterotrimeric G protein coupling to metarhodopsin II, the active photointermediate of bovine rhodopsin. Employing uv-visible spectroscopy we have investigated the nature of the interaction between the C-terminal tail of transducin and metarhodopsin II. We have provided evidence that suggests the orientation of transducin when it interacts with metarhodopsin II.

Mass spectrometry is a powerful technique for characterizing intact and digested proteins. We have optimized mass spectral methods for investigating integral membrane proteins, utilizing rhodopsin as a model system. The mass spectrometric studies provide the foundation for future investigations into agonist and antagonist interactions and the related G protein coupled receptors using molecular crosslinking.

Development and validation of new tools for generating structural constraints for conformational states of proteins that are not amiable to more traditional structural determination techniques are described. Antibody imprinting studies on rhodopsin were advanced with the work presented here. The x-ray crystal structure of the anti-rhodopsin antibody K42-41L in complex with a synthetic epitope mimetic peptide is described. These studies led to the generation of a model of the third cytoplasmic loop of the photointermediate metarhodopsin I and constraints on the conformational changes in metarhodopsin II.

CHAPTER 1

INTRODUCTION AND REVIEW OF RHODOPSIN

History of Rhodopsin

Franz Boll first discovered rhodopsin in the frog retina in 1877 [1] and rhodopsin has been studied extensively since that time. The light sensing protein found in the retina was initially called visual red or visual purple and subsequently was named rhodopsin from the Greek rodon, meaning rose due to the color of the isolated protein. This nomenclature was first used by Kuhne and subsequently Wald suggested that this nomenclature be adopted [2]. Rhodopsin is located in the rod cells in the retina and allows for the perception of black and white vision under low light conditions. It was not until 1979 that rhodopsin was recognized to be a G-protein coupled receptor [3].

Rhodopsin can easily be obtained in relatively large amounts from cattle and other retinas. Furthermore, rhodopsin can be purified in its native membrane resulting in a large number of structural and functional studies being carried out, leading to it being viewed as the prototypical member of the G-protein coupled receptor (GPCR) super-family. Studies on rhodopsin have led the field of GPCR research: rhodopsin was the first GPCR to have its amino acid sequence determined [4, 5], was the first GPCR to have its gene cloned [6], and is the first and only GPCR for which there are high resolution crystal structures of several inactivate states, determined by x-ray crystallography [7-13]. Studies employing rhodopsin as a model for the GPCR super-family have led to

discoveries that continue to have broad implications for increasing our understanding of fundamental mechanisms in signal transduction.

GPCR Super Family Classification Schemes

G-protein coupled receptors (GPCR) are the largest known family of receptors in the human genome [14]. There are at a minimum two common features shared by all G-protein coupled receptors: They have amino acid sequences that are consistent with having seven transmembrane spanning regions and contain certain indicator amino acids in the putative transmembrane regions. There is a growing trend to refer to the members of the GPCR super-family as 7-transmembrane spanning proteins (7-TM), as most of the proteins classified as GPCR's have not yet been tested for interaction with G-proteins [15-17]. A wide variety of ligands or stimulatory events, including binding of proteins, peptides, amines, odorants, hormones, lipids, ions and absorption of photons are all thought to mediate receptor activation and lead to signal transduction.

G-protein coupled receptor sequences are present in all of the sequenced eukaryotic genomes and as much as 1% of human protein coding genes are of putative genes for GPCR's [18]. With the increasing number of complete genomes sequenced; putative GPCR's are being found in plants, fungi, insects and mammals. The presence of GPCR's in fungi, plants, and insects indicates that this super-family of receptors is very ancient in origin [19, 20].

Photochemically active proteins that use vitamin A derivatives (retinal) as their chromophore are collectively termed retinal binding proteins and have been found in all domains of life. The large family of 7-TM retinal binding proteins are split into to types

based on primary sequence alignment [21]. Microbial (type 1) rhodopsins have been found in a diverse group of organisms including haloarcheaea, proteobacteria, cyanobacteria, fungi, and algae. In archea the retinal binding protein, bacteriorhodopsin was subjected to structure determination quite early and was used as a template to infer structures for known non-bacterial GPCR's [22]. There are striking similarities in the secondary structural components (7-TM spans) and functional properties (retinal being bound via Schiff base linkage in the 7^{th} TM span) between archaeal and mammalian retinal binding proteins which have led some to believe that these proteins are related. The color tuning mechanisms and thermodynamic energy profiles of the formation of bacteriorhodopsin photo-intermediates have been shown to be very similar to mammalian rhodopsin [23]. However the very low sequence homology, and striking functional differences, such as bacteriorhodopsin not coupling to heterotrimeric G-proteins, have led many to conclude that bacteriorhodopsin and mamalian rhodopsin are not related [24].

Often used methods for GPCR categorization are based on ligand specificity and conservation of amino acid residues at key locations within the putative transmembrane helices and have resulted in the development of organizational systems for segregation of G-protein coupled receptors into 5 classes: A,B,C,D, E and F [25]. More recently the GRAFS (Glutamate, Rhodopsin, Adhesion, Frizzled/taste2, Secretin) categorization scheme, has been presented, where human receptors are split into the following groups, G (glutamate receptor family, 15 members), R (rhodopsin like family, 241 non olfactory, 460 olfactory members), A (adhesion family, 24 members), F (frizzled\taste2 family, 24 members), S (secretin family, 15 members). The GRAF organization scheme was

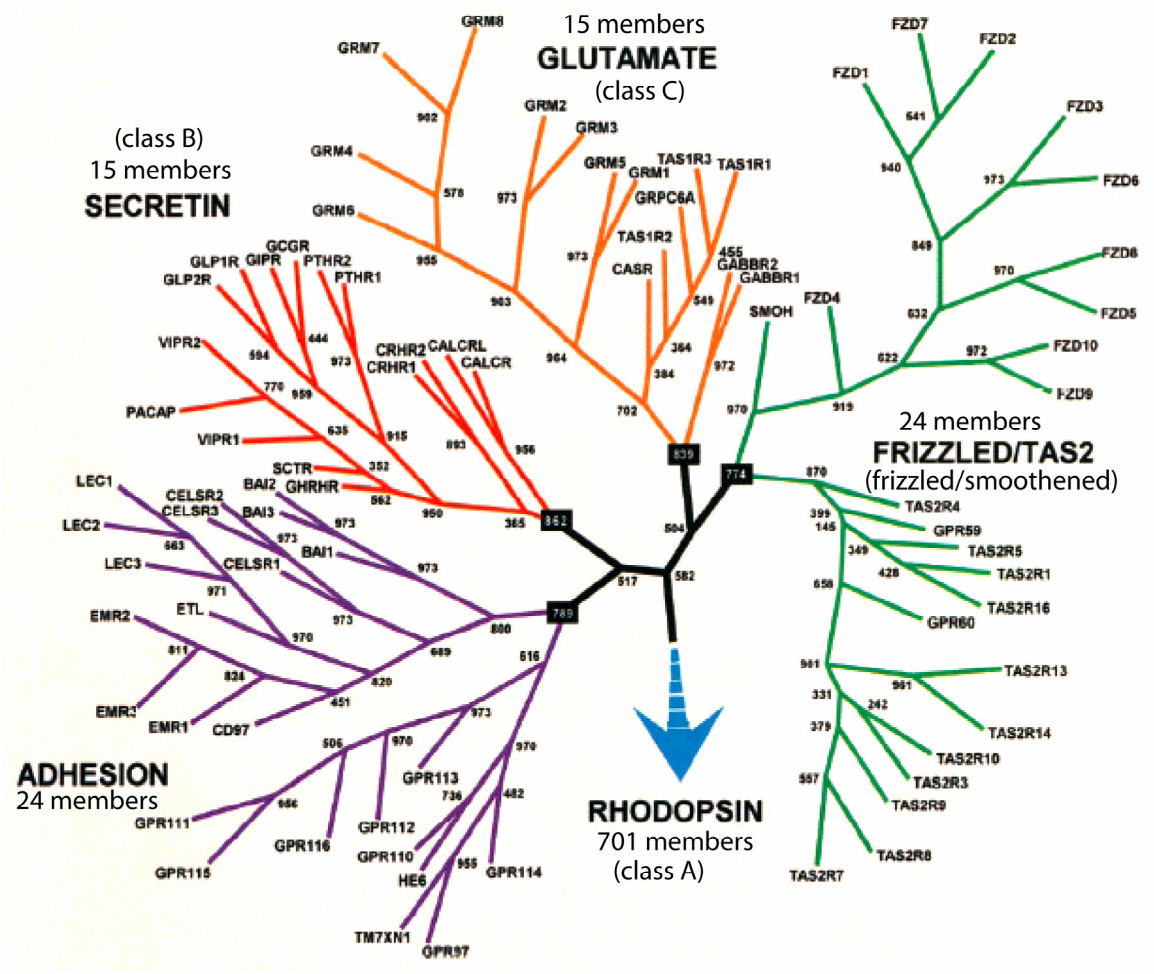


Figure 1.1 G-protein coupled receptors found in the human genome can be clustered into 5 groups based on chromosomal location and sequence alignments. The rhodopsin group is the largest and has been further subdivided into α,β,δ,γ groups (modified from [15]).

constructed by clustering receptors based on chromosomal position and conserved sequence features found in the human genome [15]. The GRAF grouping is similar to the family system for GPCR organization in that class A is similar to the rhodopsin cluster of receptors, and constitutes the largest of all families or groups in either organization method as shown in Figure 1.1 The rhodopsin receptor family is seen as having the most evolutionary success in that most of the GPCR repertoire in plants, yeast, and mammals are classified as belonging to the rhodopsin family of receptors [26]. The conserved

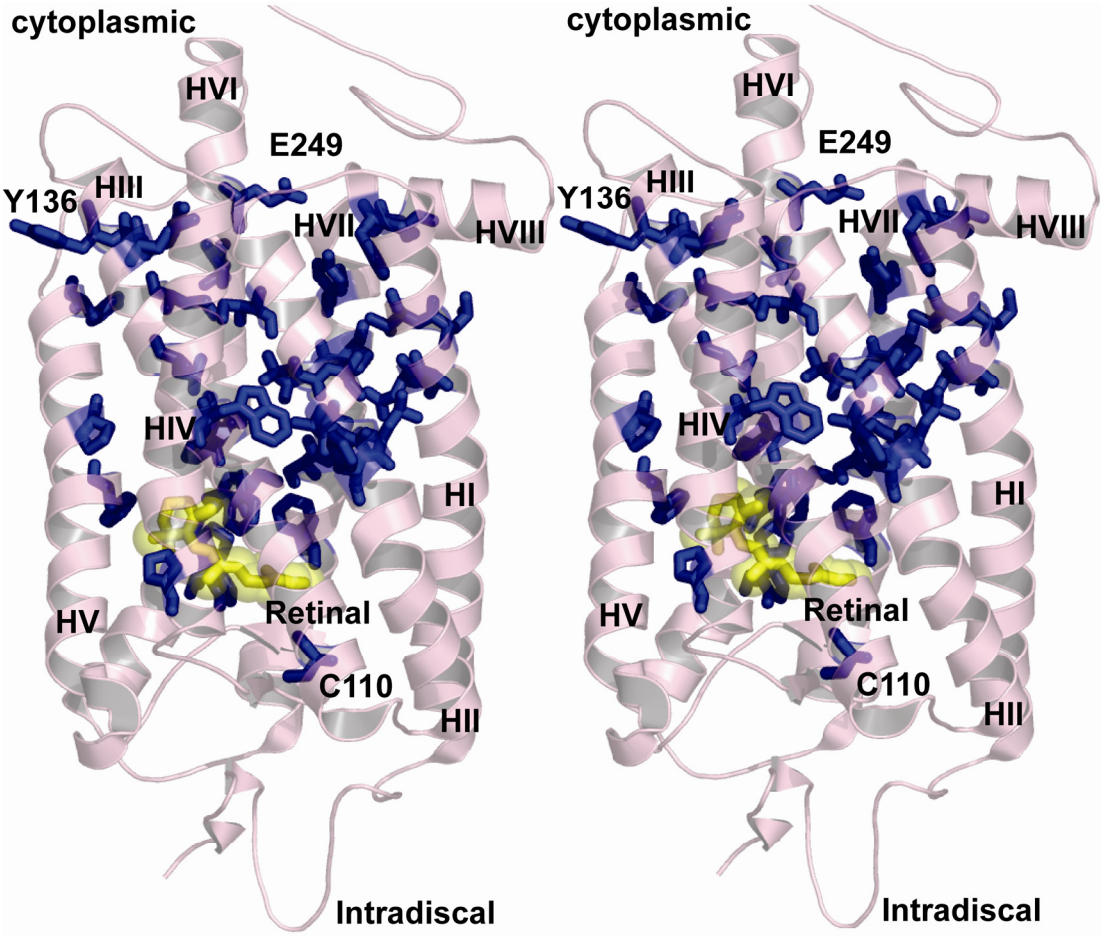


Figure 1.2. Stereo view of bovine rhodopsin. Residues that have been found to be conserved between all family A (Rhodopsin) GPCRs are colored blue and retinal is yellow.

sequence features for class A family members are displayed as blue colored sticks on 3D view of the crystal structure of rhodopsin (U119.pdb) (1.2) and colored blue on the "snake" diagram (Figure 1.3) of rhodopsin. In analyzing a set of 270 (non olfactory) class A members, 18 residues were found to be highly conserved, and present in 60% or more of the class A (rhodopsin family) sequences. Rhodopsin was used as the template for performing multiple sequence alignments. The conserved residue positions in this class A subset are as follows: in helix I G54, N55, L57, and V58, in helix II F75, L79,

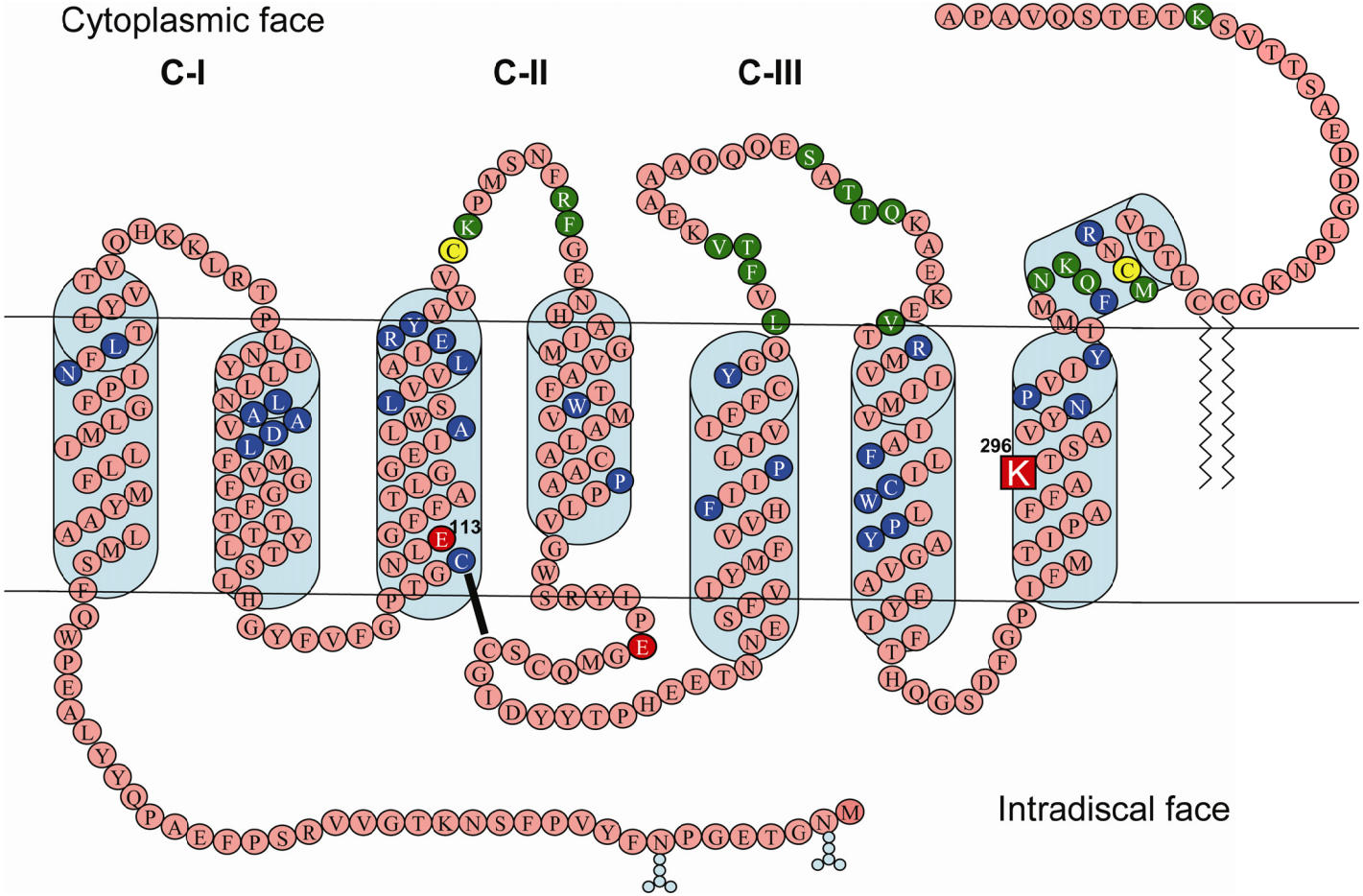


Figure 1.3.Conserved residues in the rhodopsin GPCR family. By a comparison of several hundred amino acid sequences patches of conserved residues where detected, the amino acids that are conserved in bovine rhodopsin and all rhodopsin-like GPCR's are in blue. Residues colored red are coupled to rhodopsin function, those colored green are residues that have been implicated in binding to the heterotrimeric G protein transducin, and those colored yellow are the two cysteines that can be modified readily when rhodopsin is in the rod outer segment native membrane.

A80, A82, D83, L84, L85, in helix III C110, S124, L128, I131, E134, R135, and Y136. The strongly conserved ERY present in helix III is likely to be coupled to receptor activation [27-29]. In helix IV W161 and P170 are conserved, in helix V F212, P215 and Y223 are conserved, in helix VI K249, K252, F251, C264, W265, P267, and Y268 are conserved, in helix VII L294, N298, S299, N302, P303, and Y306 (of the NPxxY motif) are conserved, and lastly in helix VIII F313 and R314 were found to be conserved [30]. Three of the conserved residues are found in the retinal binding pocket (F212, W265, and Y268) and may be involved in a shared mechanism for activation due to agonist binding.

Evolutionary trace analysis performed by Madabush et al., revealed residues conserved between related GPCR family A members [31]. By aligning the sequences of the putative 7-transmembrane spanning helices common to all GPCRs, residues linked to ligand binding, receptor activation, and G protein coupling were identified. The residues associated with ligand binding clustered near the extracellular portion (intradiscal surface) of the helical bundle of the receptor. The residues found to be associated with receptor consituative activity or folding/activity form a swith region that is located between the lignad binding pocket and the residues associated with G protein coupling. Residues that affect G protein coupling/activation are found nearest the cytoplasmic face of the receptor.

The majority of the conserved residues tend to be clustered towards the cytoplasmic side of the transmembrane spans (Figure 1.2) and the side chains are oriented into the helical bundle of dark adapted rhodopsin as can be seen in Figure 1.3. Presumably other members of the class A receptor family have a similar structure and similar side chain orientation at least in the unexcited resting state. The conserved

residues are thought to be linked to shared mechanisms of receptor activation and signal deactivation, but no detailed model of mechanisms involving most of the shared residues has been put forward. G-protein coupled receptors play critical roles in signal transduction in biological systems and are important pharmacological targets, as much as 50% of the drugs currently on the market and in the developmental pipeline target GPCR's [32]. Thus, given the high levels of similarity and evolutionary relatedness to other family A members, increased understanding of rhodopsin has the potential to have a significant broad impact on pharmacology and drug discovery.

Biological Sources and Features of Rhodopsin in Rod Cells.

Rhodopsin is present at very high concentration (~3.3 mM) in the outer segment of the highly differentiated rod photoreceptor cell in retina of the vertebrate eye, as illustrated in Figure 1.4. Bovine rhodopsin, which is highly homologous to other mammalian rhodopsins, is composed of 348 amino acids with the sequence shown in the so called "snake" diagram in Figure 1.3. Rhodopsin has two carbohydrate chains and its most abundant glycoform has a mass of ~41.7 KDa [33]. Isolation of rod outer segment membranes by discontinuous sucrose step density gradient from cattle retina (illustrated in part D of Figure 1.4) typically yields 0.5-1 mg of rhodopsin per retina [34]. Rhodopsin functions as a single photon detector with a quantum yield of 0.67, which is considerably greater than that for most man-made photo detectors [35]. Two thirds of the photon energy absorbed by 11-cis retinal is stored in a strained complex of all-trans retinal,

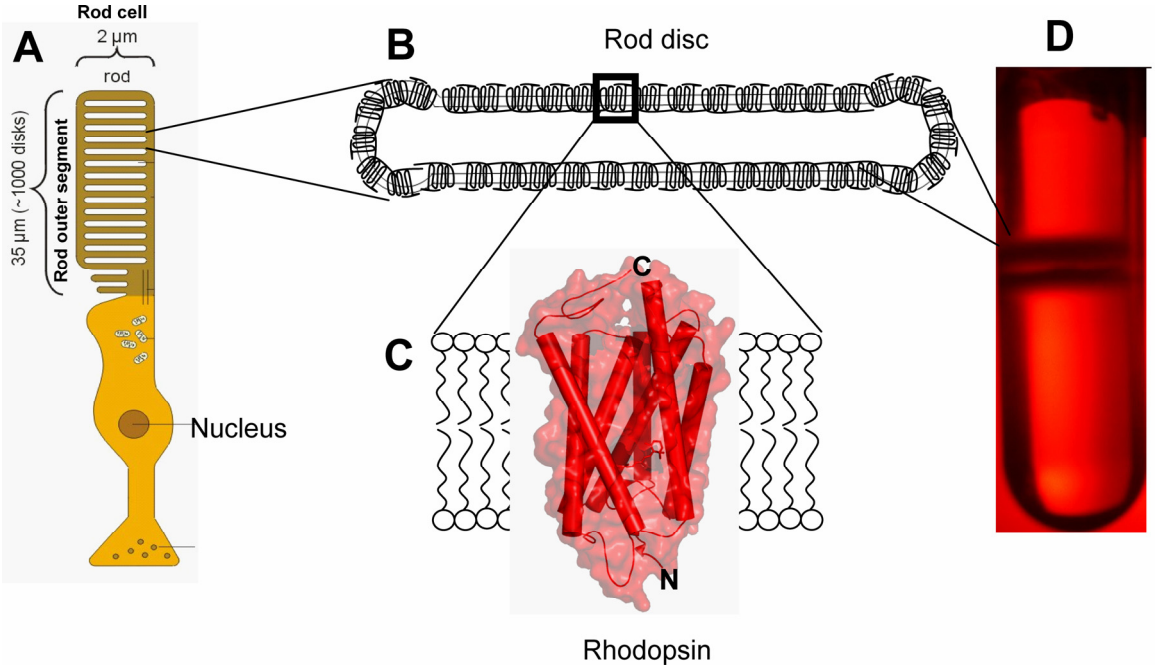


Figure 1.4. There are ~6.4x10^6 rods per vertebrate retina, and ~600-2000 disks per rod depending on the length of the outer segment. The rhodopsin concentration per rod is estimated to be 3.3 mM, there are as many as 2 x 10^4-8 x 10^5 rhodopsin molecules per rod [36, 37]. A) rod discs are localized in the rod outer segment, B) the disc of the rod cell contains very densely packed rhodopsin which may be present in biologically relevant dimers or arrays of dimers[38]. C) Rhodopsin is oriented in the disc membrane with the amino terminal tail localized in the intradiscal space and the carboxy terminal tail exposed to the cytoplasmic space of the outer segment as shown in this picture. D) Rhodopsin is typically purified from retinas by mechanical disruption, shearing off the outer segments, and isolating the rod disk membranes on a discontinuous sucrose gradient. The top band in the photograph of a sucrose gradient contains sealed rod outer segments and the lower band in the photograph contains broken rod outer segments.

bound to rhodopsin that can be trapped at -196ºC prior to any conformational change by the receptor [39]. There are as many as 10^{14} rhodopsin molecules in a single retina, yet the visual system is still capable of detecting single photons due to the intrinsic low noise level in rhodopsin [40]. The chromophore 11-cis retinal is covalently bound to lysine 296 of rhodopsin via a Schiff base linkage and functions as an “inverse agonist”, holding the protein in an inactive conformation [41].

The steps that couple the absorption of a photon by 11-cis retinal and its isomerization to the generation of a nerve impulse and the perception of vision are summarized in Figure 1.5. Briefly, upon absorption of a photon the covalently-linked

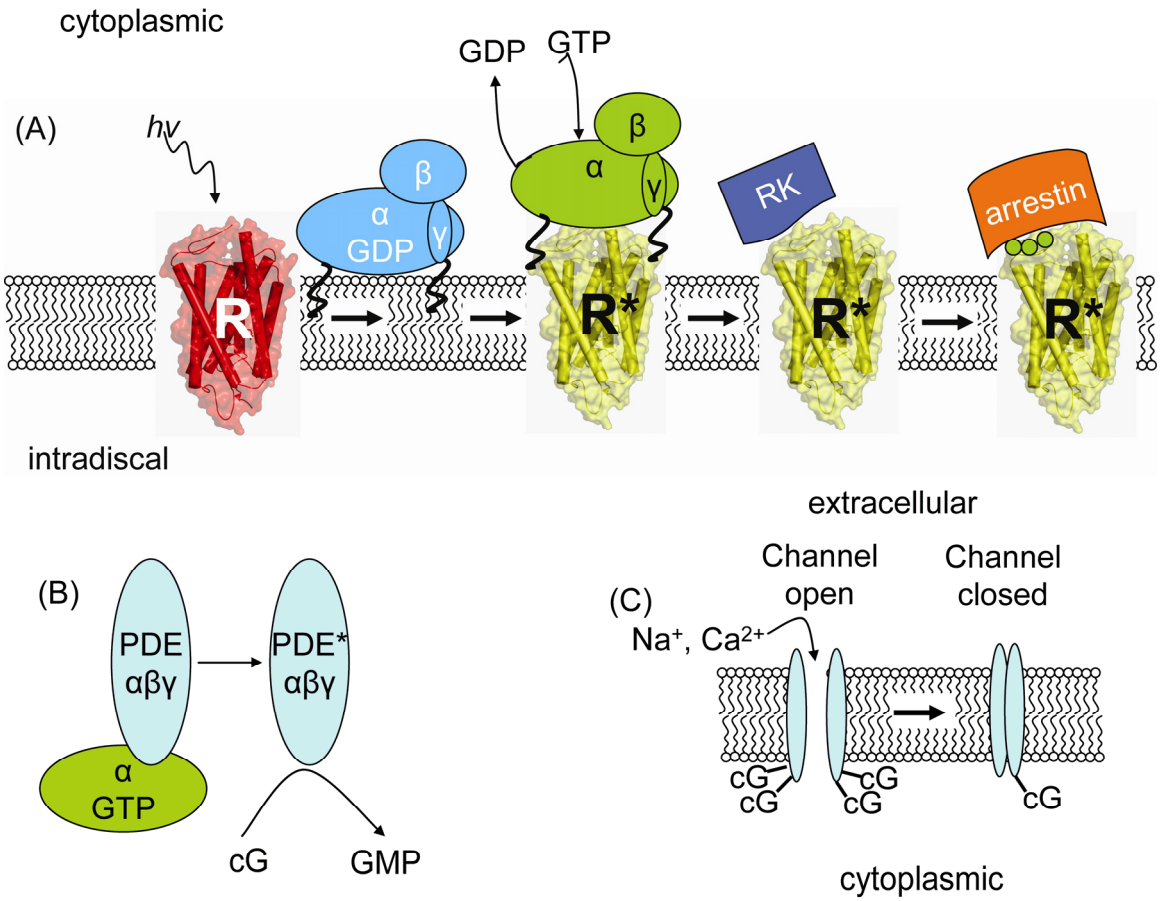


Figure 1.5. Diagram of the visual signal transduction. A) Following receptor activation by absorption of one photon by the ligand 11-cis retinal, the active conformation of the receptor metarhodopsin II, is formed in milliseconds under physiological conditions. Interactions between the activated receptor (R*) and the membrane-associated heterotrimeric G-protein transducin stimulates the release of bound GDP from the alpha subunit of the heterotrimeric G-protein. The receptor-bound alpha subunit of transducin then binds GTP; this binding event causes the release of the heterotrimer from rhodopsin and the dissociation of the alpha subunit from the beta gamma dimer. (B) The alpha subunit of transducin then activates phosphodiesterase PDE which hydrolyses cyclic GMP to GMP. (C)Reduced levels of cGMP (cG) lead to the closure of cGMP gated cation channels leading to a change in the membrane potential of the outer segment, which results in the propagation of a nerve impulse and ultimately results in the perception of vision.

chromophore undergoes a cis to trans isomerization, driving the formation of the activated rhodopsin conformation (R*). Activation of rhodopsin involves the translocation of two protons, which are thought to be required for receptor activation and G-protein coupling [42]; (1) there is a proton transfer from the protonated Schiff base linkage of retinal, resulting in neutralization of the Schiff base counter ion E113 [43, 44], and (2) there is spectroscopic evidence of proton uptake from the bulk solvent upon transition from metarhodopsin IIa to metarhodopsin IIb [45]. In the unactivated receptor the protonated Schiff base linkage is stabilized by the counter ion E113 [44] and it has been demonstrated that mutating E113 to Q results in a decrease in pKa of the protonated Schiff base from above pH 16 [46] to pH 6 and an increased sensitivity to hydroxylamine [47]. Regeneration of a E113Q rhodopsin mutant with 11-cis retinal resulted in a receptor that was capable of activating transducin in the dark [44], indicating the retinal interactions with E113 reduce constitutive activity of the receptor. A counter ion switch mechanism has been proposed where, following photoactivation, the protonated Schiff base counter ion switches from E113 to E181 in metarhodopsin I [48]. The changing amino acid interaction network with the all-trans retinal chromophore is thought to lead to the formation of the catalytically active conformation of the receptor, metarhodopsin-II [49]. The conformation of metarhodopsin II is of broad interest because it is thought to be homologous to the agonist-excited conformations of all other class A GPCR's, if not for all GPCR's.

Signal amplification is achieved by the rapid, repetitive activation of transducin by metarhodopsin II, at an estimated rate of 120 Gαt activated per second per R* [50]. When the heterotrimeric G-protein, transducin, interacts with metarhodopsin-II, it

undergoes a conformational change leading to the release of GDP. Subsequent binding of GTP results in the dissociation of transducin from rhodopsin and the dissociation of the alpha subunit of transducin from the beta and gamma subunit complex. The alpha subunit of transducin with bound GTP activates the membrane-bound cyclic GMP specific phosphodiesterase (PDE) that in turn hydrolyzes cGMP. Reduced levels of cGMP leads to the closure of cGMP-gated sodium ion channels. The closure of the ion channels result in hyperpolarization of the cell leading to a change in the frequency of the generation of nerve impulses and eventually leading to the perception of light [49].

The response to light must be rapidly quenched to avoid after-images in the visual field. The major mechanism for attenuating the response to light, following photoactivation of rhodopsin, is the phosphorylation of serine and threonine residues on the C-terminal tail of rhodopsin by rhodopsin kinase [51, 52]. Interaction between R* and rhodopsin kinase has been shown to result in the activation of rhodopsin kinase (reviewed in Maeda et al., [53]). Rhodopsin kinase is thought to bind to the second and third cytoplasmic loops of the cytoplasmic face of metarhodopsin I, II, and III. Rhodopsin kinase binds to and phosphorylates both metarhodopsin I and metarhodopsin II [54]. The transducin affinity for metarhodopsin II decreases as the number of residues phosphorylated on rhodopsin increases [55]. Arrestin binds to phosphorylated rhodopsin and blocks subsequent interactions between transducin and R* [55]. The affinity of arrestin increases as the number of phosphorylated residues on rhodopsin increases [56]. Arrestin is released from rhodopsin when retinal is lost, and phosphorylated rhodopsin decays to phosphorylated opsin [57]. Attenuation of G-protein activation by phosphorylation and subsequent binding of arrestin to activated and phosphorylated

receptors is thought to be a conserved mechanism in the GPCR super-family [58]. In some GPCR's the receptor-arrestin complex is endocytosed, where the receptor is either degraded or recycled back to the plasma membrane(reviewed in [58]).

Structural and Functional Features of Rhodopsin

Attempts to elucidate the structure and functional relationships in rhodopsin have been ongoing for approximately 34 years. Energy transfer measurements made in 1972, following labeling of rhodopsin with fluorophores, allowed for estimation of the size of the receptor as a 75Å ellipsoid form [59], which is remarkably close to what is observed in the crystal structures presently available. Very approximate models of the topological organization of rhodopsin, being composed partially of seven transmembrane spanning helices, were initially inspired by bacteriorhodopsin, limited proteolysis, and chemical modification experiments [60]. A detailed topological model of rhodopsin was not developed until the full amino acid sequence was determined, revealing that the receptor was composed of 7 putative transmembrane spanning helices [4, 5, 36]. Crystallographic studies have since discovered an unexpected 8^{th} amphipathic helix (Figure 1.6) parallel to the membrane surface and perpendicular to the transmembrane helical bundle [7].

Rhodopsin contains several post translational modifications: (1) the amino terminal Met residue is acetylated [61]; (2) residues Asn^{2} and Asn^{15} are glycosylated predominantly with $(Man)_3(GlcNAc)_3$ [62] but additional glycoforms are present (shown in chapter 3); (3) the chromophore 11-cis retinal is attached though a Schiff base linkage to Lys^{296} [63, 64]; (4) two cysteine residues Cys^{322} and Cys^{323} located at the C terminus of the protein are palmitoylated [65], and (5) two cysteines 187 and 110 form a disulfide

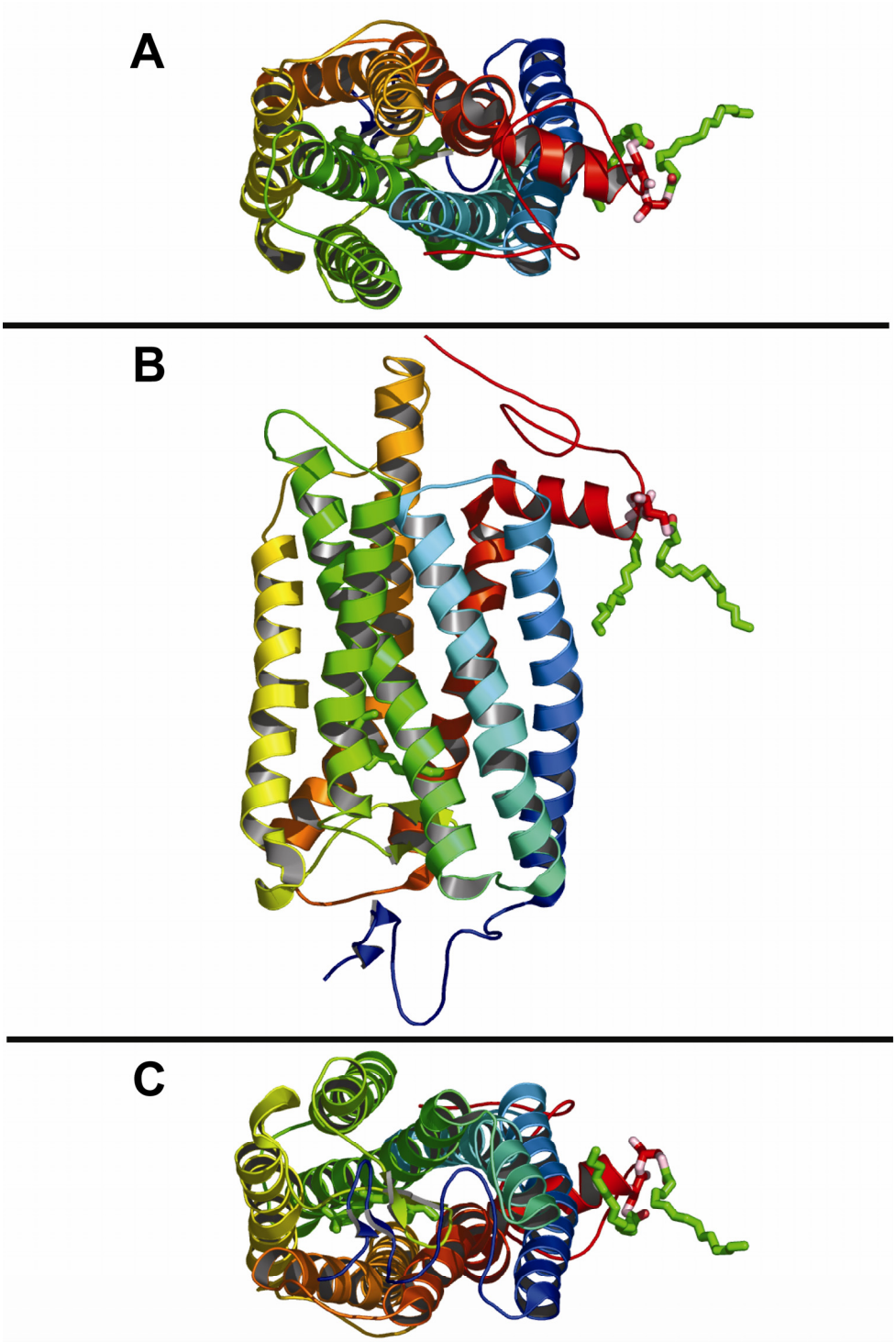


Figure 1.6. Crystal structure of unactivated bovine rhodopsin (1U1.pdb). The cytoplasmic face of rhodopsin is shown in A). B) Rhodopsin with the cytoplasmic face oriented up and the intradiscal face oriented down following a rotation of the rhodopsin by 90˚. The intradiscal face of rhodopsin in shown in panel C)

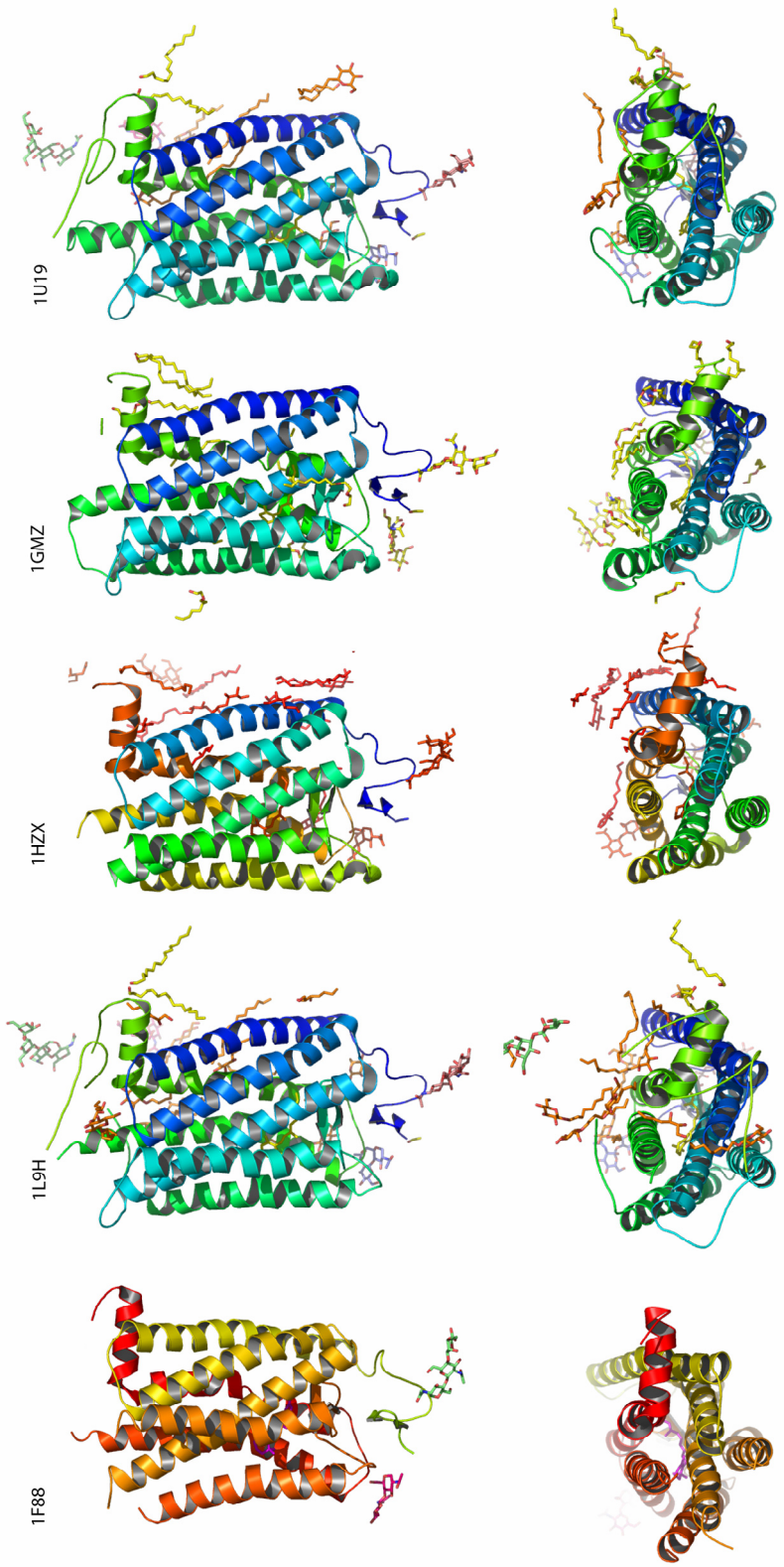


Figure 1.7. Five high resolution crystal structures of dark adapted bovine rhodopsin. Top are transmembrane views of crystal structures with the cytoplasmic face up and the amino interdiscal surface down. Below the cytoplasmic views of the 5 crystal structures 1L9H, 1F88, 1GMZ, 1HXZ, and 1U19 are shown. The resolution of these structures ranges from 2.8 Å to 2.2Å. The first crystal structure 1F88 is resolved to 2.8 Å as is 1HZX. Improvements in purification lead to improvement of resolution to 2.65Å for 1GMZ. Seven ordered waters have been resolved in structure 1L9H (2.6 Å) and 1U19 (2.2 Å).

whereas the other cysteines are reduced. The C-terminal tail is required for proper cellular trafficking to the rod outer segment (reviewed in [66]). Five high resolution crystal structures of the unactivated receptor are shown in Figure 1.7. These structures differ somewhat in resolution, ranging from 2.8Å for the first structure published (1F88) to 2.2Å (1u19) for the highest resolution crystal structure. A notable difference between these five structures is the presence or partial absence of some of the loops and portion of the C-terminal tail on the cytoplasmic face of rhodopsin. Two of the five structures (1GMZ and 1U19) have the entire cytoplasmic face and loop regions included in the structures. The CIII loop is found to take on two different orientations between the two crystal structures that include the loop. This observation, coupled with antibody K42-41L crystallographic characterization carried out by Chayne Piscitelli in the laboratory of Dr. Martin Lawrence [67] and phage display epitope mapping experiments carried out by Brian Bailey in the laboratory of Dr. Edward Dratz [68], will be discussed at some length in chapter 5. Briefly, the antibodyK4241L stabilizes MI at the expense of MII. K4241L binds to an extended conformation of the CIII loop of metarhodopsin I and this extended conformation of the CIII loop, when stabilized by antibody binding, does not allow for the formation of MII. The surfaces of the intradiscal and cytoplasmic faces of rhodopsin contain roughly 1200Å^2 in surface area on the cytoplasmic face and approximately 900Å^2 on the intradiscal face, as measured on the 1U19.pdb structure. The amino terminal tail residues 1 through 33 form a plug on the intradiscal face of rhodopsin which protrudes into the helical bundle, presumably decreasing access of solvent into the retinal binding pocket. The loop residues on the cytoplasmic face are composed of residues 64-71 for CI, 139-150 for CII, 227-241 for CIII and the highly conserved ERY motif is found at the

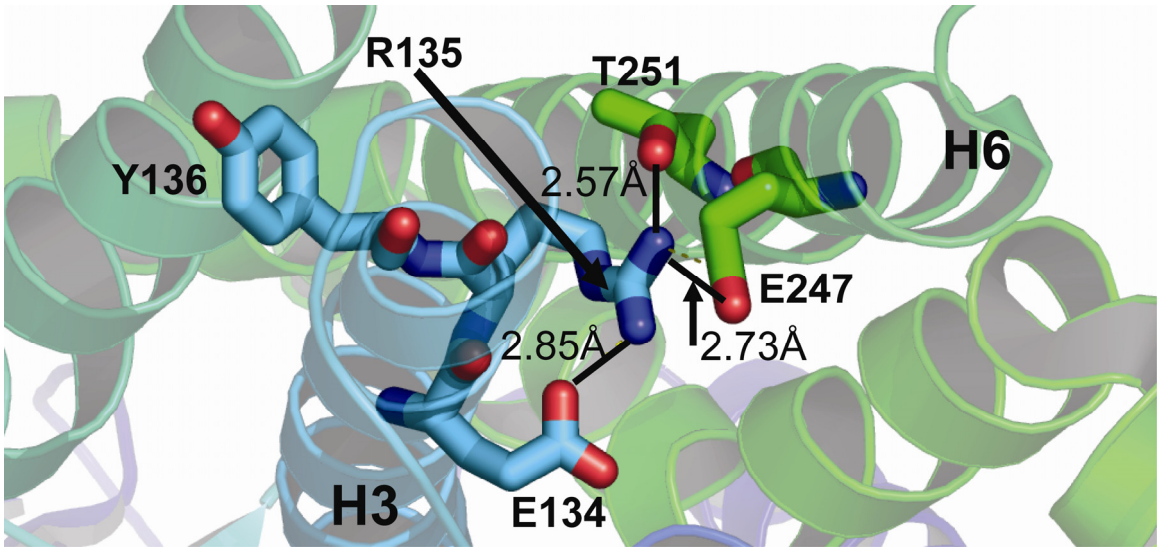


Figure 1.8. Expanded view of the interactions between helix 3 and helix 6 through the highly conserved ERY motif at the cytoplasmic end of helix 3 and residue E247 of helix 6.

end of helix 3 (structure 1U19.pdb). The arginine from this conserved ERY motif forms a salt bridge with anionic E134 and interacts with E247 and T251 of helix 6 (Figure 1.8).

Bound water molecules were detected in several crystal structures (1L9H and 1U19) and may enable an extended helical hydrogen binding network that is believed to stabilize interactions between helix 7 and helix 2 and 3. The crystal structures 1L9H.pdb and 1U19.pdb have revealed the presence of bound water molecules within the helical bundle of rhodopsin. Seven bound water molecules have been found and are bound in 4 groups [8]. The conserved NPxxY motif in helix 7 interacts through N302 and Y306, via a bound water with conserved D83 in helix 2 (Figure 1.9A and B).

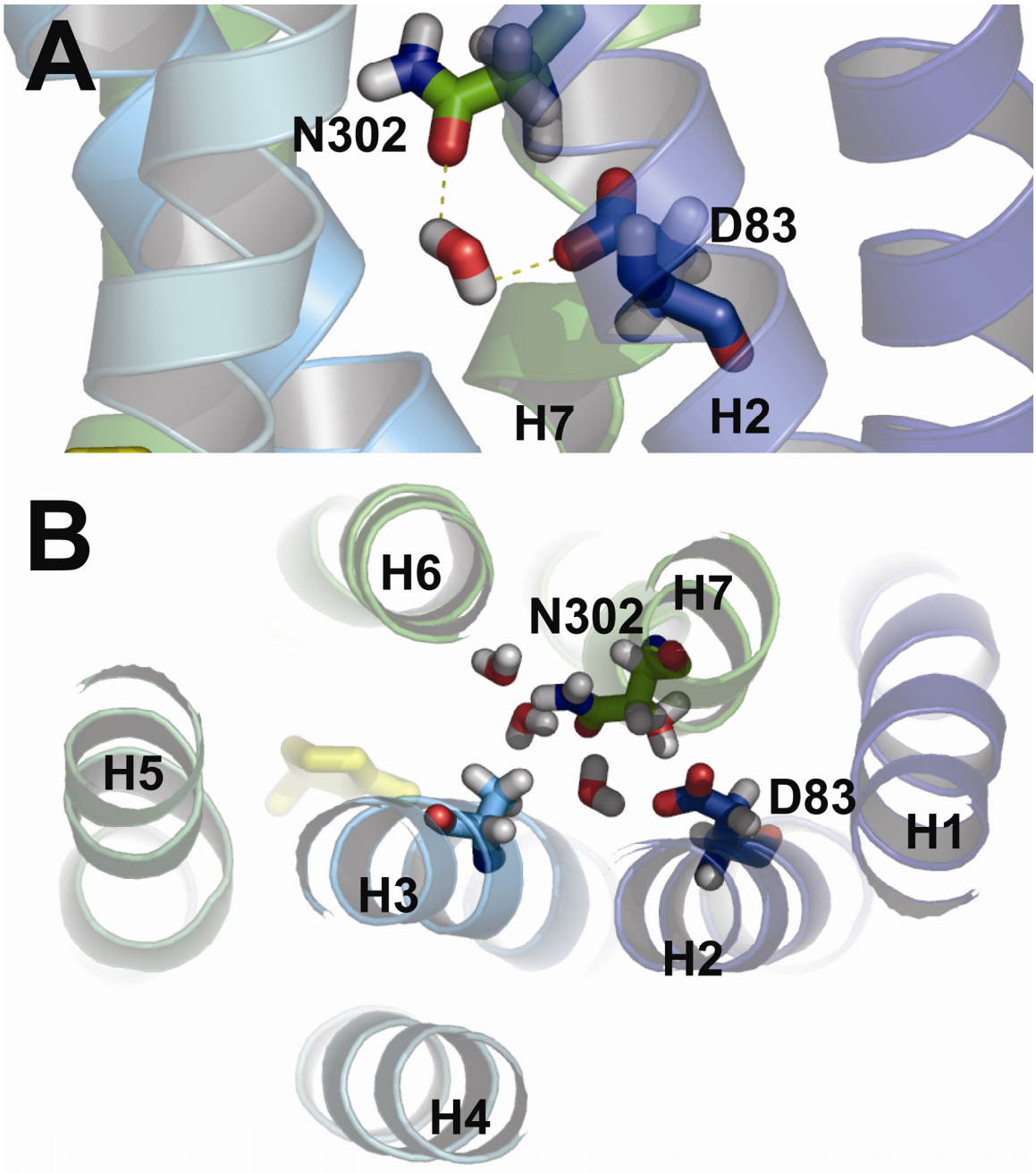


Figure 1.9. There are many ordered water molecule in the highest resolution crystal structures of rhodopsin, which are thought to be functionally important. A) A side on view of rhodopsin demonstrating the presence of bound water molecules that may extend the hydrogen bonding network between residues N302 in helix 7 and D83 of helix 2, increasing the stability of the helical bundle. B) Top down view from the cytoplasmic face showing the presence of water molecules extending hydrogen bonding networks between helix 3 and helix 7.

Conformational Changes Upon Receptor Activation

Site directed spin labeling has been used to measure differential movement of regions of rhodopsin following activation. Khorana's and Hubbell's groups, followed by others, have employed mutagenesis studies and site specific labeling of rhodopsin with spin labels to measure changes that occur following light activation (reviewed in [69]). Prior to the availability of a high resolution crystal structure Yang et al., showed by measuring disulfide formation that Cys^{65} was in close proximity with Cys^{316} when rhodopsin was in the ground state [70]. Placement of spin labels on helix 6 at several different locations suggested that changes in spin-spin interaction following receptor photoactivation were due predominantly to rigid body movements of helix 6 relative to helix 3 [71, 72]. Formation of engineered disulfide bonds between helix 3 and helix 6 has been shown to impair transducin activation [72]. Indeed the movement of helix 6 upon receptor activation is thought to be a conserved feature of family A receptor activation. Along with rhodopsin, the β2-adrenergic receptor [73-75], and the 5HT1 receptor [76] activation are thought to involve rotation of helix 6. Consistent with the notion that the helical bundle expands at the cytoplasmic face upon receptor activation, is the finding that helix 3 and helix 5 move relative to one another when binding and activating transducin as demonstrated by Yu et al., by generating split receptor mutants [77].

There are conformational changes of helix 3 near the cytoplasmic face after light excitation, demonstrated by increased spin label mobility and increased chemical reactivity of cysteine 140 upon receptor activation [72]. It was demonstrated that if either

residues 136 or 140 of helix 3, and residue 222 of helix 5 of rhodopsin form a disulfide bond, then transducin activation is inhibited [77]. However if either residue136 or 140 of helix 3 and 225 of helix 5 form a disulfide bond then transducin activation is unaffected, demonstrating that restricting the motion of helix 5, by not allowed to helix 5 to rotate in a counter clockwise fashion inhibits transducin activation. Another possible interpretation of the results by Yu et al., is that all residues near 225 are required and are involved in binding and activating transducin, and the presence of the disulfide bond interferes with the critical metarhodopsin II-transducin interaction [77]. The conformational changes of rhodopsin that have been reported to take place following activation and formation of metarhodopsin II can be summarized as follows; helix 2,3,6 and 7 are thought to move away from the center of the helical bundle and away from one another, presumably opening the helical bundle and revealing the transducin binding site. Helix 7 may undergo internal helical reorganization in the region that forms a 3_{10} helix in the inactive state assuming a regular alpha helical structure [78]. Changes in constraints holding helix 3 and helix 6 together, presumably involving hydrogen bonding networks between the conserved ERY residues of helix 3 and NPxxYF residues of helix 7 are thought to be part of the switch mechanism resulting in receptor activation [78].

Spectral Features of Rhodopsin

The spectroscopic properties of rhodopsin and photo-activated intermediates are due to changes in the environment of the retinal after excitation and during relaxation. Retinal, when free in solution, has an absorbance maximum of 370 nm, and when conjugated to an amine through a protonatable Schiff base linkage, the retinal complex

has an absorbance maximum of 440 nm, if the solution is acidified. Interestingly, free retinal in solution isomerizes upon exposure to light much more slowly and with a much lower quantum efficiency than retinal bound to rhodopsin, indicating that the isomerization event is guided by the protein environment [79]. When retinal is conjugated to rhodopsin through the protonated Schiff base linkage a red shift is observed, such that the absorbance maximum of rhodopsin is at 498 nm. Residues lining the retinal binding pocket are thought to be responsible for the red shift in the retinal absorbance. Notably, E113 acts as a counter ion to the Schiff base linkage and greatly increases the pKa, also increasing the stability of the opsin retinal complex [80].

Absorption of a photon by the chromophore 11-cis retinal leads to electronic excitation and isomerization, initially to a strained all-trans retinal. Light-activated rhodopsin relaxes, leading to the formation of a series of temporally and spectrally distinct photo-intermediates, as shown in Figure 1.10, which was adapted from Lewis et al. [81]. The spectral differences between photo-intermediates reflect changes in chromophore environment, resulting from changes in the chromophore-protein interactions. The first detectable photo-intermediate formed following photoactivation is bathorhodopsin (λmax 540), which forms in picoseconds. The retinal in bathorhodopsin is in a distorted trans configuration, as suggested by Borhan et al. [82] based on photocrosslinking studies of retinal analogs, and this was later also shown by x-ray crystallography [12]. The second photo-intermediate is blue shifted intermediate (BSI) (λmax 477 nm), which is formed in nanoseconds after bathorhodopsin and is only observed in time-resolved measurements at room temperature [83]. Lumirhodopsin (λmax 497 nm) forms in nanoseconds and formation is associated with an increased

volume of the helical bundle [84]; retinal assumes a more relaxed conformation, relative to bathorhodopsin and the β ionone ring of retinal flips towards transmembrane helix 4 during lumirhodopsin formation [13, 82, 85, 86]. Metarhodopsin I (λmax 487 nm) forms in milliseconds after lumirhodopsin and is thought to be associated with the recovery of normal hydrogen bonding to the protonated Schiff base [86]. The transition from lumi to meta I is coupled to a conformational change in the polyene chain of retinal, as observed by resonance Raman spectroscopy [87].

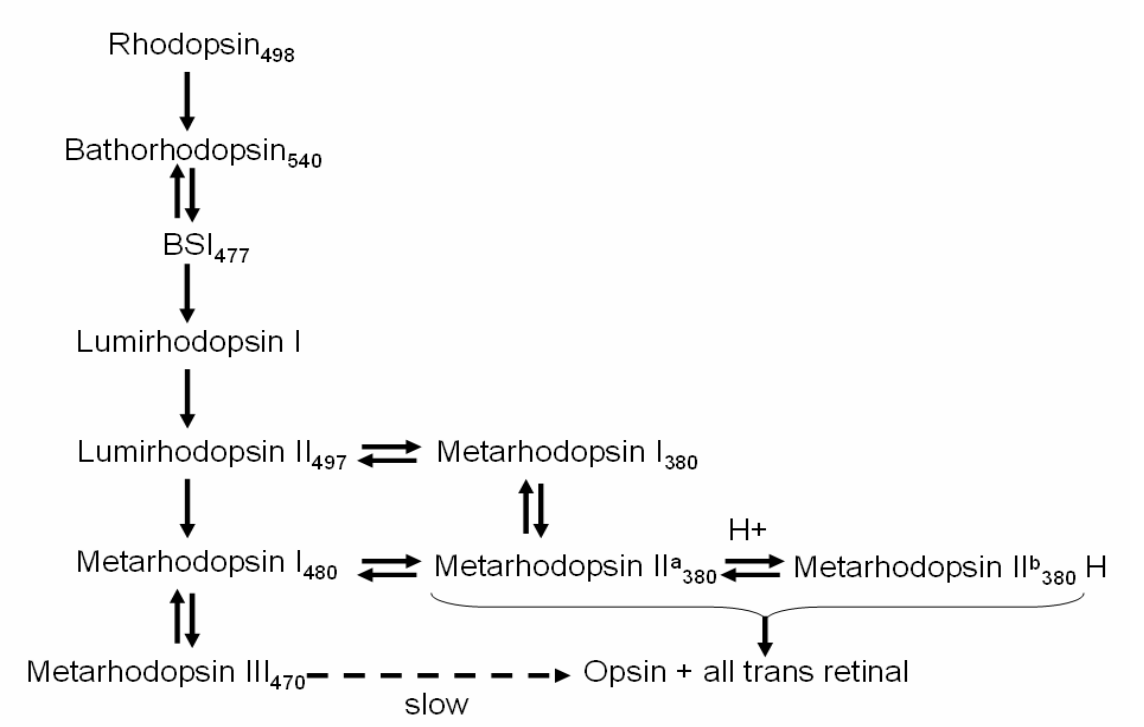


Figure 1.10. Rhodopsin photo-intermediates. Shown above is the series of spectrally distinct photo-intermediates that form following rhodopsin excitation by photon absorption. Thermal relaxation of light-excited rhodopsin occurs with the formation of the photo-intermediates above that have spectrally distinct absorbance maximums noted in subscript.

Metarhodopsin I is in dynamic equilibrium with metarhodopsin II (λmax 380 nm)[88], and metarhodopsin II has been further subdivided into the isochromatic metarhodopsin IIa and metarhodopsin IIb [45, 89]. The transition between metarhodopsin IIa and metarhodopsin IIb is coupled to the uptake of a proton from the bulk solvent [45]. Metarhodopsin IIa is thought have a more compact conformation and Metarhodopsin IIb has been proposed to be an open, active conformation of the receptor that couples to Gαt transducin [45].

Formation of metarhodopsin-II is thought to be associated with a reduction in tertiary interactions between helix 6 and helix 3 [72]. A lack of structural rearrangement of helix 6 upon metarhodopsin II formation was inferred from spin-label studies, leading to the notion that a rigid body movement of transmembrane helix 6 occurs upon metarhodopsin II formation [90]. Photocalorimetric measurements showing an increase in the in enthalpy between metarhodopsin I and metarhodopsin II are consistent with a decrease in molecular contacts upon metarhodopsin II formation [91]. Uptake of a proton from the bulk solvent is coupled to the formation of metarhodopsin IIb [45]. Charge neutralization of E134 has been proposed to lead to reduced tertiary contacts between helix 3 and helix 7, allowing for the movement of helix 3 away from helix 7, and leading to the exposure of the residues that interact with transducin and subsequently activate transducin [92]. Mutation of E134 to Q results is a mutant that is capable of activating transducin in the dark at a fraction of the light induced rate [92]. Metarhodopsin II decays into opsin and all trans retinal. Under conditions where metarhodopsin I is stabilized, metarhodopsin I will decay to form metarhodopsin III [93, 94]. Metarhodopsin III (λmax 470 nm) has been thought of as a stable storage form of

rhodopsin that can be photolyzed back to a "metarhodopsin II like" photo-intermediate [95].

The changes in enthalpy upon formation of the photo-intermediates of rhodopsin have been summarized in Figure 1.11 [23, 91]. Following capture of light energy by photolysis to form R* and retinal isomerization, there is a stepwise decrease in the enthalpy of the system, as rhodopsin relaxes through the photo-intermediates leading up to metarhodopsin I formation. The transition between metarhodopsin I and metarhodopsin II coincides with an increase in enthalpy of the system, which is presumably consistent with the reduction in tertiary contacts between the helices and a conformational change resulting in exposure of the binding site for transducin. Currently there are crystal structures of the ground state, bathorhodopsin [12], lumirhodopsin [13] and a light-activated rhodopsin photo-intermediate that contains a deprotonated Schiff

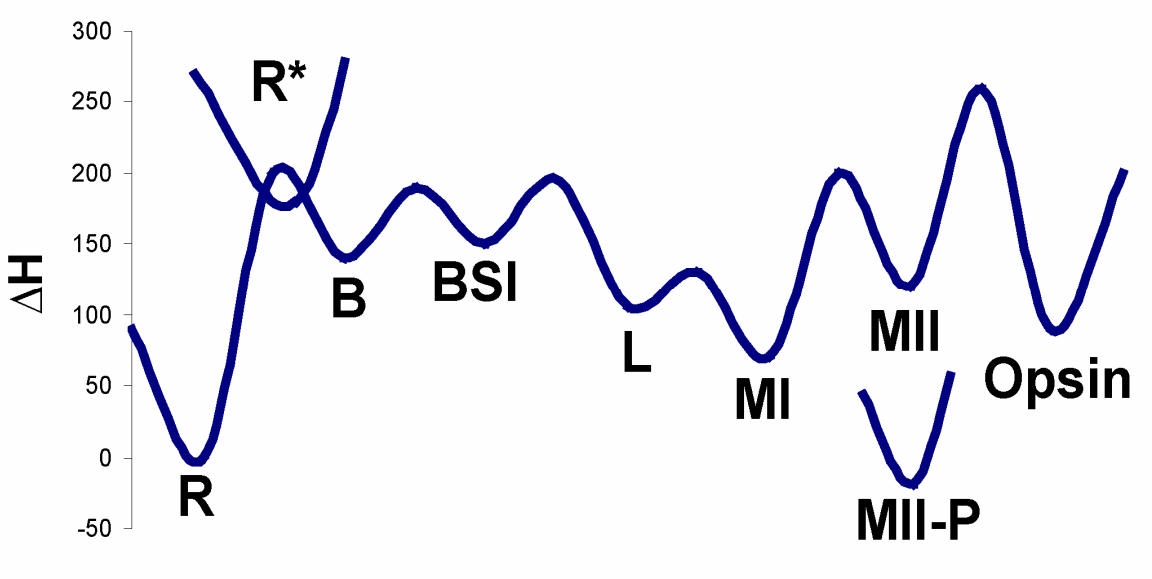


Figure 1.11. Energetics of rhodopsin and photo-intermediates, modified from Birge and Vought [23]. The ground state of rhodopsin is the most energetically stable. Following photoactivation the absorbed energy from the photon captured by R* isdissipated into the protein through a series of steps that have been discussed.

base [96]. Comparison between unactivated rhodopsin and bathorhodopsin revealed structural changes around the retinal binding pocket and the isomerization of retinal [12]. Residues that are found to change in proximity of the retinal binding pocket are **C110**, E113, T118, E122, C167, C187, M206, **F212**, **W265**, **Y268**, and K296. Residues that are bolded are conserved among all family A G-protein-coupled receptors and their involvement may constitute part of a conserved mechanism for GPCR activation. Small changes are seen when comparing the electron density of dark adapted rhodopsin to that of bathorhodopsin. The polyene chain of the chromophore takes on a highly distorted conformation in bathorhodopsin (Figure 1.12) and the distance between the protonated Schiff base and the counter ion Glu113 increases by ~0.3Å [13]. Studies of the photo-activated intermediates formed in 2D crystals of rhodopsin have shown that a 380 nm absorbing species will form and is in a temperature-dependent equilibrium with MI_{480} [97]. The 380 nm absorbing species formed in 2D crystals at physiological temperatures was purported to be MIIa [98]. Additional studies employing FTIR of 2D crystals have shown that the 380 nm species formed in 2D crystals is capable of binding to the C-terminal tail of the alpha unit of transducin but is not capable of activating transducin [97]. The recently released 3D crystal structure of a photo-activated, 380 nm absorbing (deprotonated Schiff base) species, was hypothesized to be a structure of the active state of the receptor [96]. Photo excitation of prior rhodopsin crystals has led to the shattering of the crystals, due to conformational changes in the protein. The rigid body

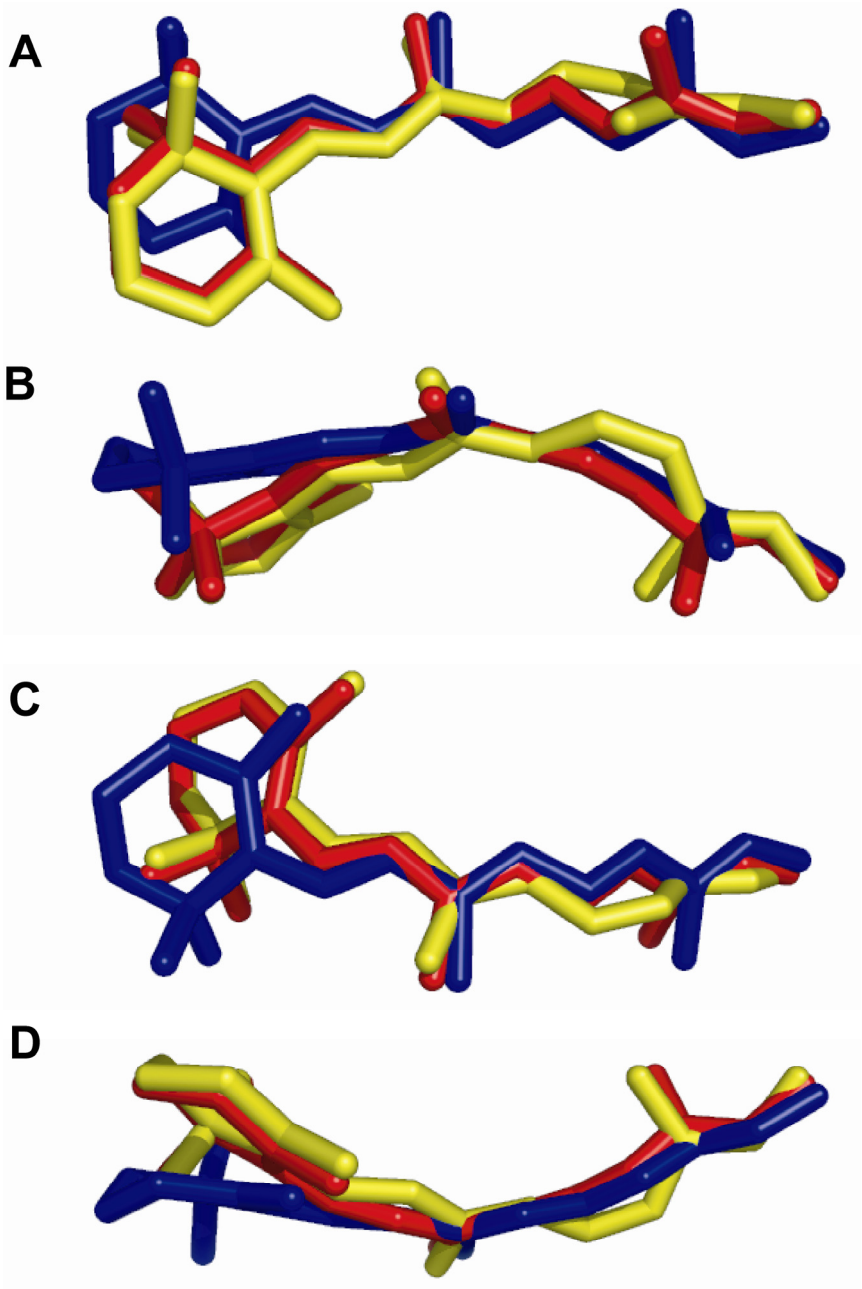


Figure 1.12. Comparison of retinal conformation in different photo excited and ground state rhodopsin crystal structures, 11-cis retinal from dark adapted rhodopsin is colored yellow, isomerized retinal from the crystal structure of bathorhodopsin is colored red, and retinal from lumirhodopsin is colored blue. A-D are views of the three different states of retinal each rotated 90 degrees about the horizontal axis. Upon formation of bathorhodopsin a distortion of the polyene chain of retinal is observed and the retinal straightens. The dominant change between retinal in rhodopsin and lumi is the movement of the β-ionone ring towards helix 3.

conformational changes suggested by the spin labeling experiments are not seen in this structure. A possible interpretation for this is that the activating conformational changes occurs at MIIb and the photo-activated conformation observed may be that of a precursor to metarhodopsin IIb. Two other species of photo-activated rhodopsin are reported to contain a deprotonated Schiff base, MI_{380} and MIIa. The experiments performed to characterize the photo-activated crystals do not allow for the discrimination between MI_{380} or MIIa and either is possible. However, it is unlikely that the structure is of MIIb, given the large amount of biophysical data suggesting that a large conformational change is required for the formation of MIIb from dark adapted rhodopsin and MI.

Metarhodopsin I-II Equilibrium

Following photoactivation of rhodopsin, meta-stable photo-intermediates are formed within milliseconds at physiological temperatures. Metarhodopsin I, the precursor to the active state of rhodopsin, is in equilibrium with metarhodopsin II, the active form of rhodopsin, and this equilibrium has been shown to be sensitive to temperature, pH, ionic strength of the buffer, and mild detergents. Binding events, kinetics, and effects on equilibrium of the meta-stable species can be observed and measured, taking advantage of the distinct spectral signatures of metarhodopsin I and metarhodopsin II following photoactivation. A method for monitoring the metarhodopsin equilibrium by UV-Visible spectroscopy following photolysis was initially developed and reported by Emeis and Hoffman and is known as the extra-metarhodopsin II assay (extra MII) [99]. Unactivated rhodopsin has an absorbance maximum at 498 nm and a molar extinction coefficient of 40,600 M^{-1} cm^{-1}, metarhodopsin I has an absorbance

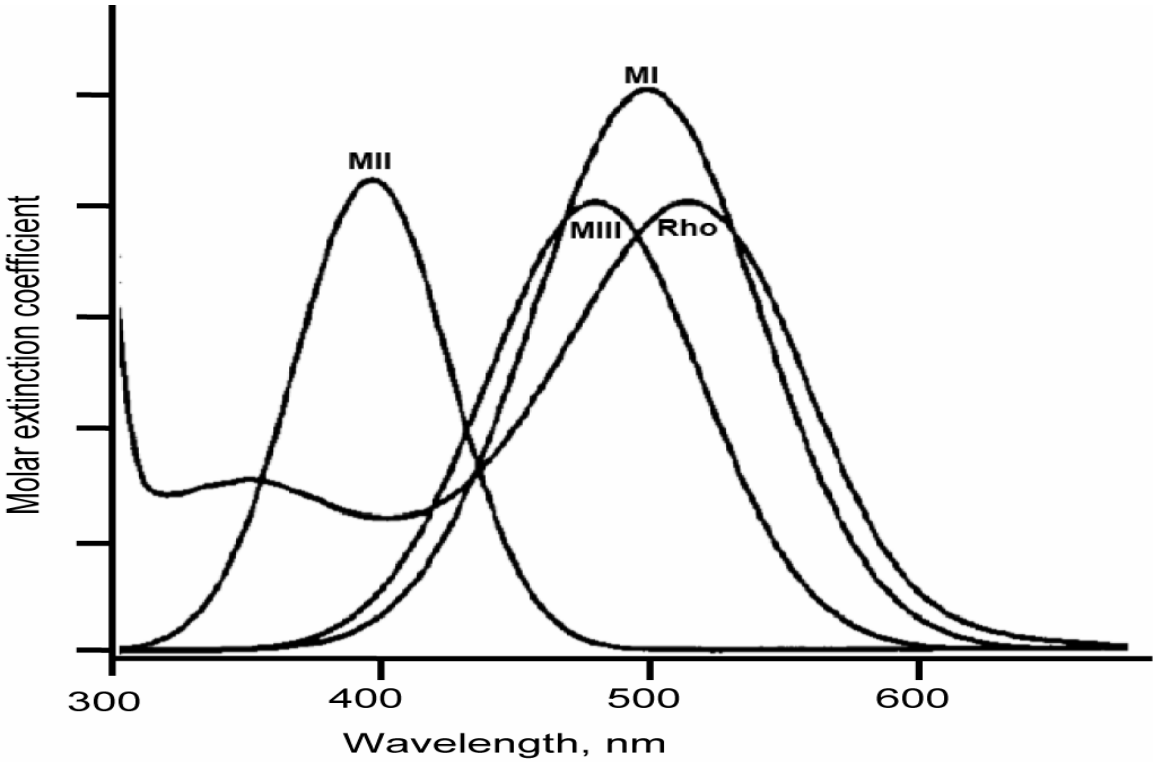


Figure 1.13. Spectral features of meta-stable species of rhodopsin adapted from Parkes et al., [100]. Spectral features for rhodopsin, metarhodopsin I, metarhodopsin II, and metarhodopsin III with their relative molar extinction coefficients are shown.

maximum of 478 nm and molar extinction coefficient of 44,000 M^{-1} cm^{-1}, and metarhodopsin II has an absorbance maximum of 380 nm and a molar extinction coefficient of 38,000 M^{-1} cm^{-1} (Figure 1.13 above) [101]. Monitoring the difference in absorbance between 380 nm and 417 nm allows the kinetic monitoring of the formation of metarhodopsin II. Absorbance changes at 417 nm are subtracted from the 380 nm absorbance change in a dual wavelength spectrometer, leading to a compensation of light scattering changes and a more accurate assessment of the MII contribution to the absorbance measurements. The isosbestic point between rhodopsin and metarhodopsin II occurs near 417 nm, thus changes in absorbance resulting from changes in the amount of light scattering of the sample can be reduced when measuring the changes in absorbance

at 380 nm and subtracting changes at 417 nm. Monitoring the formation of metarhodopsin II employing the extra meta II assay has allowed for the measurement of the kinetics of formation of MII [102], and the binding affinity of the heterotrimeric G-proteins [100, 103]. This has furthered studies in increasing the understanding of the molecular determinants for G-protein coupling and activation of rhodopsin [104]. The equilibrium binding constant of transducin to metarhodopsin II has been determined by titrating the amount of activated rhodopsin into a sample and application of a series of calibrated flashes [100].

Analysis of the metarhodopsin II light titration signal allowed for the characterization of the temperature and pH dependence of the metarhodopsin I-metarhodopsin II equilibrium [100, 102]. The pH and temperature dependence of the metarhodopsin I-metarhodopsin II equilibrium has been described by the following equation, $\ln(Ka)=-9464/(T)-1.608*(pH)+44.87$, where T is the absolute temperature in Kelvin [100, 102]. Increasing temperature is observed to shift the meta equilibrium leading to increased amounts of metarhodopsin II, as described by the formula above [102] and shown in Figure 1.14. Increasing the temperature of the photoactivation has the same effect as decreasing the pH, as can also be seen in Figure 1.14. We have applied the light titration analysis for synthetic peptide analogs of the C-terminal tail of transducin binding to MII and this is discussed in chapter 2. A method that is complementary to the extra meta-II assay involves measuring photo-regeneration of 11-cis retinal following exposure to blue light (412 +/- 12 nm), by following the absorbance change at 520-540 nm [105, 106]. In the presence of transducin or analogs of the C-terminal tail of transducin, photo-regeneration is inhibited [106]. Measuring the decay of

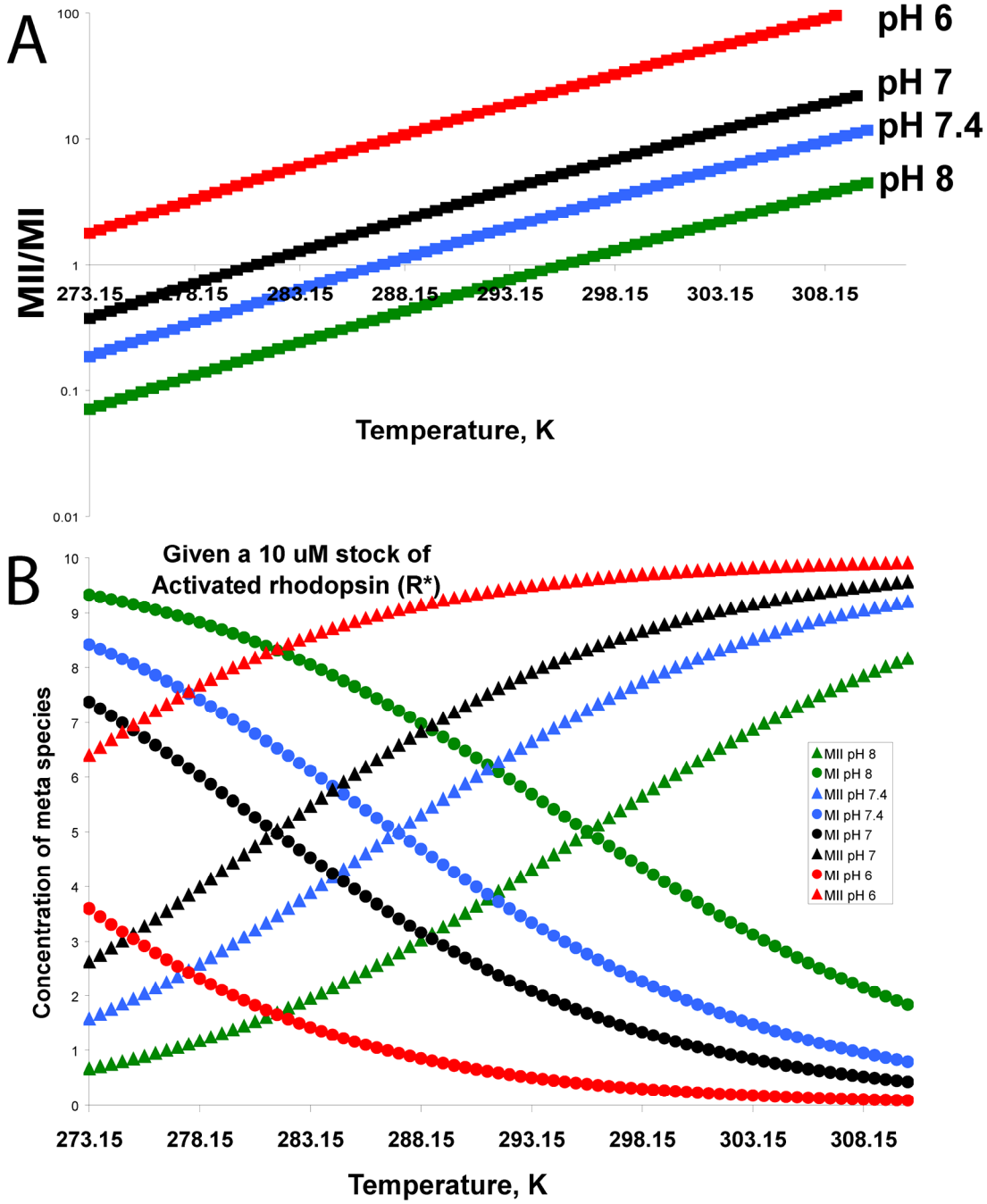


Figure 1.14. The temperature and pH dependence of the equilibrium between metarhodopsin I and metarhodopsin II can be modeled with the following equation, ln(Ka)=-9464/T-1.608*pH+44.87, where Ka is equal to the ratio of MII/MI and temperature is in Kelvin. A) The effect of temperature change on the MI/MII equilibrium is show in the four traces. Increasing temperature favors the formation of metarhodopsin II. B) The theoretical quantities of metarhodopsin I and metarhodopsin II given 10 uM activated rhodopsin and the pH and temperatures shown in A.

metarhodopsin II and the formation of opsin can also be followed by monitoring an increase in intrinsic tryptophan fluorescence [107]. This method has been applied by Heck et al., [107] and allows for discriminating between metarhodopsin II and metarhodopsin III interactions, whereas the extra meta II assay allows for the discrimination between metarhodopsin I and metarhodopsin II binding partners.

Transducin Interactions with Metarhodopsin-II

Greater understanding of the molecular determinants involved in activated receptor coupling to G-proteins will facilitate a better understanding of a potentially conserved signaling mechanism used widely in biology. It was found that the C-terminal 11 residues of the alpha subunit of the G-protein transduscin are capable of interacting with light-activated rhodopsin, stabilizing metarhodopsin II, and are capable of competing with the trimeric G-proteins for binding [108]. The C terminal tail of the alpha subunit of transducin becomes highly ordered upon binding activated rhodopsin [109, 110]. The NMR structure of the C terminal tail of the alpha subunit reveals that upon interacting with R* the peptide assumes a partially helical structure, with a beta turn of the last 4 residues [109, 110]. The last 11 residues of the alpha subunit assuming partially α helical structure upon binding to R* is consistent with the notion of the formation of an extended 5^{th} helix in the alpha subunit of transducin upon binding activated receptor [109]. The carboxyl tail of the gamma subunit of the heterotrimeric G-protein, 60-71, can also couple to activated rhodopsin if farnesylated and shift the MI-MII equilibrium, stabilizing MII [111]. The current state of understanding is that both the alpha and

gamma subunit C-terminal tails additively contribute to the coupling of the heterotrimeric G-protein to rhodopsin. Both the alpha and gamma subunit C-terminal tails have been shown to interact with and stabilize extra metarhodopsin II. The Gαt C-terminal tail (340-350) has been found to be an important contact site for transducin binding to activated metarhodopsin-II [108, 112, 113]. Binding of the Gαt C-terminal tail peptide, $^{-11}$IKENLKDCGLF^{-1}, shifts the MI ↔ MII equilibrium to stabilize MII and the amino acid sequence of the C-terminal tail of the alpha subunits of G-proteins are thought to determine receptor coupling specificity [114]. Photo-crosslinking, differential chemical modification, and mutagenesis studies all indicate that the cytoplasmic C IV surface loop (including residues in helix 8) of rhodopsin is part of the Gαt C-terminal peptide binding site [115-117]. Mutagenesis studies suggest that a hydrophobic region on the C III surface loop of rhodopsin mediates Gαt C-terminal peptide analog-receptor interactions [70]. Fluorescence quenching studies place the amino terminus of Gαt C-terminal peptide analogs near C140 during metarhodopsin-II stabilization [118]. Lastly we have shown that Gαt C-terminal peptide analogs exhibit an orientation specificity. The amino terminal residue of Gαt C-terminal peptide can be coupled to C140 resulting in metarhodopsin II stabilization, whereas if the amino terminal residue is coupled to C316 on rhodopsin, metarhodopsin II is not stabilized as discussed further in chapter 4.

CHAPTER 2

BINDING KINETICS OF PEPTIDE ANALOGS OF THE C-TERMINAL TAIL OF TRANSDUCIN

Introduction

Rhodopsin is the best understood G-protein-coupled receptor and the activated state of the receptor, metarhodopsin II, is a prototype for the agonist bound state of the large rhodopsin like family (family A) of G-protein-coupled receptors. Activation of rhodopsin occurs following the absorption of a photon by the covalently coupled inverse agonist, 11-cis retinal. The isomerization of the chromophore converts the inverse agonist to a full agonist. The photon energy absorbed by the chromophore 11-cis retinal covalently bound to K296 in rhodopsin is dissipated to the protein.

Isomerization of the chromophore is coupled to changes in the charge states of residues, notably E113 and E134 in rhodopsin, as well as changes in certain amino acid interaction networks that appear to lead to conformational changes in the photo-activated receptor (R*) [34]. The relaxation of light-excited rhodopsin occurs concurrently with the formation of a series of well studied photo-intermediates. The active conformation of the receptor metarhodopsin II is formed and is in a dynamic equilibrium with the metarhodopsin I precursor. Changes in light scattering of rod membranes following photoactivation of rhodopsin led in 1981 to the characterization of a binding signal (reflecting transducin binding to R*) [119]. At nearly the same time it was reported that in the presence of peripheral rod outer segment disc membrane proteins that an increased

amount of metarhodopsin II was produced following photolysis of 10% or less of the total rhodopsin present in a sample under conditions that favored metarhodopsin I stabilization [103]. This "extra" amount of metarhodopsin II was attributed to the binding of transducin to rhodopsin, leading to a shift in the equilibrium of the photo products, due to the fact that metarhodopsin II and the complex of transducin and metarhodopsin II both have an absorbance maximum at 380 nm. Bleaching more than 10% of the rhodopsin in the sample did not produce an extra MII signal, since all of the G-protein present was exhausted. Adding non-hydrolyzable GTP or high levels of GDP to the assay mixtures inhibited the formation of the extra metarhodopsin II signal by releasing transducin-GTP or transducin-GDP from their complex with metarhodopsin II, allowing for the conversion back to metarhodopsin I.

The metarhodopsin I-metarhodopsin II equilibrium has been shown to be pH, temperature, pressure, and anion sensitive, and it may also be shifted with addition of glycerol [88, 100, 102, 120-123]. Elevated hydrostatic pressure forces the metarhodopsin II back to metarhodopsin I in the native membrane [124]. Decreasing the pH from 8 to 6 shifts the metarhodopsin equilibrium, favoring the formation of metarhodopsin II. Conditions that favor increased freedom of movement of the receptor appear to shift the equilibrium favoring the formation of metarhodopsin II (e.g. presence of detergents, increased temperature). The rate of formation of metarhodopsin-II was shown to increase in the presence of flexible detergents relative to the rate of metarhodopsin II formation in the native membrane or in the presence of rigid detergents [123]. The formation of metarhodopsin II has been shown to involve the uptake of a proton from the bulk solvent [45], presumably neutralizing one of several negatively charged side chains that

participate in interactive networks that stabilize the inactive conformation of the receptor [44]. Cooperative binding of the heterotrimeric G-protein transducin to metarhodopsin-II has been reported [125, 126] and cooperative binding is consistent with the growing body of experimental evidence that rhodopsin may function as a dimer [37, 96, 127] in the rod outer segment or perhaps even as a tetramer [38, 128, 129].

The C-terminal peptide of the alpha subunit of transducin Gαt (340-350) has been shown to interact with metarhodopsin II and lead to stabilization of metarhodopsin II [108]. Interaction between metarhodopsin II and the heterotrimeric G-protein transducin or peptide analogs of the C-terminal tail, lead to the removal of the interacting complex from the MI-MII equilibrium and an observed increase in absorbance of the 380 nm band, due to formation of the metarhodopsin II-peptide complex. The C-terminus of the alpha subunit of the heterotrimeric G-proteins has been found to be important for G-protein coupling specificity [114, 130, 131] and may constitute a conserved mechanism of G-protein coupling and activation by G-protein coupled receptors [131]. Evidence supporting the notion that the C-terminus of the alpha subunit may impart receptor specificity was provided by the finding that changing the last three residues of the alpha subunit of heterotrimeric G-protein switched receptor coupling specificity from Gαq to Gαi [130].

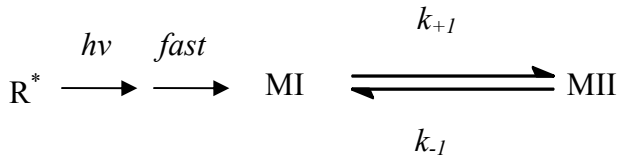
The Gαt C-terminal peptide has been reported to bind to unactivated rhodopsin [110], to MIIa [97] and metarhodopsin Ib [132]. These results seem consistent with one another, considering that it has been recently shown that there is no large rigid body movements of the helices observed when comparing the structures of unactivated rhodopsin and metarhodopsin I at low resolution [133]. Interestingly the C-terminal

residues of the gamma subunit also have been found to interact with metarhodopsin II, leading to stabilization of the active conformation of the receptor [134]. The last 11 residues of the gamma subunit have been found to assume an ordered alpha helical structure upon binding metarhodopsin II [135]. Binding of the C-terminal tail of the gamma subunit of transducin inhibits the binding of the C-terminal peptides of the alpha subunit, indicating that interactions of the heterotrimeric G-protein with metarhodopsin-II are directed in part by both the gamma and the alpha subunit C-terminal tails [136]. Evidence has been presented that the interaction between the gamma and alpha C-terminal tails and activated rhodopsin occurs in a sequential fashion. First the gamma subunit binds, then the alpha subunit binds, and this binding of the alpha C-terminal tail is coupled to the exchange of GDP for GTP and transducin activation [136]. However, the C-terminal tail and possibly other regions of the alpha subunit of transducin, interact with a complex surface on activated rhodopsin composed partially of the third cytoplasmic loop of activated rhodopsin [115, 137].

The stabilization of metarhodopsin II by transducin or transducin-mimetic peptides prevents the formation of metarhodopsin III and the decay of activated rhodopsin via metarhodopsin-I formation and subsequent hydrolysis resulting in free all-trans retinal and the apoprotein opsin [138]. There are several crystal structures of the transducin alpha subunit, however the C-terminal tail is largely or completely disordered in all of the crystal structures [139-142]. Structural features of the C-terminal tail of transducin and ultimately the structure of peptide bound to metarhodopsin II were determined by transferred NOESY NMR spectroscopy [109, 110, 138], with the most recent structure allowing for the determination of the angle of the major axis of the

peptide being about 40˚out of the plane of the membrane when bound to activated rhodopsin [109].

The formation of meta-stable photo-intermediates and the resultant kinetic and equilibrium binding constants can be described as follows (see reaction schemes 1 and 2); following activation by absorption of a photon of light several short-lived photo-intermediates are formed; metarhodopsin-I is formed in milliseconds and is in equilibrium with metarhodopsin-II. The equilibrium constant Ka has been found to be sensitive to pH and temperature. Parkes et al., provided a formula for determining Ka given the experimental conditions [100, 102], and a function describing the pH and temperature dependence of the kinetic rates of formation k_{+1} and k_{-1} was also developed by Parkes et al., [102]. The rate of formation of MII is faster at pH 6 then at pH 8. The kinetics of formation of metarhodopsin-II contains two components, a faster 380 nm absorbance change then a slow pH dependent proton uptake that correlates with the additional 380 nm absorbance. These findings have resulted in subdivision of the formation of metarhodopsin-II into metarhodopsin-IIa and metarhodopsin IIb [45]. In



RXN scheme 1

$K_a = k_{+1}/k_{-1}$

$$\text{MII + peptide} \underset{k_{-2}}{\overset{k_{+2}}{\rightleftharpoons}} \text{MII-peptide} \qquad \text{RXN scheme 2}$$

$$K_b = k_{+2}/k_{-2} = [\text{MII-P}]/[\text{MII}]x[\text{P}]_{free}$$

the presence of transducin or peptide analogs of the C-terminal tails of transducin α or γ subunits the metarhodopsin-II-peptide complex is formed as shown schematically in reaction scheme 2.

The equilibrium binding constant for the peptide Kb can be described as follows,

$$K_b = ([\text{MII-P}])/([\text{MII}]*[\text{P}]_{free}) \qquad \text{Equation 1}$$

where [P] is the free peptide concentration, [MII] is the concentration of metarhodopsin II, and [MII-P] is the concentration of metarhodopsin II peptide complex formed.

The observed kinetic rate of formation is described by,

$$k_{obs} = k_{+1}x[\text{MI}] + k_{+2}x[\text{MII}]x[\text{P}]_{free} + k_{-2}x[\text{MII-P}] - k_{-1}x[\text{MII}], \text{ and} \qquad \text{Equation 2}$$

and the Kb equilibrium constant can be expressed as,

$$K_b = k_{+2}/k_{-2}, \qquad \text{Equation 3}$$

solving equation 3 for k_{+2}, and substituting k_{+2} into equation 2 yields and then solving for k_{-2} yields ,

$$k_{-2} = (k_{obs} - k_{+1}x[\text{MI}] + k_{-1}x[\text{MII}])/(K_b x[\text{MII}]x[\text{P}] + [\text{MII-P}])\ k_{-2}, \qquad \text{Equation 4}$$

The kinetic rate constants k_{+1} and k_{-1} for the metarhodopsin I-metarhodopsin II conversion have been previously described by the two following equations;

$$\ln(k_{+1}) = -21028x(1/T) - 0.702x\text{pH} + 80.01 \text{ and}$$

$$\ln(k_{-1})=-11564x(1/T)-0.906x\text{pH}+35.14,$$

where T is the temperature of the sample in Kelvin.

Knowledge of the observed kinetics and equilibrium binding constants of peptide variants of transducin allow for determining k_{+2} and k_{-2}. Studying the effect of peptide sequence variation on the kinetics may allow the development of a better understanding of the molecular determinants present on the alpha and gamma subunits which control binding to the activated G-protein-coupled receptor.

Here we report the determination of the equilibrium binding constants for the formation of the metarhodopsin II-peptide complex employing a nonlinear least squares fit Simplex analysis of light titration experiments [100]. Peptides that differ in the -4 and -10 position of the C-terminal tail of the alpha subunit of transducin were synthesized and assayed for their ability to form a complex with metarhodopsin-II. In parallel with measuring the equilibrium binding constants for Gαt C-terminal peptide analogs we have measured and determined the binding kinetics for two different synthetic peptide analogs of the C-terminal tail of transducin. The previously reported EC50 values for these peptides give some indication of the strength of the interaction; however, EC50 values do not give an accurate measure of the binding constants and do not describe the relative on and off rate of different peptide analogs. By measuring the equilibrium binding constant of peptide analogs and measuring the k_{obs} kinetic rate we are able to determine the relative on and off rates of different peptides allowing for a better understanding of the molecular determinants for transducin-metarhodopsin II interaction.

Results

We have measured the ability of Gαt peptide analogs to bind to and form a complex with metarhodopsin-II. The different spectrophotometric signitures of metarhodopsin I and II photo-intermediates (shown in Figure 2.1) can be used to monitor the metarhodopsin-I metarhodopsin-II equilbrium. We have employed a spectrophotometric assay which involves monitoring the accumulation of metarhodopsin II-peptide complex to measure the potency of different synthetic peptide analogs derived from the C-terminal tail of the alpha subunit of transducin. The synthetic peptide of the native C-terminal tail sequence, IKENLKDCGLF, and two high affinity variants, Ac-VLEDLRDCGLF, and Ac-VLEDLRS(Abu)GLF, (Abu=amino butyric acid) were synthesized and tested for their ability to interact with and stabilize metarhodopsin-II. Following the application of small calibrated flashes of light in light titration experiments, we have monitored the formation of metarhodopsin II over 50 second intervals in the presence or absence of Gαt peptide analogs. The ability of the peptides to stabilize metarhodopsin-II shows a dosage dependence, as can be seen in Figure 2.2. The association between rhodopsin and peptide analogs reached or nearly reached equilibrium over the 50 second intervals, following flash photolysis as shown by the plateau in the change in absorbance at 390-417 nm after each flash (Figure 2.2). When peptide was not added to the rhodopsin sample, only a small amount of change in the 390-417 nm absorbance was observed after the first flash, but further flashes gave no additional detectable change. The small change that does occur after the first flash is likely due to the presence of endogenous transducin in the rod outer segment preparations (Figure 2.2,

light blue line). As increasing amounts of light-activated rhodopsin(R*) were generated and the peptide concentration became limiting, no more metarhodopsin II peptide complex could be formed even with additional bleaching (Figure 2.2, yellow line).

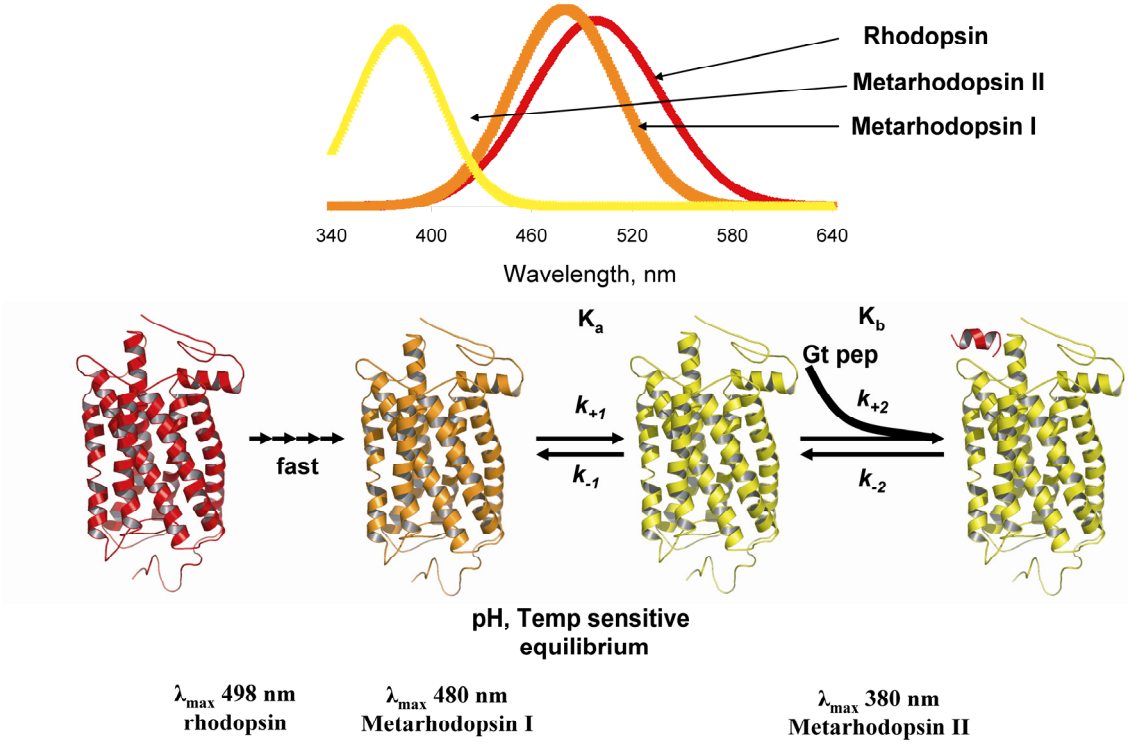


Figure 2.1. Rhodopsin/extra-MII reaction scheme. Dark adapted rhodopsin has a maximum absorbance at 498 nm. Following photolysis rhodopsin forms several spectrally distinct photo-intermediates (reviewed in chapter 1). Metarhodopsin I forms in milliseconds at physiological conditions and is in equilibrium with metarhodopsin II. These meta-stable species have distinct spectral signatures as shown in the above illustrative synthetic absorbance traces. Metarhodopsin I has an absorbance maximum at 480 nm and metarhodopsin II has a absorbance maximum at 380 nm. Monitoring the accumulation of metarhodopsin II can best be done by monitoring the change in absorbance at 390 nm and subtracting the change at 417 nm which is due to changes in light scattering in membrane suspensions, allowing for very sensitive kinetic measurements of MII formation. Addition of peptide analogs of the C-terminal tail of transducin alpha and gamma subunits both result in shifting the apparent MI/MII equilibrium.

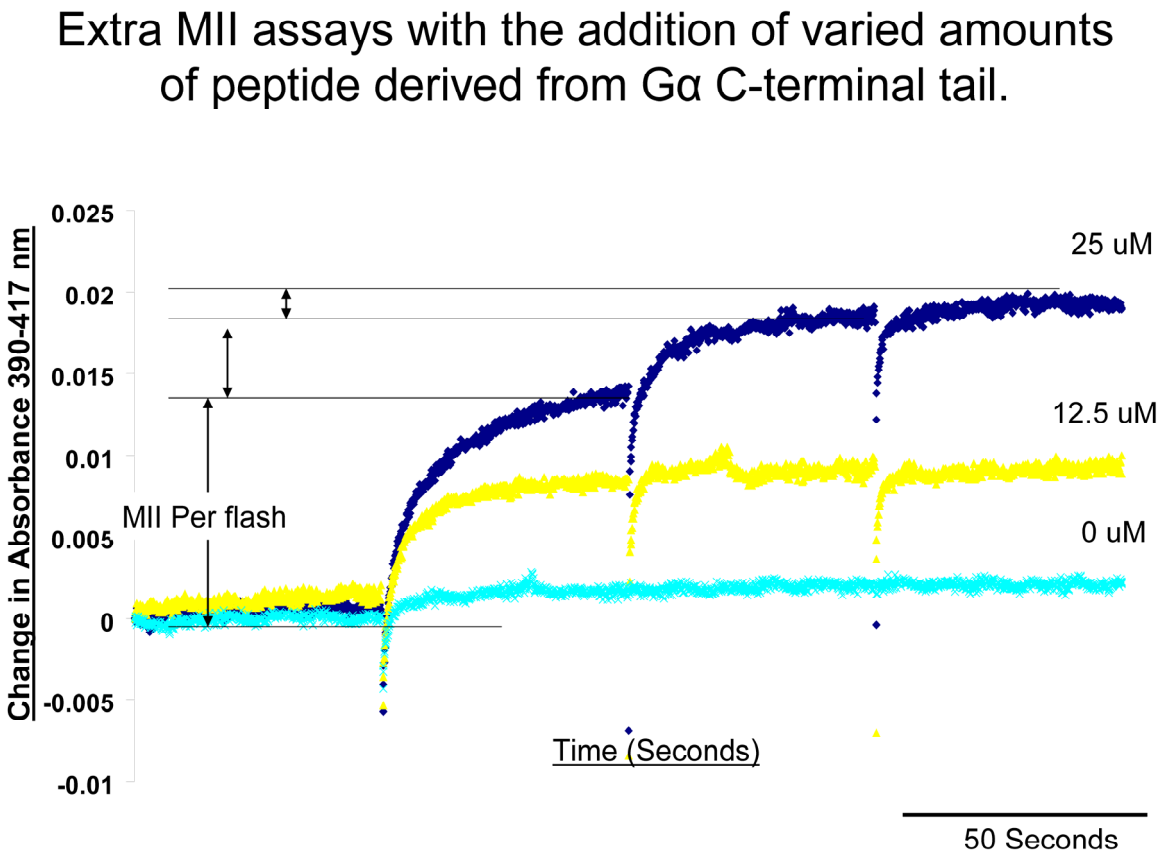


Figure 2.2. Light titration of rhodopsin, measuring the effects of successive light flashes and the addition of varied amounts of peptide analogs of the C-terminal tail of Gαt. Changes in absorbance at (390-417)nm were monitored in a Olis/Shimadzu UV3000 dual wavelength spectrophotometer. Following the application of a flash of light that bleached ~ 8% of the total rhodopsin present in a sample, the absorbance changes were monitored and the activated rhodopsin was allowed to approach equilibrium. Typically 20 flash intervals were monitored to approach complete bleaching and the first 3, are shown here for clarity. The amount of metarhodopsin II formed shows a peptide dose dependence, at lower concentrations of peptide (12.5 uM) the effective peptide concentration is exhausted after 1 flash interval. However, doubling the concentration results in peptide being able to stabilize over twice as much metarhodopsin II.

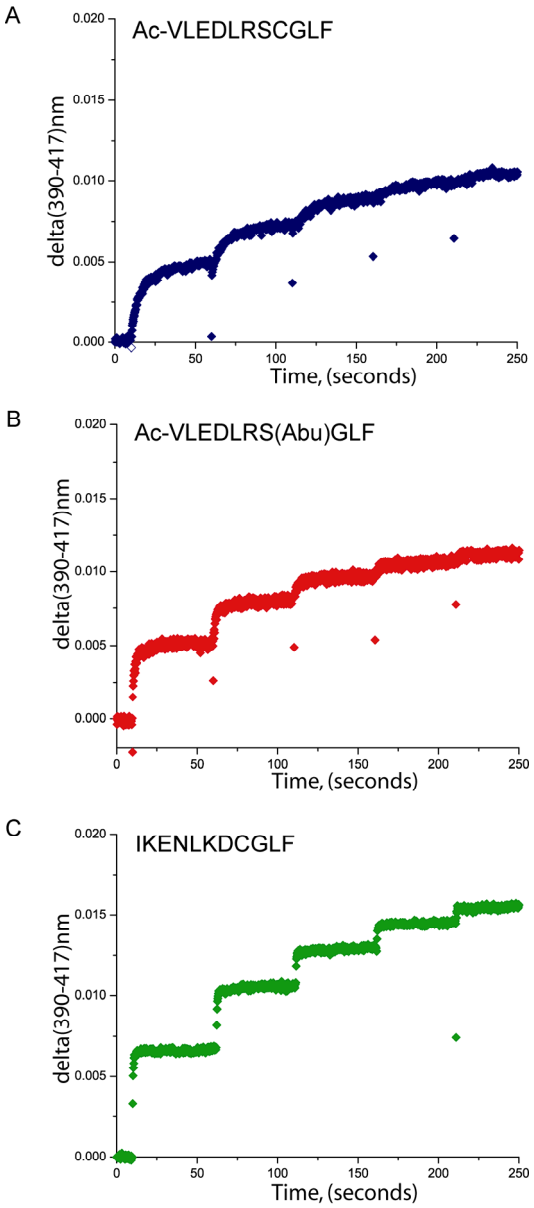


Figure 2.3. Light titration of peptide analogs of the C-terminal tail of Gαt. Rhodopsin in rod outer segments was present at a concentration of 5 uM in buffer B (materials and methods) at pH 8 and 4º C. The change in absorbance due to the accumulation of metarhodopsin-II peptide complex was monitored following photolysis of 8% of the total rhodopsin per flash. 20 flash intervals were monitored (5 are shown for clarity). The amount of metarhodopsin II peptide complex per flash is determined by monitoring relative change in absorbance from one flash interval to the next, after the system has reach equilibrium. These amounts of metarhodopsin II formed per flash are then used in the Simplex analysis for the binding of each peptide, allowing for the determination of the equilibrium binding constants to each peptide.

However, with an increased amount of peptide more metarhodopsin can be stabilized with successive light flashes (Figure 2.2, dark blue line). Light titrations of synthetic peptide analogs of the Gαt c terminal tail VLEDLRSCGLF (3A), IKENLKDCGLF (3B), and AcVLEDLRS(Abu)GLF (3C) were performed. Shown in Figure 2.3 for clarity are 5 of the total 20 flash intervals measured. Following the light titration measurements for a peptide, the amount of complex formed after each flash was equal to the absorbance change, determining the equilibrium binding constant (Kb) of the peptide is accomplished by solving the series of 4 equations below;

(1) $[R^*]= [MI]+[MII]+[MII-P]$

(2) $[P]_{total}= [P]_{free}+[P]_{bound}$

(3) $Ka=[MII]/[MI]$

(4) $Kb=[MII-P]/([MII]*[P]_{free})$

Given the assayed concentration of peptide added, the concentration of rhodopsin, the fraction of rhodopsin bleached per flash (the amount of R* generated), and the equilibrium constant for the formation of metarhodopsin I and metarhodopsin II (Ka), a least squares fit was performed, fitting the observed change in optical density with a predicted change in optical density employing the following equation; $\Delta OD=\Delta[R^*]\Delta\varepsilon(rh\rightarrow MI)+ (\Delta[MII]+ \Delta[MII-P])\ \Delta\varepsilon(MI\rightarrow MII)$. The differential extinction coefficients used were -5500 M^{-1} cm^{-1}, for the transition from rhodopsin to metarhodopsin I and 33000 M^{-1} cm^{-1} for the transition between MI and MII. The equilibrium binding constant Kb, was determined for two of the three peptides. An

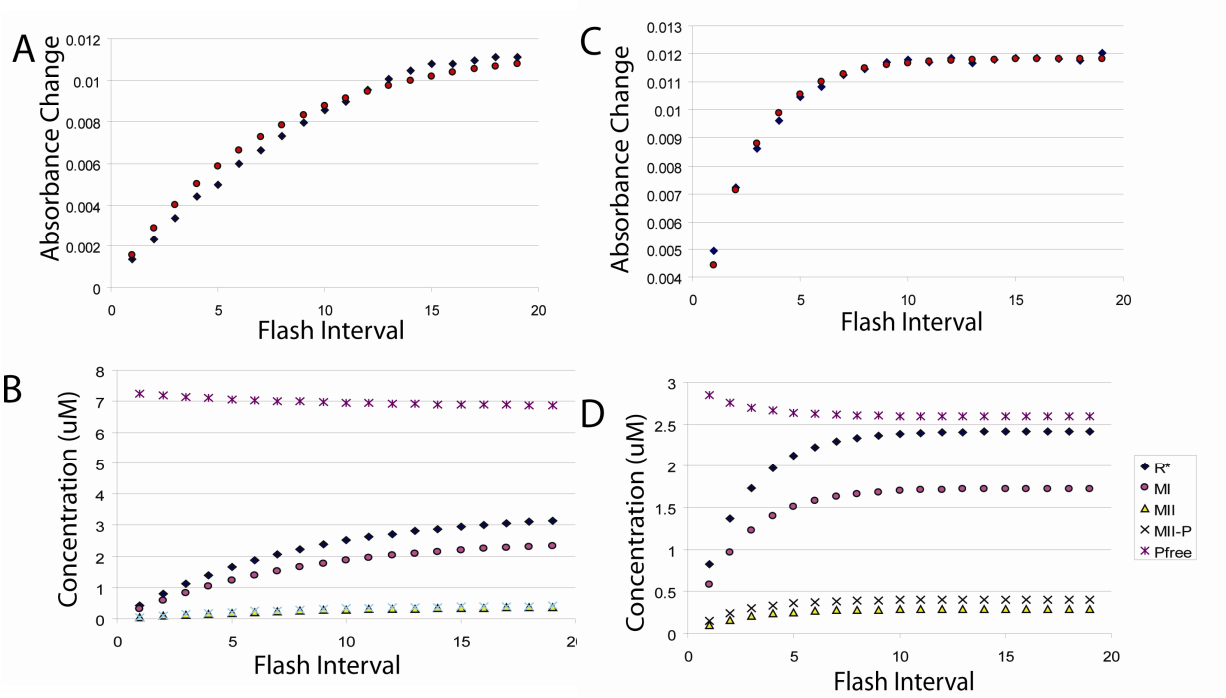


Figure 2.4. Simplex C analysis of light titration for peptides Ac-VLEDLRD(Abu)GLF (A) and Ac-VLEDLRSCGLF (C). The change in absorbance following light excitation of rhodopsin was measure for 20 flash intervals (blue diamonds). The values of change in absorbance and reactant concentrations were used as an input to the Pascal program SimplexC[100], which performs a down hill nonlinear least squares fit on the absorbance change data (red circles). The output of the Simplex analysis fit includes simulated data plotted along with the experimental results for each peptide and the extrapolated concentration of all of the species present in sample mixture as shown in B for peptide Ac-VLEDLRS(Abu)GLF and in D for peptide Ac-VLEDLRSCGLF, which allows for the determination of the equilibrium binding constant Kb.

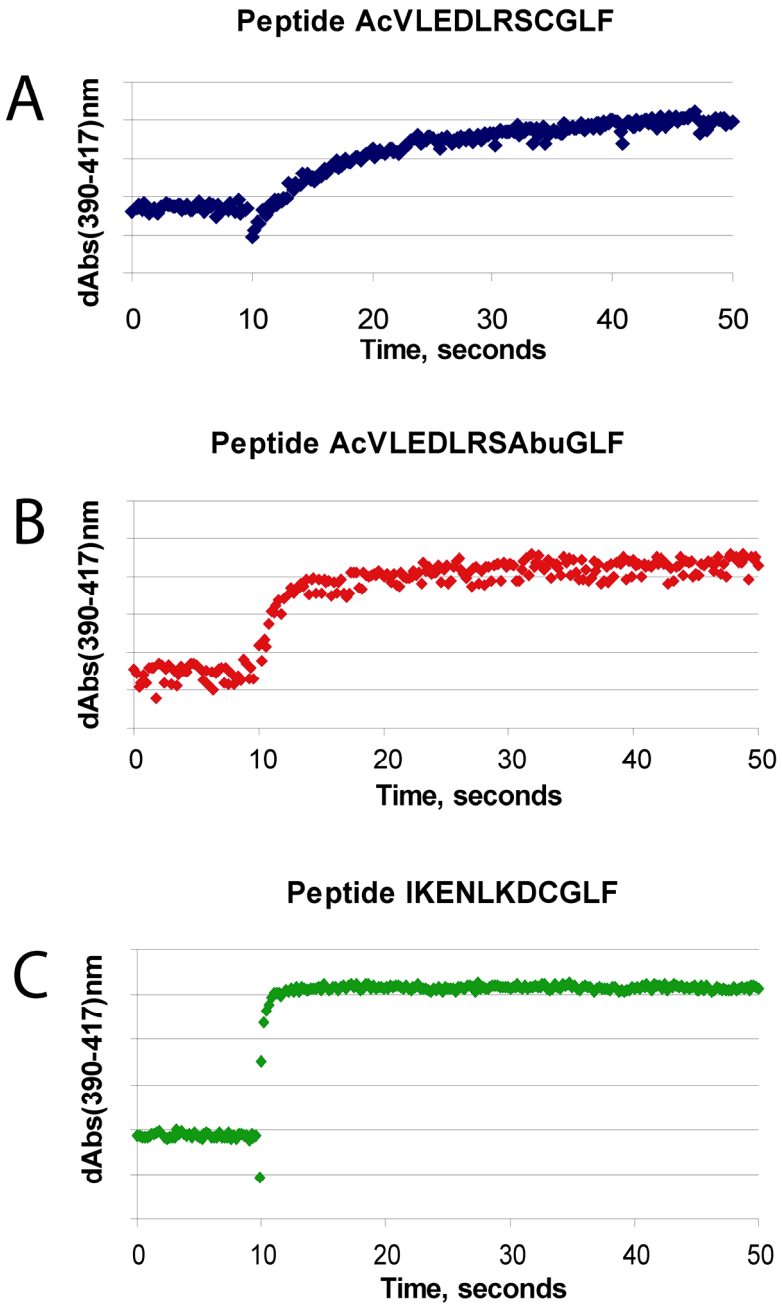


Figure 2.5. Peptide analog of the C-terminal tail of transducin interact with rhodopsin with different observed kinetic rates. A) peptide AcVLEDLRSCGLF has the lowest EC50 and the slowest observed rate of formation, B) peptide AcVLEDLRS(Abu)GLF shows an intermediate observed kinetic rate of interaction with metarhodopsin II, and C) the native peptide IKENLKDCGLF binds with the lowest affinity however has the fastest observed kinetic rate of interaction with metarhodopsin II.

Protein or Peptide	k_{obs} s^{-1}	k_{+2} μM^{-1} s^{-1}	k_{-2} s^{-1}	Kb μM-1	Kd μM	EC50 μM
Transducin	ND	1.16[136]	152[136]	30[100]	0.03[100]	ND
Ac-VLEDLRSCGLF	0.13	0.14	0.26	0.53	1.9	1.1 (3.6)
Ac-VLEDLRS(Abu)GLF	0.19	0.14	0.8	0.17	5.8	10.6 (1.2)
IKENLKDCGLF	1.79	10.2	5.7	0.001	1209	1209(2.7)[112]

Table 2.1. Kinetics of peptide interactions with metarhodopsin-II.

example of solving for Kb by fitting the absorbance data employing the program SimplexC is shown in Figure 2.4.

Shown in Figure 2.4A is the average change in absorbance at 390-417nm per flash interval, after light-excited rhodopsin has formed and closely approached or reached equilibrium, due to the formation of metarhodopsin II-peptide complex and small amounts of metarhodopsin II which are in equilibrium with both metarhodopsin-I and metarhodopsin II-peptide complex. The absorbance change over 20 flash intervals was used as the input to the SimplexC program, the poor quality of the fit seen in Figure 2.4A is likely the result of the model for the formation of metarhodopsin II being incorrect. The model used currently has metarhodopsin I in equilibrium with a single metarhodopsin II species, however there is evidence for two forms of metarhodopsin II, MIIa and MIIb, where MIIa forms rapidly and MIIb forms with a slower kinetic rate constant [45].

The observed kinetic rate of formation of metarhodopsin-II peptide complex (k_{obs}= $k_{+1}x$[MI]+$k_{+2}x$[MII]x[P]$_{free}$+$k_{-2}x$[MII-P]-$k_{-1}x$[MII]) appears to be peptide-dependent (Figure 2.5). Previously it has been reported that the rate of formation of metarhodopsin-II peptide complex does not differ due to the identity of the peptide analog [143]. However upon close inspection of the published data [143] there are readily apparent differences in the rates of formation of metarhodopsin II-peptide complex due to the

presence of different peptide analogs when comparing kinetic traces. The native low affinity peptide shows the fastest rate of formation of metarhodopsin II peptide complex (Figure 2.5 C), the cysteine to amino butyric acid high affinity analog (Ac-VLEDLRS(Abu)GLF) shows an intermediate kinetic rate and, unexpectedly, the peptide with the highest affinity shows the slowest rate of formation (Figure 2.5 A) which seems counter-intuitive. The kinetic on rate (k_{+2}), and off rate (k_{-2}) were determined employing classical kinetic relationships and conservation equations from the observed kinetic rate of formation and equilibrium binding constant for the peptides and are reported in table 2.1. Given the observed rate of formation of metarhodopsin-II peptide complex, which can be expressed as follows ($k_{obs}= k_{+1}x[MI]+k_{+2}x[MII]x[P]_{free}+k_{-2}x[MII\text{-}P]-k_{-1}x[MII]$), the kinetic rates for the formation of MII from MI and MI from MII, and the equilbrium binding constants the on rate (k_{+2}), and off rate (k_{-2}) can be calculated.

Discussion

The equilibrium for the binding of peptide to rhodopsin is schematically depicted in Figure 2.1. We have titrated solutions of Gαt C-terminal peptide analogs with light-activated rhodopsin and monitored the accumulation of metarhodopsin II-peptide complex formed by measuring the change in absorbance (Figures 2.3 and 2.4). This method was initially developed by Parkes et al., and applied to determining the equilibrium binding constants for the intact heterotrimeric G-protein. The equilibrium binding constant of transducin was reported to ~30 uM^{-1} at pH 8 and 0º C, or an equivalent Kd of approximately 0.03 uM. The Kb value determined for the high affinity analog of transducin (AcVLEDLRDCGLF) was found to be 0.53 uM^{-1}. The intact

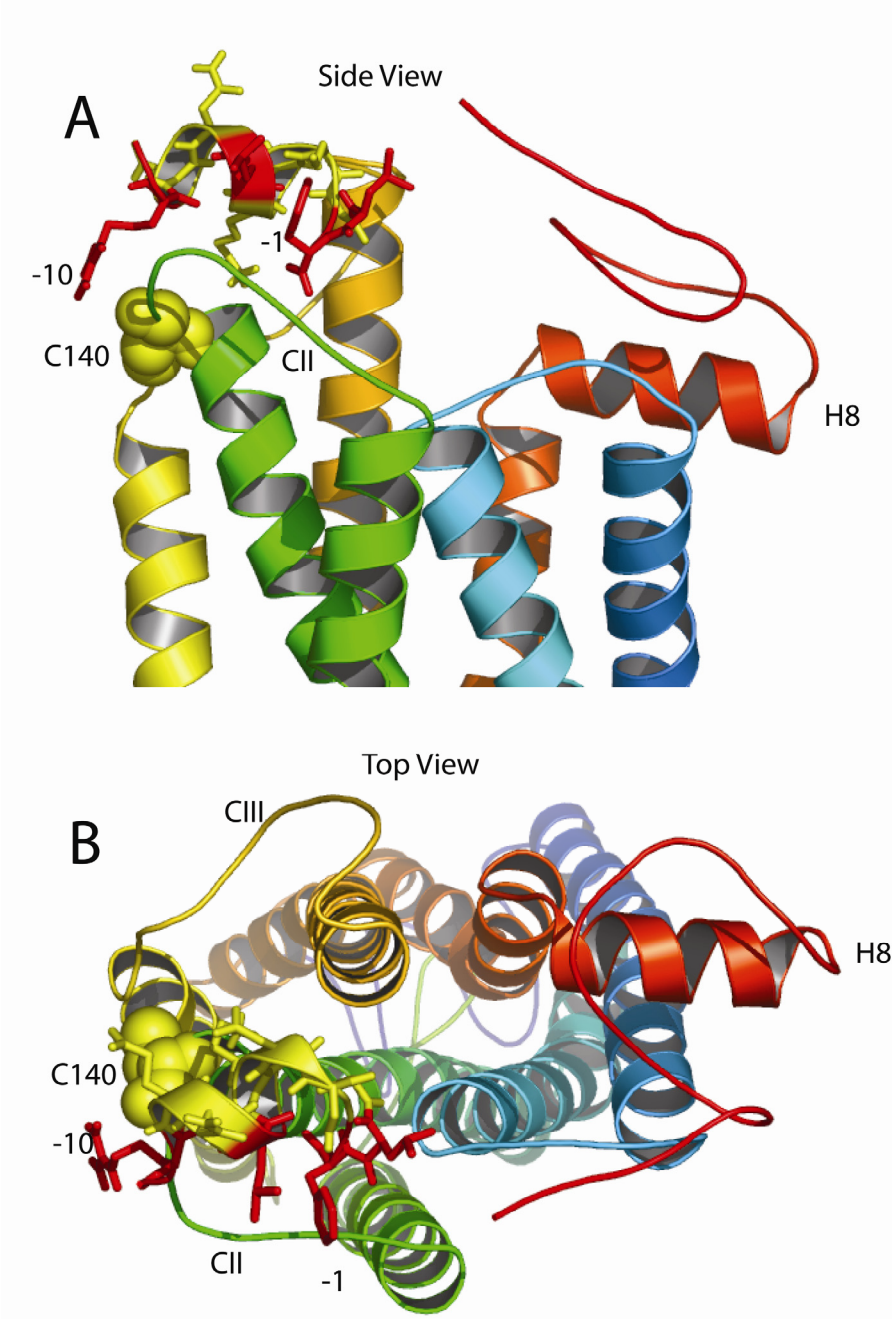


Figure 2.6. Rigid body docking of a analog of the c terminal 11 residues of transducin alpha subunit (1LVZ.pdb) onto structure of unactivated rhodopsin (1U19.pdb) employing Cluspro (a web based rigid body docking program). A) A side view of the cytoplasmic surface of rhodopsin is shown and B) a top down view of the cytoplasmic face is shown with the peptide docked near residue C140 at the top of helix 3. The hydrophilic]C-terminal residues -1F,-2L,-7L,-10R,-11I are colored red and the residues -3G,-4S,-5D,-6K,-8N,-9E of the c terminal peptide are colored yellow. The hydrophobic surface of the peptide is facing the receptor which is consistent with the notion of the peptide interacting with a hydrophobic surface that is exposed when metarhodopsin II is formed.

heterotrimeric G-protein shows greater affinity for metarhodopsin II than the native C-terminal tail peptide which has a reported EC50 value of ~1.2 mM [112]. For low affinity peptides the dissociation constant (Kd) is approximately the same as the EC50, given that at the EC50 very little peptide is bound by activated rhodopsin.

A model of rhodopsin interacting with the C-terminal tail of transducin is presented in Figure 2.6. The C-terminal tail of the alpha subunit of transducin forms an amphipathic helix. We docked the NMR structure of the C-terminal tail of the alpha subunit of transducin [109] to dark adapted rhodopsin, illustrating how the hydrophobic face of the peptide might bind to a complementary hydrophobic face on metarhodopsin II, favoring the formation of the metarhodopsin II-peptide complex. The model presented in Figure 2.6 is consistent with chemical crosslinking data further discussed in chapter 4. Interestingly, residues at positions -2,-7, and -10 in the peptide, that have been found to modulate affinity are found on the hydrophobic face of the peptide, which is likely to be in contact with the surface of the receptor, as shown in our docking results.

Of the peptides studied, the relative potency of peptide AcVLEDLRSCGLF is greater than that of AcVLEDLRSAbuGLF, where these two peptides differ only with respect to at the -4 position. Substitution of a -CH3 group for the –SH of cysteine when the residue at the -4 position is changed from cysteine to aminobutyric acid reveals that increasing the hydrophobicity of the peptide results increases affinity. The potency of the peptide in its ability to bind to metarhodopsin II decreased with decreasing hydrophobicity at -4 where peptide activity of valine> methionine> cysteine> serine [112, 118]. Consistent with the findings of Aris et al., we find that replacing the cysteine

at the -4 position with aminobutyric acid leads to an increase in the Kd or a decrease in the net strength of the interaction between metarhodopsin II and the peptide.

At elevated temperatures the binding constant increases, indicating a tighter binding and this has been interpreted as indicating that the interaction between metarhodopsin II and transducin is dominated by hydrophobic interactions [100]. The presence of leucine residues at the -2 and -7 position of the C-terminal peptide has been implicated as being part of a hydrophobic patch of residues that become ordered upon interaction with metarhodopsin-II [138]. Leucine or closely related residues at the -2 and - 7 position are highly conserved in G-protein alpha subunits in mammals (table 2.2) and are required for effective G-protein receptor coupling, indicating that a highly conserved feature of G-protein coupling to receptor is likely a hydrophobic interaction [114]. Transducin has been reported to couple to a sub-species of metarhodopsin I, metarhodopsin Ib. The role of both leucines at the -2 and -7 positions was investigated

Alpha subunit	Amino acid sequence
	-11 -10 -9 -8 -7 -6 -5 -4 -3 -2 -1
α_t	I K E **N L** K D C G **L** F
α_{i1}	I K N **N L** K D C G **L** F
α_{i2}	I K N **N L** K D C G **L** F
α_{i3}	I A N **N L** K E C G **L** F
α_{o1}	I A N **N L** R G C G **L** Y
α_{o2}	I A K **N L** R G C G **L** Y
α_z	I Q N **N L** K Y I G **L** C
$\alpha_{q,11}$	L Q L **N L** K E Y N **L** V
A_{12}	L Q E **N L** K D I M **L** Q
consensus	**h x x N L + x x x L x**

Table 2.2. Gα C-terminal tail sequences

and it was shown that leucine -2 played a more dominant role in coupling leading to MIb stabilization than leucine -7 [132].

Changing lysine at the -10 position to leucine in peptide analogs leads to a large increase in the affinity of the peptide for metarhodopsin-II [112]. With the exception of changing the residue at the -10 position to aspartic acid, the changing of lysine at position -10 showed a clear trend that increasing the hydrophobicity of the residue leads to a decreased EC50 value of the peptide for binding to metarhodopsin II [144]. Interestingly, we have found that chemical crosslinking of a truncated version of a C-terminal tail analog of transducin, leading the last two residues is capable of stabilizing metarhodopsin II when it is crosslinked to cysteine C140 through modification of the amino terminal residue of peptide VLEDLRD(Abu)G. This observation, along with the reported effect of changing the leucine at the -2 position to alanine leading to a great reduction in the MIb and MII stabilization [132], suggests that the role of the C-terminal residues is one of increasing the affinity of the peptide through primarily a hydrophobic interaction, and it is required for the effective formation of metarhodopsin II transducin complex. However, the last two residues are not absolutely required for metarhodopsin II stabilization upon peptide interaction.

The relative low affinity of the native C-terminal tail sequence is possibly due in part to the fact that there are likely to be several points of interaction between metarhodopsin II and the intact heterotrimeric G-protein, as indicated by studies that have shown that both the alpha and gamma C-terminal tails are capable of stabilizing metarhodopsin II [143]. However, it is unclear how both the C-terminal tail of the alpha

and gamma subunit could interact at the same time given that the footprint of the heterotrimeric G-protein is larger than the surface of monomeric rhodopsin.

Rhodopsin functioning as a single photon detector requires an efficient mechanism for signal amplification. Rapid amplification of GTP exchange following excitation by very low numbers of photons has perhaps developed at the expense of high affinity binding to the heterotrimeric G-protein transducin. The balance between specificity and sensitivity is exemplified by the photo-transduction system. The observed low affinities of the C-terminal peptides of the alpha and gamma subunits of transducin is thought to be due to a required rapid turnover of the R*-transducin complex necessitating the interaction between these two proteins be relatively low affinity in nature.

Materials and Methods

Rod Outer Segment Preparation

Dark adapted frozen bovine retinas were obtained from Schenk Packing Co. (Stanwood, WA). Retinas were initially suspended in ice cold buffer A (0.05 M monobasic potassium phosphate, 0.015 M dibasic potassium phosphate, 1 mM $Mg(OAc)_2$, 1 mM DTT, 0.1 mM EDTA, pH 7.0, sparged with argon, 45% w/v sucrose) resulting in a final sucrose concentration greater than 30%. ROS were sheared from the retinas by vigorous mechanical shaking [145]. Briefly, the shaken retinas were centrifuged in a Sorval HB-4 swinging bucket rotor at 7,000 RPM for 10 minutes, pelleting large pieces of intact retina and leaving ROS in the supernatant. The supernatant was then poured into a 200 ml graduated cylinder through a gauze lined funnel and diluted 2x with cold buffer A without sucrose, resulting in a sucrose

concentration less than 15% allowing for the pelleting of the rod outer segments. The diluted supernatant was then poured into 4 Oakridge tubes and centrifuged at 11,000 RPM for 30 minutes, pelleting the crude ROS. Further enrichment of the ROS was achieved by isolation on discontinuous sucrose gradients (27.0%, 28.7%, 34.0%, and 38.0%). Crude ROS is diluted v/v with buffer A containing 27% sucrose and layered on the top of the discontinuous sucrose gradient and was spun for 45 minutes at 13,000 RPM in the Sorval HB-4 rotor. The ROS will localize at between the 27.0% and 28.7% region in the sucrose gradient. ROS isolated from the discontinuous sucrose gradient were stored in liquid nitrogen until use. The purity of the rod outer segments was determined by measuring the ratio of total protein absorbing at 280 nm to photo activatable rhodopsin at 500nm. Rhodopsin concentrations were calculated from the difference spectrum (unbleached-bleached) at 500 nm (Δ500) in the presence of 3% lauryldimethylamine-oxide (LDAO), using a molar extinction coefficient of 40,600 M^{-1} cm^{-1}. A typical $OD_{280}/\Delta 500$ ratio for the rod outer segments was approximately 2. All manipulations of retinas, rod outer segments (ROS), and rhodopsin were carried out under dim red light, unless otherwise indicated.

Peptide Synthesis

Synthetic peptides were prepared using a Rainin Protein Technologies PS3 peptide synthesizer and standard Fmoc chemistry on PEG resin (Advanced Chemtech). All peptides were deprotected and cleaved from the PEG resin by incubation in a cleavage cocktail containing 90% TFA, 5% thioanisole, 5% ethandithiol for 2 hours at room temperature. Cleaved peptide was precipitated by addition of 25 fold excess ethyl

ether. The precipitant was pelleted by centrifugation and excess ethyl ether was decanted. Synthetic peptides were purified by RP-HPLC, dryed and stored for short term at -20˚ C. Purified peptide masses and sequences were confirmed by MALDI-TOF mass spectrometry (Bruker Biflex III) using α-Cyano-4-hydroxy-cinnamic acid (Bruker part no. 201344). Stock solutions of the peptides were prepared by dissolving the peptide in buffer B (50 mM HEPES, 100 mM NaCl, 1 mM $MgCl_2$) at pH 8, immediately prior to use.

Light Titration Experiments

Rhodopsin rod outer segment membranes to be used in light titration experiments were suspended in buffer B and the final pH adjusted to pH 8.0. For each light titration experiment, an aliquot of rhodopsin (3-5 uM) was bleached by a series of millisecond flashes with orange light from a xenon flash lamp filtered through an OG515 long pass filter at 50 second intervals, and absorbance changes were measured during each interval. Stock solutions of synthetic Gαt peptides were made by dissolving peptide in buffer B and then added to assay solutions resulting in a final concentration of 5-8 uM. Each flash bleached ~8% of the rhodopsin. The appearance of metarhodopsin-II was detected by monitoring the difference in absorbance between 390 nm and 417 nm (390-417) [100] , using an Olis/Shimadzu UV-3000 dual wavelength spectrophotometer, equipped with a temperature controlled cuvette holder. Typically 20 flash intervals were monitored for each light titration experiment. All light titration experiments were performed at 4 ˚C and the sample compartment was purged with dry nitrogen gas.

Equilibrium Binding and Kinetic Analysis
of Synthetic Gαt C-terminal Tail Analogs

Determination of the equilibrium binding parameters was accomplished employing the Pascal program SimplexC obtained from Parkes and Liebman [100]. The change in absorbance following light excitation and sample equilibration was measured from the light titration data for each flash. These change in absorbance at 390-417 nm after the system reached equilibrium following photolysis was averaged over a ten second interval and these values where used as the input to the fitting program SimplexC. The observed kinetic rates for formation of metarhodopsin II-peptide complex for the second flash interval after any residual G-protein had reacted were determined employing Global Works (OLIS).

CHAPTER 3

MASS SPECTROMETRIC ANAYLSIS OF G-PROTEIN COUPLED RECEPTORS RHODOPSIN AND CCR5

Introduction

Mass spectrometry of biomolecules advanced greatly as a field in the late 1980's and early 1990's with developments in electrospray ionization (ESI). Electrospray ionization is a soft ionization method, that forms ions in the gas phase without extensive fragmentation, and was referred to as "putting wings on molecular elephants" by developer John Fenn [146]. More recent developments in ESI have allowed for mass spectral analysis of large intact proteins and multi-protein complexes [147]. Developments in ESI and mass analyzers have extended the upper limits of mass analysis to such a extent that intact viruses can be detected, where the upper mass range detected to date is reported to be ~40 Mda (reviewed in [148]).

Electrospray Ionization

Ion formation during ESI consists of three major steps, (1) the creation of an electrically charged spray, (2) reduction of droplet size of the spray by heating, (3) generation of fully desolvated ions. The creation of an electrically charged spray is achieved by spraying ion-containing solutions through an electrically conducting needle held typically at an electric potential of 3-4 kV, with reference to a counter electrode. The droplets containing ions in the liquid exposed to the electric field repel each other

and form a “Taylor cone”. The Taylor cone is formed by the desolvation of ions in droplets and an increase in charge density in the droplets until Coulombic repulsion results in the explosion of droplets and generation of a fine spray largely containing single molecules.

Mass spectrometric studies of integral membrane proteins are often plagued by limited amounts of purified protein, sample losses due to irreversible aggregation during handling (poor solubility), poor recovery of peptides from digests following liquid chromatography ,ionization suppression, and analyte adduct formation due to the presence of strong acids and detergents needed to solubilize the intact proteins and digested peptides. The presence of detergents is typically required for the solubilization and purification of membrane proteins, but most detergents interfere with obtaining adequate MS signals. In addition to troublesome detergent mass adduct formation, when sufficient removal of detergent has not been achieved, ionization suppression due to the matrix effects of detergent molecules may result poor mass spectra [149]. Thus detergents must be removed or the concentration greatly reduced to allow the interpretation of mass spectra of membrane protein samples.

Analysis of chemically and proteolytically cleaved rhodopsin fragments by mass spectrometry has fostered the development of methods to analyze integral membrane proteins and has allowed for the determination and characterization of several post translational modifications present on rhodopsin. The molecular weight of intact rhodopsin and proteolytically cleaved rhodopsin was detected at low resolution by matrix assisted laser desorption-time of flight (MALDI-TOF) [150]. The location of the fatty acid moieties on the carboxyl terminal tail of rhodopsin was confirmed by MS analysis

[150]. A comparison of a synthetic peptide and the rhodopsin-derived C-terminal tail peptide was required to interpret the MS and tandem MS/MS mass spectral data at the time [151]. Phosphorylation of rhodopsin by rhodopsin kinase as a means of receptor attenuation following photoactivation was investigated by initially digesting the intact photo-excited rhodopsin with protease Asp-N, isolating the C-terminal peptide fragment by HPLC, and then analyzing the resultant peptide by ESI in a triple quadropole mass spectrometer [152]. Papac et al., further analyzed this showing MS/MS sequencing of the C-terminal tail using a four sector machine to reveal a phosphorserine residue [153]. The nature of the heterogeneity of the two glycosylated asparagines was observed by Barnidge et al., [154] in MALDI-TOF mass spectrometric analysis of tryptic fragments of the C-terminal tail of rhodopsin.

The coupling of proteolysis and mass spectral analysis of peptide fragments is a powerful technique that has fostered more detailed characterization of rhodopsin. Following cleavage of rhodopsin with trypsin, fractionation by HPLC in octylglucoside, and subsequent analysis by MALDI-TOF mass spectrometry, Barnidge et al. were able to detect five rhodopsin fragments comprising 54% of the amino acid sequence of rhodopsin [154]. Many of the detected fragments included transmembrane spanning regions, thus this method represented an advance in techniques, since one of the major limitations of the application of HPLC and mass spectrometry to membrane proteins is poor recovery of hydrophobic peptides. Full sequence coverage of the CNBr fragments of rhodopsin was later reported by Ball et al., in an ESI LC/MS method [155]. Detection by MALDI-TOF of all of the peptide fragments derived from cyanogen bromide cleavage of rhodopsin was reported Kraft et al., [156]. The method reported by Kraft et al.,

represented an advance in technique, since it required only a few picomoles of peptide mixture spotted on the MALDI target, compared to several thousand picomoles of rhodopsin digest initially loaded onto C18 columns prior to analysis by ESI-MS in the method developed by Ball et al., [155]. Analysis of rhodopsin fragments by MADLI-TOF mass spectrometry has the potential for high mass accuracy and increased sensitivity; however detection by HPLC-ESI methods has proven to be a more robust approach. Improvements in mass spectrometry technology have led to LC-ESI method being more versatile and effective, if not as sensitive as MALDI-TOF.

The detection of all of the digest fragments of rhodopsin by LC-MS/MS was accomplished employing a strategy where cyanogen bromide-digested rhodopsin was separated by liquid chromatography and detected by ESI in an ion trap [155]. Advances in instrumentation have reduced the required amount of sample from several thousand picomoles [157] to subpicomol quantities [158]. Studies investigating the potential sites of interaction between the heterotrimeric G-protein and rhodopsin used the previously developed mass spectrometric methods [115, 116]. Rhodopsin was used as a model system to develop methods for generating structural constraints for membrane proteins employing mass spectrometry and chemical crosslinking [159]. The proximity of neighboring regions on rhodopsin have been examined by application of heterobifunctional crosslinking reagents to specific residues on rhodopsin, followed by the measuring of the amounts and location of intramolecular crosslinks formed by FT-ICR MS [159].

An important impact of mass spectrometric studies of rhodopsin has been the development of methods that are applicable to other integral membrane proteins where

sample quantities are limited. Bovine rhodopsin has served as a model system for developing mass spectrometry methods for integral membrane proteins, due to the relative ease in which large amounts of protein can be obtained from bovine retina, approximately 0.3-0.5 mg per retina.

Mass spectrometric analysis of integral membrane proteins has been demonstrated for several proteins. Mass spectral characterization and topology modeling of the glycine receptor has been achieved after applying limited proteolysis and ESI LC/MS characterization of the putative loop region that extends into the aqueous medium outside the membrane domain of this ligand-gated anion channel [160, 161]. Detection of the peptides of the complete amino acid sequence of the integral membrane protein aquaporin O was reported employing both MALDI-TOF and capillary liquid chromatography coupled to tandem mass spectrometry [162]. Glycosylation sites and amino acid polymorphisms were characterized in the integral membrane protein cytochrome b employing both MALDI-TOF and nanospray MS/MS analysis of purified cytochrome isolated from human neutrophils [163]. The success of the previous studies is in part due to advances in mass spectrometric technology and method development largely utilizing bovine rhodopsin as a model integral membrane protein, as explained below.

Currently we are investigating the interactions between metarhodopsin-II and the heterotrimeric G-protein alpha subunit C-terminal tail, employing chemical and photo crosslinking experimental approaches. The Gαt C-terminal tail interactions with rhodopsin stabilize the active conformation of the receptor, metarhodopsin-II. We have detected metarhodopsin II stabilization following chemical crosslinking of peptide

analogs of the C-terminal tail of the alpha subunit of transducin to light-excited rhodopsin [104]. Peptide chemically crosslinked to rhodopsin was detected both by MALDI-TOF mass spectrometric studies of intact rhodopsin and ESI-LC/MS TOF of cyanogen bromide digested rhodopsin peptides discussed in greater detail in chapter 4. Additionally, the related GPCRs, CCR5 and CXCR4, both coreceptors required for HIV infection, are currently under investigation with attempts to localize the sites of photocrosslinked agonist and antagonist compounds employing mass spectrometry are ongoing. Critical to the success of these studies is the development of methods for the mass spectral analysis of the peptides derived from these integral membrane proteins. Here we present the comparative analysis of bovine rhodopsin CNBr digests on four different mass spectrometers a Bruker Esquire 3000 ion trap, an Agilent XCT nanospray ion trap, (with and without Chip LC), a Bruker microTOF which couples ESI to a time of flight mass detector and a Bruker FT-ICR MS. Optimization of detection methods employing rhodopsin as a model system has been performed and these efforts have fostered greatly improved detection of the related and medically important CCR5.

Results and Discussion

Cyanogen bromide (CNBr) digestion functions under strong acid conditions, where even the most stubborn protein is effectively denatured and solubilized. Cleavage of most membrane proteins is achieved employing CNBr. The CNBr cleavage reactions of rhodopsin and CCR5 take place in high concentrations (70%) of trifluoroacetic acid (TFA), with 30% water being essential to complete the cleavage reaction. CNBr digestion cleaves at the C- terminus of methionine residues leaving either a homoserine

or homoserine lactone. Peptides containing these residues are detected with a mass loss of 30 Daltons or 48 Daltons, respectively from the theoretical masses of the methionine-containing peptide (Figure 3.1).

There are 16 methionine residues in the amino acid sequence of rhodopsin, resulting in seventeen theoretical digest products. The average and monoisotopic masses of the CNBr produced peptides are shown in the "snake" diagram of rhodopsin in Figure 3.2 and listed in table 3.1. Following cleavage of rhodopsin by CNBr the sample is freeze dried several times to remove excess CNBr and TFA. Preparation of sample for HPLC MS analysis requires the initial solubilization of peptides with neat TFA or formic

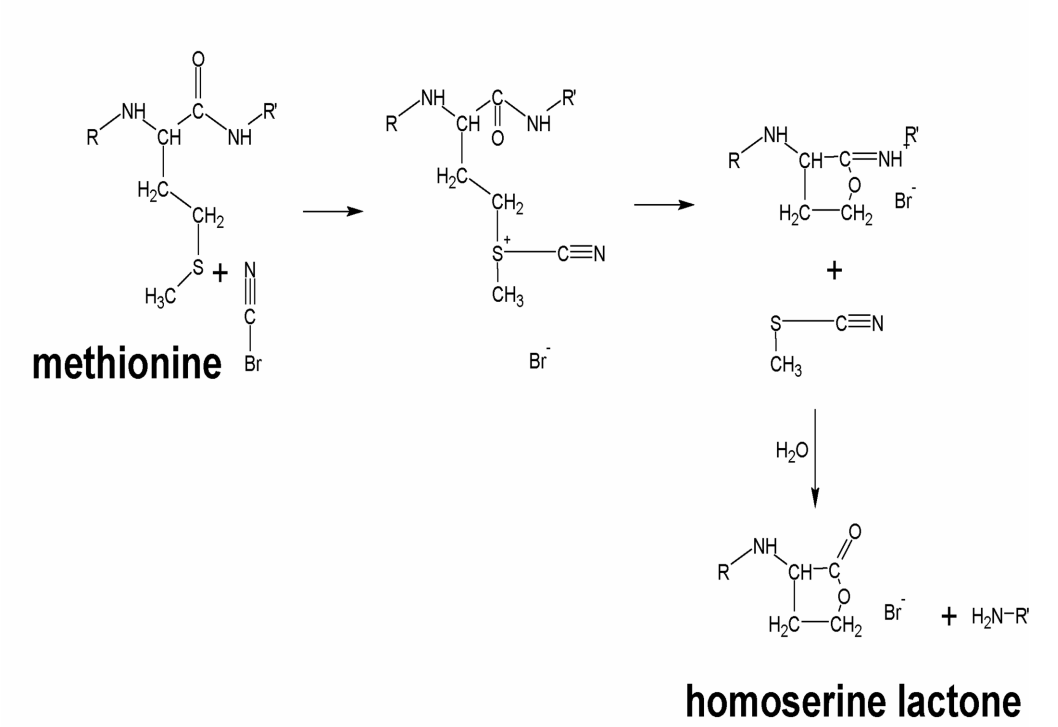


Figure 3.1. Chemical cleavage at methionine residues. Reaction of cyanogen bromide with methonine residues.

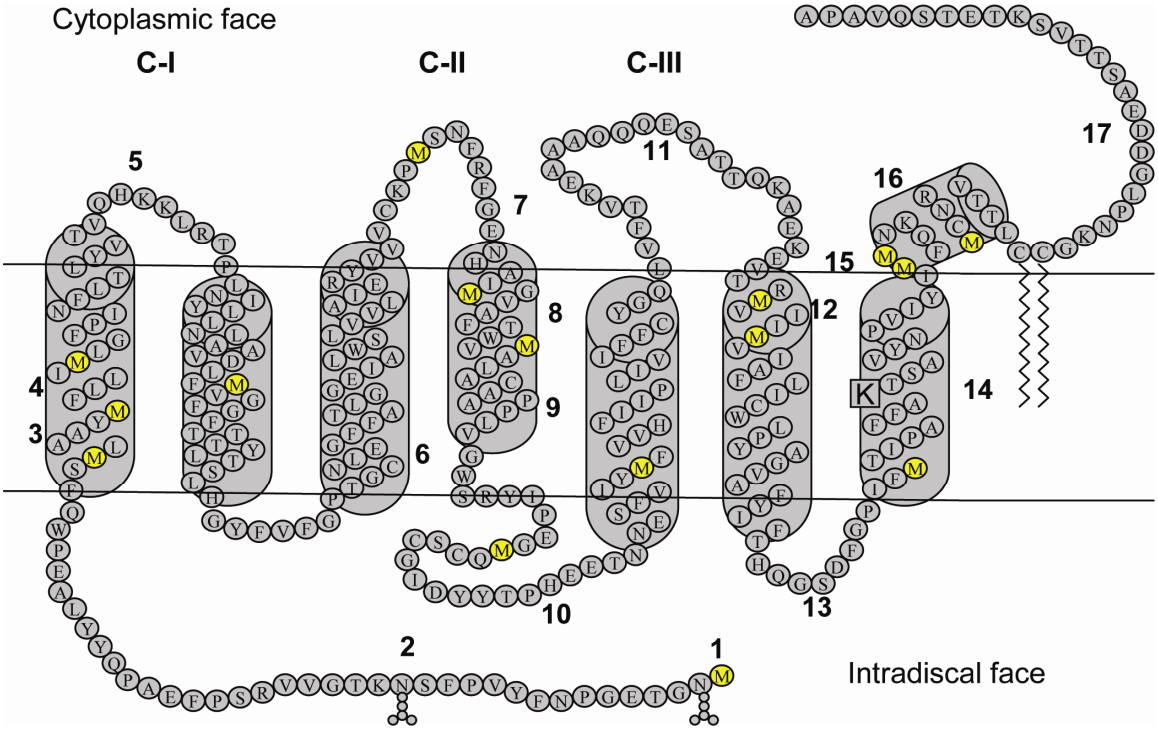


Figure 3.2. Snake diagram of bovine rhodopsin. Methionine residues are colored yellow. Peptide fragments generated by CNBr digest of rhodopsin are numbered and this numbering system will be used throughout the text.

acid. The presence of some acids such as TFA leads to ion suppression [164]. TFA has been shown to greatly reduce the ionization of basic analytes [165]. There is a trade off between effective recovery and solubilization of sample and a subsequent reduction inionization. Recently neat formic acid has been used in the initial sample preparation and in HPLC solvents, leading to improved detection without any noticeable problems such as formylation of serines and threonines in the peptide samples.

Following CNBr digest of rhodopsin, the cleavage of the amino terminal methionine and after residue 309 results in single homoserines or homoserine lactones which are not detected by our mass spectrometric methods. The remaining 15 fragments can be detected with different efficiencies, depending on reverse phase column solid

phase, mobile phase, and method of ionization. Ball et al., demonstrated similarities in elution profile when separating peptides on C4, C8, and C18 columns [155]. A draw back of the Ball method was the very large amount of rhodopsin peptides needed for the analysis, which has been improved upon in later work [158].

Mass spectrometric analysis of rhodopsin employing three different mass analyzers was performed. Electrospray ionization coupled to a quadropole ion trap (QIT), time of flight (TOF), or ion resonance cyclotron Fourier transform (ICR-FT) mass analyzers were used to detect rhodopsin digest fragments. For these three mass spectrometers the ionization methods were very similar if not identical, thus the

Fragment number	Monoisotopic mass	Residue number	HPLC index
1	143.0577	1	
2	6497.8374	2-39[a]	11
3	520.2771	40-44	6
4	588.3761	45-49	8
5	4241.4259	50-86	14
6	6353.2692	87-143	15
7	1374.6555	144-155	5
8	862.4463	156-163	7
9	2159.1112	164-183	9
10	3005.2762	184-207	2
11	5315.8335	208-253	12
12	427.2920	254-257	3
13	3580.8172	258-288	13
14	2198.1902	289-308	10
15	101.04762	309	
16	1097.5315	310-317	1
17	3598.9341	318-348[b]	4

Table 3.1. Theoretical cyanogen bromide digest products.
[a] mass for major glycoform.
[b] dominant detected mass contains 2 fatty acid modifications.

differences in the signal were partially due to differences in the chromatography, but mainly due to differences in the mass analyzers.

The resolution of the three different mass analyzers varied greatly. Resolution is defined as m/Δm, where m is an observed mass and Δm is the resolvable mass difference between two adjacent masses typically measured from the mid line of the full width at half maximum peak height. Increased resolution allows for improved mass accuracy. The monoisotopic distribution of ions becomes observable at higher resolution, the charge state of a ion can be accurately determined and the mass deconvolution of several charge states becomes possible as the resolution increases above where isotopic resolution is apparent. The Esquire 3000 has a relatively low resolution of around 1000, the microTOF has a reported resolution of 10,000, and in theory the ICR-FT has a resolution of several hundred thousand. Ion cyclotron resonance Fourier Transform (ICR) FT mass spectrometers have the highest mass accuracy or capability. However, these instruments are very expensive, hard to run, and require dedicated personel to maintain. Time of Flight mass spectrometers have the advantage that these instruments offer a very robust technology in practice, allowing for use with minimal training and relatively minimal maintenance. The mass accuracy and sensitivity of ESI-TOF is less than the FTMS, however, the ease of use provides an important practical benefit.

Analysis of rhodopsin with the microTOF and the HPLC separation of all of the peptide fragments were optimized to the extent that we have successfully detected all of the peptide fragments following cyanogen bromide digestion. Table 3.2 shows the masses detected and mass errors associated with a typical peptide mass detection when the rhodopsin CNBr digest is analyzed on the Bruker microTOF. The base peak

chromatogram of a typical LC/MS analysis of rhodopsin and by the microTOF is shown in Figure 3.3. In this analysis of a CNBr-digested rhodopsin sample, approximately 150 picomoles (pmoles) of total digest product were loaded onto a 20 x 2.0 mm mercuryMS LC/MS cartridge containing 5µ Luna C18(2) solid phase. The peptide fragments were initially solubilized in 10 µl formic acid, 10 µl isopropanol, and 80 µl nanopure water then separated by reverse phase HPLC and introduced into the mass spectrometer at a flow rate of 200 µl/minute, using a linear gradient of 100% isopropanol with 0.5% formic acid starting 2 minutes after injection over 22 minutes. 17 fragments of rhodopsin were detected and the mass error ranged from ~40 to 2 parts per million (ppm) with an average of error of 17.3 ppm. Generally the larger the fragment, the greater the observed mass error. The average resolution obtained was 3600, which provides good resolution of the isotope peaks for most of the peptides of rhodopsin (an example of this monoisotopic resolution can be seen in Figure 3.6C).

Multiple peaks for fragments 5, 9, 10, 14, and 17 were routinely detected in the HPLC chromatogram, which was not expected. It is possible that the peptides are associated with other rhodopsin peptide fragments during the HPLC separation and this association leads to the formation of two populations observed as two or more peaks. Alternatively, the peptides may be separated into two populations based on a conformational equilibrium that is slow over the HPLC separation time. Fragment 17 contains cysteine 322 and 323 that are both modified with the palmitoyl moieties and elutes consistently in two peaks. The difference in mobility in the two fragment 17 peaks (17A and 17B) of the C-terminal tail of rhodopsin is not due to differences in detectable

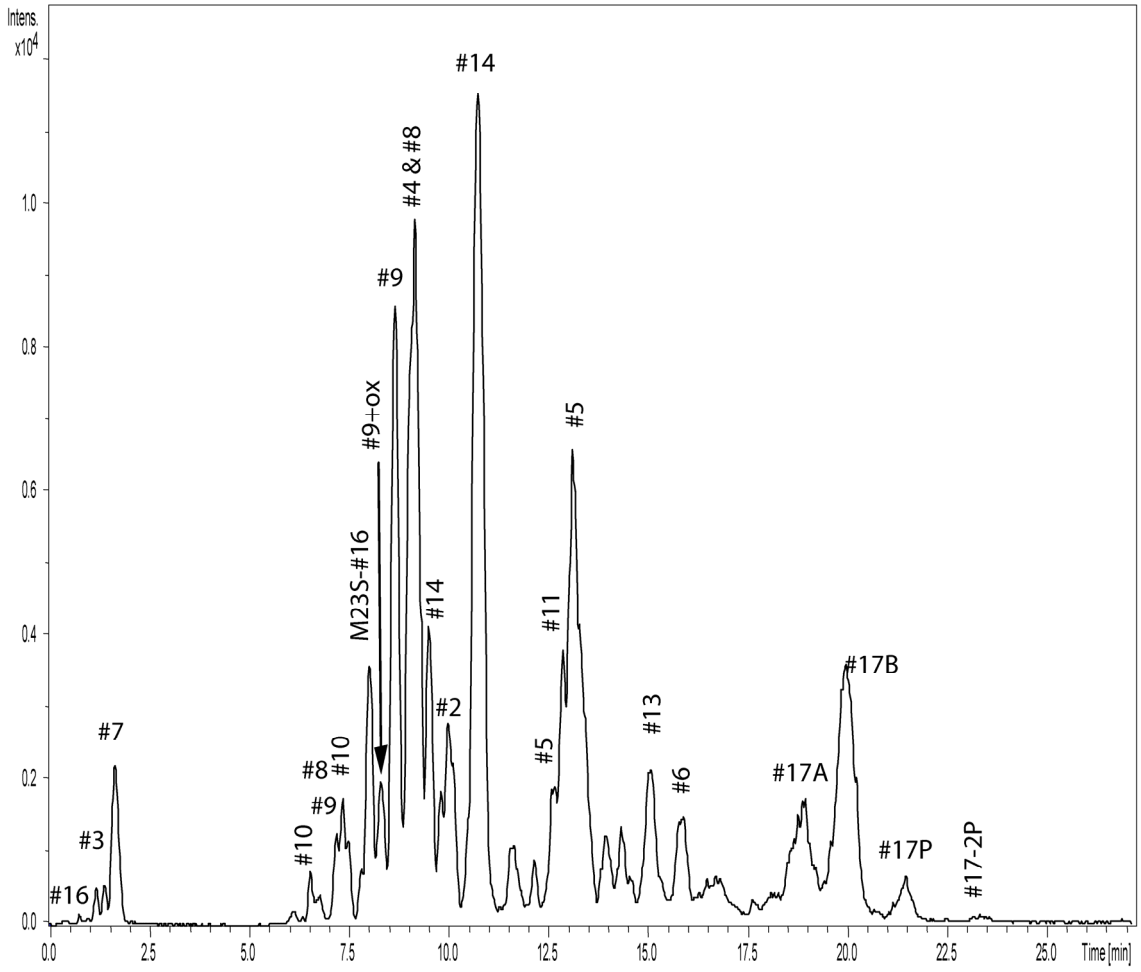


Figure 3.3. Base peak chromatogram of bovine rhodopsin CNBr digest analyzed on the microTOF. Approximately 150 pmoles of rhodopsin CNBr peptide digest was analyzed, resulting in the detection of 15 of the 17 digest fragments. Additionally oxidation products of peptide fragment #9 were detected as well as the singly and doubly phosphorylated C-terminal tail fragment #17.

post-translational modifications, as the masses for the peptides observed for each peak are the same. There is not a significant abundance of any detectable peptide co-eluting with the C-terminal peptides for either fragment 17 peak which might have been interacting with the peptide to increase or decrease mobility in the HPLC.

Fragment number	Monoisotopic Mass	Residue number	Theoretical masses for detected charge state	Observed masses error (ppm)
1	ND	1		ND
2	6497.8374	2-39	1625.209	1625.2608 (31.7)
3	520.2771	40-44	520.2771	520.2771
4	588.3761	45-49	588.3761	588.3748 (2.2)
5	4241.4259	50-86	1061.106	1061.1263 (18.7)
6	6353.2692	87-143	1589.067	1589.0458 (13.5)
7	1374.6555	144-155	1374.6555	1374.6396 (11.5)
8	862.4463	156-163	862.4463	862.444 (2.7)
9	2159.1112	164-183	1080.056	1080.0519 (3.4)
10	3005.2762	184-207	1503.138	1503.1819 (29.1)
11	5315.8335	208-253	1329.708	1329.7303 (16.5)
12	427.2920	254-257	ND	ND
13	3580.8172	258-288	1194.2724	1194.3115 (32)
14	2198.1902	289-308	1099.595	1099.5883 (6.2)
15	ND	309	ND	ND
16	1097.5315	310-317	1097.5315	1097.4878 (39.8)
17	3598.9341	318-348	1200.31136	1200.6731 (18)

Table 3.2. LC/MS analysis of rhodopsin fragments on a Bruker microTOF

Thus we have come to the tentative conclusion that the multiple peaks for fragment 17 are due to a slow conformational equilibrium that affects the net mobility of the fragment 17 peptide resulting in two peaks. Co-elution of fragments 4 and 8 and near co-elution of fragments 5 and 11 appears to be due to their similar hydrophobicity as indicated in the theoretical HPLC index (table 3.1). The HPLC index represents a theoretical retention profile for peptide fragments analyzed by LC-MS and was calculated employinG-protein prospector [166]. The method developed for the HPLC separation of rhodopsin allows for the separation of a peptide containing the oxidation product of tryptophan leading to a second slower eluting peak in the base peak chromatogram of fragment 9 as seen in Figure 3.3.

Mass fingerprinting for the identification of unknown proteins is possible when high mass accuracy is achieved using bioinformatics tools such as the Matrix Science

search tool Mascot. The lower abundance ions in the mass spectrum were examined in an attempt to determine if peptides from rhodopsin or other proteins could be co-eluting with the C-terminal tail peptide 17, leading to the observed change in elution time and the presence of two peaks in the base peak chromatogram. A total of nine masses are detectable in the mass spectrum of the first peak containing the C-terminal tail of rhodopsin (#17A, Figure 3.3) which is a quite complex looking peak with many shoulders. We searched the mass spectrometry protein sequence data base (MSDB) using Matrix Science Mascot, searching all known mammals, since the bovine genome is not complete We only accepted possible peptide identification if the mass error was 50 ppm or less, resulting in the tentative assignment of three of the 9 peptides. The top assignment was a peptide from bovine latrophilin-2, this is a G-protein coupled receptor found in the brain, lung and liver. Notably, the peptides identified for this GPCR due not share similarity in sequence to bovine rhodopsin [167]. Upon close inspection of peak 17B, (Figure 3.3) there are 7 masses present that cannot be assigned to rhodopsin and when searching with Mascot are not attributed to bovine.

Activation of rhodopsin by light excitation is followed by phosphorylation on the carboxyl terminal tail by a G-protein receptor kinase GRK1 [55]. The phosphorylation reduces the affinity of the heterotrimeric G-protein for metarhodopsin II and leads to an increased affinity of visual arrestin followed by the quenching of the G-protein signal amplification. Digest fragments showing the presence of 1 and 2 phosphorylations by characteristic 80 Dalton mass increases are shown in Figure 3.3 and Figure 3.4 fragment with #17-P and fragment #17-2P eluting after fragment 17. The presence of

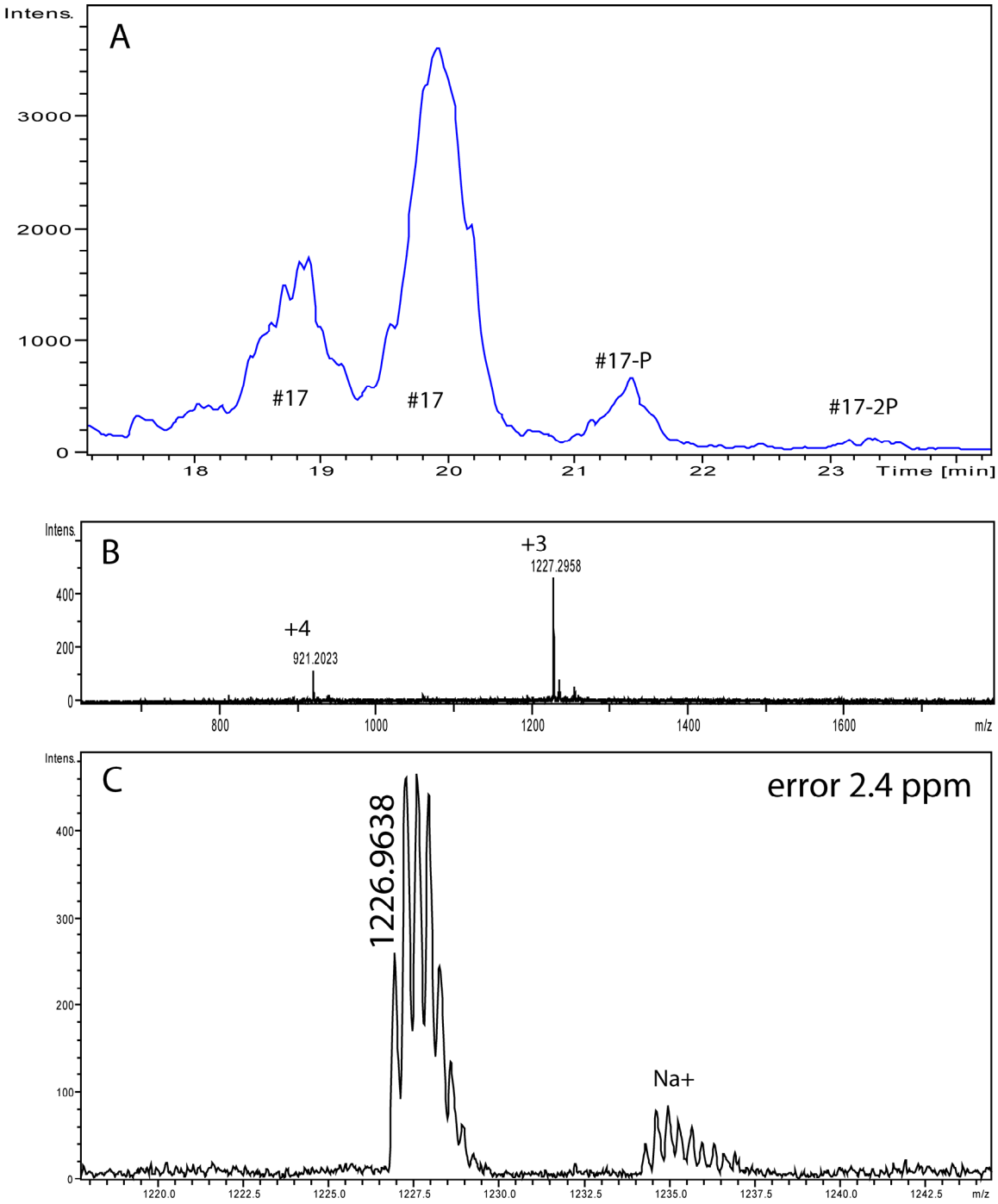


Figure 3.4. Detection of the phosphorylated c terminal tail of rhodopsin. A) Base peak chromatogram of fragment #17 which is the carboxyl most fragment containing two cysteines that are each modified with a palmitoyl fatty acid anchoring helix 8 to the lipid bilayer. B) Shown is an averaged mass spectra for the peak labeled #17-P, a mono phosphorylated c terminal tail of rhodopsin. C) An expanded view of the plus 3 ion together with the sodiated form of the peptide shown in panel B.

masses consistent with the phosphorylation of the C-terminal tail of rhodopsin eluting after the non phosphorylated fragment was initially surprising. Phosphorylation increases the hydrophilicity of a peptide however this has previously been shown in some cases to result in reduced retention of peptides in reverse phase HPLC seperation and in some data presented increased retention in reverse phase chromatography of rhodopsin [152].

In studies on mouse S opsin and bovine rhodopsin, peptides derived from the C-terminal tail following endoproteinase Asp-N digest of intact receptor resulted in peptide fragments that eluted earlier than the unphosphorylated C-terminal tail [168]. Phosphorylation of different serine residues on the C-terminal tail of rhodopsin causes different shifts in mobility as was shown by Lee et al., since phosphorylation at S338 causes earlier elution than phosphorylation at S343 [169]. Elution order of peptides following phosphorylation is affected by intrinsic peptide properties, solvent pH, and perhaps other detailed properties of the HPLC solvents.

G-protein coupled receptors are typically glycosylated on the amino terminal region and asparagine residues at positions 2 and 15 are N- glycosylated in rhodopsin. The dominant composition of each sugar moiety is 3 N-acetylglucosamine sugars (each 203.0794 Da) and 3 hexose sugars (each 162.0528 Da). The glycosylated amino terminal fragment #2, elutes from the HPLC column at approximately 48% B and appears quite heterogeneous in composition (Figure 3.5). The dominant charge state for this fragment observed is the plus four. Masses consistent with 2 glycosyl chains with 3 GlcNAC and 3 hexose each and the addition of up to four additional hexose sugars are detected.

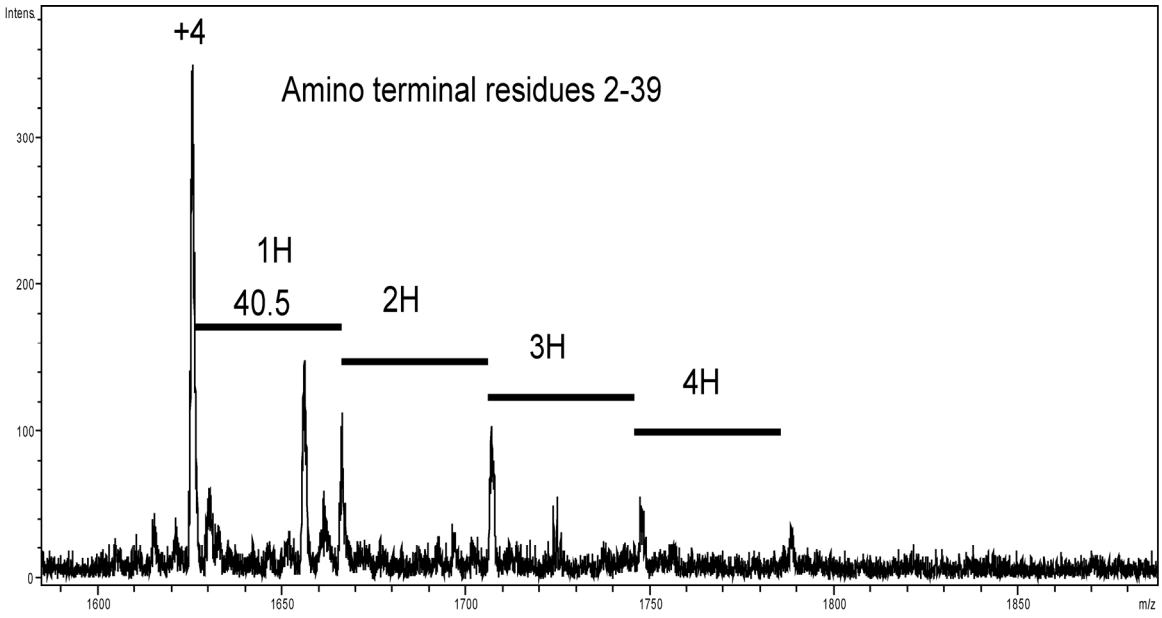


Figure 3.5. Glycosylated amino terminal fragment of rhodopsin detected on the microTOF. Several glycoforms co-elute with the amino terminal fragment of rhodopsin are. The dominant glycosylation detected is the addition of 3 GlcNAc and 3 hexose sugars on two residues. Peptides with up to 4 additional hexose sugars are detected and labeled 1H to 4H above.

Electrospray ionization often results in the generation of multiply charged ions. During the desolvation of the ion-containing droplets positive charges are greatly concentrated in the droplet. Under the ionization and detection conditions reported here many charge states are typically detected for the larger rhodopsin fragments. The maximum entropy deconvolution routine in the data analysis software package from Bruker was used to deconvolute the masses of individual rhodopsin peptides where several charge states were apparent in the mass spectra and the resulting calculated neutrally charged parent ion spectra show improved signal to noise and multiple isotope peaks, shown in Figure 3.6. Fragment 6 of rhodopsin is the largest fragment generated when cleaved by cyanogen bromide, the +4, +5, +6, +7, and +8 charge states are shown in Figure 3.6 panel A and the deconvoluted spectrum is shown in panel B.

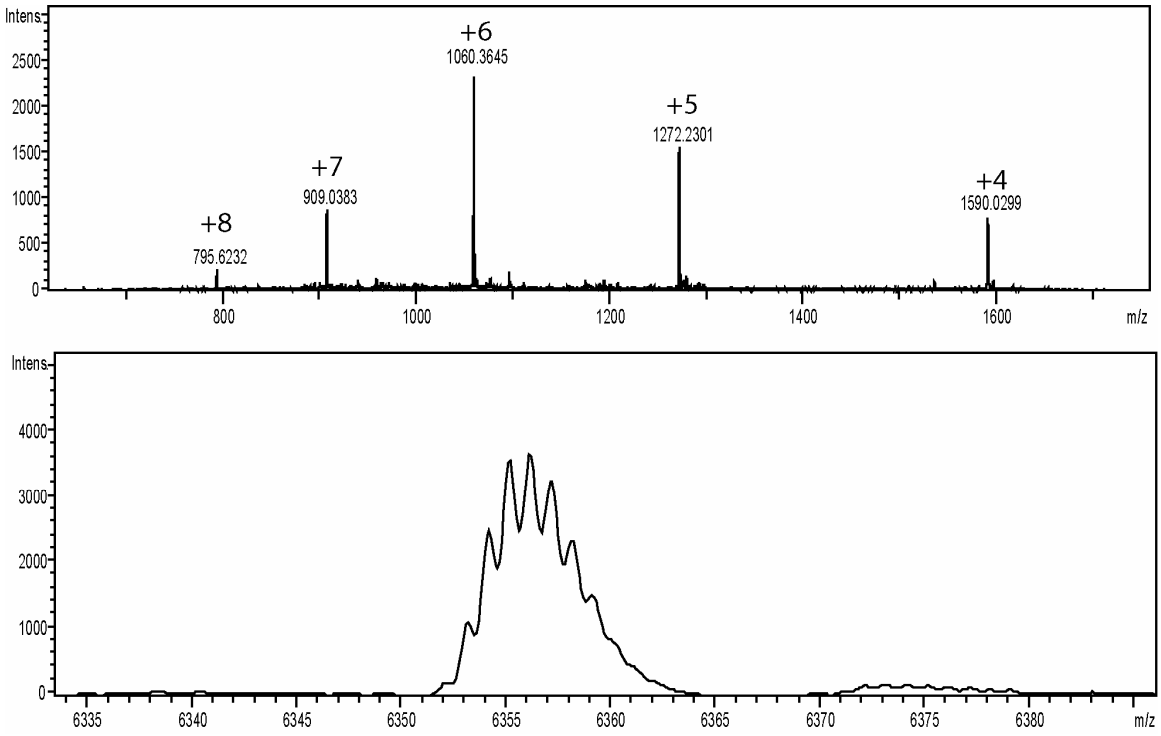


Figure 3.6. Maximum entropy deconvolution of the charge states shown in panel A, these are derived from fragment 6, the largest CNBr fragment yielded from a CNBr digest of rhodopsin.

Analysis of rhodopsin digest was also carried out on a similar instrument to the Bruker microTOF, a Bruker FT -ICR MS. Approximately 10 to 15 pmoles of total rhodopsin digest product was injected and analyzed on the ICR-FT resulting in very large signals as compared to 150 pmoles injected on the microTOF. The base peak chromatogram for the data acquired on the FTMS is shown in the top most panel of Figure 3.7 with the extracted ion chromatograms for the resultant 15 CNBr fragments shown below. The comparable base peak chromatogram and extracted ion chromatograms for analysis of rhodopsin on the microTOF are presented in Figure 3.8. The signal to noise on the FTMS appears much better and the sensitivity of the FTMS instrument is at least 10

times better. However, with our optimized method on the microTOF we are able to detect and interpret more features in the mass spectral signal from rhodopsin as compared to analysis of rhodopsin CNBr peptide digest on the FTMS. A comparison between the signals in the microTOF for a single time point for several peaks is shown in Figure 3.9. At first glance it appears that the microTOF performs better than the FTMS instrument. This is not supported by the deconvoluted spectra presented in Figures 3.10 and 3.11. When comparing the deconvoluted signal from the microTOF in Figure3.10 to similar data from the FTMS in Figure 3.11 it appears that the microTOF has similar resolution compared to the FTMS. The development of methods for the mass spectrometric analysis of rhodopsin on the microTOF resulting in comparable results to FTMS analysis is a significant step forward for achieving our research goals. The FTMS instrument at Sandia National Laboratories has added functionality, peptides of interest can be exhaustively fragmented and sequences as has been demonstrated by Novak et al., [170]. Samples of interest can be prescreened in house on the microTOF to asses their merits and if they look very promising these same samples can be sent to these collaborating facilities for FTMS/MS analysis.

We have analyzed rhodopsin digests on two different ion traps, the Bruker Esquire 3000 and the Agilent XCT ultra II with chip HPLC nanospray. These instruments are low resolution, but have the capacity to perform MS/MS experiments. MS/MS experiments involve initial detection of a mass of interest in the ion trap, typically an abundant ion at any given time, this is then called the parent ion. Following the initial detection of a mass of interest (the parent ion) a narrow mass range including the parent ion is isolated in the ion trap, then the ions are excited enough to increase the

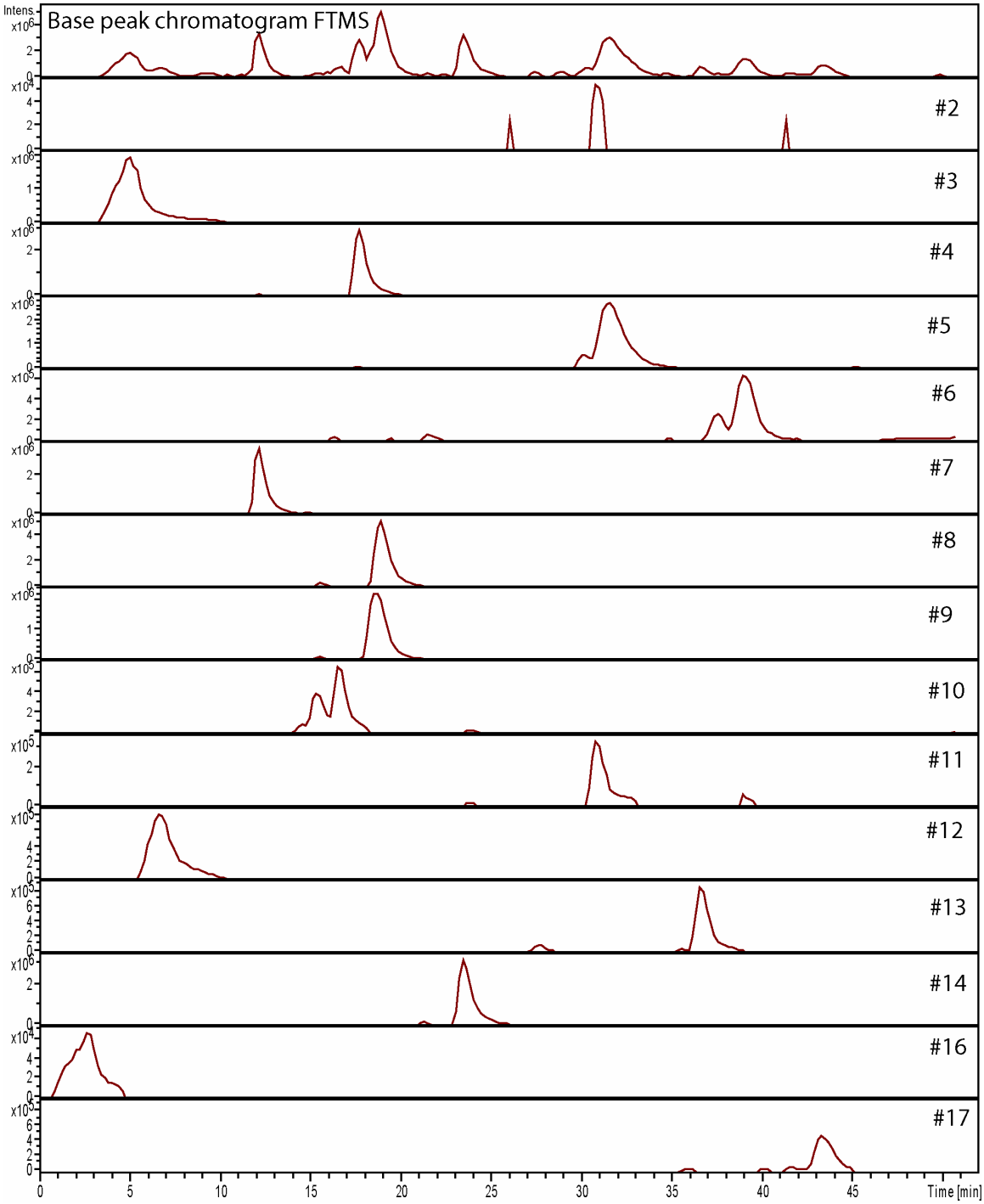


Figure 3.7. Base peak chromatogram of rhodopsin CNBr digest is shown in the top most panel and extracted ion chromatograms for fragments 2 through 17 are shown below. Rhodopsin fragment numbering is for each extracted ion chromatogram the same as that shown on the snake diagram in Figure 3.1.

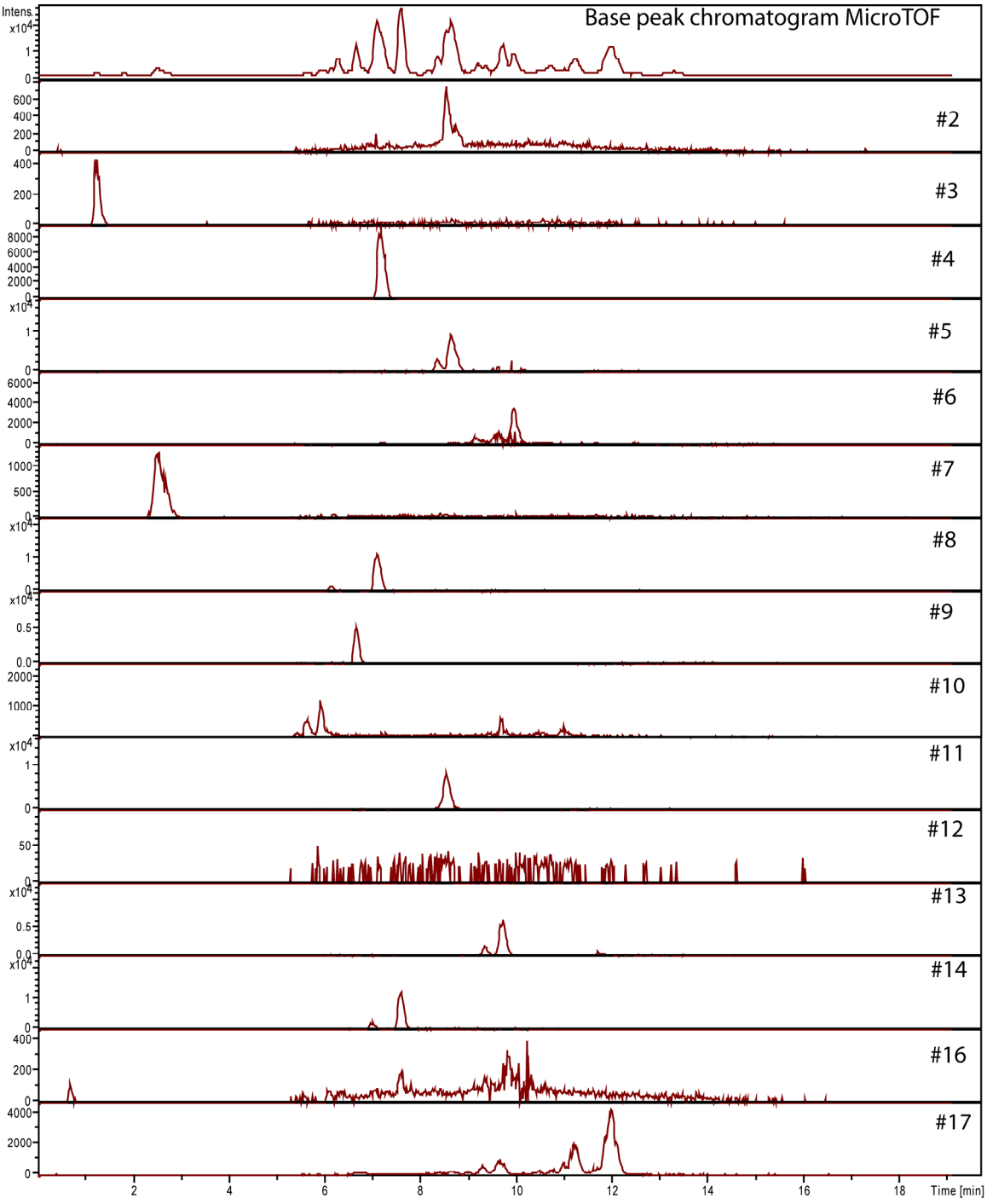


Figure 3.8. Base peak chromatogram of rhodopsin CNBr digest is shown in the top most panel and extracted ion chromatograms for fragments 2 through 17 are shown below. Rhodopsin fragment numbering is for each extracted ion chromatogram the same as that shown on the snake diagram in Figure 3.1

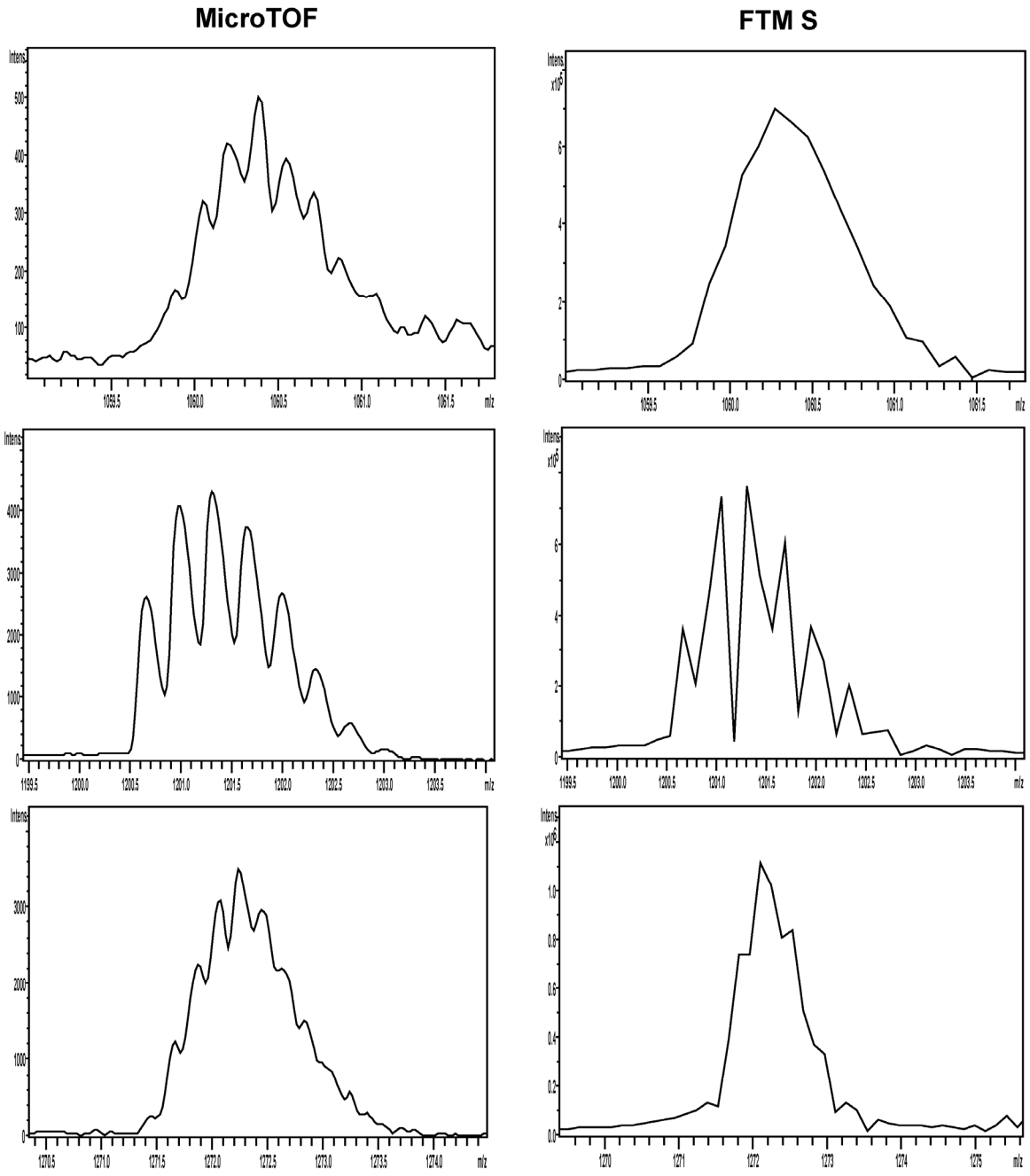


Figure 3.9. Comparison between the observed resolution between the microTOF and the FTMS analysis of CNBr digested rhodopsin. Glycosylated amino terminal tail is not detected on the FTMS and phosphorylated carboxy terminal tail peptides were also not detected. The mass error between the two instruments is comparable and following deconvolution the chromatograms of the ions look comparable.

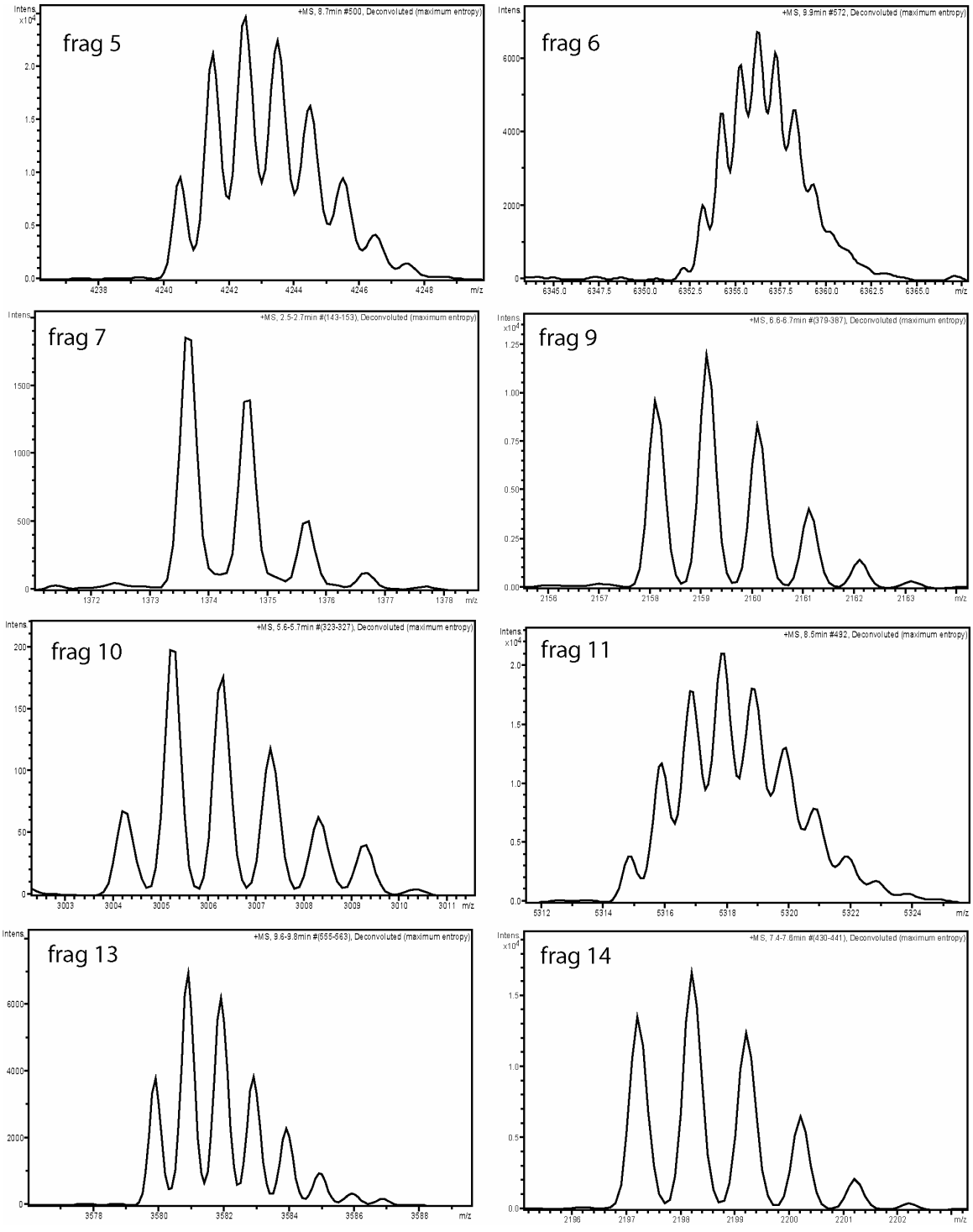


Figure 3.10. Maximum entropy deconvolution of the larger CNBr digest peptide fragments of rhodopsin detected on the microTOF.

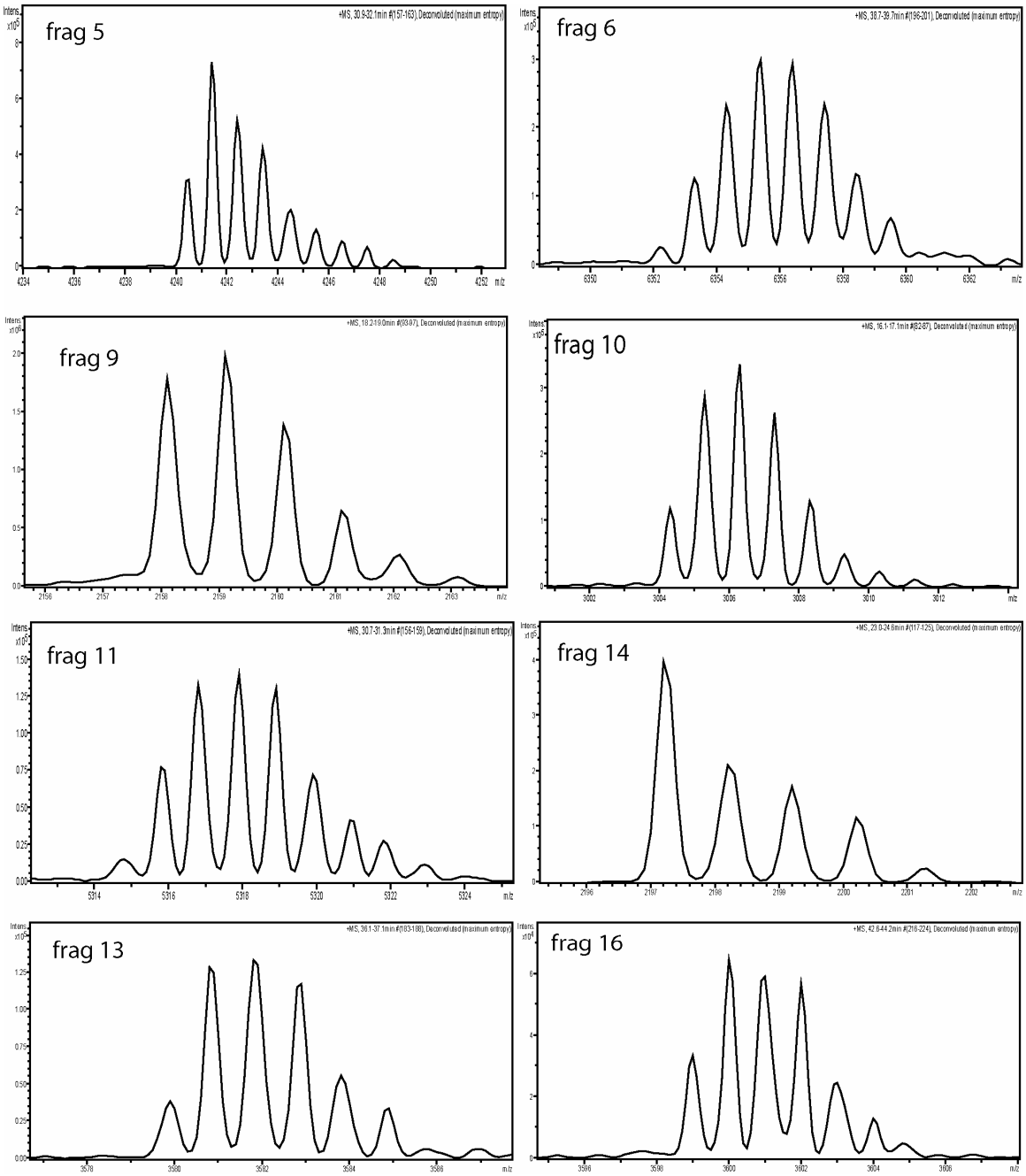


Figure 3.11. Maximum entropy deconvolution of the larger CNBr digest peptide fragments of rhodopsin detected on the FTMS.

rate of collisions between parent ion and a inert collision gas typically helium. The induced collisions cause the parent ion to fragment, and these fragments are detected in subsequent scans of the masses present in the ion trap. The fragments of the parent ions are referred to as the daughter ions. The redundant nature of the MS/MS fragment ladder partially compensates for the lack of high mass accuracy in the ion trap, allowing for determination of peptide sequences derived from a protein of interest. Amino acid sequencing of peptides derived from proteins can be accomplished by MS/MS mass spectrometry, and in favorable cases allow for the determination of the location of a modification, such as the location of a crosslinked ligand or post translational modification on the protein of interest.

The ionization on the esquire 3000 is a very robust configuration and we see no effects on ionization due to different solvents. A typical LC-MS/MS base peak chromatogram is shown in Figure 3.12. Analysis of rhodopsin CNBr digest samples allowed for the detection of 70% of the protein sequence routinely. With the change in chromatographic columns to the short Phenomenex Luna, peptides that can be assigned to the entire sequence of rhodopsin can be detected and MS/MS data provides confirmation for the identity of most of the detected peptide masses. However, the very large CNBr fragments, with m/z greater than a 2000 do not fragment well and thus this instrumental approach is limited.

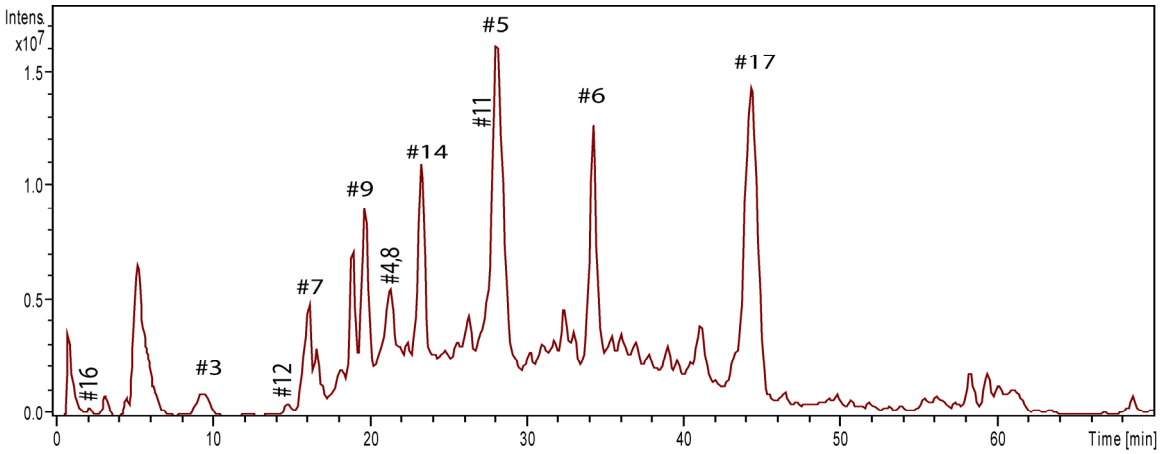


Figure 3.12. Esquire 3000 ESI ion trap analysis of bovine rhodopsin CNBr digest.

The ionization of the rhodopsin peptide digest sample was not as robust for the initial hardware configuration of the Agilent XCT plus, where the spray of analyte was introduced into the mass spectrometer through a fused silica capillary. At high % organic liquid chromatography mobile phases the quality of the spray degraded until there was negligible ion current. The lack of ability to spray and thus ionize analyte at high organic solvent compositions presented a major challenge for the successful detection of hydrophobic fragments of membrane proteins. The Chip LC micro fluidics sample introduction developed by Agilent has led to great improvements in the quality of the spray and the ionization of sample at low and high organic. The Chip LC also provided an increase in sensitivity of the instrument, as well as a much faster MS duty cycle, in comparison to the Esquire, allowing for better MS/MS sequence coverage. A typical HPLC base peak chromatogram for the XCT ultra is shown in Figure 3.13.

The MS/MS of several rhodopsin peptides are shown in Figure 3.14 though 3.16. The ion traps provide a means of determining sequence data that the microTOF is not currently capable of providing. The XCT trap with Chip LC nanopsray is capable of

providing much better MS/MS data then the Esquire 3000 as can be seen when comparing the MS/MS for peptide #7 in Figure 3.14 (esquire data) with 3.15 (XCT ultra data). In the Esquire only 6 daughter ions are detected following fragmentation of the parent ion as compared to 15 daughter ions being detected when a similar sample was analyzed on the XCT ultra II with Chip LC.

Significantly intact rhodopsin was also detected by mass spectrometry on the microTOF, development of quantitative methods for determining the amount of modification pre digestion will facilitate investigation of chemically and photo crosslinked peptides to rhodopsin. Intact rhodopsin can be detected in the microTOF

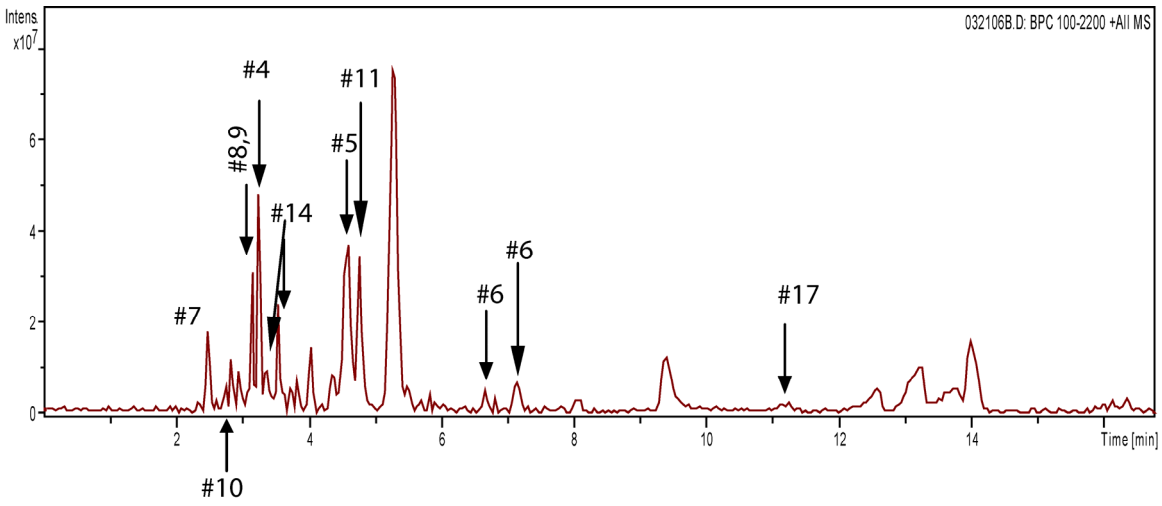


Figure 3.13. Base peak chromatogram of a CNBr digest of bovine rhodopsin separated on the XCT Ultra II with Chip LC front end.

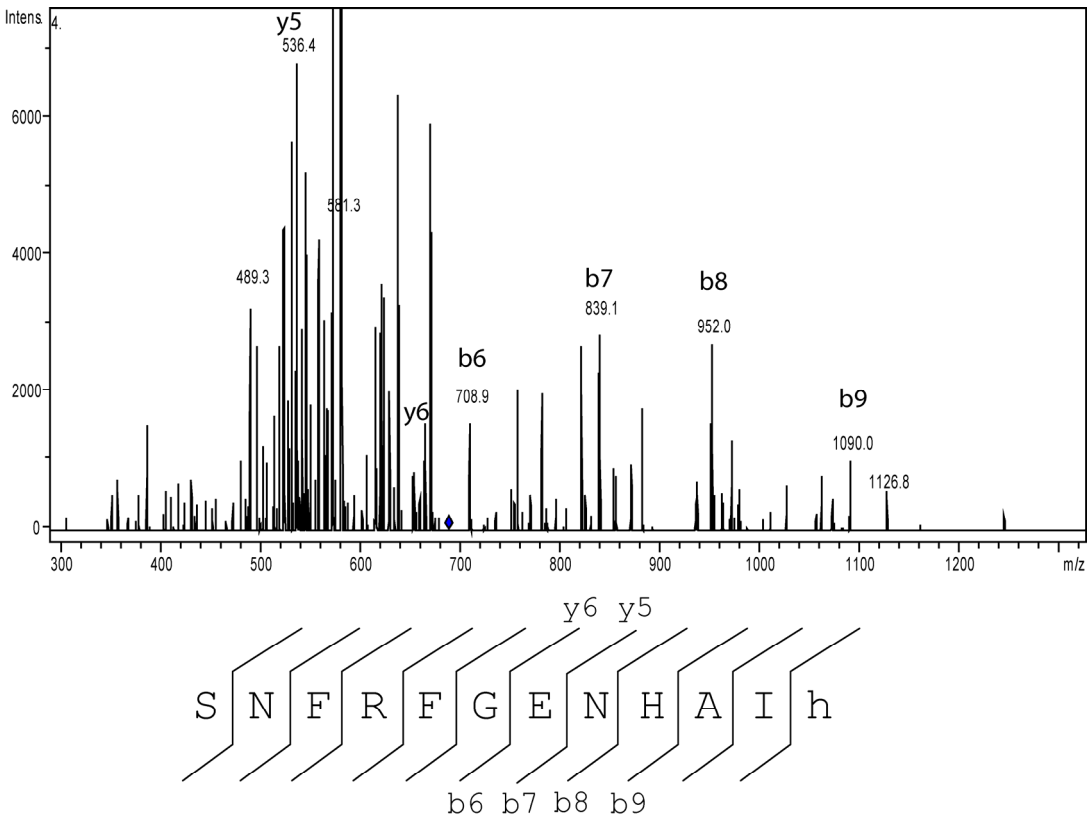


Figure 3.14. MS/MS spectrum of fragment #7 of rhodopsin from analysis with the esquire 3000 QIT.

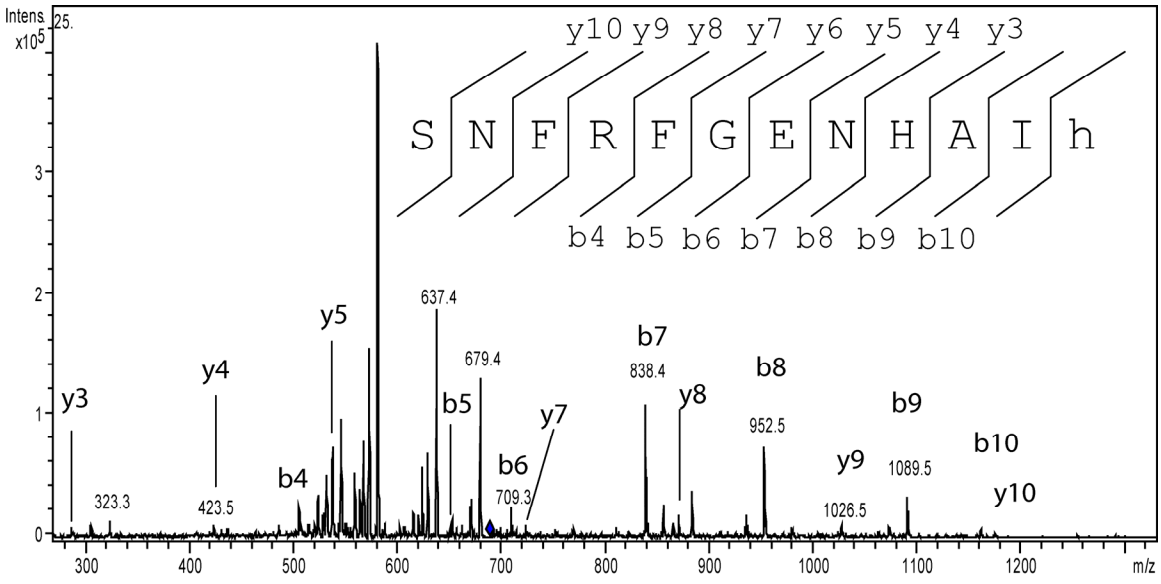


Figure 3.15. MS/MS spectrum of fragment #7 of rhodopsin from analysis with the XCT nanospray.

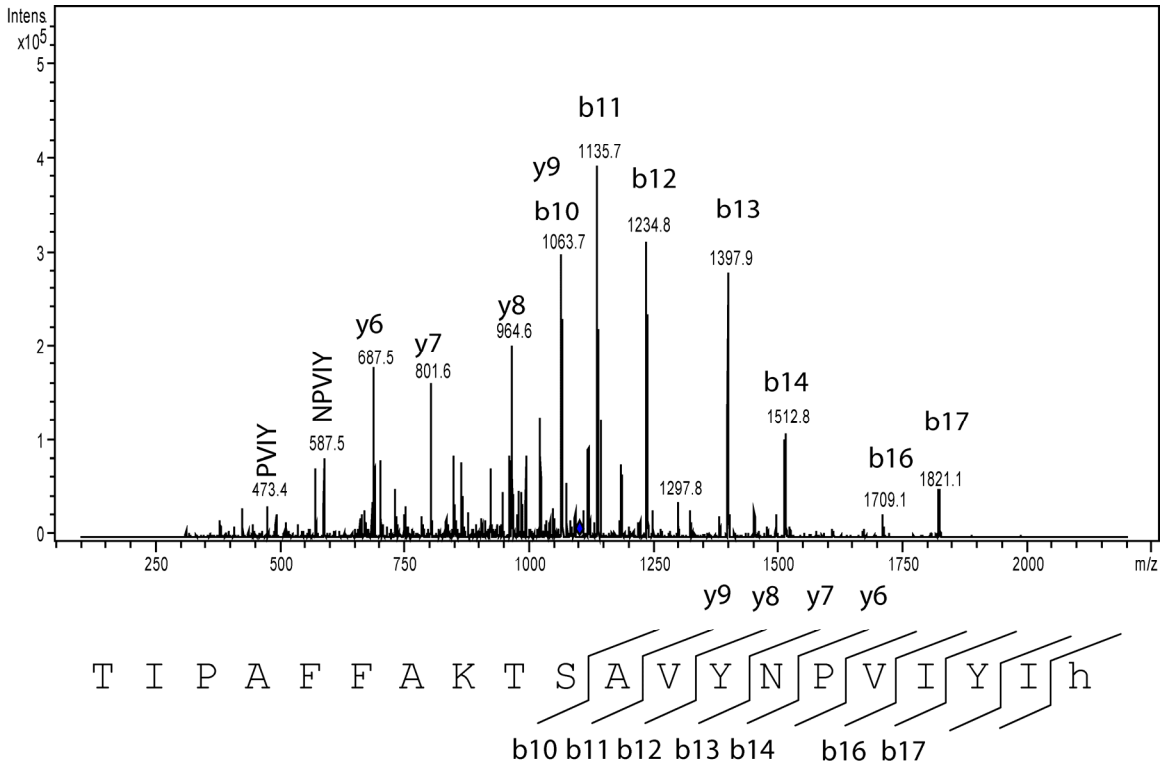


Figure 3.16. MS/MS spectrum of fragment 14 from bovine rhodopsin detected on the XCT ultra II.

prior to reduction and alkylation (Figure 3.16). Deconvolution of the multiply charged species of intact rhodopsin allows for the generation of a calculated neutral charge state spectrum showing the dominant rhodopsin glycoform and additional glycoforms. The resolution is sufficient for the detection of the dominant glycoform with the addition of a sodium adduct (+21).

CCR5 is a member of the rhodopsin family of G-protein coupled receptors and is one of the co-receptors required for HIV infection. CCR5 binds the natural ligands, MIP1α, MIP1β, and RANTES. In addition several small molecule inhibitors have been developed. The successful development of mass spectrometric methods allowing for the

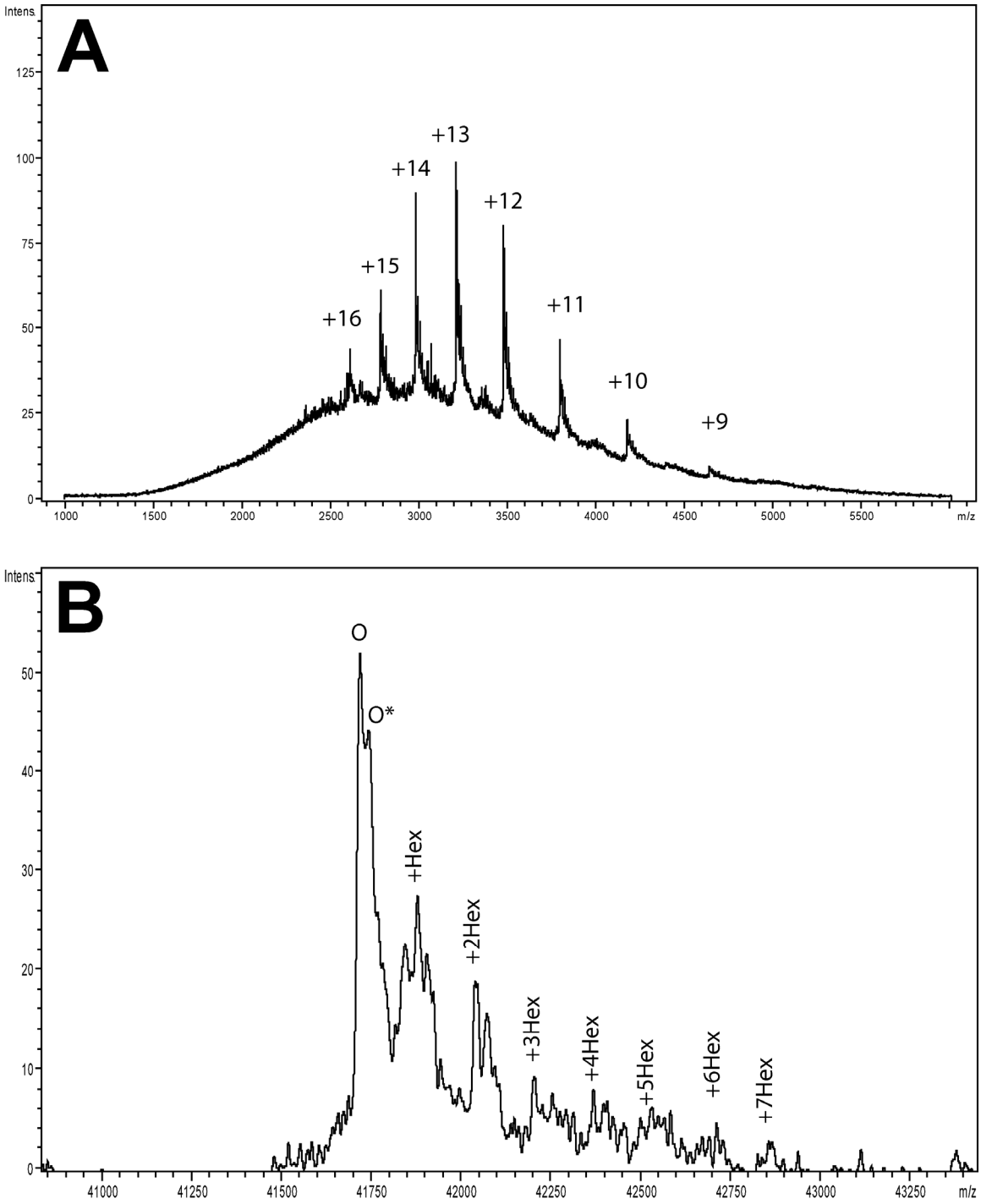


Figure 3.17. Direct infusion of Opsin ESI TOF detection. Panel A is the mass spectrum of intact Opsin ionizing forming many multiply charged ions. B) The deconvoluted mass spectrum with the peak labeled O having a mass consistent with that of opsin with 2 fatty acids and the dominant glycoform, heterogeneity in glycosylation can be detected with masses consistent with the additions of hexose. The resolution is sufficient to detect mass shifts of as little as 23 AMU due to a sodium adduct labeled O*.

detection of the intact CCR5 and the peptide fragments will facilitate studies in identifying the binding sites for these ligands after crosslinking. CCR5 was expressed in canine kidney cells at the National Cell Culture Center, transfected with a codon-optimized CCR5 construct [171]. The construct contained the last nine C-terminal residue epitope of rhodopsin to allow for affinity purification, using a well behaved anti-rhodopsin antibody 1D4 [171]. A "snake" diagram of CCR5 is presented in Figure 3.18.

A 3D model of CCR5 shown in Figure 3.19 is based on a 3D model of CCR5 generated based on the dark adapted rhodopsin crystal structure 1U19 [9] employing the homology modeling program LOOPP [172]. CCR5 is cleaved into only seven fragments by cyanogen bromide, at 6 methionine residues. The theoretical masses are shown in table 3.3.

CCR5 contains several post translational modifications, (1) the receptor is glycosylated on serines at the 6 and 7 position , (2) two tyrosines are sulfonated on the amino terminal [173], and (3) may be modified on the C-terminal tail with up to 3 palmitoyl fatty acids. The post-translational modifications lead to considerable mass heterogeneity, which increases the difficulty of identifying peptides containing modifications in a mass spectrum. The base peak chromatogram for a CNBr digest of CCR5 is shown in Figure 3.20. Five of the seven fragments of CCR5 resulting from CNBr digest were detected by LC-MS analysis in the microTOF. The mass spectra for the detected CNBr fragments of CCR5 are shown in Figure 3.21 . Surprisingly even the largest fragment H containing 110 residues was detected.

Currently we have been able to detect fragments containing helix 2 through 6 and roughly half of helix 1 and 7. Having developed the methods for the detection of the

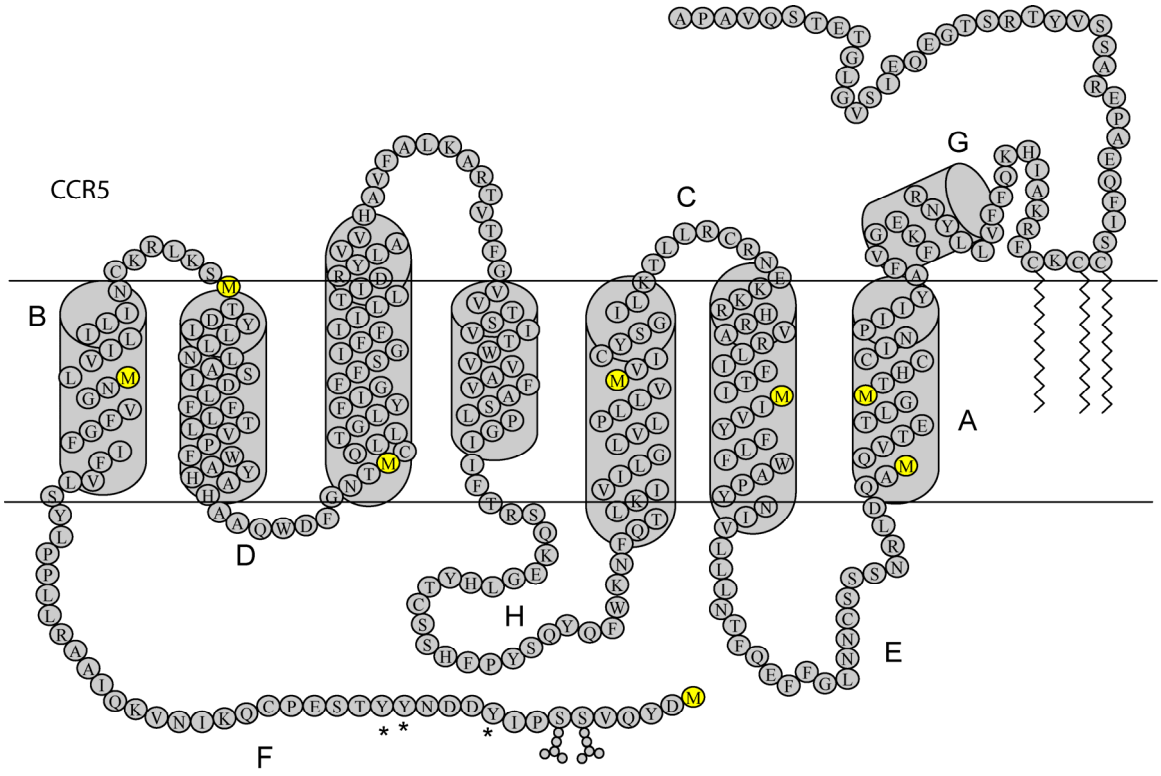


Figure 3.18. Snake diagram of CCR5. A molecular model of CCR5 was generated by threading of the primary amino acid sequence of CCR5 onto the rhodopsin structure 1U19.pdb. Cyanogen bromide cleavage points are colored yellow and the lettering of each digest fragment on the snake diagram is consistent with the lettering in table 3.3.

sequence	Frag.	Mass (M+1)	m/z observed.
280-287	A	830.43	+1
50-64	B	1814.14	+2,+3
211-241	C	3893.25	+3,+4,+5,+6
65-100	D	4130.07	+2,+3,+4
242-279	E	4545.27	+2 through +7
2 49	F	8176.66	ND
288-362	G	8970.49	ND
101-210	H*	12610.93	+5 though +13

Table 3.3 Cyanogen Bromide fragments of CCR5.

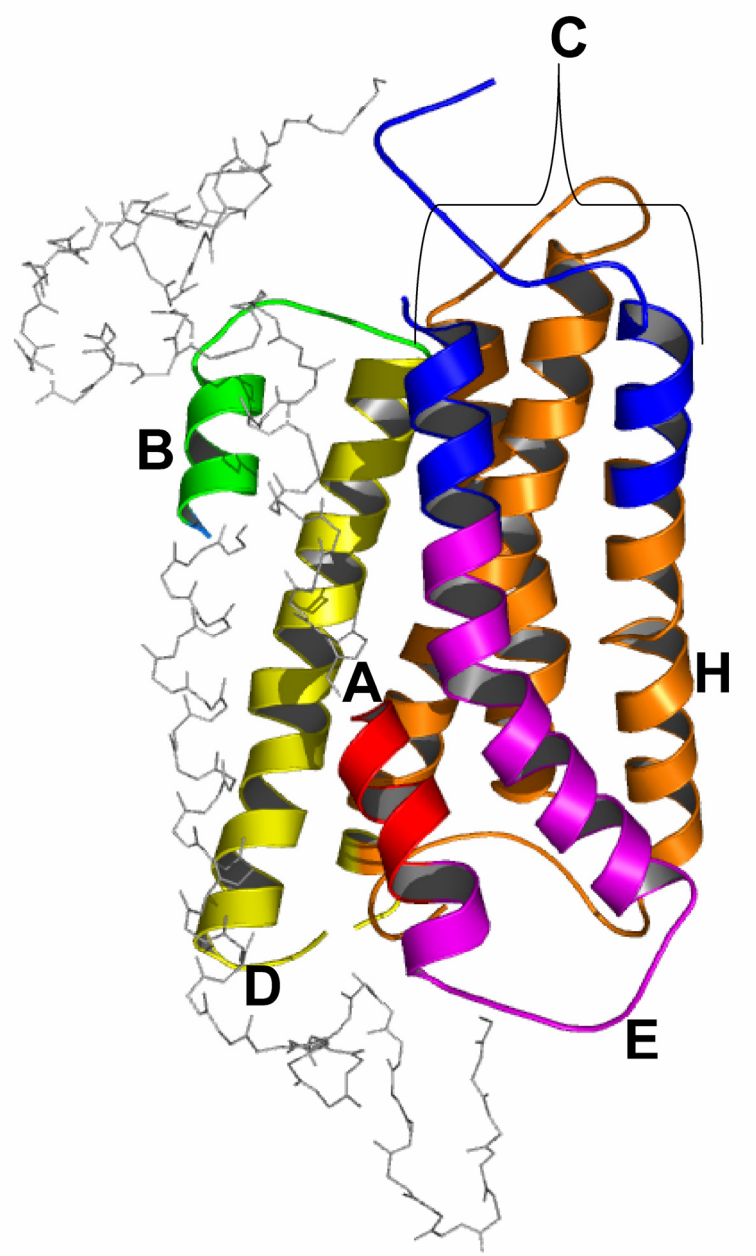


Figure 3.19. Model of CCR5. The fragments detected by mass spectrometric analysis of CNBr digested rhodopsin are labeled and color coded. Fragment A contains residues 280-287 and is colored red, B contains residues 50-64 and is colored green, C contains residues 211-241 and is colored blue, D contains residues 65-100 and is colored yellow, E contains residues 242-279 and is colored pink, and H contains residues 101-210 and is colored orange.

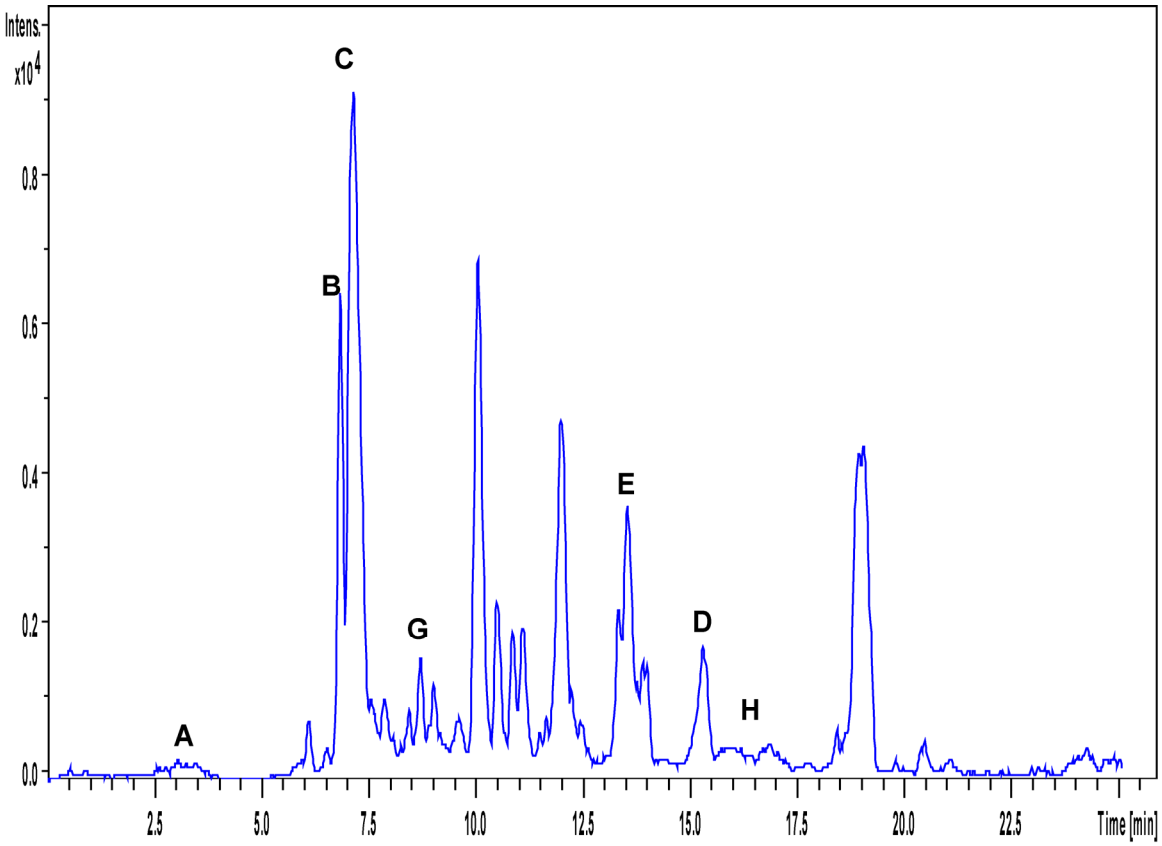


Figure 3.20 Base peak chromatogram of CNBr digest of CCR5.

transmembrane regions of CCR5 makes it more likely that employing these mass spectrometric methods for the detection of the receptor following crosslinking of ligands of interest will result in the identification of ligand binding sites on CCR5.

Employing rhodopsin as a model system for method development of the mass spectrometric analysis of integral membrane proteins has led to significant advances in these analytical techniques. The inherent difficulty in expressing and purifying large quantities of most integral membrane proteins increases the usefulness of a protein like rhodopsin as a pilot test system, given its abundance from a readily available biological source and ease of purification once again illustrating the relevance of utilizing rhodopsin

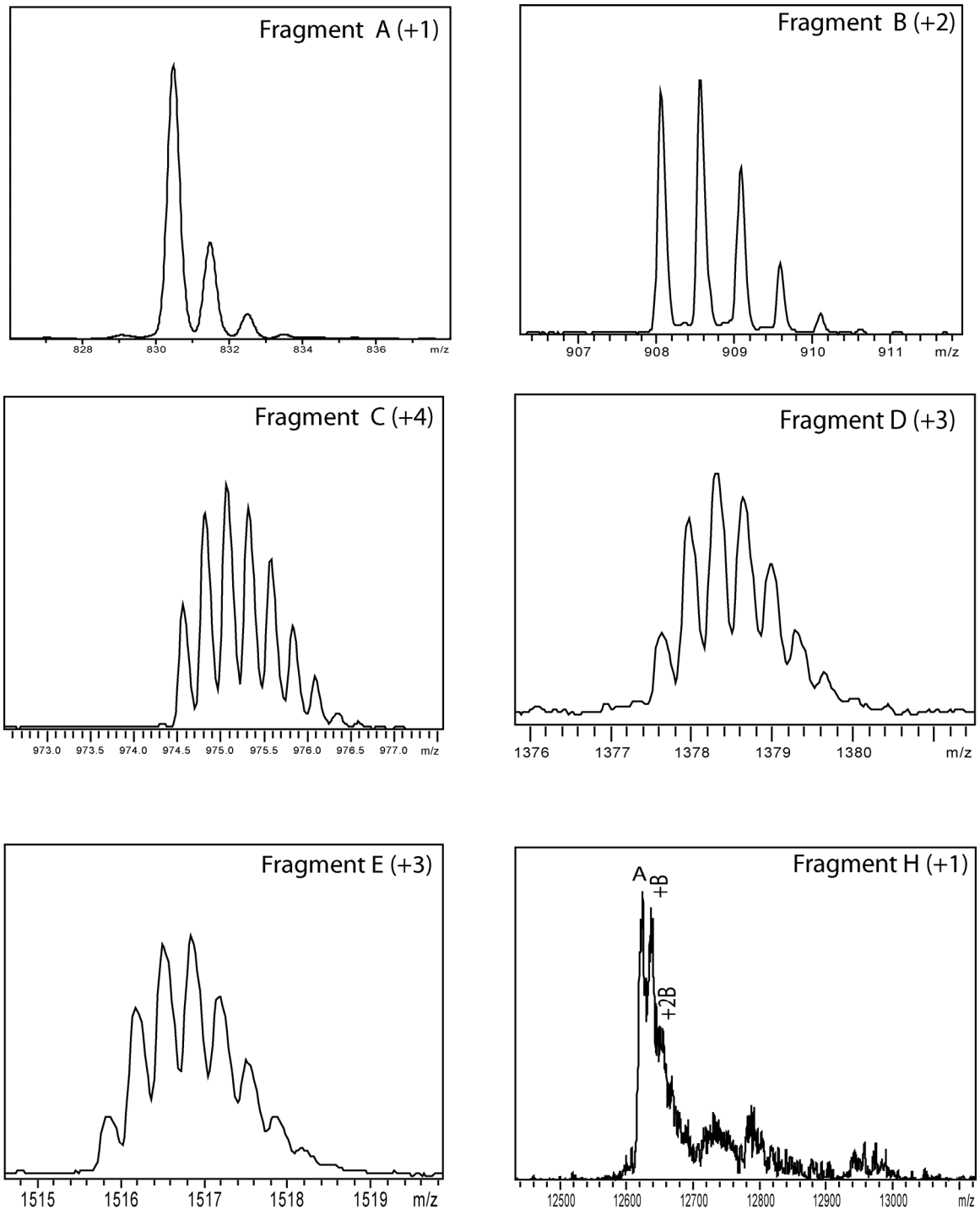


Figure 3.21. Mass spectra of CCR5 CNBr digest fragments detected in the microTOF.

as a prototype for other integral membrane proteins. We have demonstrated that with rhodopsin we have adapted and improved methods leading to the detection of the glycosylated fragments amino terminal peptide as well as the phosphorylated C-terminal tail. Employing methods developed for rhodopsin we have made advances in mass spectrometric studies of CCR5 such that we can detect all of the transmembrane helices which may lead to success in detecting and identifying sites of ligand binding. Detecting minor components in a complex mixture is the challenge presented when attempting to detect conjugated ligands in studies leading to increased understanding of agonist and antagonist binding as well as G-protein coupling in the case of GPCR's. It is our hope that these initial mass spectrometric studies of rhodopsin will facilitate further investigations of G-protein coupling to rhodopsin and ligand binding for the co-receptors involved in HIV infection.

Materials and Methods

Rhodopsin Sample Preparation

Rhodopsin rod outer segments were initially prepared as described in chapter 2 materials and methods. The concentration of rhodopsin present in an aliquot was initially determined by measuring a UV visible difference absorbance spectrum in the presence of LDAO, as described in chapter 2. Typically a 500 µl aliquot of 30 uM rhodopsin in native membranes was reduced by addition of 10 µl tributyl phosphine(Sigma, T-7567) and alkylated by the addition of 10 µl of 4-vinyl pyridine(Sigma, V3204). The reduction and alkylation reaction was typically allowed to proceed at room temperature tumbling for 1-4 hours. Rhodopsin samples are pelleted and resuspended in 95 % ethanol,

disrupting the pelleted rhodopsin by bath sonication prior to centrifugation and resuspension to remove excess tributyl phosphine,4-vinyl pyridine, and to extract some of the lipids was repeated 3-5 times. The washed rhodopsin pellet is then resuspended in acetone and pelleted, and then pellet is then allowed to air dry for several minutes. After excess acetone has been removed by air drying the rhodopsin pellet is dissolved in a minimal amount of TFA (Pierce, 28903), typically 100 ul. A fresh stock solution of cyanogen bromide (ICN biomed) in TFA is made ~500 fold molar excess of CNBr to rhodopsin is added to the rhodopsin dissolved in TFA. The final concentration of TFA is reduced to 70% by addition of Nanopure water. The rhodopsin CNBr cleavage reaction is then foil wrapped and allowed to tumble slowly overnight at room temperature. To quench the cleavage reaction water 10 fold excess v/v of Nanopure water is added resulting in the precipitation of the hydrophobic peptides derived from rhodopsin. The cleavage reaction was then lyophilized to dryness and resuspended in water, the lyophilizing and resuspension was repeated 3x to removing excess cyanogen bromide and TFA. Typically two to three hundred micrograms of digest product was weighed out and dissolved in 10-40 µl 100% formic acid (Fisher, FX0440-5) by vortexing, then an equal volume of isopropanol (EMD PX1838) was added and then the dissolved material was mixed well by vortexing. Lastly the final volume of the solubilized rhodopsin digest peptides was adjusted with addition of Nanopure water resulting in the final formic acid and isopropanol concentrations of 5% respectively. The sample was centrifuged at 14.5 K for 5 minutes to remove any insoluble particles the supernatant was then carefully withdrawn and then analyzed by LC/MS.

CCR5 Expression and Purification

CCR5 extraction and purification was performed by Dr. Royce Wilkenson in the laboratory of Dr. Martin Teintze. Breifly, CCR5 was expressed using a codon-optimized construct with a C-terminal rhodopsin epitope tag transfected into canine kidney cells following published methods [171]. CCR5 is affinity purified sing 1D4 antibody on agarose beads from detergent solubilized membranes isolated from large quantities of cells cultured at the National Cell Culture Center. Preparation of CNBr digested CCR5 was performed in the same fashion as described for rhodopsin by Dr. Royce Wilkenson.

Capillary HPLC-QIT

Mass spectrometric analysis of peptide fragments from rhodopsin CNBr digest were performed on an Esquire 3000 were separated on home made C18 columns or on a Luna guard cartridge 2 x 20 mm (Phenomenex, 00M-4252-BO-CE). Home made columns were constructed with 15 cm peek tubing ,inner diameter 0.25 mm (upchurch peek tubing1531B), unions, ferrels, and frits for column construction were purchased (unions u435, ferrel u401x, frit c407x) and packed with Vydac C18 (10-15 um particle size and 300Å pore size (Cat. No. 218TPB1520)) using a pressure bomb constructed in house. Approximately 2 ml of slurry was prepared fresh and placed in a resuvour of with stirring magnet and this was loaded into the pressure bomb. The amount of solvent that passed through the column was monitored, when 1-1.5 ml of solvent had passed through the column the bomb was depressurized and the column assembly was completed by cutting 2 cm off of the end of the tubing and placement of the of a union. Employing an

Agilent 1100 capillary LC system typically 50 µl of rhodopsin digest (150-300 pmoles) was injected onto the reverse phase column and eluted over 70 minutes with a solvent flow rate of 100 ul/min when separating on the Luna column or 40 µl per minute on the hand packed column. The HPLC gradient started at 100% A (water with 0.5% formic acid) and 0% B (100% isopropanol with 0.5% formic acid) ramping to 100% B over 50 minutes followed by washing the column at 100% B for 20 minutes. The Esquire was set to perform MS/MS on any ion appearing at an intensity of 25K counts or greater, after the acquisition of 2 MS/MS spectra on an ion it was then ignored for 1 minute.

MicroTOF

Mass spectrometric analysis of rhodopsin peptide fragments performed on a Bruker microTof were separated on a Phenomenex Luna C18(2) guard cartridge (part number 00M-4252-B0-CE). Rhodopsin peptides (50-300 pmoles) were eluted from the column at a flow rate of 200 µl per minute starting at 100 % A for 2 minutes then ramping to 100% B over 25 minutes followed by 2 minutes at 100% B.

Nanospray –QIT

Mass spectrometric analysis of rhodopsin peptide fragments on a Agilent XCT Ultra with 43 mm Chip LC column was performed typically loading 10 to 50 picomoles of peptide mixture. Peptides were eluted from the Chip LC column running a 17 minute gradient ramping from 0% B to 100% B. Solvent A contained 5% ACN, 95% Nanopure water and 0.5% formic acid and solvent B contained 2:1 isopropanol:acetonitrile with 0.5% formic acid. Flow rates were typically 0.4 µl per minute over the course of the gradient. The XCT ion trap was set on Ultra scan rate and performed MS/MS on any ion

with greater intensity than 25000 counts. Data analysis was performed using Data Anlysis v 3.3 (Bruker).

FT-MS

Analysis of rhodopsin by ICR-FTMS was performed as has been reported previously by Kruppa et al.,[170] and more recently by Jacobsen et al.,[159]. Breifly, samples were analyzed at Sandia National Laboratories, approximately 500 pmoles of rhodopsin digest was injected onto a PLRP/S column (5 um particle size, 0.2 x 150 mm, Michrom Biosources) and seprated using solvents and gradients as follows: solvent A, 0.5% formic acid, 2.5% acetonitrile, 2.5% isopropanol, 95% water; and solvent B, 50% acetonitrile, 40% isopropanol, 10% water, 0.4% formic acid; gradient in solvent B, 0 to 1 minute 0-1% , from 1 to 5 minutes change in B from 1-20%, from 5 minutes to 40 minutes change in B from 20-70%, from 40 minutes to 45 minutes change from 70-99% B and from 45 to 50 minutes hold at 99% B. The chromatographic separations were performed at 25ºC at a flow rate of 5 µl /minute using an Agilent 1100 capillary HPLC system. Mass spectrometry was performed using a APEX II FTMS equipped with a 7.0 Tesla superconducting magnet and an Apollo ESI ion source (Bruker Daltonics).

Mass Spectral Analysis of Intact Rhodopsin.

Intact rhodopsin was detected by ESI-TOF. Sample preparation for direct infusion of intact rhodopsin was as follows 100 µl of 100 uM rhodopsin in rod outer segments was suspended in 50 mM hydroxyl amine pH 7.5 and exposed to light to remove the retinal, then pelleted and suspended in chloroform to remove the native lipids. The rhodopsin precipitated in chloroform and was washed with water by vortexing to

remove residual salts. The rhodopsin pellet was then dissolved in 50 µl of neat formic acid and adjusted to a final volume of 100 µl with isopropanol. The rhodopsin in formic acid and isopropanol was then diluted 1:100 with 50% acetonitrile: 50% water and direct injected into the Bruker microTOF using a syringe pump at 200 µl per hour.

CHAPTER 4

METARHODOPSIN-II STABILIZATION BY CROSSLINKED Gαt C-TERMINAL PEPTIDES

Introduction

The G-protein coupled receptor (GPCR) super-family constitutes more that 1% of the human gene complement and controls a very wide range of physiological processes [15, 174]. Rhodopsin is the best understood GPCR and is the photoreceptor protein in the rod cells of the retina, where it functions as a single photon detector for dim light vision. Rhodopsin is a prototypical GPCR, being the only GPCR for which high resolution crystal structures are available but the high resolution crystal structures reveal only the unactivated resting state of the receptor[7, 9-11, 24, 175]. More recently several photo-intermediates structures have been determined at much lower resolution [12, 13, 96].

Absorption of a photon by the covalently coupled 11-cis retinal chromophore causes isomerization of the retinal and activates rhodopsin. Photoactivation of rhodopsin leads to the formation of a series of short-lived photo-intermediates that culminate in an equilibrium between metarhodopsin I (MI, with peak absorbance near 480nm) and metarhodopsin II (MII, with peak absorbance near 380 nm), that is established in milliseconds at physiological temperatures[34].

Metarhodopsin II is the conformation of the receptor that binds to and excites G-proteins, but little is known about the detailed molecular structure of metarhodopsin II.

We have proposed a model for the membrane surface features of metarhodopsin I, that is the direct precursor to metarhodopsin II, based on x-ray diffraction analysis of an epitope peptide complex with an antibody that stabilizes metarhodopsin I [176]. Spin-spin interactions in electron spin resonance have shown that upon formation of metarhodopsin-II the transmembrane helical bundle expands at the cytoplasmic face of rhodopsin and the largest movement appears to be helix VI moving away from the core of the helical bundle [69]. The binding of the G-protein transducin stabilizes metarhodopsin II and leads to the release of GDP from the complex leaving an empty nucleotide binding pocket on the G-protein. In the presence of GTP, the binding of GTP causes the release of Gα and Gβγ from the membrane. The molecular mechanism of the coupling of GPCR's and G-proteins is a major unsolved problem in cellular signaling, which if it were better understood is expected to have many important implications for pharmacology.

The C-terminal tail (340-350) of the heterotrimeric G-protein alpha subunit (Gαt) has been found to be an important contact site for transducin binding to and stabilizing activated metarhodopsin-II [108, 112, 113]. Binding of the Gαt C-terminal tail peptide, $^{-11}$IKENLKDCGLF^{-1}, shifts the MI ↔ MII equilibrium to stabilize MII and the amino acid sequence of the C-terminal tail of the alpha subunits of G-proteins are thought to determine receptor coupling specificity [114]. Photocrosslinking, differential chemical modification, and mutagenesis studies all imply that the cytoplasmic C IV surface loop (including residues in helix 8) of rhodopsin is part of the Gαt C-terminal peptide binding site [115-117]. Fluorescence quenching studies of a bimane probe linked to site specific thiols and quenching by tryptophan residues place the amino terminus of Gαt C-terminal

peptide analogs near C140 during metarhodopsin-II stabilization [118]. Mutagenesis studies suggest that a hydrophobic region on the C III surface loop of rhodopsin mediates Gαt C-terminal peptide analog-receptor interactions [70], but a detailed structure of the MII-G-protein interaction that triggers signal amplification is not available.

In the present study, we found that analogs of the C-terminal tail of Gαt can stabilize MII when they are covalently bound with a specific N↔C polarity to one of the two native reactive cysteines, C140 and C316 on the cytoplasmic face of rhodopsin. Of the two reactive cysteines in dark-adapted rhodopsin, C316 is most reactive presumably due to side chain orientation leading to greater solvent exposure as can be seen in Figure 4.1. C316 will react with α-haloacetyl compounds readily, while under the same conditions C140 shows little to no reactivity [177-179]. N-maleimide derivatives have been shown to modify both C140 and C316 in dark-adapted rhodopsin and 316 can be blocked selectively with 4,4-dithiodipyridine (DTP) [180] before the maleimide coupling [177, 178, 181].

We used synthetic peptides that differed in the placement of a thiol crosslinking group, either at the N-terminus or the C-terminus of the Gαt 340-350 peptide analogs to establish the N → C orientation of the covalent binding of the reactive peptide relative to C140 or C316 on rhodopsin. By selectively crosslinking the Gαt C-terminal tail peptide to either C140 or C316 on rhodopsin and measuring the stabilization of metarhodopsin-II by the crosslinked peptides, we assessed the orientations of the peptides on the rhodopsin surface that are able to stabilize metarhodopsin-II. This information obtained provides evidence on the nature of productive Gα transducin-metarhodopsin-II interactions, that we anticipate will provide a foundation for planned experiments that can provide much

more detailed information on the amino acid residues of the light-activated rhodopsin which are critical for interacting with Gαt and for triggering GTP/GDP nucleotide exchange.

Results

The C-terminal eleven residues (340-350) of the alpha subunit of transducin are capable of shifting the MI ↔ MII equilibrium by binding to and stabilizing MII [108]. We synthesized a panel of Gαt C-terminal tail peptide analogs containing thiol reactive groups, shown in Table 4.1, and assessed their capacity to shift the MI↔MII equilibrium. There are 10 endogenous cysteines in rhodopsin which are shown in Figure 4.1A. Two of the endogenous cysteines are disulfide bonded to one another (C110 and C187) and 2 are modified with the palmitoyl fatty acid (C322 and C323). The remaining 6 cysteines exhibit very different reactivity. The two cysteines, 140 and 316, rendered as red colored space filling models in Figure 4.1A, are the only two cysteines that are substantially reactive in the native membrane in unactivated rhodopsin. Cysteine 316 has been shown to be much more reactive than 140, most likely due to differences in solvent exposure as can be seen in Figure 4.1B.

Peptide amino acid sequence	Peptide name
Biotin-VLEDLRD(Abu)GL(Dpr)-IA	B-23S-IA
IA-VLEDLRD(Abu)GL(Dpr)	IA-23S
Maleimide-VLEDLRD(Abu)GL(Dpr)	M-23S
IA-VLEDLRD(Abu)GL(Dpr)-IA	IA-23S-IA
IA=iodoacetyl, Abu=α amino butyric acid, Dpr= α,β, - diamino propionic acid	

Table 4.1. Gαt C-terminal peptide analogs

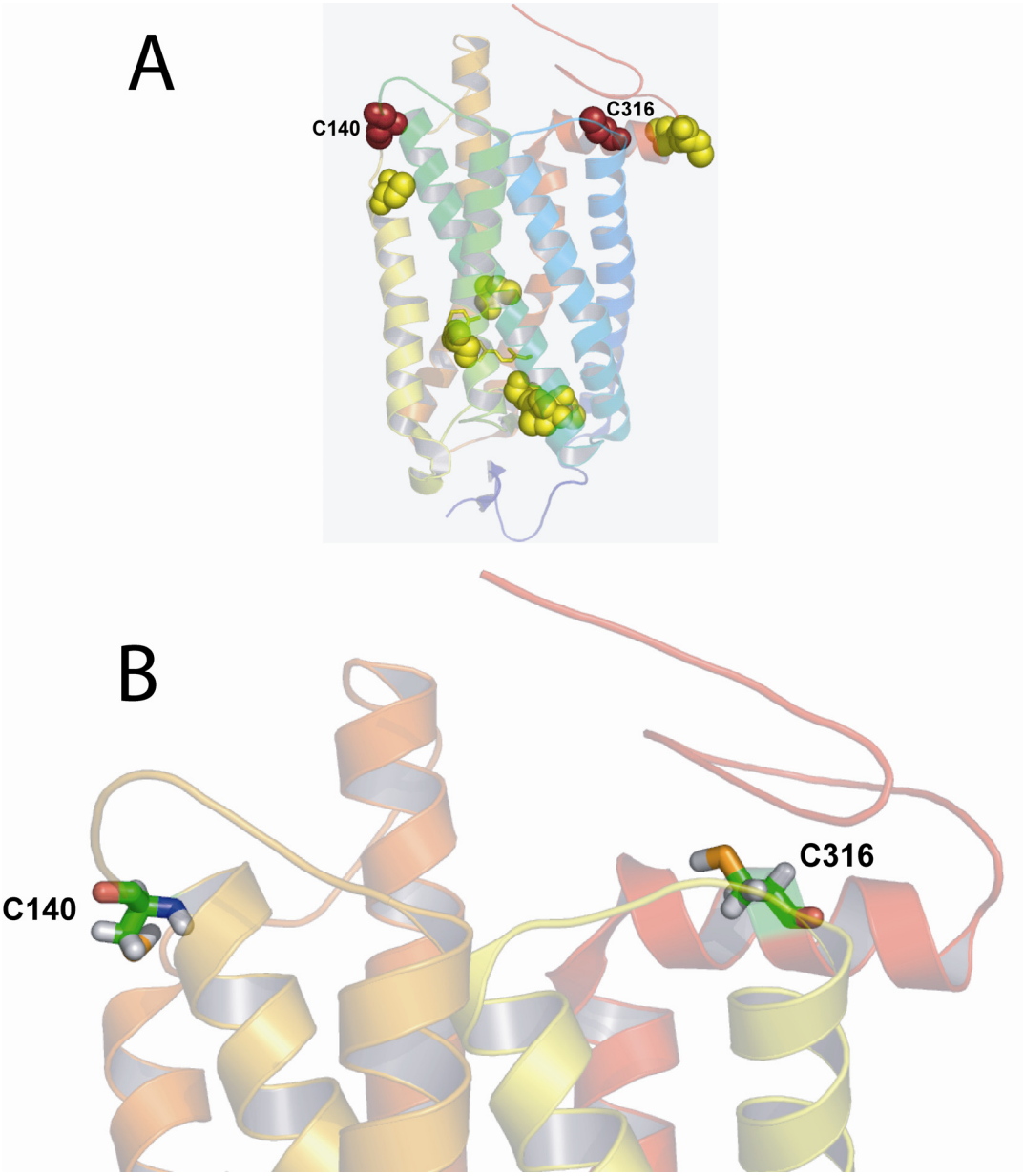


Figure 4.1. Endogenous cysteines present in rhodopsin. The structure of unactivated rhodopsin (1U19.pdb) is shown in A, the ten cysteine in rhodopsin are rendered in space filled models, in yellow are the 8 cysteines that are unreactive in the dark and colored red are the two cysteines, C140 and C316 that are reactive in the dark. An expanded view of the cytoplasmic face of rhodopsin in B shows the different side chain orientation which may explain in part the differential reactivates of C316 (most reactive) and C140 (least reactive). The sulfhydral of C140 is oriented parallel to the lipid bilayer and may be shielded from interactions with reagents in the bulk solvent by the CIII loop. C316 is solvent exposed thus the observed high level of reactivity may be due to an increased solvent exposure as observed in the crystal structure.

The residues on rhodopsin that have been found to be required for effective Gαt binding are shown in Figure 4.2, rendered as green sticks on the dark adapted rhodopsin crystal structure.

Peptide IA-23S-IA (Table 4.1) with thiol-reactive iodoacetate groups on both the N- and C-termini was chemically crosslinked to C316 under conditions where C140 does not react with iodoacetate derivatives. The covalent addition of crosslinked peptide to intact rhodopsin was detected by MALDI-TOF mass spectrometry in the linear mode, as shown in Figure 4.3. The MALDI spectrum of the intact rhodopsin is rather broad due to heterogeneous glycosylation and the inherent low resolution of linear MALDI-TOF spectra of large proteins. The mass shift of the MALDI signal of the crosslinked rhodopsin (Figure 4.3, blue trace) indicates that there was little or no unmodified rhodopsin remaining after peptide crosslinking and that there is approximately one peptide coupled per rhodopsin molecule under these conditions. The somewhat broader, asymmetric MALDI signal of the crosslinked sample may reflect the high laser power needed to obtain spectra of the complex, although a small portion of the rhodopsin might have more than one peptide crosslinked per rhodopsin molecule, contributing to the asymmetric tail on the high mass side of the MALDI spectrum.

We found that chemical coupling of the bifunctional peptide IA-23S-IA to cysteine 316 in non-activated rhodopsin, followed by photoactivation, led to a shift in the MI↔MII equilibrium toward MII, as shown in Figure 4.4A (red circles). Prior to removal of excess uncrosslinked peptide the amount of metarhodopsin-II that was stabilized (blue triangles), and the amplitude of this response is very similar to the maximum amount of metarhodopsin-II stabilization that can be obtained by fully

functional, high affinity Gαt C-terminal peptides or the intact heterotrimeric G-proteins [112, 182]. Following removal of excess free peptide, the shift in the MI↔MII equilibrium toward MII was reduced but still present, indicating that peptide crosslinked to C316 leads to substantial metarhodopsin-II stabilization (Figure 4.4A, red), but that non covalent peptide also contributes to the MII stability. The presence of two reactive coupling sites, one at each end of the peptide, makes it possible for the peptide to cross link to the reactive cysteine on the cytoplasmic face of rhodopsin in two orientations (N-

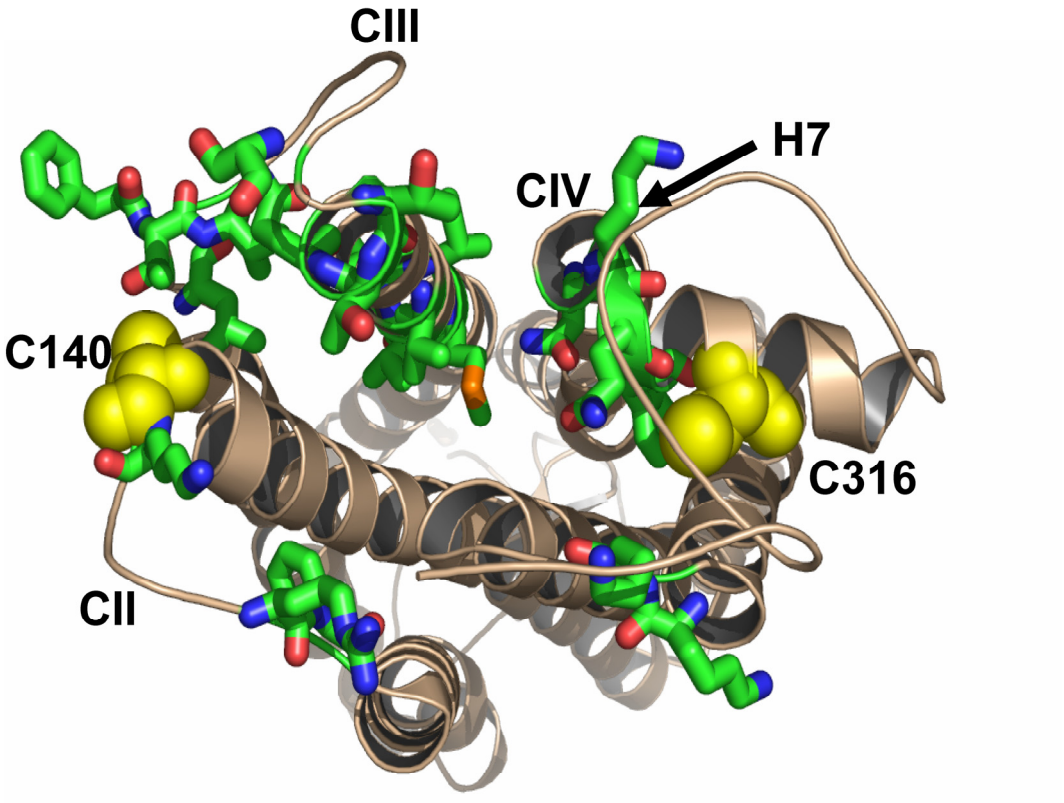


Figure. 4.2. The dark-adapted rhodopsin crystal structure (1U19) [9] illustrating the spatial distribution of the residues that have been implicated in mediating the interaction of Gt (340–350) C-terminal tail peptide with metarhodopsin-II [116, 118, 183, 184]displayed in green in stick format. Cysteine 140 and 316 are rendered as yellow spheres.

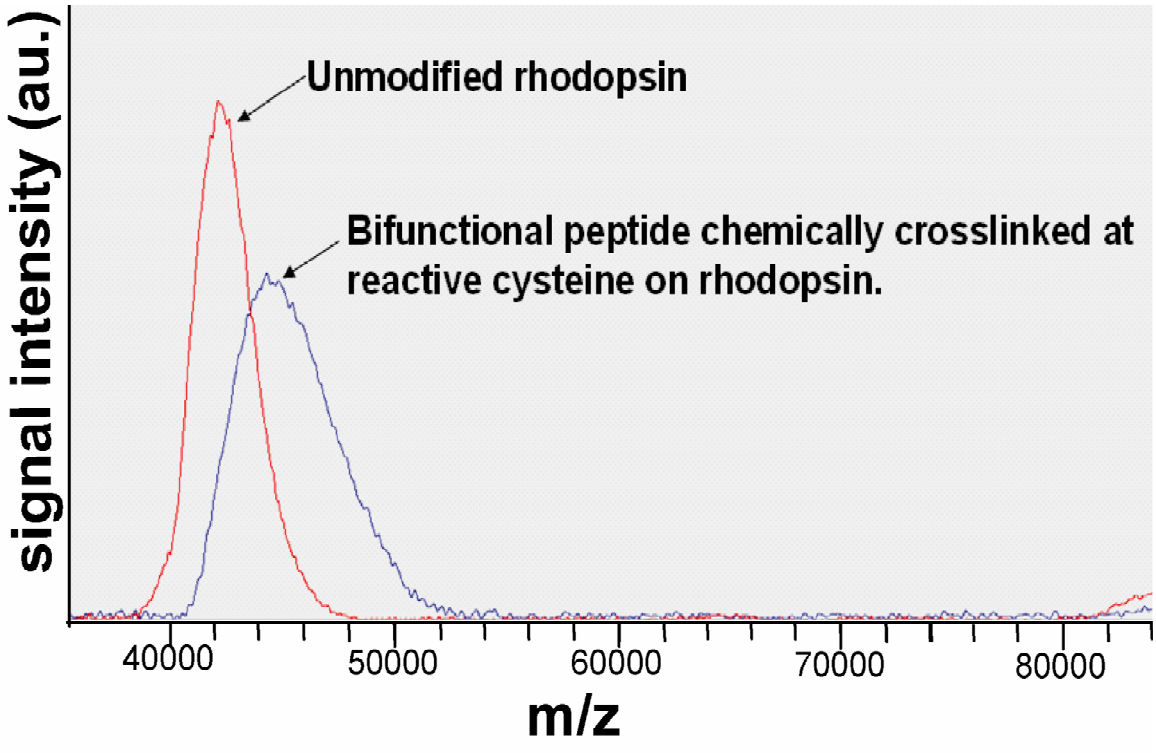


Figure. 4.3. MALDI-TOF of intact rhodopsin. Modified (black trace) and unmodified (blue trace) intact rhodopsin was analyzed by MALDI-TOF mass spectrometry. Following chemical crosslinking of peptide IA-23S-IA a rhodopsin mass shift was detected relative to an unmodified rhodopsin sample that shows little unmodified rhodopsin remaining in the modified sample and approximately one peptide added per rhodopsin, as discussed in the text.

linked or C-linked to C316) which leaves the peptide orientation that stabilizes metarhodopsin-II uncertain. If rhodopsin labeling with IA-23S-IA resulted in approximately one peptide crosslinked per rhodopsin molecule as indicated in Figure 4.4, and washing off uncrosslinked peptide by centrifugation leaves only partial MII stabilization, not all of the crosslinked peptide orientations are capable of shifting the MI-MII equilibrium and some of the MII stabilization observed in the presence of excess peptide must be due to the non-covalently linked peptides being bound leading to metarhodopsin II stabilization.

Evaluation of the orientation of the peptide crosslink that leads to metarhodopsin-II stabilization was carried out by chemically crosslinking peptides with either the N-terminal or the C-terminal residues modified with the thiol crosslinking reagents iodoacetate-SE or maleimide-SE. The C-terminal modified peptide IA-23S (Table 4.1) was able to stabilize metarhodopsin-II when the peptide is free in solution, as shown by measuring the shift in the MI-MII equilibrium prior to the removal of excess peptide from the crosslinking reaction (Figure 4.4B red circles). However, following the removal of excess free peptide by centrifugation, the metarhodopsin-II stabilization is absent (Figure 4.4B, black squares). Thus, the peptide chemically crosslinked to C316 by its N-terminus is not capable of stabilizing metarhodopsin-II. We believe that the IA-23S peptide peptide crosslinks to C316, since C316 is the most reactive thiol in rhodopsin and reacts vigorously with alkyl halides[177] similar to the reactive group place on the peptide, but we are unable to confirm this crosslink using mass spectral methods. A negative result with mass spectral detection of this crosslink in not sufficient to conclude that the crosslink did not occur.

Initially blocking cysteine 316 with 4,4-dithiodipyridine (DTP) [180] and then coupling the more reactive maleimide-containing peptide M-23S (Table 4.1) allowed for selective coupling of peptide M-23S to cysteine 140 on rhodopsin. The extent of modification of cysteine 316 with DTP can be monitored and quantified

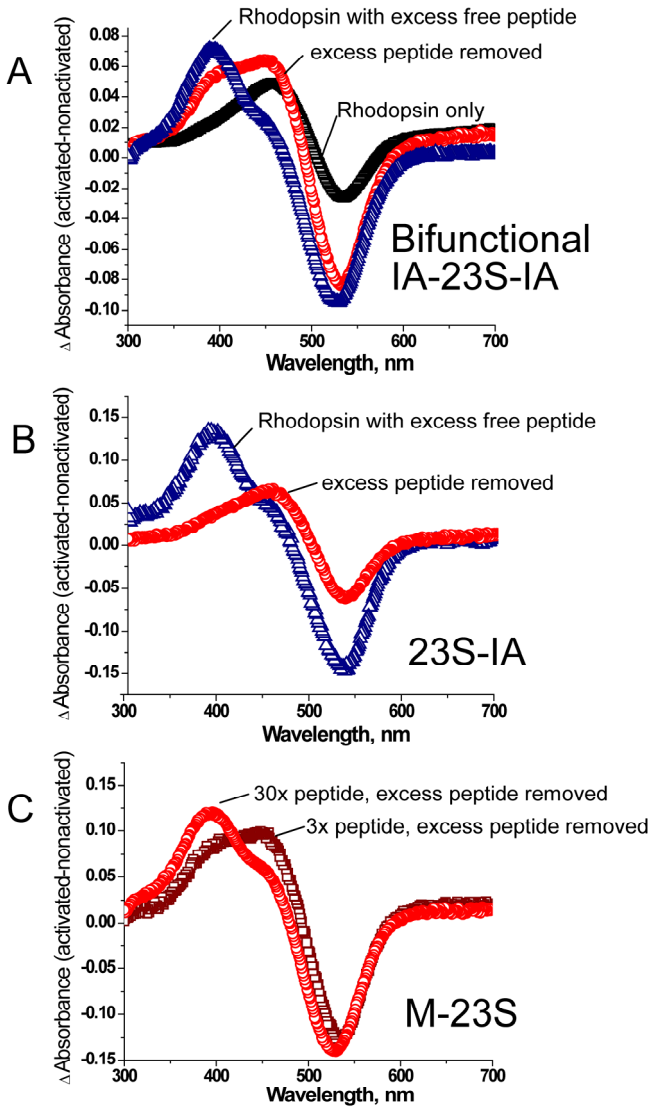


Figure 4.4. Rhodopsin difference absorbance spectra showing the shifts in the metarhodopsin-I metarhodopsin-II equilibrium following chemical crosslinking of Gt C-terminal tail peptide analogs. (A) Peptide IA-23S-IA was incubated with rod outer segments (10 uM) at pH 8 at 4 °C overnight. Absorbance difference spectra were measured for rhodopsin (black squares), rhodopsin with the addition of peptide IA-23S-IA after incubation overnight prior to the removal of excess uncoupled peptide (blue triangles) and following removal of excess uncoupled peptide (red circles). (B) Peptide IA-23S was incubated with rod outer segments (10 uM) at pH 8 and 4 °C overnight. Absorbance difference spectra were measured before (red circles) and after removal of uncrosslinked peptide (black squares). (C) Peptide M- 23S threefold molar excess (dark red squares) or 30-fold molar excess (bright red circles) was incubated with rod outer segments (10 uM), that had been treated with 4,4'-dithiodipyridine to block C316, at pH 8 at 4 °C overnight. The absorbance difference spectra were measured after removal of uncrosslinked peptide in the curves shown.

spectrophotometrically by the color change due to the DTP reaction. Cysteine 316 on rhodopsin was quantitatively blocked with DTP (data not shown), followed by overnight incubation with peptide M-23S. Covalently linking the amino terminus of M-23S to C140, followed by washing off excess free peptide and photoactivation led to very substantial stabilization of metarhodopsin-II, as shown by the absorbance difference spectra (Figure 4.4C). The extent of peptide mediated metarhodopsin-II stabilization increased following incubation of rhodopsin with increasing amounts of peptide M-23S crosslinking followed by washing the unreacted peptide off the membrane. This effect was observed comparing the amount of metarhodopsin-II stabilized following incubation of rhodopsin with a 3 fold molar excess of peptide M-23S (Figure 4.4C, dark red squares) compared to incubation of a 30 fold molar excess of peptide (Figure 4.4C, red circles). The 30 fold molar excess stabilized the maximum amount of MII that can be stabilized under any conditions.

Following the crosslinking of peptides the rhodopsin samples were extracted from lipids and digested with CNBr followed by analysis of the peptide digests were analyzed by HPLC-MS. The extracted ion chromatograms for the peptide fragment containing cysteine 140 with and without peptide crosslinked is presented in Figure 4.5. The deconvoluted mass spectra for the modified and unmodified C140 containing peptide is shown in Figure 4.5, providing direct evidence for the functional modification of rhodopsin by the crosslinked peptides.

Chemical crosslinking of the biotin-containing peptide B-23S-IA (Table 4.1) to rhodopsin allowed us to biotin-affinity purify and identify the crosslinking site on C316 by mass spectrometry on cleaved peptide fragments. In the absence of an affinity tag like

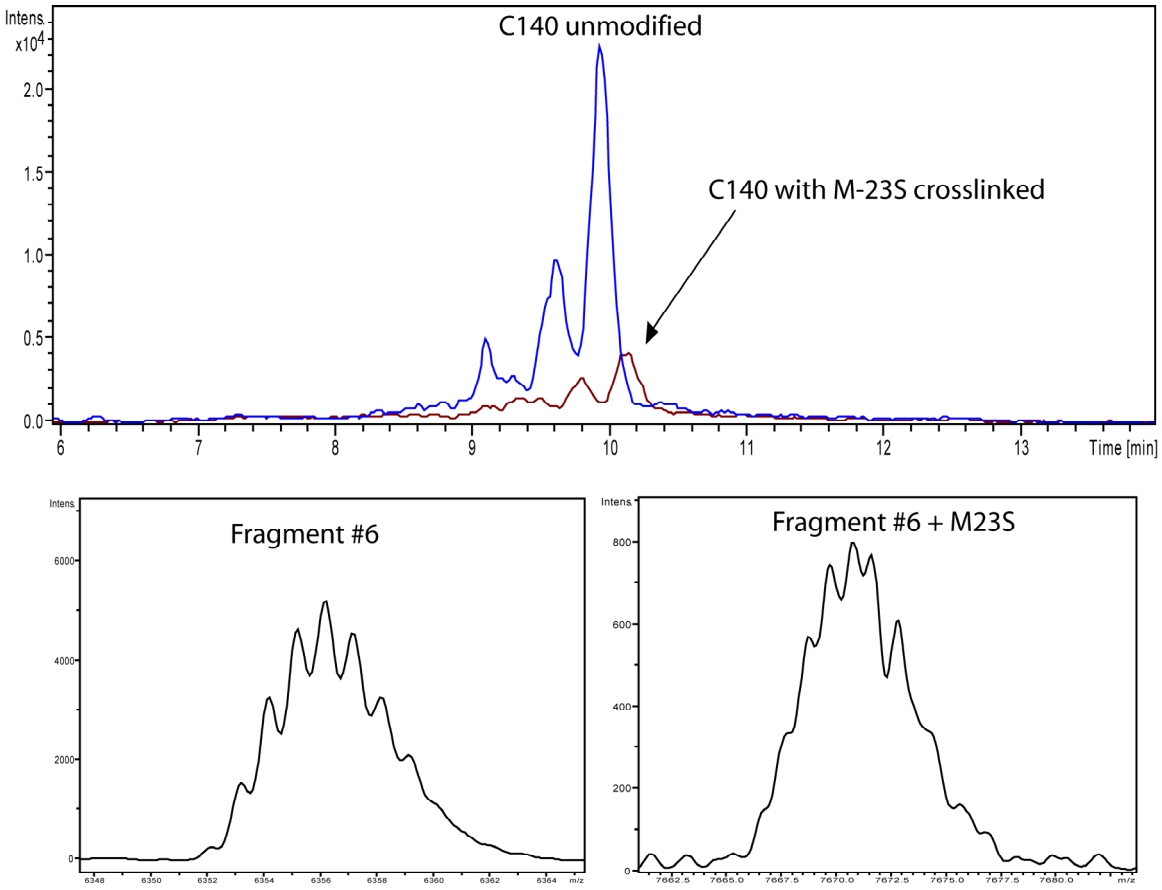


Figure 4.5. Extracted ion chromatogram of C140 unmodified and modified peptide. Following rhodopsin digestion with cyanogen bromide the peptides were separated by reverse phase HPLC, ionized by electrospray ionization and detected in a time of flight mass analyzer. The peptide containing C140 has a theoretical monoisotopic mass of 6353.2692 and observed deconvoluted mass of 6353.2 an error of 10 ppm. The modified peptide elutes after the of unmodified peptide and has a theoretical mass of 7667.1147 and an observed mass of 7667.7 an error of 76 ppm.

biotin we were unable to detect the peptide crosslinking to sites in rhodopsin by MALDI-TOF, due to differences in ionization efficiency of the different CNBr peptide fragments as well as differences in ionization efficiency before and after crosslinking. Chemical crosslinking of peptide B23S-IA by the C-terminus to C316 on rhodopsin, followed by washing off the unreacted free peptide and photoactivation, led to strong metarhodopsin-II stabilization, as evidenced by the increase of the 390nm-417nm absorbance difference

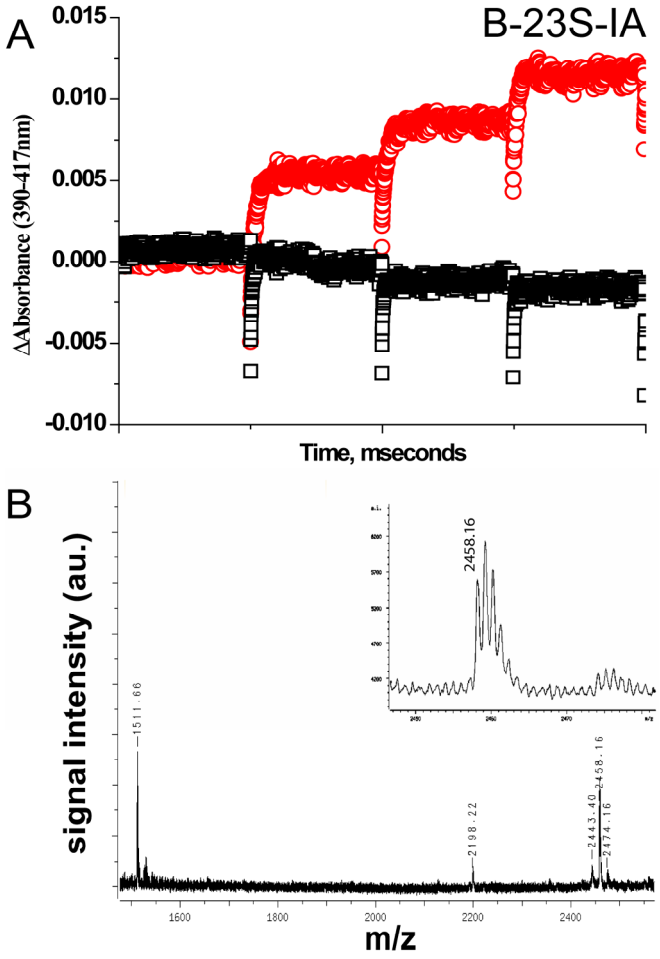


Figure. 4.6 Crosslinking peptide B23S-IA to C316 on rhodopsin leads to the stabilization of metarhodopsin-II. Peptide B23S-IA was incubated with rod outer segments (10 uM) at pH 8 at 4 °C overnight and uncoupled peptide was removed by centrifugation. (A) Metarhodopsin-II formation following flash photolysis of rhodopsin in the absence of peptide (black squares) or in the presence of B23S-IA crosslinked to rhodopsin after unreacted peptide was removed (red circles) was monitored for the difference in absorbance (390–417 nm). Four hundred and seventeen nanometers is the isosbestic point between MI and MII and 390nm provides the highest signal to noise for monitoring the levels of MII. Flash photolysis bleached 8% of the total rhodopsin per flash. (B) MALDI-TOF mass spectrum of a CNBr cleavage product of rhodopsin showing peptide B-23S-IA crosslinked to the rhodopsin peptide containing C316. After coupling to peptide B-23S-IA, washing off unreacted peptide by centrifugation, and measurement of metarhodopsin-II stabilization—rhodopsin was chemically cleaved with CNBr. Peptide fragments coupled to the biotin-containing B23S-IA were affinity purified using streptavidin-Dyna magnetic beads, detected by MALDI-TOF mass spectrometry and found to be coupled to 310NKQFRNCh317 (theoretical mass 2458.50, observed mass 2458.16).

peptide to C316 was confirmed by MALDI-TOF mass spectrometry following cleavage induced by a series of light flashes in a light titration series (Figure 4.6A). The amplitude of the light titration response due to metarhodopsin-II stabilization was essentially equivalent to the maximum stabilization that can be obtained with G-protein of Gαt C-terminal peptides(data not shown). The chemical crosslinking of the biotin-containing rhodopsin at methionines by CNBr and affinity enrichment of biotin-containing peptides from the rhodopsin, using streptavidin bound to magnetic beads (Figure 4.6B).

Discussion

Interactions between G-protein coupled receptors and the alpha subunit of the heterotrimeric G-proteins have been reported to involve residues on the CII, CIII, and CIV cytoplasmic loops in several different GPCR's [114]. The residues that have been implicated in mediating interactions of the C-terminal peptide of Gαt with metarhodopsin-II are illustrated in Figure 4.1. Evidence for the interacting residues illustrated was based primarily on site-specific mutagenesis experiments, which might alter protein interactions by changing protein conformation, rather than revealing direct sites of interactions and thus some of the putative interactive sites shown in Figure 4.1 could well be "false positives".

Hydrophobic interactions between rhodopsin and the C-terminal tail of Gαt have been proposed. The Cys^{-4} residue of the C terminal tail of Gαt may be involved in a hydrophobic interaction, since substitution with amino butyric acid, where the methylene-sulfhydryl group is replaced with an ethyl group, maintains the activity of the C-terminal peptide, whereas a cysteine to alanine substitution reduces the metarhodopsin-II

stabilizing activity of the peptide 3-fold [112]. It has been shown that replacing the positive charge contributed by the lysine in the -10 position with leucine increases the affinity of the C-terminal Gαt peptide analog (VLEDLKSCGLF, called 23S) for binding and stabilizing metarhodopsin-II ~ 3 fold [182]. The native C-terminal Gαt peptide has a higher off rate than the high affinity 23S analogs, presented in chapter 2, which is consistent with the native sequence being able to support a larger G-protein amplification by light-excited rhodopsin, but with lower affinity. We have chosen to use the high-affinity C-terminal Gαt peptide analog in these crosslinking studies, as the increased affinity and large residence time of this peptide presumably will favor specific binding.

Interactions between rhodopsin's fourth cytoplasmic (C IV) loop (now known to include helix 8) on the cytoplasmic surface and Gαt peptide analogs have been implicated, since replacing ^{310}NKQ^{312} on rhodopsin with the homologous sequence from the beta 2 adrenergic receptor abolished the capacity of the Gαt C-terminal peptide, IRENLKCGLF to inhibit rhodopsin photoregeneration [106]. Photocrosslinking, differential chemical modification, and mutagenesis studies all indicate the C IV loop (helix 8) is part of the Gαt C-terminal peptide binding site [115-117]. Fluorescence quenching studies place the N-terminus of Gαt analogs near C140 during metarhodopsin-II stabilization [118].

Mutagensis studies suggest that a hydrophobic region on the C III loop of rhodopsin mediates Gαt C-terminal peptide analog-receptor interactions [70]. Placement of a heterobifunctional, thiol-photo activatable, crosslinking reagent on an engineered cysteine at position 240 on the C3 loop of rhodopsin allowed for the detection of a region of transducin involved in the coupling of Gαt to rhodopsin. Residues ^{342}ENLK^{345} of the

C-terminus of Gαt was crosslinked to residue 240 on the CIII loop of rhodopsin, but the crosslinked residue on Gαt was not determined [115]. C140 and S240 are 15Å apart in the crystal structure of the unactivated receptor. Thus, the crosslinking results of Cai et al., place ^{342}ENLK^{345} of the C terminal region of the transducin 340-350 tail peptide somewhat near C140 on rhodopsin during transducin-metarhodopsin-II coupling, but do not provide more detailed information regarding the relative orientation of transducin when interacting with activated rhodopsin. The Gαt C-terminal tail has been shown to assume an ordered secondary structure when binding to metarhodopsin-II by transferred NOESY NMR experiments [110, 138, 185]. The angle of the bound C-terminal Gαt peptide, with respect to the average helical axis of metarhodopsin-II was determined to be 40º+/- 4º [186], however the NMR experiments provided no evidence for the binding sites of the C-terminal Gαt peptide on metarhodopsin-II.

When the N-terminus of the Gαt peptide analog M-23S (table 4.1) was crosslinked to C140, and the excess free peptide was washed off, substantial metarhodopsin-II stabilization was observed (Figure 4.3C). A dose-response was obtained; increasing the amount of peptide incubated with rhodopsin, presumably led to an increased amount of covalent coupling of peptide which led to a increased amount of metarhodopsin II stabilized (Figure 4.3C). If the amino terminus of synthetic peptide analogs of the Gαt C-terminal tail is crosslinked to the C140 residue on the cytoplasmic tip of helix 3 of rhodopsin, this is a sufficient placement of the peptide to shift the metarhodopsin equilibrium to strongly stabilize metarhodopsin-II.

The cytoplasmic ends of helix 3 and helix 5 have both been implicated in Gαt C-terminal 340-350 peptide binding (Figure 4.1 and 4.2). These helices are not required to

move apart for transducin activation as demonstrated with "straight jacketed" mutants with restricted motion due to engineered disulfides [187, 188]. The crosslinking of peptide M-23S to C140 and the resultant metarhodopsin-II stabilization is consistent with the notion that there is a Gαt C-terminal binding site partly composed of the cytoplasmic regions of helix 3 and helix 5.

Detection of peptides crosslinked to rhodopsin by mass spectrometry has been accomplished as seen in Figures 4.5 and 4.6B. A quantitative analysis of the amount of crosslink present is problematic due to the potential for ion suppression from matrix effects and a apparent reduction in ionization efficiency due to the addition of the peptide crosslink to the native peptide. The relative ionization efficiency is unknown for the peptide fragments post modification. The error associated with the masses detected for the unmodified peptide was 10 ppm and the error for the modified peptide is 76 ppm reflecting a decrease in signal to noise for the detection of the modified peptide.

Crosslinking peptide B23S-IA to C316 by the C-terminus also led to strong metarhodopsin-II stabilization, as shown by light titration experiments (Figure 4.6A). Light titration data can provide information on the ligand binding constant [100] (although binding constant analysis was beyond the scope of the present work). Residues near the 8^{th} helix of rhodopsin have been reported to be involved in interactions with the C-terminal Gαt peptide [106]. When peptide IA-23S is crosslinked to C316 by the peptide's N-terminus, metarhodopsin-II is not stabilized (Figure 4.4B), therefore the metarhodopsin-II stabilizing effects of peptide crosslinks are sensitive to the orientation of the crosslinked peptide on the surface of rhodopsin. The observation in Figure 4.4A that free bifunctional IA-23S-IA fully stabilizes MII (blue curve), but washing off the

free peptide leaving the crosslinked peptide (Figure 4.4A) only partially stabilizes MII (red curve), suggests that if the peptide is crosslinked to C316 by the inactive N-terminal end that the unproductive peptide can swing out of the way and allow a free peptide to bind and stabilize MII.

We have found that chemically crosslinking the C-terminal peptide of Gαt at the amino terminal region of C2 loop and at the middle of helix 8 both result in strong MII stabilization, if the peptides are crosslinked in suitable N → C orientations. Site directed spin labeling studies imply that upon receptor activation helix 7 and helix 3 move away from one another, helix 6 moves away from helix 3 and helix 8, and there is increased mobility and possible structural rearrangement near residue C140 [69]. A disulfide crosslink between C316 and C65 does not abolish receptor activation of transducin, indicating that CI and helix 8 need not move apart greatly during receptor activation [70, 189, 190].

The NMR structure of the peptide analog of the C-terminal tail of Gαt bound to metarhodopsin-II measures 17Å end-to-end from amino terminus to the extended side chain of Leu^{-3} in the most refined bound peptide structure [186], whereas the distance between C140 and C316 in dark-adapted rhodopsin is 28Å. Our finding that crosslinking peptides to either C140 or C316 on rhodopsin leading to metarhodopsin-II stabilization was unexpected, given that the conformational changes in the transmembrane helices that are thought to take place during metarhodopsin-II formation would tend to increase the distance between crosslink sites C140 and C316 [69], rather than decrease the distance.

How can essentially identical Gαt peptide analogs crosslinked by their C-terminus to C316 or by their N-terminus to C140 both lead to metarhodopsin-II stabilization when

these regions are 28Å apart in rhodopsin and the peptide is only 17Å long when bound to metarhodopsin-II? One way to rationalize these findings would be if helix 8 of rhodopsin where to rotate (clockwise viewed from the cytoplasmic side as shown in Figure 4.2 and 4.7) about the axis of helix 7 upon formation of MII. Such a rotation of helix VIII could greatly decrease the distance between C316 and C140. A movement of helix 8 towards C140 could bring a large fraction of the residues that are reported to be involved in the contact interface for Gαt C-terminal tail peptide on rhodopsin much closer together, as can be seen in Figure 4.2 and Figure 4.7. Consistent with a rotation of helix 8, moving C316 closer to C140 upon formation of MII is the finding of Yu, Kono and Oprian that C140 and C316 could not be crosslinked in dark-adapted rhodopsin, but could be crosslinked after light excitation [188]. Such a rotational motion of H8 on the surface of rhodopsin can not be excluded by any other measurements that have been reported [188, 191] and could explain how essentially the same peptide crosslinked to residues that are ~28Å apart in rhodopsin could have similar capacities to stabilize metarhodopsin-II by interacting with similar residues in a more compact pocket resulting from the rotation of helix VIII decreasing the distance on the surface of rhodopsin between C140 and C316.

Alternatively, peptides crosslinked to C316 in productive orientation could be interacting with a largely different set of residues on metarhodopsin-II relative to the interactions of the peptides crosslinked to C140. Metarhodopsin-II has been divided into isospectral species called MIIa or MII* and MIIb or $MIIH^+$ [45, 89, 192]. The transition from MIIa (MII*) to MIIb ($MIIH^+$) involves the uptake of a proton from the bulk solvent

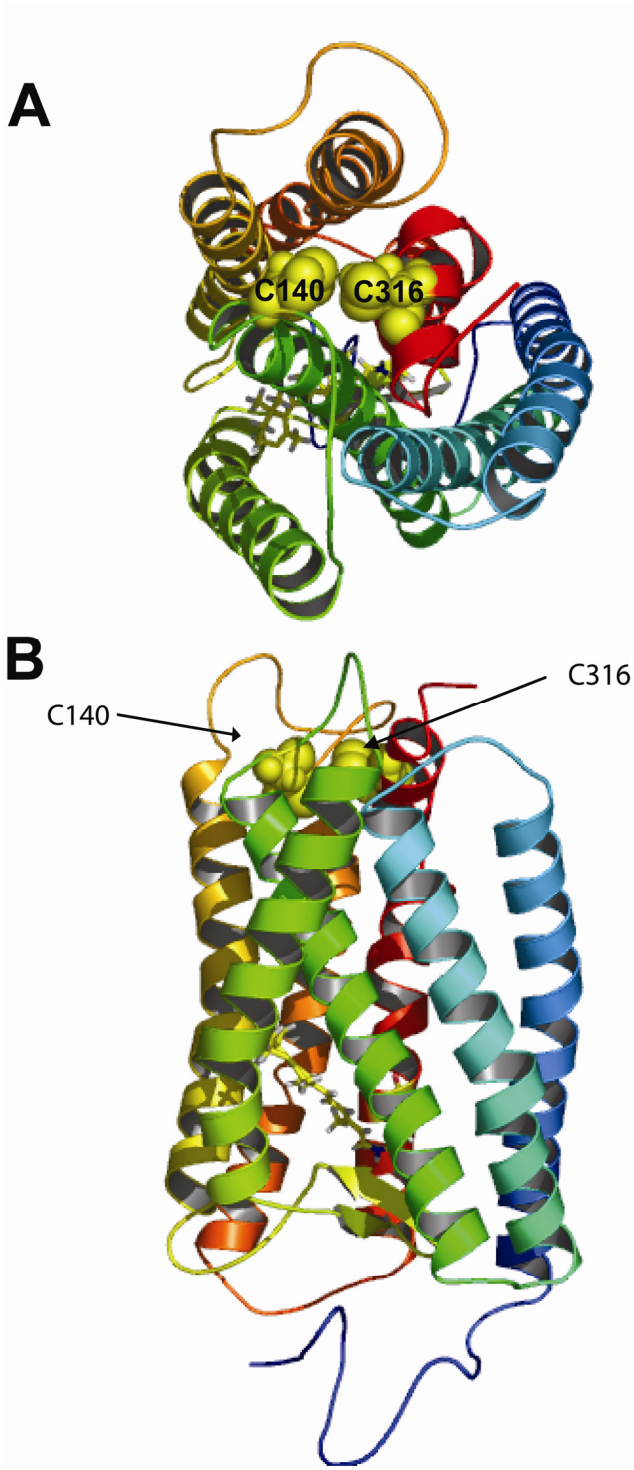


Figure 4.7. Model of metarhodopsin II generated by Gouldson et al., [193]. A view of the cytoplasmic face of the metarhodopsin II model is shown in A and a view in the plane of the membrane is shown in B, with C140 and C316 rendered as space filled models colored yellow. Experimental suggests that HVIII may move towards HIII reducing the distance between C140 and C316

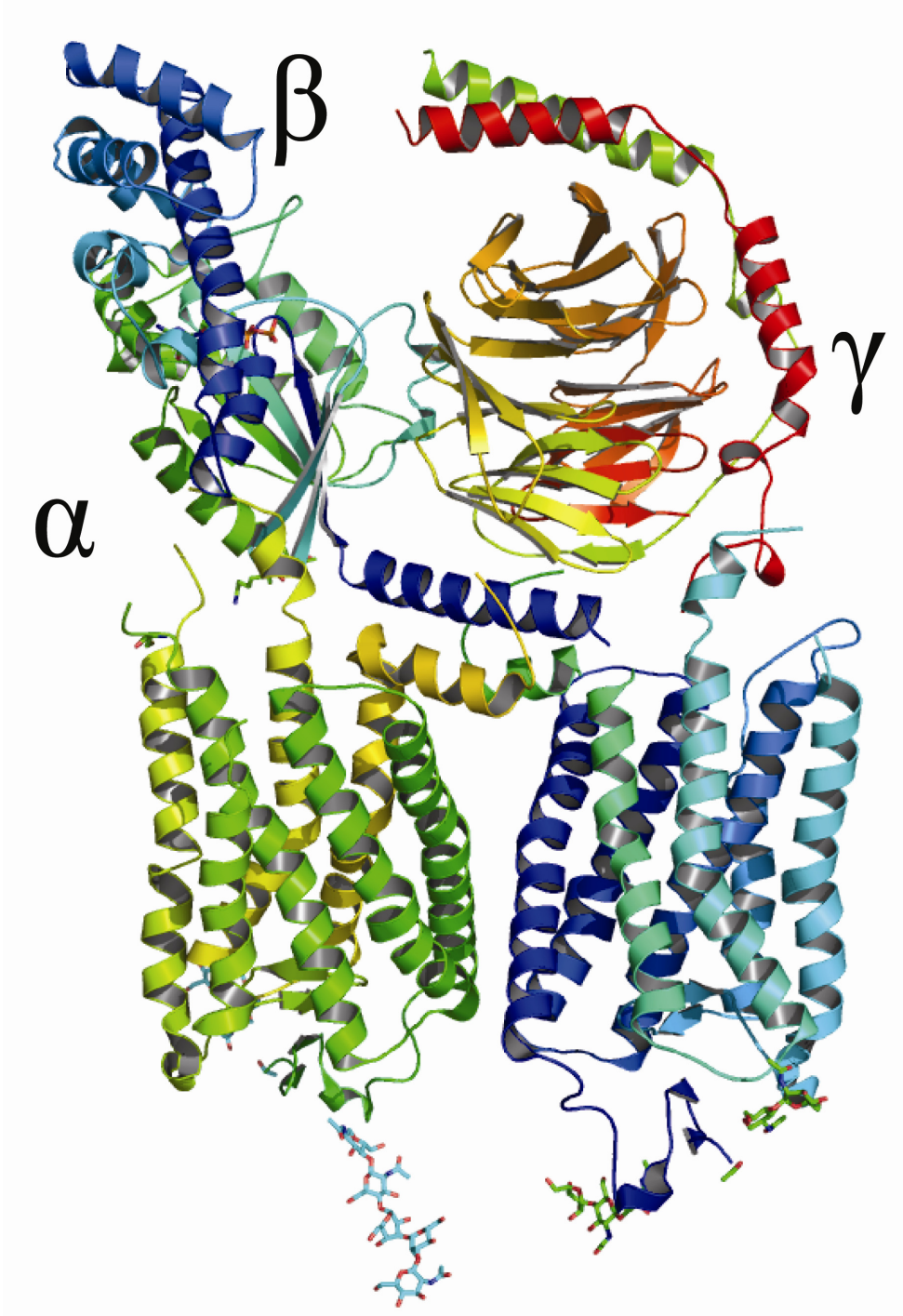


Figure 4.8 Model of interaction of heterotrimeric G-protein with a rhodopsin dimer. The structural model of the heterotrimeric G-protein (1GOT.pdb) has been docked by hand on the cytoplasmic face of the rhodopsin dimer present in the structure of the protonated Schiff base of photo-activated rhodopsin (2I37.pdb).

mediated by E134 and may involve the opening up of the cytoplasmic face of rhodopsin upon formation of metarhodopsin-IIb [45, 194]. In FTIR studies of 2D crystals of rhodopsin it was found that a high affinity C-terminal synthetic peptide of Gαt was able to bind to a photoactive species believed to be MIIa [97]. Metarhodopsin-II stabilization observed by peptides crosslinked at C140 or C316 could be different isospectral metarhodopsin-II species, which may also be consistent with a previously proposed two site sequential fit mechanism for G-protein activation [143]. We speculate that when the C-terminal Gα peptide is crosslinked at C316 via the peptide C-terminus, it might stabilize the more compact MIIa, whereas the peptide crosslinked to C140 via the peptide N-terminus could bind to and stabilize MIIb. Note that MIIb is thought to be the conformation that activates the G-protein. Considering the crosslinking results of Cai et al., [115], the fluorescence quenching results of Janz and Farrens [118] and our chemical crosslinking results together, it is sufficient and it may be necessary for the N-terminus of the C-terminal Gαt 340-350 peptide tail of transducin to bind near C140 on helix 3, when C-terminal Gαt peptides stabilize the active MII conformation of the receptor.

Recently a structure of photo-activated rhodopsin dimer has been published by Salmon et al., [96]. The photo-activated receptor was found to contain a deprotonated Schiff base which is present in both MIIa or MIIb. The structure of the heterotrimeric G-protein transducin (1GOT.pdb) was docked by hand onto the cytoplasmic structure of a dimer of rhodopsin present in the structure of the photo-activated deprotonated Schiff base. Interestingly it is possible to position the amino terminal portion, $^{-11}$IKE^{-9}, of the C-terminal tail of the alpha subunit of transducin near C140 consistent with the crosslinking results presented here, which then leads to the subsequent positioning of the C-terminal

tail of the gamma subunit of transducin near the C140 on the second rhodopsin in the dimer (shown in Figure 4.8). The modeling of the heterotrimeric G-protein on the crystallographic dimer of rhodopsin is consistent with biochemical data indicating that the alpha and gamma subunits bind to a shared region on rhodopsin [106, 135, 136].

Materials and Methods

Rod Outer Segment Preparation

Rod outer segments were prepared as previously described in chapter 2.

Peptide Synthesis

Synthetic peptides were prepared using a Rainin Protein Technologies PS3 peptide synthesizer and standard Fmoc chemistry. The amino acid analog, Fmoc diamino propionic acid (Dpr) (Advanced Chem Tech) was immobilized on PAC resin (Perceptive Biosystems) in a separate reaction, as recommended by the resin supplier. Iodoacetate was added to both reactive amines of peptide VLEDLRD(Abu)GL(Dpr) using SIA (N-Succinimidyl iodoacetate) (Pierce) following the manufacturers directions . Biotinyl-succinimidyl ester (B-SE) (Molecular Probes) was added to the N-terminus of peptide VLEDLRD(Abu)GL(Dpr), while the peptide was on the wang resin. After the biotinylated peptide was cleaved from the resin (in 95% TFA, 3% water, 2% thioanisole), iodoacetate succinimidyl ester (S-IA) was added to the free amine on the side chain of Dpr to yield the final product, biotin-VLEDLRD(Abu)GL(Dpr)-IA (B23S-IA). Maleimide succinimidyl ester (SMCC) was added to the amino termini of the peptide VLEDLRD(Abu)GL(Dpr) while it was immobilized on Wang resin. Peptide Maleimide-

VLEDLRD(Abu)GL(Dpr) (M23S) was cleaved form the resin (in 95% TFA, 3% water, 2% thioanisole). All synthetic peptides were purified by RP-HPLC. Purified peptide masses and sequences were confirmed by MALDI-TOF mass spectrometry (Bruker Biflex III) and LC MS/MS mass spectrometry (Agilent XCT Ultra). Stock solutions of the peptides were prepared by dissolving the peptide in buffer B (50 mM HEPES, 100 mM NaCl, 1 mM $MgCl_2$) at pH 8, immediately prior to use.

Chemical Coupling of Peptides to Rhodopsin

Two reactive cysteines C140 and C316 are solvent-exposed on the cytoplasmic surface of rhodopsin in intact disk membranes. Peptides were crosslinked selectively to C140 or C316 on rhodopsin in rod outer segment membranes after the plasma membranes were disrupted by exposure to low salt conditions. To selectively couple peptide to C140, C316 was blocked by first reacting it with 4,4'-dithiodipyridine (DTP) [177, 179-181, 195-198]. Rod outer segment stock solutions were pelleted and resuspended in 10 mM Tris pH 7.2, to break plasma membranes by osmotic shock and dissociate disk membranes in the low salt, and adjusted to a final concentration of 20 μM rhodopsin. A 4 fold molar excess of DTP was added to the rhodopsin sample being stirred in a temperature controlled cuvette holder (Quantum Northwest). The thiopyridone reaction product was monitored at 30 second intervals in a Cary-50 UV Vis spectrophotometer (λmax 323nm, ε7800). Following blocking of ~one cysteine per rhodopsin, the ROS membranes were washed 3x by centrifugation to remove unreacted DTP. Peptide IA-VLEDLRD(Abu)GL(Dpr) or Biotin-VLEDLRD(Abu)GL(Dpr)-IA were added in a 30 fold molar excess and allowed to couple to rhodopsin overnight at

4ºC. Excess peptide was removed from the samples by centrifugation, followed by resuspension in buffer B at pH 8 prior to spectroscopic analysis.

Light Titration Experiments

Rhodopsin rod outer segment membranes that were used in light titration experiments were suspended in buffer B and the final pH adjusted to pH 8.0. For each light titration experiment, an aliquot of rhodopsin was bleached with a series of millisecond flashes with orange light from a xenon flash lamp filtered through an OG515 long pass filter at 50 second intervals, and differential absorbance changes were measured using a dual wavelength spectrophotometer (shimadzu UV 3000) during each interval. Each flash bleached ~8% of the rhodopsin. The appearance of metarhodopsin-II was detected by monitoring the difference in absorbance between 390 nm and 417 nm (390-417) [100] , using an Olis/Shimadzu UV-3000 dual wavelength spectrophotometer, equipped with a temperature controlled cuvette holder. All light titration experiments were performed at 4 ˚C and the sample compartment was purged with dry nitrogen gas.

Difference Absorbance Spectral Measurement and Analysis

Absorbance spectra of rhodopsin in native membrane suspensions with and without peptide crosslinking were measured in a Cary 50 spectrophotometer with a temperature controlled sample holder and a special Cary detector assembly that was mounted directly behind the cuvette in the sample compartment, designed to capture a large fraction of the light scattered by the turbid samples. Rhodopsin samples were placed in the temperature controlled sample holder and the temperature was allowed to equilibrate at 1˚C at pH 8.0 while purging the sample compartment with dry nitrogen.

Spectra of unactivated rhodopsin were measured and then samples were illuminated with >500 nm light from a Fiber Photics Illuminator 150 for 10 seconds, using an OG515 long pass filter and fully bleached absorbance spectra were acquired. The pH of the samples was measured following recording of spectra.

Mass Spectrometry

The presence of chemically crosslinked peptides linked to rhodopsin was confirmed by mass spectrometry. Chemical crosslinking to intact rhodopsin was detected by MALDI-TOF mass spectrometry of intact rhodopsin [150]. Following chemical crosslinking an aliquot of rhodopsin-containing membranes were pelleted and resuspended in neat formic acid, diluted 10 fold in 50% acetonitrile, spotted on a MALDI target, mixed with 2,5-Dihydroxybenzoic acid matrix (Bruker Daltonics), mass spectra were measured in linear mode. Following chemical crosslinking of peptide B23S-IA to C316,(5μM rhodopsin and 5μM peptide in 20mM Hepes, 150mM NaCl, pH 7.5, stirred on ice for 1hr in the light) the rhodopsin was chemically cleaved with CNBr as described below and analyzed by MALDI-TOF mass spectrometry [156]. For cleavage the rhodopsin was solubilized in 1% LDAO and reduced and alkylated by incubation with 20mM DTT for one hour at room temperature followed by one hour incubation with 100mM iodoacetamide wrapped in foil. Following reduction and alkylation the samples were cleaved with CNBr (ICN biomed) by first precipitating with TCA (Fisher) to remove lipids and then resuspending and washing in ethanol 3x to remove excess reagents. Rhodopsin samples were then dissolved in a minimum of neat trifluoroacetic acid and cleaved with the addition of 500x molar excess CNBr in 70% trifluoroacetic

acid. The cleavage reaction was terminated by diluting 10x with water, freezing and lyophilizing to dryness. Samples were resuspended in water and lyophilized to dryness three times to remove excess trifluoroacetic acid and cyanogen bromide. Biotinylated peptides were enriched after washing off free peptide before and cleavage, following the method of Girault et al., using magnetic streptavidin beads (Dynabeads M-280) prior to MADLI-TOF mass spectrometric analysis [199]. A dilution series of the digest to be analyzed was made in 20/80 water/acetonitrile before mixing 1:1 to 3:1 with saturated MALDI matrix in 20/80 water/acetonitrile (α-cyano-4-hydroxycinnamic acid). Typically, 0.1 to 0.3 μL of matrix/sample mixture was spotted. Rhodopsin peptides derived from CNBr digest of rhodopsin were analyzed by LCMS on the Bruker microTOF as previously described in chapter 3.

CHAPTER 5

ANTIBODY IMPRINTING OF G-PROTEIN COUPLED RECEPTORS.

Introduction to Antibody Imprinting

Antibody imprinting involves the mining of information about the structure of the antigen present in an antibody. Antibodies recognize the interactive surface features of a protein antigens called epitopes. Such epitopes are comprised of consecutive stretches of amino acid residues in a protein or in a discontinuous epitope, residues that are in close spatial proximity as a result of the folding of a protein, but do not represent consecutive residues in the primary sequence of a protein. Antibodies that recognize discontinuous epitopes contain information about the spatial proximity of residues in the native folded protein or alternative folded conformation of a native protein.

The antibody residues that impart specificity, mediating antigen binding are collectively referred to as the paratope. Antibody imprinting provides a method for gathering and interpreting the structural information present in the antibody paratope. The paratope is structurally complimentary to the antigen epitope and thus the paratope contains information about the antigen, much like the fossilized foot print from a dinosaur contains information about the foot of the dinosaur. Filling in the imprint of the foot print of the dinosaur allows for detailed inspection of the shape and structure of the ancient foot. Similarly filling in the antigen imprint on the antibody by selecting peptides from random libraries allows the detailed inspection at the molecular level of shape,

charge, and polarity of the antigen epitope. The antibody imprinting method involves the selection of peptides binding to the antibody that mimic the residues on the antigen that comprise the epitope. The antibody epitope is recovered by aligning the amino acid sequences of the mimetic peptide onto the primary amino acid sequence of the antigen. In addition, determination of the 3D conformation of the mimetic peptides when bound to the antibody by x-ray crystallography [176] or NMR [200] can provide detailed structural information on the folding of the antigen epitope surface and this may facilitate improved modeling of the antigen epitope conformation. In cases where antibodies have been or can be selected to stabilize normally transient conformations of a protein, antibody imprinting may allow structural characterization of transient protein conformations or protein features that have eluded crystallization [68, 176, 201].

In previous work, the antibody imprinting technique has been used to identify a consensus peptide sequence that mimics a discontinuous epitope on the surface of the transmembrane host defense protein flavocytochrome b [200-202] and validate consensus sequences derived from phage display analysis of anti-actin antibodies with surface features revealed in the x-ray crystal structure of G-actin. In one case the consensus epitope peptide selected with anti-flavocytochrome antibody 44.1 was mapped to two discontinuous regions of the protein that are folded closely together on the intact protein, but are 150 residues and two transmembrane spans apart in the protein primary sequence. The structure of the antibody bound peptide was determined by transferred NOESY NMR studies and provided constraints that allowed modeling of the native epitope [200].

Bailey et al. initiated antibody imprint studies of light-excited rhodopsin in order to probe its normally transient meta-stable conformations [68]. This work utilized a

panel of monoclonal antibodies developed against light exposed rhodopsin; all of the antibodies were assayed for the capacity to discriminate between metarhodopsin I and metarhodopsin II and were examined by antibody imprinting. Included in this library was antibody K42-41L, a murine monoclonal antibody first described by Adamus, et al. [203]. Adamus, et al., concluded that the primary contribution to the epitope of K42-41L was contained within the C3 loop of rhodopsin (residues 230-252) by showing that a peptide fragment representing the C3 loop effectively competed with rhodopsin for binding to K42-41L. In contrast, peptides representing the other surface loops of rhodopsin did not show detectable competitive activity for this antibody. The interaction of K42-41L with light-excited rhodopsin was also examined, providing preliminary evidence that this antibody inhibited formation of metarhodopsin-II and stabilized metarhodopsin I [68].

Bailey et al. employed two different random peptide libraries displayed on phage to select small peptides that bind to K42-41L [68]. Ninety phage clones were selected from the J404 9-mer peptide library [204] and sequenced. Sequence alignment of the bound clones yielded the consensus sequence peptide TGALQERSK. This peptide was found to compete effectively with rhodopsin for binding to K42-41L but differed very substantially in sequence from the C3 surface loop sequence of rhodopsin. The x-ray crystal structure of the consensus mimetic epitope peptide bound to antibody K42-41L and a model for the role of the C3 loop in the metarhodopsin I-metarhodopsin II transition have been proposed and was reported by Piscitelli et al., [176] and are presented below.

The successful application of antibody imprinting to flavocytochrome b and bovine rhodopsin were encouraging and stimulated further pursuit of immunological reagents to be used in antibody imprinting studies of the conformational epitopes present on rhodopsin following receptor activation. Given the transient nature of the meta-stable species of rhodopsin, more recent efforts have been made to select single chain Fv (scFv) antibodies from random libraries that bind to and stabilize the meta-stable light stimulated rhodopsin species. The screening of a large group of monoclonal antibodies was also undertaken in hopes of finding antibodies that bind to and stabilize the distinct metarhodopsin species preferentially.

Single Chain Fv Selection

An alternative to generation of monoclonal antibodies in mouse spleen cells is the selection of single chain Fv (scFv) antibodies from random libraries displayed on the pIII protein of M13 phage, in a similar fashion to the selection of phage displayed random peptides. Single chain Fv antibodies are comprised of variable heavy and variable light chain domains of an antibody typically linked together in a single chain by a poly-glycine amino linker sequence. The scFv are displayed as a fusion to the amino terminus of the minor coat protein pIII. The pIII protein of the M13 phage is required for bacterial infection and the display of large fusion proteins like scFV on the pIII reduces or completely abolishes phage infectivity.

A method for displaying large fusion proteins on the pIII protein is to construct the scFv library in a phagmid which then requires the use of a helper phage when amplifying the library during round of affinity selection, amplification, and screening. A

phagemid is simply a plasmid that bears a phage origin of replication allowing processing of the phagemid DNA during phage amplification in infected bacteria, allowing for the generation of pIII-scFv fusion proteins. The use of a scFv phagemid library requires the use of helper phage which, following bacterial super-infection, provides wild-type pIII proteins for assembly into the phage progeny resulting in phage displaying pIII-scFv and wild-type pIII allowing the scFv-carrying phage to be infectious.

The scFv library used here is the ETH-2 human phagemid library. The ETH-2 library is a modified version of the phage library described and used by Pini et al., [205]. The diversity of any phage library is limited by the transformation efficiency in the initial generation of the library. Greater diversity is achieved in the ETH-2 library by combining four sub-libraries that are generated by independent electroporation steps to reduce the effects of limited electroporation efficiency which result in low diversity libraries. Three antibody germ-line segments were used in the creation of the ETH-2 library, DP-47 for the heavy chain and DPK-22 and DPL-16 for the light chain [206]. Diversity was engineered into the scFv library heavy chain complementarity determining region 3 (CDR3) by addition of 4 to 6 random residues at the following position $^{92}CAR(X)_{4\text{-}6}FDY$ (colored blue in Figure 5.1). Additionally six amino acid positions (32, 50, 91, 93, 94, and 96) in the CDR3 of the light chain were randomized colored green as shown in Figure 5.1.

The ETH-2 scFv library was screened for scFv that bind to light-activated rhodopsin in native rod outer segment disk membranes at low pH where metarhodopsin II is stabilized or at high pH where metarhodopsin I is stabilized, as depicted schematically in Figure 5.2. We biotinylated bovine rhodopsin in rod outer segment disk membranes

with a disulfide cleavable linker EZ-Link Sulfo-NHS-SS-biotin and attached the rhodopsin to the wall of plastic tubes by interaction with pre-absorbed Neutavidin (Pierce). Bovine rhodopsin bound to the tubes was exposed to light at either pH 6 or pH 8 and an aliquot of naive scFv library was added and incubated with the photo-activated rhodopsin. Following the removal of unbound scFv by a series of washes, the bound

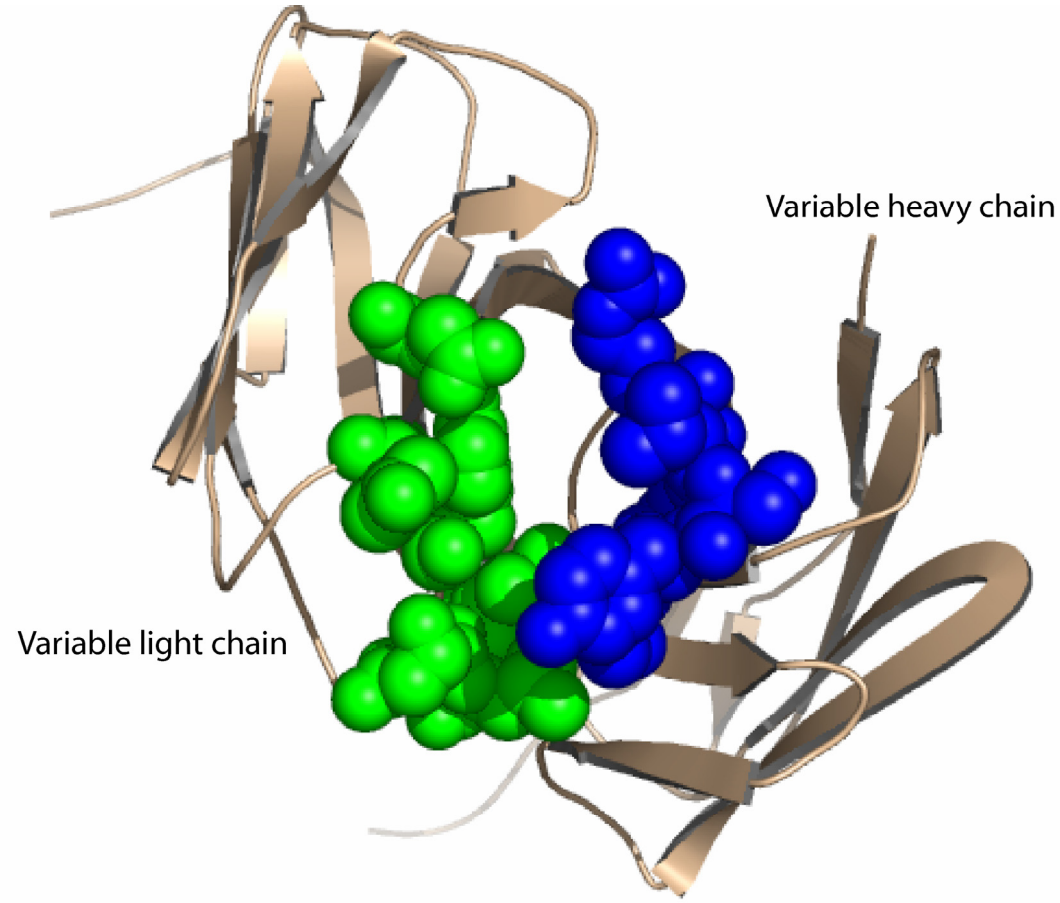


Figure 5.1. Positions on the single chain Fv that are randomized in generation of the ETH-2 library are shown as space filled residues. The green space filled residues are positions on the light chain of the scFv that are randomized and blue spheres are positions on the heavy chain that are randomized in the library construction.

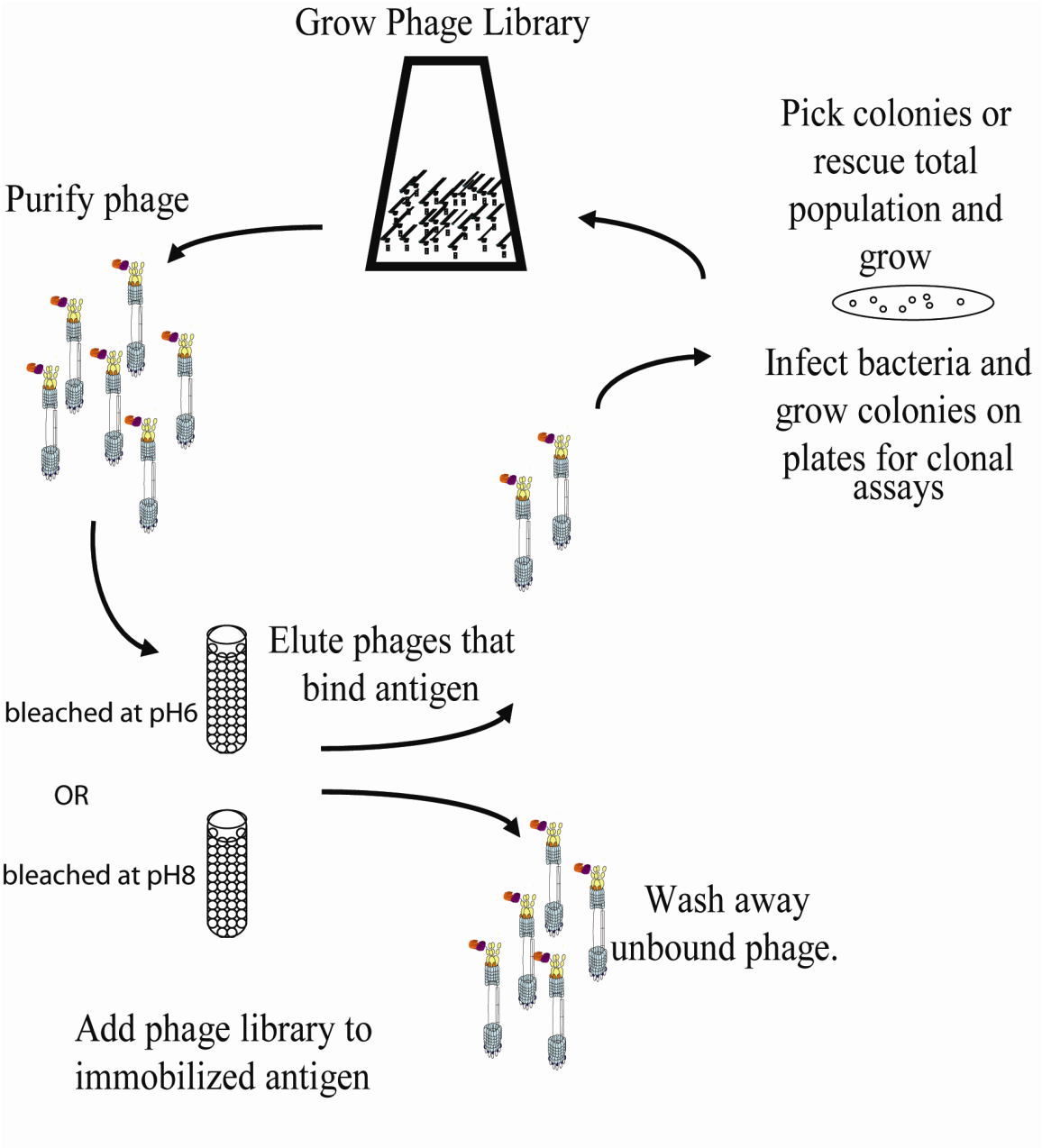


Figure 5.2. Scheme for scFv selection with immobilized photo-activated rhodopsin native in rod outer segment disk membranes as the "bait" protein. Three rounds of affinity selection were performed, immunotubes were coated with rhodopsin in native rod outer segment disk membranes and then an aliquot of naïve phage library was incubated with the immobilized biotinylated rhodopsin bound to neutravidin coated plastic tubes, weakly bound and unbound phage were then washed away and binders were eluted by cleavage of a disulfide biotin linker (Pierce EZ-Link Sulfo-NHS-SS-biotin). The eluted phage were then used to infect *E. coli* cells, the phage population was grown for amplification of binders and prepared for subsequent rounds of selection.

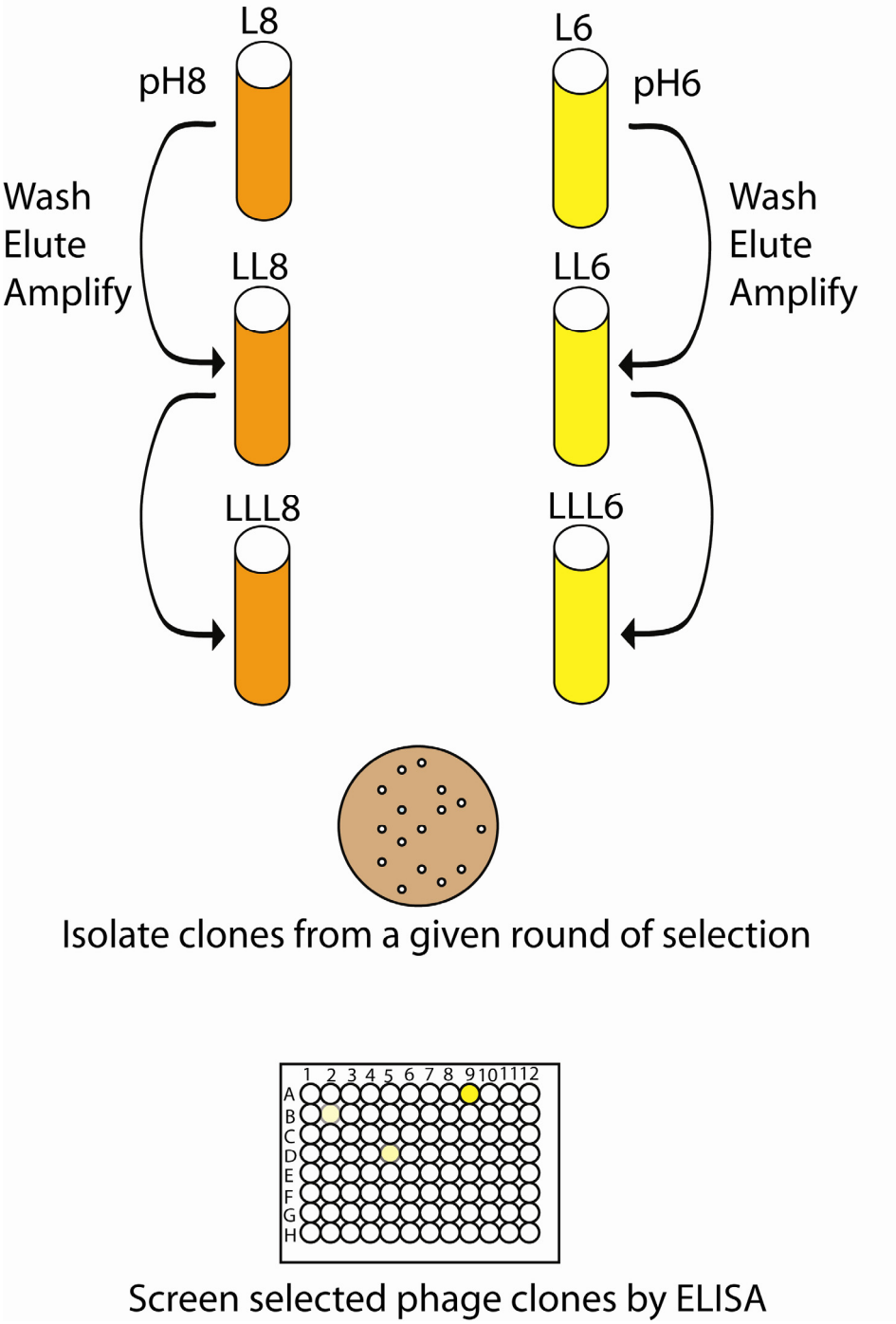


Figure 5.3 Schematic of scFv selection against immobilized bovine rhodopsin. Nunc immunotubes were coated neutravidin and exposed to biotinylated unactivated bovine rhodopsin in phosphate buffered saline at pH 6 or pH8. Three rounds of affinity selected against photo-activated rhodopsin were performed and the resultant scFv displaying phage clones were assayed for rhodopsin binding by ELISA.

scFv were eluted by cleaving the sulfhydryl liable linker holding the rhodopsin to the tube using 50 mM DTT. The rhodopsin scFv complexes were then used to infect TG-1 *E. coli* and the selected population of phage was amplified for use in the next round of affinity selection. Three rounds of affinity selection of scFv against light exposed rhodopsin were performed at pH 6 and pH 8 as depicted in Figure 5.3. Following affinity selection, phage clones were screened for binding to light exposed rhodopsin by ELISA (as shown in Figure 5.4). Following the ELISA screen of light exposed rhodopsin

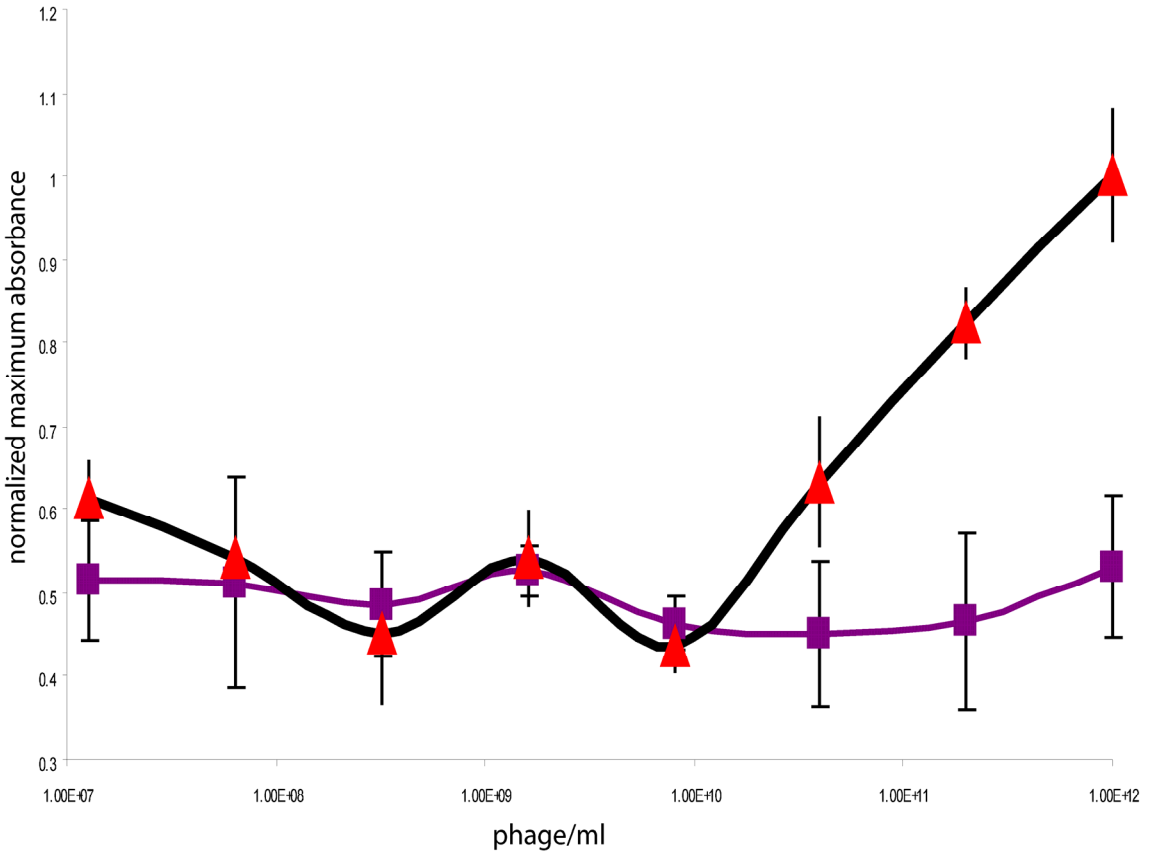


Figure 5.4. ELISA using HRP-anti-M13 antibody showing the scFv LLL6A9 clone displayed on phage binding to light exposed rhodopsin preferentially relative to bovine serum albumin. Binding of scFv was measured to light exposed bovine rhodopsin (red triangles) or bovine serum albumin (blue squares). Phage displaying scFv from the third round of affinity selection binds to rhodopsin preferentially relative to BSA.

binders, the variable regions in the scFv were sequenced and attempts were made to express the rhodopsin binding scFv. The titers of phage were assayed following each round of selection, 10^2 phage/ml were present following the first round of selection. The titer increased to 10^4 phage/ml following the third round of selection. Following three rounds of selection ScFv displaying phage clones were assayed by ELISA and this revealed that there were few candidate clones that showed significant binding to rhodopsin. However one clone of interest that showed binding to light exposed rhodopsin was found and called LLL6A9. This phage clone was found among scFv present following three rounds of selection against light exposed rhodopsin in buffer at pH 6 (see Figure 5.3). ScFv LLL6A9 was assayed by ELISA for the ability to bind to light exposed rhodopsin relative to binding to bovine serum albumin (BSA) shown in Figure 5.4. Phage clone LLL6A9 bound to bleached rhodopsin preferentially relative to BSA but showed only modest binding affinity given detection of binding required high numbers of phage greater than 10^{10} per ml (Figure 5.4). Many attempts were made to express soluble scFv LLL9A6 by infecting HB 2152 *E. coli* cells. The scFv construct in the ETH-2 phagemid library contains an amber stop codon, which in suppressor cells such as TG-1 *E. coli* will be read through and scFv pIII fusion proteins are produced, however in non suppressor HB2152 *E. coli* the amber stop codon is recognized and a scFv fusion proteins are not generated. A soluble scFv is produced and should be targeted to the periplasmic space of the HB2152 *E. coli* cells. It would be desirable to pursue the scFv selection and expression with a more robust display system.

Monoclonal Antibody Screening

Given the difficulties in expressing selected scFv, we returned to screening hybridoma cell culture supernatants from a large number of monoclonal antibody cell cultures for antibodies with interesting binding properties. A panel of hybridoma cell lines expressing anti-rhodopsin antibodies were acquired and screened for metarhodopsin I/II binding as part of a collaborative effort with the laboratory of Dr. Paul Hargrave. The properties of some these antibodies are shown in table 5.1. All antibodies were assayed for the ability to bind to immobilized dark or light exposed rhodopsin and for binding

Antibody ID	Rhodopsin competition[a]	Peptide competition[a]	Western Blot[a]	Meta species discrimination	Binding Bleached or Unbleached rhodopsin
451-68	+	I-II,III-IV,323-348	+	Meta I (pH 7.4)	Both(both)
507-12	+	(III-IV), 323-348	+	Meta I (pH 6.0 and pH 7.4)	Both (light)
423-55	+	III-IV,323-348	+	None	Both(dark)
464-16	+	2-32,II-III	+	Meta I	Both(light)
441-16	+	ND	+	Meta I	Both
541-27	+	2-32, (IV-V,V-VI)	**NT**	Meta I (pH 7.4 but not pH 6.0)	Both
253-41	+	ND	**Weak**	None	Both

Table 5.1. Analysis of a panel of mouse anti-rhodopsin antibodies. A panel of approximately 100 monoclonal antibodies was screened for the capacity to bind preferentially to activated (bleached) or unactivated (unbleached) rhodopsin by ELISA. Additionally the antibodies were assayed for the ability to shift the MI-MII equilibrium in the "extra meta II assay" as described in the materials and methods. [a]Assays performed in the lab of Paul Hargrave
NT= not tried

being abolished by addition of soluble rhodopsin in a competitive binding assay. All antibody binding was able to be competitively inhibited. The epitopes of the antibodies were coarsely screened in peptide competition assays. The peptide competition assays tested soluble synthetic peptides, whose sequences were derived from the cytoplasmic loop amino acid sequences of rhodopsin, for their ability to abolish antibody binding.

Antibody activity was assayed by immunoblot; all of the antibodies assayed were capable of recognizing rhodopsin on a blot. The antibody binding to bleached or unbleached rhodopsin was assayed in the presence of high affinity analog peptide AcVLEDLRS(Abu)GLF, which stabilizes metarhodopsin II, to examine if any of the antibodies showed strong preference for metarhodopsin II over rhodopsin. Three of the antibodies, 507-12, 441-16, and 464-16 showed a distinct preference for binding to light-activated rhodopsin over unactivated rhodopsin by ELISA (data not shown). Lastly the antibodies were assayed for the ability to bind to and shift the metarhodopsin equilibrium employing the extra MII assay. Antibody 507-12 was able to shift the metarhodopsin equilibrium favoring the accumulation of metarhodopsin I (Figure 5.5 A). This antibody has been found to bind to the c terminal tail and weakly to the C2 loop of rhodopsin that connects helix 3 and 4 on the cytoplasmic face of the receptor, the end of helix 3 is thought to undergo a conformational rearrangement upon metarhodopsin formation thus further investigation of this antibody is advisable. Antibody 451-68 does not shift the MI/MII equilibrium, consistent with the ELISA results showing equal binding to bleached and unbleached rhodopsin (Figure 5.5B). Antibody 441-16 (Figure 5.5C) shifts the metarhodopsin equilibrium, reducing the amount of metarhodopsin II present. Interestingly antibody 541-27 when assayed at pH 6.0 as shown in Figure 5.5D does not

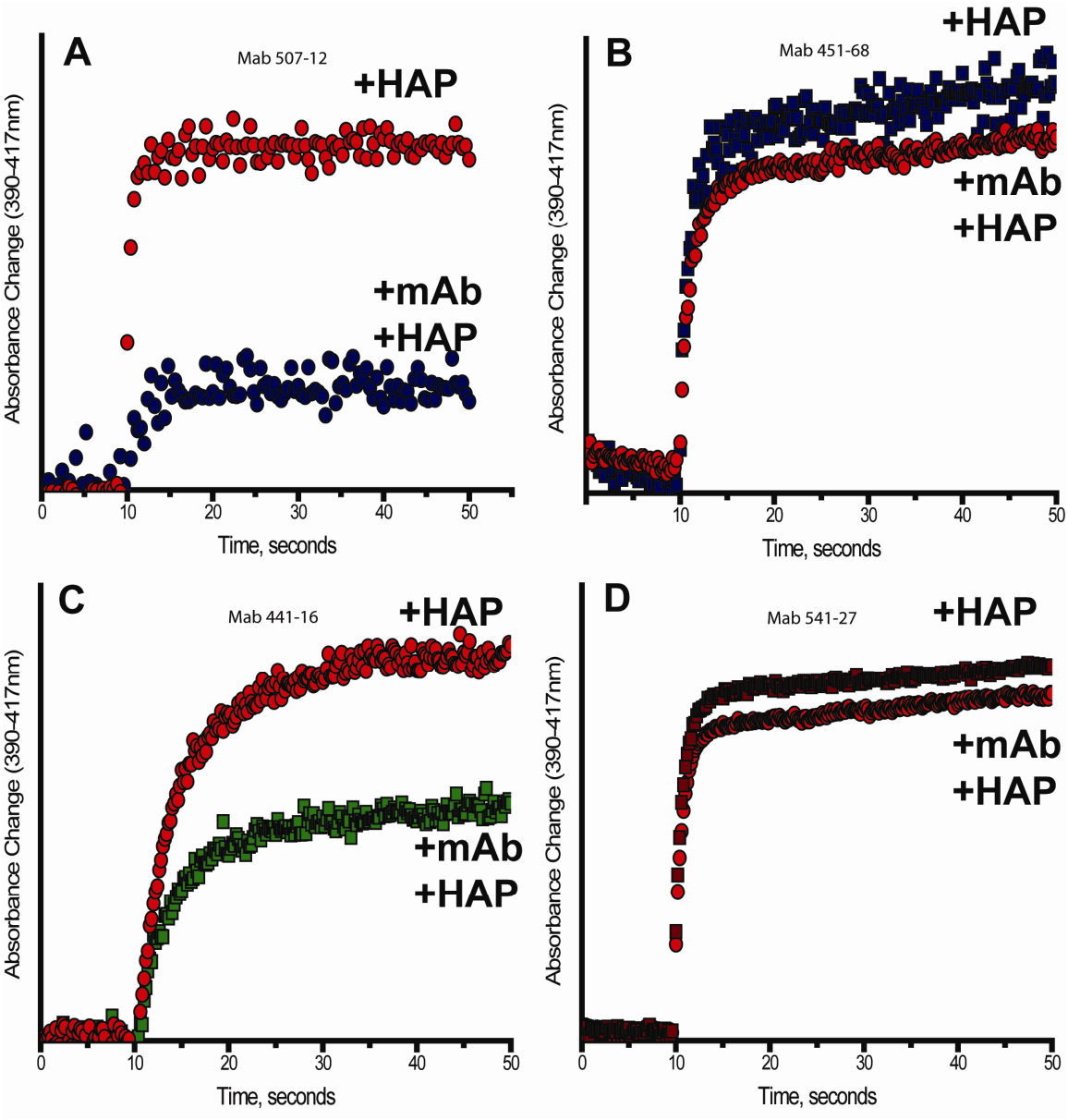


Figure 5.5. Extra MII assay of several anti-rhodopsin antibodies. A) Antibody 507-12 shifts the MI/MII equilibrium favoring the stabilization of metarhodopsin I at b pH 7.5 in the presence of high affinity peptide (HAP) Ac-VLEDLRS(Abu)GLF. B) Antibody 451-68 does not shift the MI/MII equilibrium at pH 6 and 2ºC. C) Antibody 441-16 shifts the MI/MII equilibrium favoring the stabilization of MI at pH 6 and 2ºC. D) Antibody 541-27 does not shift the MI/MII equilibrium at pH 6.0 and 2ºC.

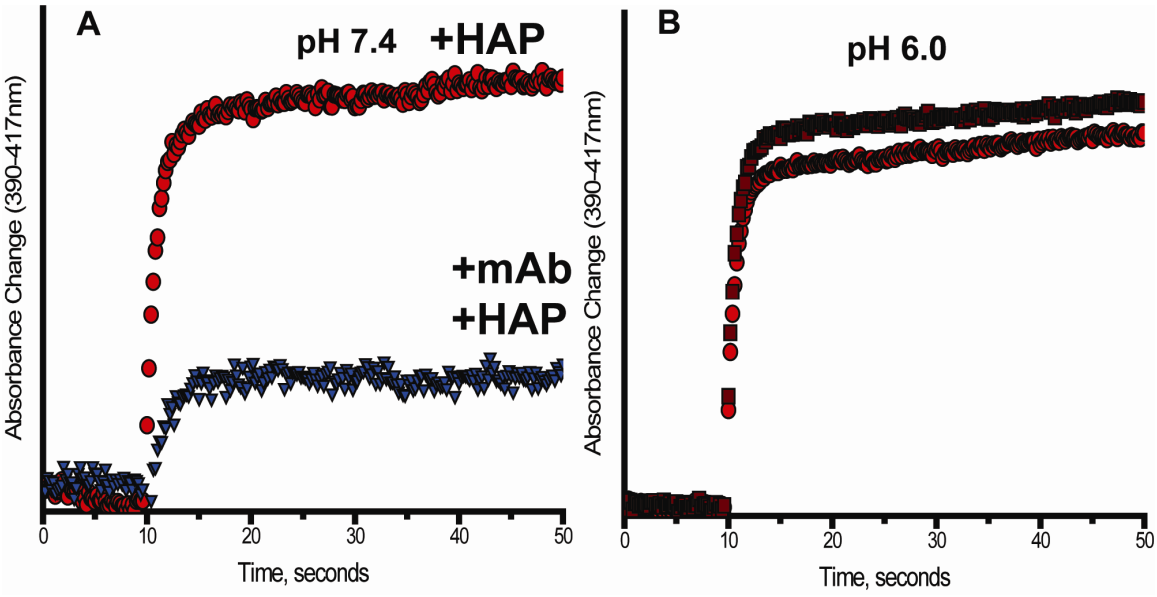


Figure 5.6. Antibody 541-27 shows discrimination between MIIa and MIIb. A) Antibody 541-27 is capable of shifting the MI/MII equilibrium favoring the stabilization of MI when metarhodopsin II is stabilized due to the presence of high affinity peptide derived form Gαt, B) however at pH 6 the antibody is not capable of shifting the MI/MII equilibrium.

appear to shift the metarhodopsin equilibrium, however when assayed at pH 7.4 and in the presence of metarhodopsin II stabilizing peptide antibody 541-27 appears to reduce the amount of metarhodopsin II stabilized by peptide (Figure 5.6).

Metarhodopsin II has been subdivided into the isospectral species metarhodopsin IIa and metarhodopsin IIb [45]. Metarhodopsin IIa is thought to form following retinal isomerization, expansion of the retinal binding pocket [45] and an internal proton transfer resulting in the neutralization of the Schiff base counter ion E113. Formation of metarhodopsin IIb is coupled to the uptake of a proton from the bulk solvent, and is thought to be associated with an opening up of the helical bundle at the cytoplasmic face, allowing the binding of the C-terminal tail of transducin or peptides derived from the C-terminal tail. The binding of antibody 541-27 to light-excited rhodopsin leading to a shift

in the MI/MII equilibrium in the presence of peptide but not at low pH suggests that additional elements are exposed upon peptide binding and the antibody 541-27 recognizes these regions and then shifts the MI/MII equilibrium reducing the amount of MII.

Structural Characterization of Antibody K42-41L with Mimetope Bound

Five crystal structures of dark-adapted rhodopsin have been determined [7-11], greatly enhancing our understanding of the inactive, dark-adapted state. Collectively, these structures provide a framework within which detailed conformational changes associated with formation of metarhodopsin-I and metarhodopsin-II may be addressed. Further, the structures imply that several elements on the cytoplasmic face of dark-adapted rhodopsin are flexible, including the C3 loop and the C-terminal tail. Portions of the C3 loop are disordered in three of the five structures reported to date [7, 8, 10], while the structures of Li et al. (PDB ID 1GZM) [11] and Okada et al. (PDB ID 1U19) show the C3 loop, but in two very different conformations. The C3 loop is "ordered" in these structures (1GZM and 1U19) but the B-factors for the C_α atoms are high (rising above 100 $Å^2$), suggesting that each of these models represents a family of closely related conformations, rather than a single, sharply defined structure. This data, together with site-specific spin labeling [69], suggests that the C3 loop and C-terminal tail are dynamic structural elements in the dark-adapted state. Dunker and coworkers [207, 208] have recently pointed out that cell-signaling proteins often interact through highly flexible regions which form well structured signaling complexes so that specificity can be

obtained without the requirement for forming extremely tight and slowly changing complexes.

A 5.5 Å electron crystallographic study of metarhodopsin-I has recently been published [209]. Comparison of this intermediate-resolution electron density map with the X-ray structures of dark-adapted rhodopsin shows that the transmembrane structure of metarhodopsin-I is quite similar to that of the dark-adapted ground state. Thus, it appears formation of metarhodopsin-I occurs without large rigid-body movements of the transmembrane helices, implying that the large conformational changes thought to accompany formation of metarhodopsin-II occur later in the photo bleaching process. The cryo-EM map shows clear density for most of metarhodopsin-I, image reconstruction from tilt series of 2D crystals provides much lower resolution for surface features than the transmembrane portions (due to the "missing core" of information from the incomplete tilt series). Structural information for metarhodopsin-II is more limited, though models have been proposed [86, 210]. These models are based in large part on site-specific spin labeling studies that demonstrate a substantial conformational change upon formation of metarhodopsin-II [70, 71, 90], but do not provide atomic resolution.

In this work we report further characterization of the interaction of antibody K42-41L with dark-adapted and light-excited rhodopsin. We show that K42-41L can discriminate between metarhodopsin-I and metarhodopsin-II, inhibiting formation of metarhodopsin-II while stabilizing metarhodopsin-I under several conditions. Chayne Piscitelli in the laborartory of Dr. Matrin Lawrence has determined the crystal structure of Fab K42-41L bound to a peptide that mimics the native epitope (TGALQERSK). Geometric constraints taken from the structure of the peptide in the K42-41L/peptide

complex were used to model the conformation of the native epitope on metarhodopsin I. This model suggests that K42-41L recognizes a different extended conformation of the C3 loop that is an accessible intermediate between the different compact conformations of the C3 loop seen in two crystal structures of dark-adapted rhodopsin (1GZM and 1U19). The discriminating ability of K42-41L indicates that the conformation of the C3 loop that binds K42-41L can be attained in either dark-adapted rhodopsin or metarhodopsin-I, but this C3 loop conformation must be significantly different from that required to form in metarhodopsin-II. Taken together, the structural and functional data indicate that the equilibrium between inactive metarhodopsin-I and active metarhodopsin-II conformation is dependent upon the conformation of the C3 loop as described further in the following text.

Conformational States of Rhodopsin and the Activity of K42-41L

Photoisomerization of the retinal cofactor causes rhodopsin to rapidly progress through a series of intermediates that leads to an equilibrium between metarhodopsin-I and metarhodopsin-II, as diagrammed in Figure 5.7A. The retinal is lost at longer times, resulting in the eventual appearance of the apoprotein opsin (Figure 5.7A). We find using ELISA assays, that the relative affinity of K42-41L for dark-adapted rhodopsin is quite similar to that for opsin, the original antigen used for production of K42-41L (Figure 5.7B). This suggests that the K42-41L epitope may be accessible in both opsin and dark-adapted rhodopsin.

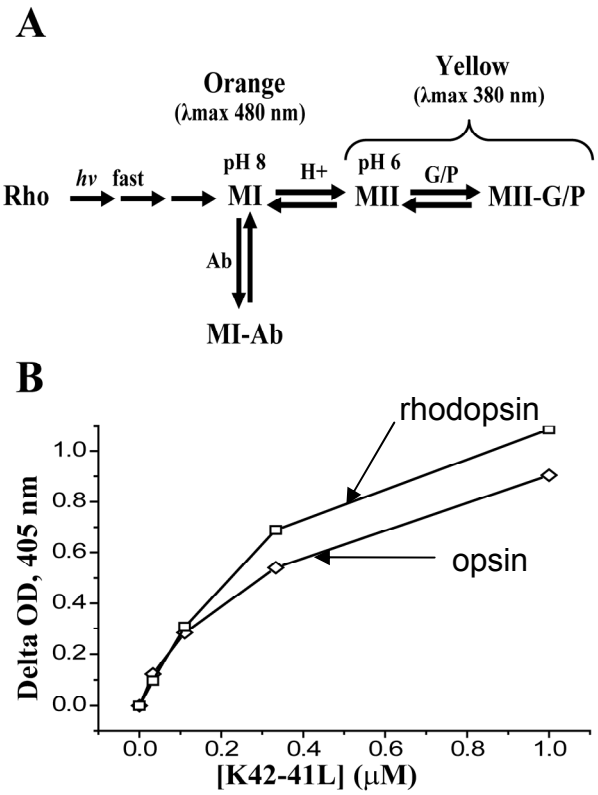


Figure 5.7. A) Schematic diagram of the light excitation pathway of rhodopsin. After exposure to visible light (hv) the pink-colored rhodopsin (Rho) undergoes a series of rapid (fast) conformational changes ending in an equilibrium mixture of the orange-colored metarhodopsin-I (MI) and yellow-colored metarhodopsin-II (MII). MII interacts with and is stabilized by the heterotrimeric G-protein (G) transducin or certain peptide segments of transducin (P) to form yellow-colored complexes (MII-G/P). The color changes of the different conformational forms of the protein allow spectroscopic monitoring of the photolysis of rhodopsin, the position of the equilibrium between MI and MII, and the formation of MII-G or MII-P complexes. The position of the MI/MII equilibrium is sensitive to pH and MI is favored under mild alkaline conditions (pH ~8) while MII is favored under mild acid conditions (pH ~6). MII slowly breaks down to orange-colored MIII, followed by formation of the colorless apoprotein opsin (chromophore-free) not shown in this diagram. Opsin production is too slow to contribute under the conditions studied in the present experiments, unless explicitly indicated. B) ELISA assay demonstrating that the K42-41L antibody recognizes the original antigen, opsin (open diamonds), and dark-adapted rhodopsin in native retinal rod disk membranes (open squares) with essentially equal affinity. The dark-adapted or fully light-bleached membranes were bound to ELISA plates, washed and presented with a dilution series of antibody K42-41L. Bound antibody was detected as described in the text.

Effect of K42-41L on the Metarhodopsin-I ↔Metarhodopsin-II Equilibrium

Antibodies that preferentially recognize a specific meta-stable state of rhodopsin are expected to influence the equilibrium between metarhodopsin-I and metarhodopsin-II. Metarhodopsin-I is orange in color while metarhodopsin-II and its complex with transducin or certain transducin peptides are yellow in color (Figure 5.7A). Thus the appearance of metarhodopsin-I and metarhodopsin-II, as well as the equilibrium between these two meta-stable species, can be followed spectrophotometrically. A convenient way to observe the metarhodopsin-I ↔ metarhodopsin-II equilibrium is to follow the change in absorbance between metarhodopsin-II (at 380 nm or with better signal to noise at 390 nm) and the nearby metarhodopsin-I/metarhodopsin-II isosbestic point at 417 nm [100]. The native rhodopsin-containing ROS membrane suspensions are optically turbid, however, the light scattering of the suspensions is quite similar at 390 and 417 nm. Thus, differences in light scattering between the two wavelengths due to slight settling of membranes or changes in membrane scattering observed after light excitation , are strongly attenuated in the ΔA(390 nm-417 nm) signals[102].

The conformational equilibrium of light-excited rhodopsin is sensitive to several factors that preferentially stabilize particular meta-stable states (Figure 5.7A), with pH ~8 stabilizing metarhodopsin-I and pH ~6 stabilizing metarhodopsin-II.
Binding of transducin peptides that mimic the C-terminal tail of the transducin alpha subunit [182], or the farnesylated C-terminal peptide of the transducin gamma subunit [111] stabilize metarhodopsin-II. In the absence of transducin or transducin peptide mimetics, a series of light flashes results in light-activated rhodopsin in which the

metarhodopsin-I↔metarhodopsin-II equilibrium greatly favors metarhodopsin-I, under typical assay conditions of pH 8 and 4 ^{o}C. As shown in Figure 5.8A the addition of the high affinity transducin α subunit C-terminal peptide analog Ac-VLEDLRSAbuGLF shifts the metarhodopsin-I↔metarhodopsin-II equilibrium, greatly favoring the formation of metarhodopsin-II. The complete transducin or other transducin peptides show similar effects, but with different affinities. Optical monitoring under conditions that may affect the stability of metarhodopsin-II is termed the "extra meta-II assay". In Figure 5.8A each flash excited approximately 8% of the total rhodopsin present and equilibrium is reached in about 40 seconds after each flash at 4 ^{o}C.

In order to examine the interaction of K42-41L with light-excited rhodopsin, the antibody was added to the extra meta-II assay. Addition of K42-41L to the peptide-stabilized extra meta-II assay, at a pH where MI is favored in the absence of peptide, (Figure 5.8A) resulted in a large decrease in formation of metarhodopsin-II. In a related version of the assay, shown in Fig. 5.8B, where metarhodopsin-II is stabilized instead by low pH (6.7) and the kinetics for the formation of metarhodopsin-II are much faster. Introduction of K42-41L into this low pH extra meta-II assay also results in a reduction in formation of metarhodopsin-II (Figure 5.8B).

The decrease in metarhodopsin-II could be due to several factors. K42-41L might possibly inhibit formation of metarhodopsin-I, and thus the subsequent formation of metarhodopsin-II (Figure. 5.7A), or K42-41L might preferentially stabilize metarhodopsin-I, resulting in loss of the meta-II signal. While the extra meta-II assay is very useful for measuring the kinetics of the light excitation process and for “light

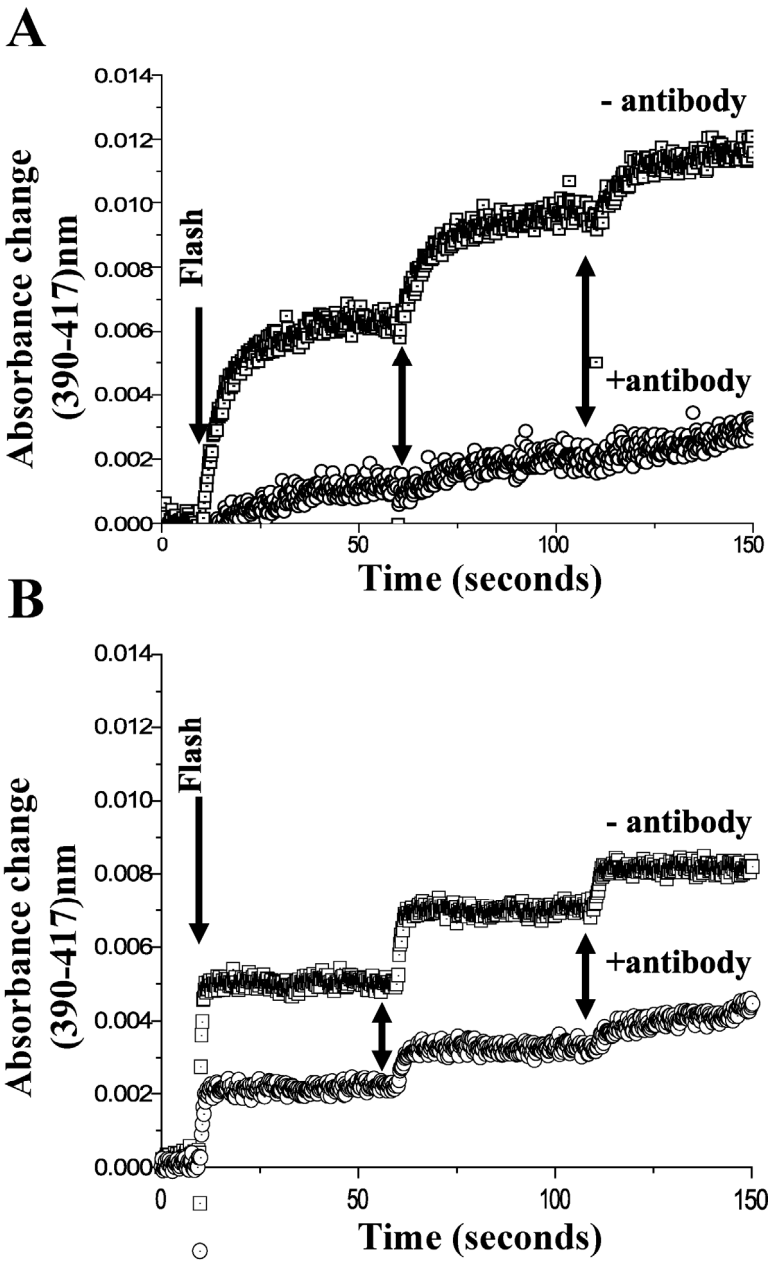


Figure 5.8. K42-41L inhibits formation of metarhodopsin-II. A and B demonstrate photolysis of rhodopsin upon a series of light flashes that bleach ~8% of the total rhodopsin per flash. Three consecutive flash intervals are shown, the arrows indicate the time points at which flashes were provided. The square symbols represent metarhodopsin-II stabilized in the absence of antibody K42-41L while circles represent samples incubated with antibody K42-41L. A) Metarhodopsin-II stabilized at pH 8 by the addition of the Ac-VLEDLRSAbuGLF peptide, a high affinity analog of the C-terminal tail of the transducin alpha subunit. B) Metarhodopsin-II stabilized at pH 6.7, as described in Experimental Procedures.

titration" of the amount of active metarhodopsin II, full absorption spectra are more definitive in confirming the identities of photolysis intermediates. However, the light scattering of the membrane suspensions tends to strongly distort the optical absorbance spectra. Thus dodecyl maltose, a mild detergent that dissolves the membrane, was addedto reduce light scattering and greatly improve the clarity of the optical spectra. However, the presence of dodecyl maltose increases the rate of the MI → MII reaction and shifts the MI/MII equilibrium towards metarhodopsin-II [123]. Under the conditions of this experiment (pH 7.2, 4°C, 2.0 mM DM) the absorbance spectra deconvolution into MI and MII components show that the equilibrium ratio of MII/MI is 1.2 (accounting for the higher extinction coefficient of MI). Under the same conditions in the native membrane the MII/MI ratio would be ~3-fold lower (i.e. 0.4) [100]. Deconvolution of the full light-dark difference spectra reveals components that are due to the loss of rhodopsin and the gain of metarhodopsin-I and metarhodopsin-II (Figure 5.9). The loss of rhodopsin absorbance at 498nm is evidenced by the negative lobe of the difference spectra in Figures 5.9A and 8C and the equilibrium ratio of metarhodopsin-I and metarhodopsin-II can be seen in the components of the absorbance spectra in Figures 5.9B and 5.9D. Addition of the K42-41L antibody causes a decrease in metarhodopsin-II, with an absorbance maximum near 380 nm and an increase in the formation of metarhodopsin-I, with a maximum near 480 nm (Figure 5.9B and 5.9D). Thus the deconvoluted difference spectra support the conclusions from the light titration experiments showing that K42-41L destabilizes metarhodopsin-II, pulling metarhodopsin-I into an antibody stabilized complex although

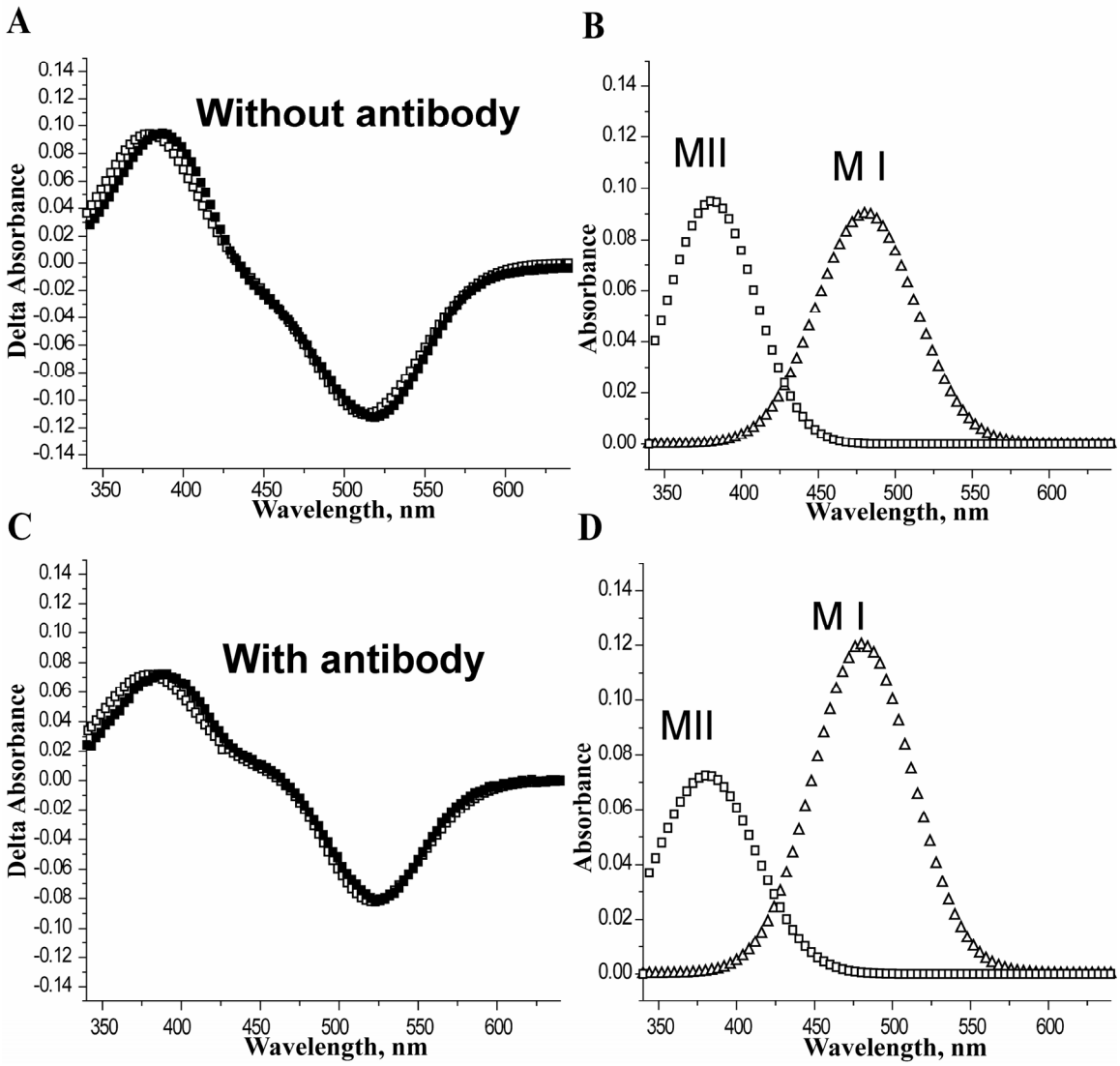


Figure 5.9. Effect of antibody K42-41L on the UV-Vis absorbance spectra of 3.2 μM light-excited rhodopsin in 2.0 mM dodecyl maltose solution, pH 7.2. A) Difference absorbance spectrum (dark-adapted rhodopsin minus bleached rhodopsin) without antibody K42-41L (solid squares) and simulated difference spectrum (open squares). B) Deconvoluted absorbance spectra. The triangles indicate MI and open squares indicate MII, the spectrum of the loss of dark-adapted rhodopsin was omitted for clarity. The sum of the three deconvoluted spectra (dark-adapted, MI and MII) fit the difference spectrum in A (solid squares). C) Difference spectra in the presence of 1.6 μM antibody K42-41L (solid squares) and the simulated difference spectra (open squares). D) Deconvoluted absorbance spectra showing an increase in the amount of MI and decrease in MII upon the addition of the antibody.

the effects are modulated by the presence of detergent sufficient to dissolve the membrane.

Adamus and coworkers [203] have demonstrated the reactivity of antibody K42-41L toward a peptide containing residues 230 through 252 of the C3 loop. The random peptide phage display epitope mapping data of Bailey et al. [68] indicated strongly that K42-41L epitope includes the rhodopsin residues Gln^{238} and Glu^{239}. FINDMAP, a computational epitope mapping algorithm designed to match target protein sequences to epitope peptides [68, 211], pointed to a lower scoring alternative mapping in the rhodopsin sequence, namely the 243-252 region of the C3 loop. We synthesized the alternate epitope candidate peptide T^{243}QKAEKEVTR^{252} and performed competition ELISA in order to determine if this peptide could compete for antibody binding to rhodopsin. In contrast to the consensus peptide used for co-crystallization (TGALQERSK), the peptide representing residues 243 through 252 of the rhodopsin sequence did not compete with K42-41L for binding to rhodopsin (data not shown), indicating that the epitope for K42-41L does not include the C-terminal portion of the C3 loop.

The Structure of K42-41L and the Epitope Mimetic, TGALQERSK

The ability of K42-41L to discriminate between metarhodopsin-I and metarhodopsin-II provides an impetus for structural characterization of the epitope mimetic peptide in complex with its antibody. Such studies could be expected to elucidate relationships between the light-induced conformational changes of metarhodopsin-I and metarhodopsin -II and the activity of K42-41L. In particular, these

studies would be expected to provide information on the conformation of the epitope peptide when it is bound to the antibody and delineate factors influencing the conformational features that are inconsistent with the formation of meta-II rhodopsin.

The amino acid sequence of the antibody K42-41L was determined by molecular cloning of the light and heavy genes form total RNA extracted from the mouse hybridoma cells expressing antibody K42-41L, as a necessary prelude to the interpretation of the x-ray electron density in terms of the polypeptide sequence. The amino acid sequence of the complementarity determining regions (CDR) for the K42-41L light and heavy chains (included in the PDB submission of the structure, 1XGY) reveals that the antibody has a relatively long CDR L1 loop (16 residues) and a short CDR H3 loop (8 residues). This combination of loop lengths is typical for antibodies raised against peptides, but is less commonly seen in antibodies against full-length proteins [212]. However, Adamus et al. previously showed that the C3 loop of rhodopsin contains primary determinants for recognition by K42-41L, and this combination of loop lengths would be consistent with an interaction between K42-41L and an extended conformation of the C3 loop [212].

The antigen-binding Fab fragment of K42-41L was purified and co-crystallized with the TGALQERSK peptide. The structure was determined at 2.7 Å resolution by molecular replacement with two copies of the Fab/peptide complex in the asymmetric unit C. Piscitelli in Prof Martin Lawrence's lab. There was clear electron density for kappa light chain residues 1 through 211 (chains A and C) and IgG1 heavy chain residues

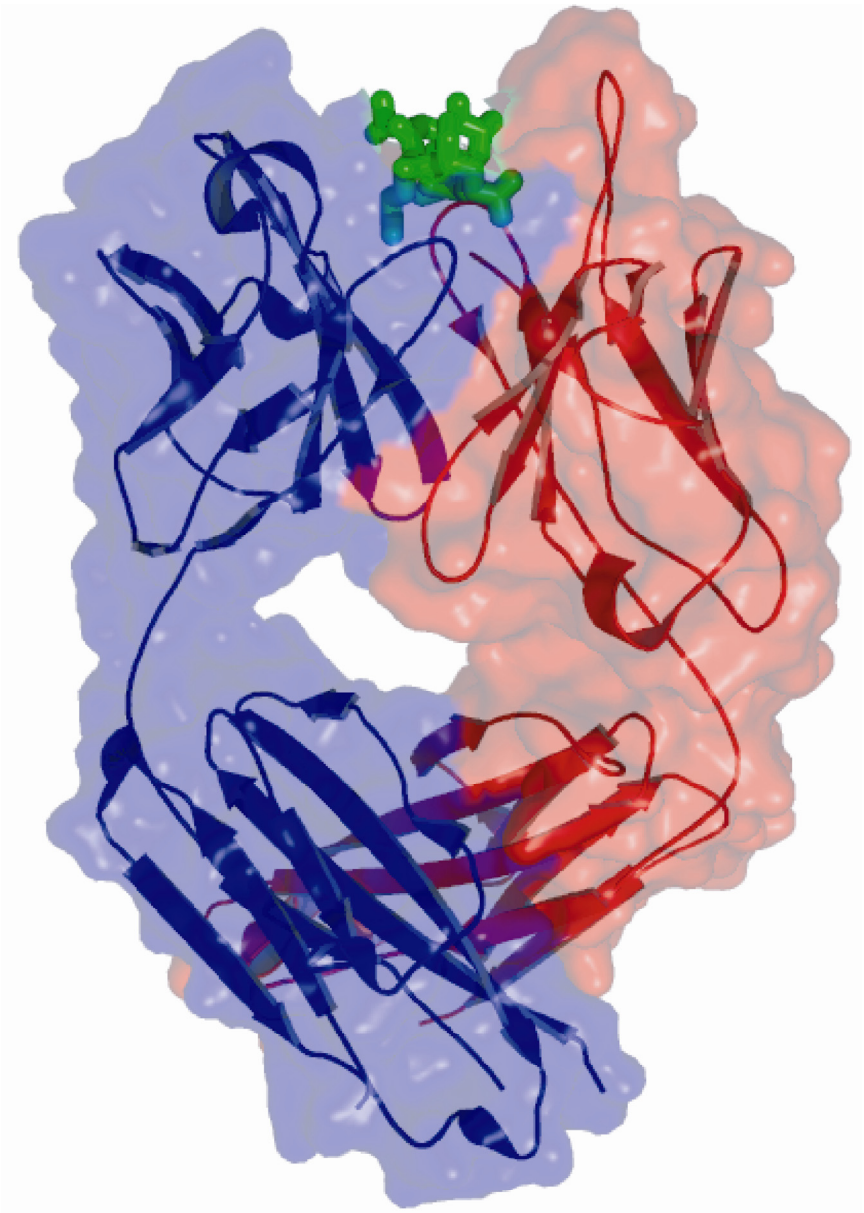


Figure 5.10. Co-crystal structure of Fab fragment derived from the monoclonal antibody K42-41L and epitope mimetic peptide TGALQERSK (1XGY.pdb). The co-crystal structure of antibody and peptide reveal that the peptide interacts with the antibody in the canonical antigenic recognition site located between the variable loops of the heavy (Blue) and light (red) chains of the Fab fragment. The last three residues of the consensus peptide are not resolved in the crystal structure and the consensus is weak in the phage selected peptide mimetic display epitope mapping for those three residues[68].

1 through 129 and 133 through 214 (chains B and D).

A striking feature of the antibody is a concave antigen recognition site (Figure 5.10). This feature is a direct result of the long L1 and short H3 loops of the antibody. Strong density for the first 6 residues (TGALQE) of the peptide was found within the concave antigen recognition site of each Fab. These residues are well ordered with a mean B-value of 32. The peptide adopts an α-helical structure of approximately one and a half turns with the first, second, fifth and sixth residues pointing down into the antigen binding site (T, G, Q and E), while the third and fourth residues of the peptide lie on the opposite side of the helix with their side chains solvent exposed (A and L). Not surprisingly, the four residues of the peptide that interact with the antibody are also the most strongly conserved amongst the peptides isolated from the diverse random peptide library displayed on phage [68]. Threonine and glycine at positions P1 and P2 show 62% and 86% conserved identity, respectively, in peptides selected by the antibody from the random peptide library. The glutamine and glutamate at positions P5 and P6 show even greater conservation with nearly 100% identity in all peptides sequences from the phage selected by the antibody (Figure 5.11).

In keeping with their high degree of sequence identity in peptides selected by the antibody from phage display [68], the glutamine and glutamate residues of the peptide appear to form the most specific interactions between the peptide and the antibody in the crystal structure of the complex. The glutamine side chain extends into a pocket in the antibody in which its amide group forms two complementary hydrogen bonds to the amide group of Asn^{H35}, while the glutamate side chain extends into a complementary pocket, forming hydrogen bonds to the hydroxyl group of Tyr^{L35} and the guanidinium

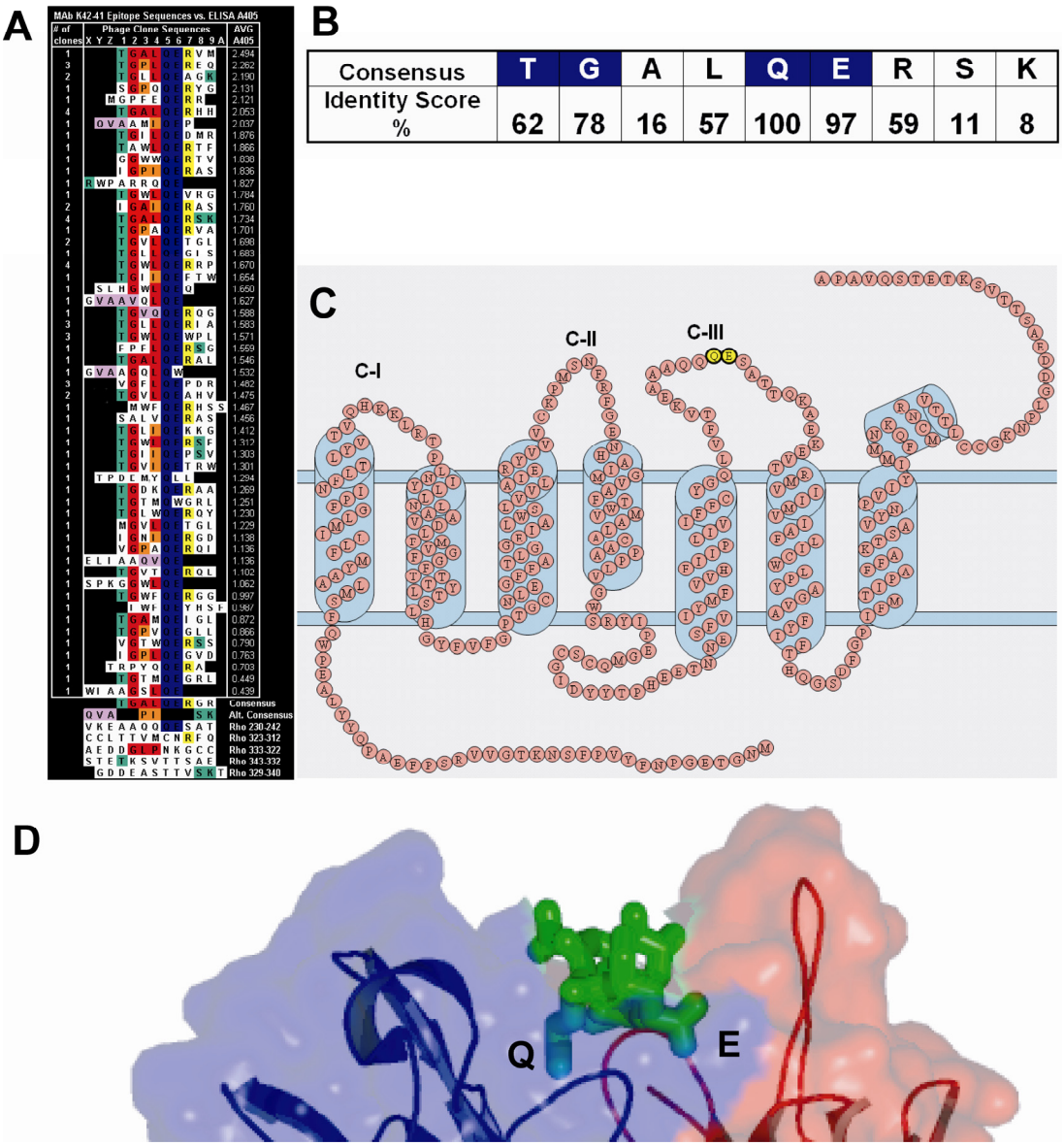


Figure 5.11. A) Epitope mapping of Antibody K4241L resulted in the selection of peptides which are found to have the consensus sequence of TGALQERSK. B) The frequencies of residues in the consensus mimetic peptide, position QE exhibit the greatest conservation. C) The strongly conserved QE present in the consensus peptide was mapped to the only QE pair present in the primary sequence of bovine rhodopsin, consistant with previous reports of the epitope of K42-41L being at least partially contained in the C3 loop. D) A representation of the crystal structure of K42-41L with the consensus epitope mimetic peptide bound. The strongly conserved QE pair make the most intimate contacts with K42-41L, providing a rationale for the high level of conservation of these residues in the peptides selected from the random peptide library.

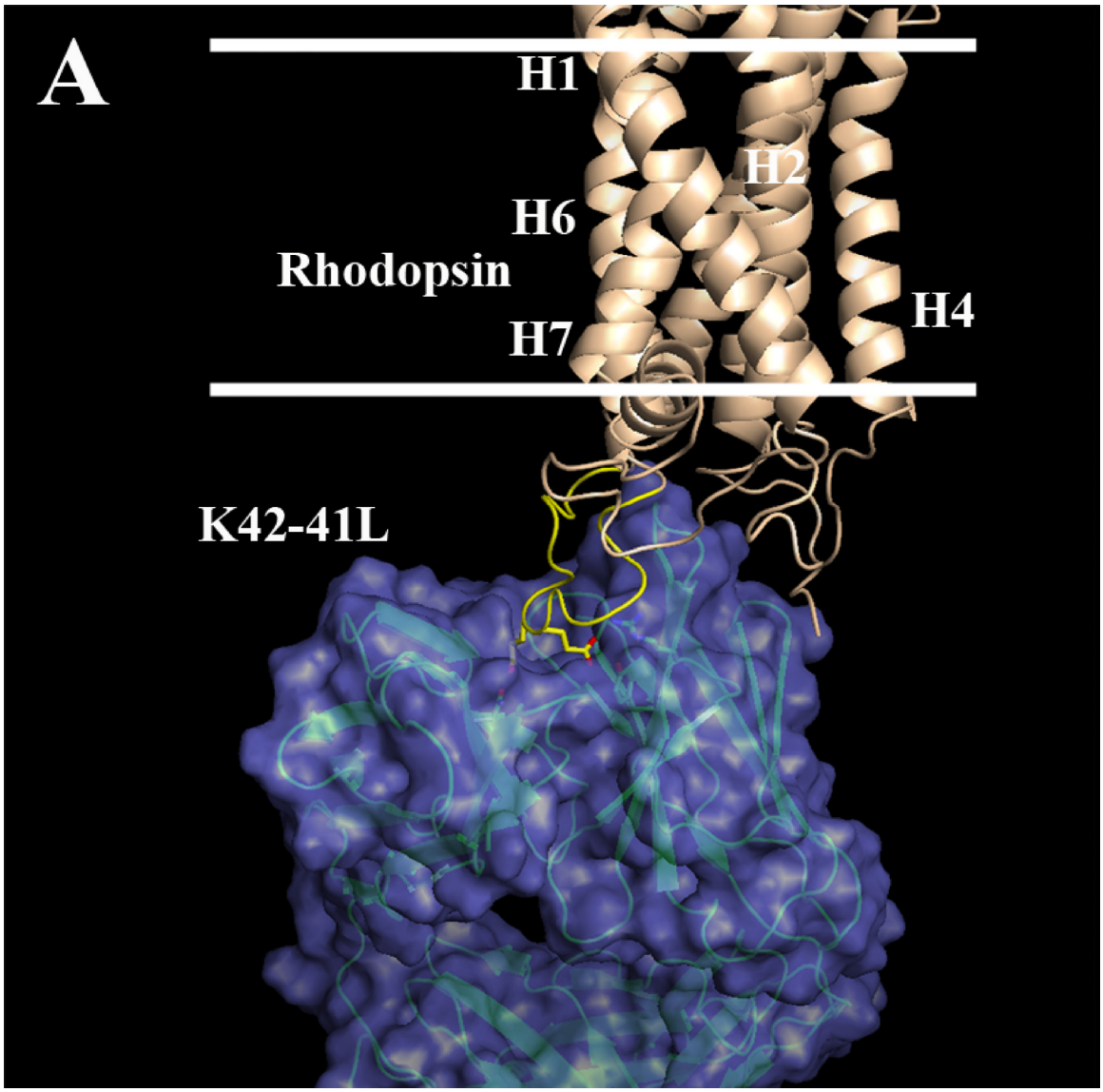


Figure 5.12. The crystal structure of antibody K42-41L docked onto a model of the extended conformation of the CIII loop of rhodopsin [176].

group of Arg^{L50}. The apparent specificity with which these residues are bound strongly suggests that the Gln and Glu residues of the antibody bound peptide are representative of the conformation of the C3 loop residues Gln^{238} and Glu^{239} in the K42-41L complex with rhodopsin. Gln^{238} and Glu^{239} are the only Gln-Glu pair in the rhodopsin sequence.

Spectroscopic assays show that binding the K42-41L antibody shifts the MI/MII conformational equilibrium away from agonist-activated metarhodopsin-II to the inactive metarhodopsin-I precursor. Such an analysis is inherently more difficult for other native GPCRs, because they lack the clear spectroscopic conformational signatures that are provided by rhodopsin. K42-41L shifts the equilibrium towards metarhodopsin-I when metarhopsin-II has been stabilized in either of two different ways. This occurs when metarhodopsin-II is stabilized "physiologically" by the binding of high affinity G_α C-terminal peptides, or when metarhodopsin-II is stabilized "biochemically" at low pH (6.7) in the native membrane (Figure 5.8). The K42-41L antibody was also shown to bind the dark-adapted conformation and opsin (Figure 5.7B).

The ability of K42-41L to discriminate between metarhodopsin-II versus dark-adapted and metarhodopsin-I, implies that similar conformations are accessible in the dark-adapted and meta-I states, but that there is a significant and distinct conformational change as metarhodopsin-I transitions to metarhodopsin-II [176]. This is consistent with the electron crystallographic studies of Ruprecht et al. on a photostationary state of rhodopsin that was highly enriched in metarhodopsin-I [209]. The 5.5 Å resolution structure indicated that the conformation of the meta-I state is rather similar to that of the ground state, and that conformational changes later in the photobleaching process (presumably at meta-II) lead to disruption of the crystal lattice packing in the 2D protein crystals.

Biochemical and structural evidence strongly suggest that K42-41L recognizes an extended conformation of the C3 loop that can be reached as an intermediate between the trigonal and tetragonal crystal structures of dark-adapted rhodopsin [176]. Energy

minimization and molecular dynamics computational runs succeeded in pulling additional elements of the C3 loop into contact with the antigen recognition site of K42-41L in an epitope/antibody docking model, however these computational exercises failed to show significant antibody interactions with residues on the C2 loop or the C-terminal tail. These computations are consistent with his the activity of K42-41L is primarily due to its interaction with the C3 loop. While the antibody is relatively large and might physically block the MII-stabilizing Gα C-terminal peptide from interacting with rhodopsin, the antibody also inhibits the formation of low pH stabilized metarhodopsin-II that does not require the binding of an additional ligand. In the case of low pH stabilized metarhodopsin-II, the activity of the antibody cannot be due to steric interference with a stabilizing ligand.

The C3 loop has been the subject of extensive mutational analysis. This includes the work of Yang et al. [70] who, using scanning cysteine mutagenesis, reported that the $Q^{238}C$ and $E^{239}C$ mutants exhibit normal photo-bleaching behavior and normal rates of Gt activation. They found that mutation of residues 226, 229, 230, 233, 234, 242, 243 or 244 all showed significant reduction in Gt activation, but showed normal stabilization of metarhodopsin-II. More recently, Natochin et al. [184] demonstrated that conversion of the entire C3 loop to polyalanine inhibits activation of transducin. The ability of cysteine and polyalanine mutants to form metarhodopsin-II strongly suggests that the conformational role of the C3 loop in the meta-I/meta-II transition is partially independent of sequence-specific interactions.

Altenbach et al., have used site-specific spin labeling to investigate the mobility of residues in the C3 loop [90]. They found a general gradient of mobility such that

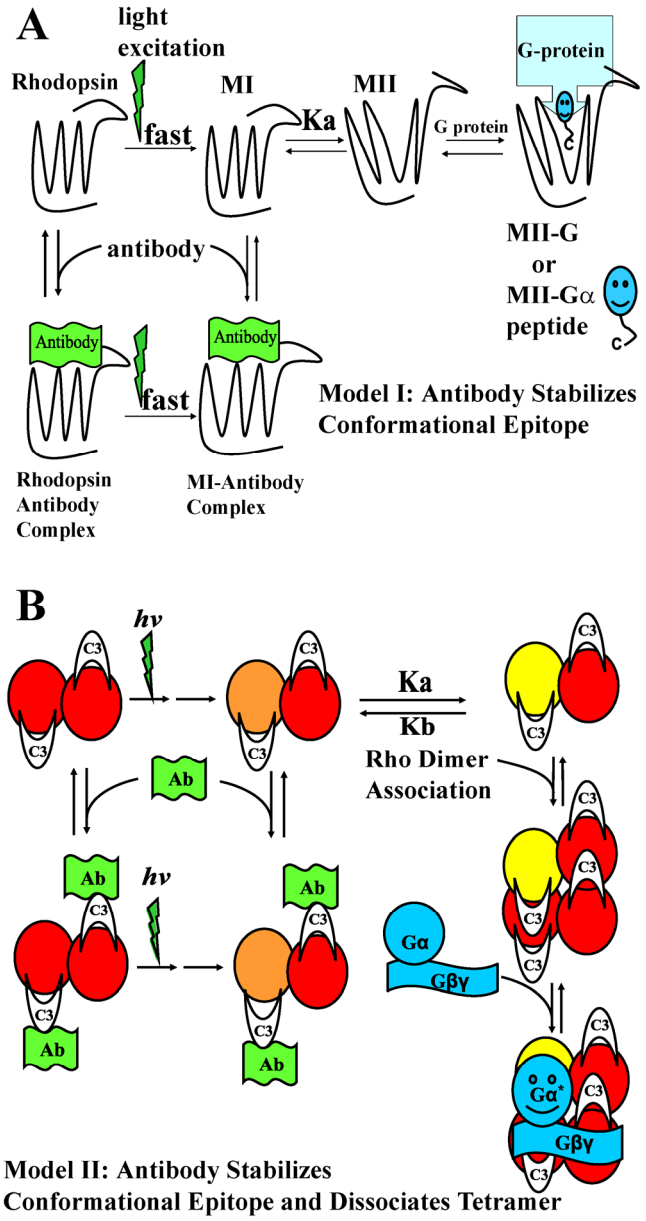


Figure 5.13. Schematic models for the stabilization of metarhodopsin-I by antibody K42-41L. A) Model 1. Antibody K42-41L binds to a conformational epitope that is accessible in the MI monomer, but not in MII, shifting the MI ↔ MII equilibrium toward MI. B) Model II. Dark adapted rhodopsin is depicted in red, metarhodopsin-I in orange, and metarhodopsin-II in yellow. In this model, the C3 loop of light-excited rhodopsin participates in the formation of a rhodopsin tetramer that contains a single MII molecule. The heterotrimeric G-protein binds with greater affinity to the excited tetramer than to an excited monomer or dimer, shifting the equilibrium towards formation of metarhodopsin-II. Bound antibody inhibits the ability of the C3 loop to participate in tetramer formation, and therefore reduces the affinity of $Gt_{\alpha\beta\gamma}$ for light-activated rhodopsin, shifting the MI/MII equilibrium towards formation of metarhodopsin-I.

mobility is lowest in the transmembrane helical segments and increases with distance from the aqueous/hydrophobic boundaries in the protein. The observed mobility is thus consistent with the exposure of the apex of the C3 loop allowing for interaction with K42-41L and a resulting shift in the MI/MII equilibrium.

The simplest model for the activity of K42-41L is that the antibody stabilizes a conformation of the C3 loop within the rhodopsin monomer that precludes formation of metarhodopsin-II (Figure 5.13A). The transition to metarhodopsin-II may be dependent upon an interaction between the C3 loop and other elements within the monomer. Antibody bound to the C3 loop might physically restrict the loop from forming these necessary interactions. Perhaps more likely possibility is suggested by extensive studies using electron spin resonance to probe conformational changes in rhodopsin. These studies follow changes in spin probe exposure or spin-spin interactions in site-specific spin-labeled rhodopsin [69, 71]. The spin-label results provide relatively low-resolution information, but it seems clear that expansion of the packing of several transmembrane helices occurs on the cytoplasmic side of the membrane during the formation of metarhodopsin-II. The largest movement, approximately 9 Å, appears to occur in helix 6 [69, 71]. The C3 loop connects helix 5 with helix 6. Thus, movement of these two helices relative to one another would separate the ends of the C3 loop, stretching it across the increased distance, pulling the loop towards the surface of the membrane. By binding to an extended conformation of the C3 loop that projects into the cytoplasm (Figure 5.12), K42-41L might interfere with the movement of helix 6, essentially holding it on a short leash, and thus block formation of metarhodopsin-II (Figure 5.13A).

An alternative mechanism for the destabilization of metarhodopsin-II and the

stabilization of metarhodopsin-I by the antibody (Figure 5.13B) is suggested from evidence that rhodopsin may exist as a dimer, or higher order oligomers or aggregates in the plane of the membrane [213]. Filipek, et al. [128] suggest that transducin may actually bind most favorably to a tetrameric rhodopsin assembly, consisting of three dark-adapted and one light-excited species. Their favored model, referred to as "model IV-V", postulates a critical role for the C3 loop in formation of the active tetramer. Though the oligomeric IV-V model of Filipek et al. does not require cooperative G-protein binding, cooperative rhodopsin/G-protein interactions have been reported [125, 126, 214], further suggesting the possibility of multimeric interactions. There is a variety of evidence relating dimerization or oligomerization of other GPCRs and evidence for increased stability of the agonist-excited conformations (conformations thought to be homologous to metarhodopsin-II) [215]. Thus in our Model II, binding of K42-41L to the C3 loop of rhodopsin would inhibit the biological activity of the receptor by promoting dissociation of the tetramer, consequently destabilizing metarhodopsin-II as diagrammed schematically in Figure 5.13B.

Experiments using primarily monomeric and some dimeric rhodopsin in dodecyl maltose micelles indicate that K42-41L destabilizes metarhodopsin-II and stabilizes metarhodopsin-I (Figure 5.9). Though this data supports the active-monomer model, it does not necessarily exclude the active-tetramer model, since changes in aggregation of detergent solublized receptor could occur upon light-excitation. Indeed, preliminary experiments at lower dodecyl maltose concentrations, where formation of dimeric and tetrameric rhodopsin are favored [216, 217], result in somewhat greater stabilization of metarhodopsin-I by K42-41L (Angel and Dratz, unpublished). Thus, it is possible that

the mechanism by which K42-41L inhibits formation of metarhodopsin-II includes elements of both models (Figure 5.13A and 5.13B). Arguments in support of the monomeric rhodopsin-G-protein activation mechanism have recently been summarized [218].

The flexibility of the C3 loop is likely to be related to its biological role. Highly flexible residues are frequently involved in protein-protein interactions during signaling events (13, 14). Entropic considerations suggest that increased flexibility allows the tightness of binding to be modulated, while maintaining a high specificity [207, 208]. Strikingly, the C-terminal tail of the transducin Gα subunit [108] is also disordered in crystal structures [139-141], and becomes ordered when interacting with metarhodopsin-II [109, 110]. Specific interaction of light-excited rhodopsin and transducin is required for visual excitation, but the complex cannot be too tight or the turnover would be too slow to provide the required high amplification of the transducin signals [107].

The observation that K42-41L can stabilize the dynamic C3 loop in a conformation that inhibits formation of metarhodopsin-II appears to be significant. Dark-adapted rhodopsin is locked in an inactive conformation by the reverse agonist 11-cis retinal. Photoconversion to the all-trans retinal agonist releases the protein to allow an equilibrium between the inactive metarhodopsin-I and the active metarhodopsin-II which excites the G-protein. Most other GPCRs have a much higher constitutive activity than rhodopsin [219] and presumably can fluctuate between MI-like and MII-like conformations even in the absence of agonists. Further ongoing studies of antibodies or other compounds that stabilize metarhodopsin-I or metarhodopsin-II-like states may facilitate the development of novel means for attenuating or activating GPCRs, leading to

advances in experimental and biomedical applications.

Materials and Methods

Rod Outer Segment Preparation

Rod outer segments were prepared as described in chapter 2.

Light Titration Experiments

Rhodopsin rod outer segment membranes used in light titration experiments (31) were suspended in buffer A (50 mM HEPES, 100 mM NaCl, 1 mM $MgCl_2$) and the final pH was adjusted for the given experiment. Prior to light titration experiments, working stock solutions of rod outer segments were briefly sonicated at 30% with a microprobe sonic dismembranator (Fisher) and rhodopsin concentrations were determined by measuring the Δ500 of an aliquote of rhodopsin in 3% LDAO. The concentrations of rhodopsin were then adjusted to 7.5 uM by addition of buffer A at the appropriate pH. For each light titration experiment, an aliquot of rhodopsin was bleached with a series of millisecond flashes at 50 second intervals and absorbance changes were measured during each interval. Each flash bleached ~8% of the rhodopsin. The appearance of metarhodopsin-II was detected by monitoring the difference in absorbance between 390 nm and 417 nm (390-417) [100] , using an Olis/Shimadzu UV-3000 dual wavelength spectrophotometer equipped with a temperature controlled cuvette holder and a sampling compartment purged with dry nitrogen gas. All light titration experiments were performed at 4 ˚C.

For measurement of low pH stabilized metarhodopsin-II, aliquots of rod outer segment were diluted in buffer A at pH 6.7. For assays that included antibody, the antibody was present at a concentration of 2.0 μM. The peptide Ac-VLEDLRSAbuGLF, a high affinity analog of the C-terminal tail of the transducin alpha subunit, was used to stabilize metarhodopsin-II at pH 8.0 [112]. Light titration assays involving peptide were done with buffer A at pH 8.0. Synthetic peptides were synthesized employing a Protein Technologies PS3 peptide synthesizer and purified by HPLC. The purified peptide masses were determined by MALDI-TOF mass spectrometry. Stock solutions of the peptides were prepared by dissolving the peptide in buffer A at pH 8.0.

Difference Absorbance Spectra

Absorbance spectra of rhodopsin with and without antibody K42-41L were measured in a Cary 50 spectrophotometer with a temperature controlled sample holder and sampling compartment purged with dry nitrogen. Absorbance spectra were acquired at 4 ˚C at pH 8.1. Rhodopsin stock solution (38 μM) was made by diluting rod outer segments in buffer A containing 5 mM dodecyl maltoside (CALBIOCHEM). The final rhodopsin concentration was 3.2 μM and the final dodecyl maltoside concentration was 2.0 mM. Rhodopsin samples were placed in the temperature controlled sample holder and the temperature was allowed to equilibrate. Spectra of unactivated rhodopsin were measured. The sample was then illuminated with >500 nm light from a Fiber Photics Illuminator 150 for 10 seconds while the absorbance spectra were acquired. The pH of the samples was measured following recording of spectra. Difference spectra were deconvoluted by fitting the summed synthetic Gaussian curves for metarhodposin-I,

metarhodopsin-II and rhodopsin.

ELISA

Enzyme-linked immunosorbent assays (ELISA) were performed using polyvinyl chloride microtiter plates coated with bovine rhodopsin in purified rod outer segments (ROS). The rhodopsin was prepared by adding 1 mL of 10 mM PBS, pH 7.4, to a 200 μL aliquot of 300 μM rhodopsin in dark or light-exposed ROS, followed by brief sonication. 100 ul aliquots of rhodopsin solution were added to microtiter plates under dim red light and incubated at 4 ^{o}C for 8 hours, washed 3 times with PBS and then blocked with 5% (w/v) milk protein, 0.02% NaN_3 in PBS. A serial dilution of K42-41L was added to the coated and blocked microtiter plate to measure antibody binding to dark-adapted rhodopsin and light-exposed opsin. For competition ELISA, microtiter plates were prepared as described above with addition of antibody K42-41L to all wells of the microtiter plates at a concentration of 1 μg/ml. Stock solutions (5 mM) of synthetic peptides TQKAEKEVTR-NH_2, TGALQERSK and TETSQVAPA were made in PBS and the peptides were added in the amount indicated per assay. The microtiter plates were incubated for 4 hours on an orbital shaker at room temperature and then rinsed 3 times with PBS to remove unbound antibody. Binding of antibody K42-41L was detected by the addition of alkaline phosphatase conjugated goat anti-mouse antibody (GAM-AP) (Zymed) diluted 1:10,000 in PBS. Following the addition of GAM-AP, plates were incubated for 4 hours at room temperature on an orbital shaker and washed 3 times with PBS. Following the addition of NBT/BCIP substrate, bound GAM-AP was detected by measuring absorbance at 405 nm

Sequencing of K42-41L

The DNA sequence of the antibody was obtained as follows: Total mRNA was extracted from a mouse hybridoma cell line producing antibody K42-41L [220] using the QuickPrep mRNA purification kit (Amersham). Variable heavy and variable light chain cDNA were amplified from the total mRNA using a set of degenerate mouse variable heavy and variable light chain primers [221]. Amplified variable heavy and variable light chain DNA was gel purified and sequenced. The amino acid sequence of K42-41L was verified, in part, by mass spectrometry and Edman degradation.

Single Chain Fv Selection

ScFv selection was performed as described in the ETH-2 phage display manual, briefly scFv selection was performed by initially biotinylating bovine rhodopsin with NHS-SS-Biotin (Pierce, Cat. No. 21331, EZ-Link Sulfo-NHS-SS-biotin), coating the immunotube (Nunc, Cat. No. 4-44202) with neutravidin (Pierce cat. No. 31000) 50 ug/ml for 4 hours at room temperature. Immunotubes were then blocked with 2% MPBS (2% powdered milk in PBS, 5.84 g NaCl, 4.72 g Na_2HPO_4, and $NaH_2PO_4.2H_20$, pH 7.2 in 1 liter) 2 hours at room temperature. Approximately 10^{12} to 10^{13} phage were then diluted in 4 ml 2% MPBS and added to immunotube with immobilized antigen and tumbled 60 minutes at room temperature and then let to stand for 60 minutes at room temperature. The supernatant was removed and placed into a second immunotube, the immunotube where the initial selection occurred was washed 10 times with PBS containing 0.1% tween-20. Bound phage were then eluted by addition of 500 ul PBS containing 50 mM DTT in PBS, cleaving a sulfhydral liable linker.

TG-1 *e. coli* cells (1.75 ml) at an OD of 0.4 were infected with 250 ul of the eluted phage at 37ºC for 30 minutes to be used for successive rounds of amplification and phage titering. Phage titer was determined by spotting several dilutions of infected cells on TYE plates (15g bacto-agar, 8g NaCl, 10g Tryptone, 5g yeast extract in 1 liter) containing 100 ug/ml ampicillin and 1% glucose. Following infection of TG-1 cells culture is pelleted and resuspended in 50 ul of 2xTY and plated on a TYE plate containing 100 ug/ml ampicillin and 1% TYE and incubated overnight at 37º C. After incubation overnight 7 ml of 2xTY media containing 15% glucose is added to the TYE plate and the cells are loosened with a glass spreader and removed,1ml of the recovered cells are used a freezer stock. 50 ul of the recovered cells was used to inoculate 50 ml of 2xTY containing 100 ug/ml ampicillin and 1% glucose and grown at 37ºC until OD 600 is 0.4. Phage for second round selection are generated by taking 10 ml of the 50 ml culture and adding $5x10^{10}$ helper phage (VCM) and incubated without shaking for 30 minutes at 37ºC in a water bath. Infected bacteria are then pelleted by low speed spin and resuspended in 2xTY containing 100 ug/ml ampicillin, 50 ug/ml kanamycin and 0.1% glucose and grown overnight at 30ºC. resultant phage were then PEG precipitated from bacterial culture supernatant after removal of bacterial cells by low speed centrifugation.

ScFv Screening by ELISA

Bacterial clonies were picked from the titer plates following each round of selection used to inoculate 200 ul 2xTY in sterile 96 well plates (Costar, Cat. No. 3790) and incubated overnight at 37ºC with shaking. Cells where then pelleted by centrifugation and supernatant removed and resuspended in 2xTY containing 100 ug/ml

ampicillin, 1% glucose and incubated for 2 hours as 37ºC. Following incubation 25 ul of 2xTY meida containing 10^9 helper phage/ml was added and ultured for 1 hour at 37ºC. The cells are then pelleted and resuspended in 200 ul 2xTY containing 100 ug/ml ampicillin and 50 ug/ml kanamycin and was grown overnight at 30ºC with shaking. The cells were then pelleted and the supernatant was then used directly in the ELISA assay. Phage containing supernatant 200 ul was added to 96 well ELISA plate and incubated for 4 hours at 37ºC or overnight at 4ºC. Unbound phage was removed by washing 5 times with PBS. The presence of phage was detected with the addition of HRP-anti-M13 5000X dilution (Amersham Pharmacia, 27-9421-01) and incubating for 4 hours at 37ºC or overnight at 4ºC. The HRP was developed with the addition of TMB substrate solution (Sigma, T-8665) and recorded on a TECAN saphire plate reader.

Screening of Anti-rhodopsin Monoclonal Antibodies

A 10 ug/ul stock solution of rhodopsin was made by briefly sonicating at 30% with a microprobe sonic dismembranator (Fisher) ROS membranes and diluting in PBS pH 6.0, 100 ul of stock solution of rhodopsin was added to each well of a Nunc maxisorp 96 well assay plate, covered with aluminum foil and incubated at 4˚ C in the dark for 5-8 hours. Following incubation the 96 well assay plate was rinsed with PBS 5 times, then blocked by adding 200 ul 5% (w/v) milk protein, 0.02% NaN_3 in PBS, wrapping in aluminum foil and incubating at 4˚ C in the dark for 5-8 hours then rinsed 5 times with PBS pH 6. Monoclonal antibody cell culture supernatant was assayed for the capacity to recognize bleached rhodopsin over dark adapted by adding 150 ul cell culture supernatant and 100 ul PBS to a pair of plates, followed by serial dilution of 50 ul volumes in 7 more

wells. Antibody K4241L was included as a positive control on eac plate. One plate a pair of samples was then exposed to light and one was left unbleached and incubated at 4˚ C in the dark for 2 hours. The ELISA plates were then washed 5 times with PBS pH 6.0. Bound antibodies were detected by addition of 150 ul (1:10000 dilution in PBS) of alkaline phosphatase conjugate anti-mouse antibody (Zymed) and incubated at 4˚ C in the dark for 1 hour, followed by rinsing 5 times with PBS. ELISA signal was developed by addition of 150 ul of 9.8% diethanolamine, 0.5 mM $MgCl_2$, p-nitrophenyl phosphate (Sigma N-9389). ELISA signal was read at 405 nm at 10 minute intervals on a TECAN safire.

CHAPTER 6

VALIDATION OF EPIALIGN EMPLOYING MODELSYSTEMS, LYSOZYME AND INTERLEUKIN-10

Introduction

Antibody epitope mapping allows for the revalation of structural information regarding the conformation of a protein that an antibody recognizes [68, 201, 222]. Often structural information provides insight into the functional properties of a protein. Traditional structural determination methods such as NMR and x-ray crystallography have resulted in the deposition of ~15488 non redundant structures in the protein data bank , however the human proteome has been estimated to contain as many as 120,000 proteins [223]. Given the large number of proteins of unknown structure, developing non-traditional methods for generating structural information regarding proteins that are not amenable to traditional structure determination methods such as NMR and x-ray crystallography is likely to have very broad impact in the area of structural genomics/proteomics. To address some of the short comings of traditional structural determination methods we have developed the computer program FINDMAP, which facilitates antibody epitope mapping employing phage display and was successfully applied in mapping of the discontinuous epitopes of several anti-rhodopsin antibodies [68].

Phage Display

Generation of random-insert libraries, displayed on the amino terminus of gene product 3, a minor coat protein (pIII) on the filamentous bacteriophage was initially demonstrated by Smith [224]. Application of phage displaying random peptide libraries to isolate antibody epitope mimetics was initially reported by Scott and Smith, since that time many antibody epitopes have been mapped by this method [225] (reviewed in [226]). The selective pressure used when employing phage display is typically the capacity of the library variants to interact with a bait protein.

Protein and peptide libraries have been successfully displayed on each of the viral coat proteins of the filamentous phage, however the most common display formats are either gene product 3 (pIII) or gene product 8 (pVIII) as displayed schematically in Figure 6.1. A strength of phage display technology is the coupling of the phenotype of each member of the library to its genotype, which allows the rapid isolation and determination of the selected amino acids resulting from several rounds of affinity selection. The pIII minor coat protein of filamentous phage is present in 3 to 5 copies on one tip of the tubular viron (Figure 6.1) and is composed of 3 domains; N1, N2, and CT. The N1 domain is made up of the first 68 residues of the protein and facilitates the translocation of the viral DNA into the cytoplasm of the infected bacteria, as well as coat protein insertion into the bacterial membrane. The N2 domain of the pIII protein consists of residues 87 to 217 and mediates binding of the virus to the f pilus of the bacterium. The carboxy terminal domain consisting of the last 150 residues is involved in forming

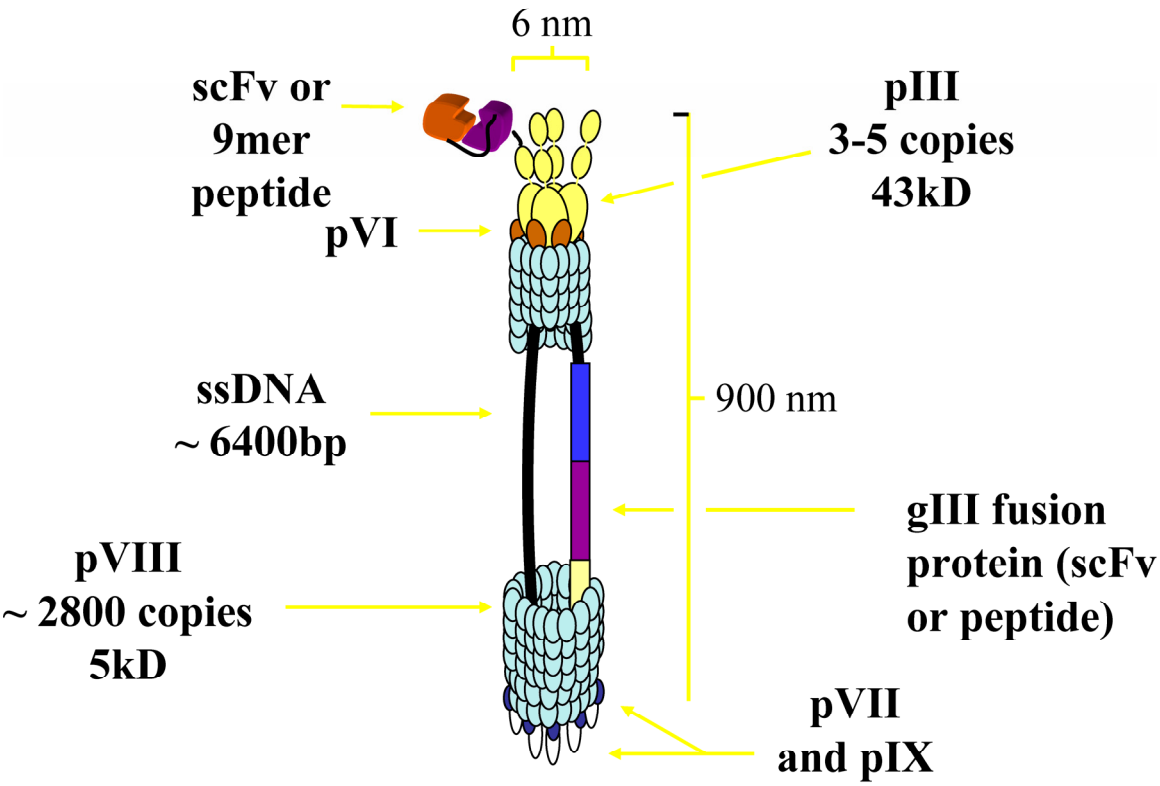


Figure 6.1. M13 phage schematic representation. Typically display libraries are constructed by fusion of peptide or protein to the pIII or pVIII of the phage.

stable virus [221]. An x-ray crystal structure of the two N-terminal domains of the pIII has been solved (1G3P.pdb) [227], presently there is no crystal structure of the C-terminal domain.

The amino terminal domain of the pIII has a theoretical isoelectric point of 4.3. The electrostatic potential of the surface of the pIII N1 and N2 domains was calculated using GRASS and is displayed in Figure 6.2 [228]. The top of the N1 domain is shown

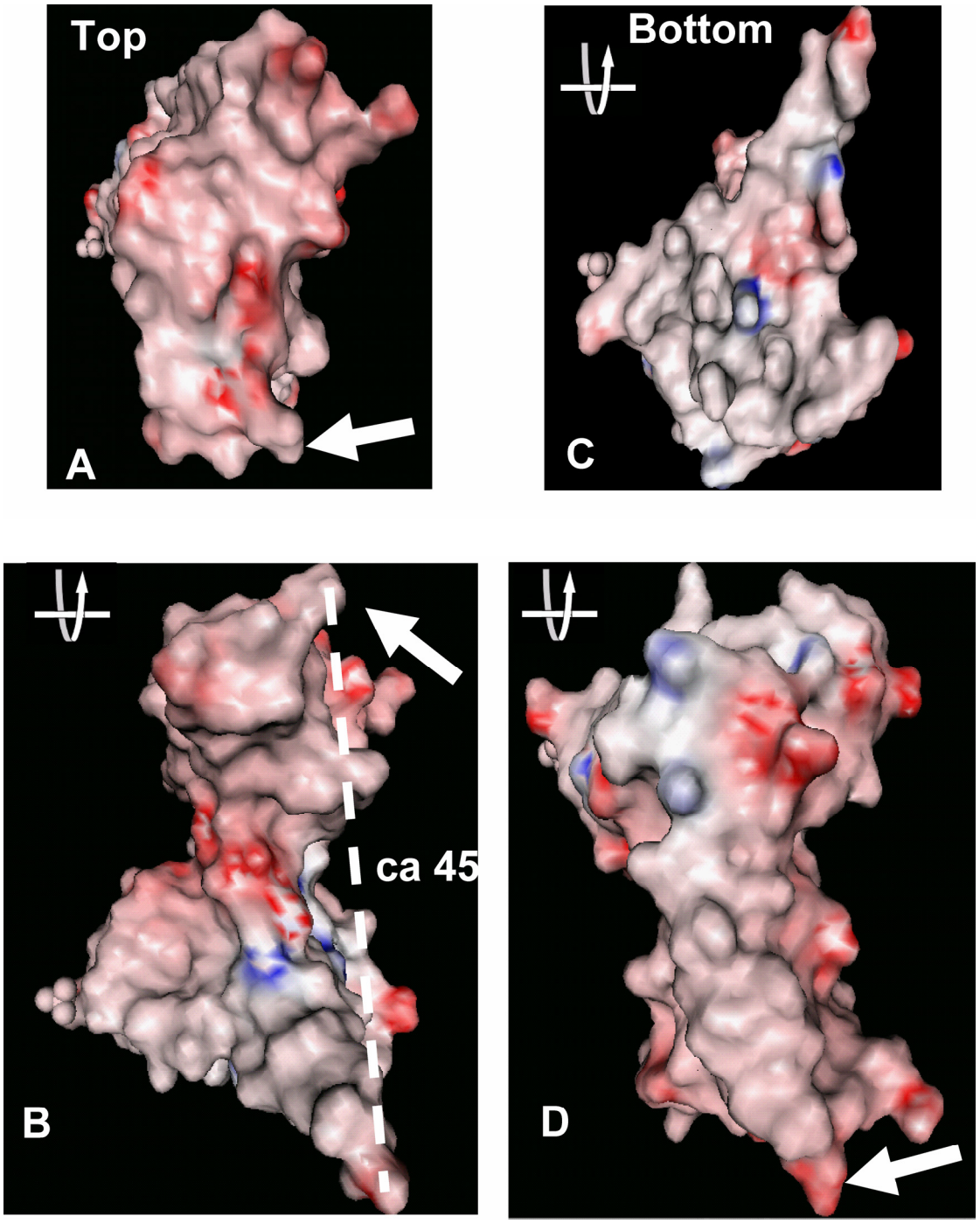


Figure 6.2. Display of the electrostatic potential of the N1 domain of the pIII protein of the M13 phage, red is positive electrostatic potential and blue is negative electrostatic potential. A) The "top" of the pIII protein is relatively planar; the arrow is pointing at the amino terminus which is the point of fusion of displayed peptide and proteins. B, C, and D are views of the electrostatic surface of the pIII following a series of rotations of 90º; the arrow again shows the amino terminus of the pIII protein.

in Figure 6.2-A, this perspective is showing the relatively planar surface of the N1 domain and the white arrows show the N-terminal point of random peptide attachment. The calculated electrostatic potential surface of the N1 domain reveals that the pIII domain is negatively charged in proximity to the point of peptide display. There are a few positively charged regions on the surface of the pIII protein as can be seen in all orientations of the pIII N1 and N2 domains in Figure 6.2. The major coat protein is present in ~2800 copies on the wild type phage. The pVIII is ~5000 Daltons and has a cluster of positive charges at the carboxy terminus that interact with the viral DNA and the amino terminus appears to present a net negative charge. The pI of the entire pVIII protein is 8.4 however much of the pVIII is buried in interactions with neighboring pVIII proteins only the last 3 amino acids of the pVIII on the carboxyl end have been show to be liable to proteolytic cleavage. The tight packing of the pVIII that results in protection from proteolytic cleavage and the acidic nature of the other coat proteins results in the assembled viron having a low isoelectric point [229].

Computational Methods for Epitope Mapping

Currently there are several computer programs developed for mapping antibody epitopes using peptide mimetic sequences derived from phage display [211, 230-233]. The methods for antibody epitope mapping implemented in the programs Sitelite[230], 3Dex [232], Mapitope [231, 234], MIMOX [233] and Pepsurf [235] require a 3D model of the antigen for the mapping of the epitope, whereas MIMOP [236], and Findmap/EpiAlign [211] are capable of mapping antibody epitopes employing the primary sequences of antigen and mimetic peptides. Computational methods for

determining the epitope of an antibody, using mimetic peptides selected from random peptide libraries displayed on M13 phage, have been applied to proteins of known structure [68, 201, 231, 234, 237] and unknown structure [68, 202, 222, 231, 238, 239]. Findmap and the more recent implementation of the algorithm called EpiAlign are capable of mapping an antibody epitope given the sequence of selected peptides from phage display and the primary amino acid sequence of the target protein, ultimately generating distance constraints providing structural information regarding the native fold of the protein under investigation. Methods that require a 3D structure of the antigen are of limited utility given we do not know the structure for the majority of all proteins.

The structure based strategies for mapping of antibody epitopes all allow for the mapping of mimetic peptide residues onto the structure of the antigen, considering side chain proximity. The residues in the mimetope need not be sequentially related in the primary sequence of an antigen but are seen as representing a conserved patch of residues found in the native 3 dimensional fold of the antigen. Mapping discontinuous epitopes employing random peptide phage displayed libraries was reported, where the structural epitope is known due to the availability of a co-crystal structure of the antibody bound to antigen [231]. Following the selection of peptides with anti-GP120 antibody b12 from random peptides displayed on phage, the statistical significance of the frequency of occurrence of di-peptide elements in the selected peptides was determined. Di-peptide elements are then mapped onto the structural model of the antigen following a set of rules; the Cα carbons of a mapped di-peptide do not have to be mapped to two consecutive residues but can not be more than 8Å apart in 3D space, the side chains of the mapped amino acids can be not further than 12 Å apart in 3D space and both residues

must be solvent exposed on the antigen. The resultant largest spatial clustering of connected di-peptides (a residues being mapped to a common position between each mapped pair of di-peptides) are thought to constitute the best candidate for a correctly mapped epitope.

FINDMAP and EpiAlign

We have developed an algorithm for mapping an antibody epitope with the goal of revalation the structural information present in the antibody epitope employing random peptide phage display [211]. Following selection of peptides and determination of the amino acid sequences of the selected peptides, the peptide sequences are used as probes and are aligned to the primary amino acid sequence of the target protein of interest (Figure 6.3). We score the alignment of a probe to the target sequence based on an alignment scoring function that is comprised of two components, (1) a **gap cost score**, allowing for the insertion of gaps in the alignment of the relatively short probes to the much longer target sequence allowing for the recovery of a discontinuous epitope defining regions and (2) the **substitution score**, allowing for non identity between mimetic probe amino acids and actual amino acids present in the epitope of a target protein of interest.

The gap cost function contains two user defined values, the **gap cost slope** and the **maximum gap cost**. When aligning a short polypeptide to the relatively long amino acid sequence of a protein the gap cost slope is the value that an aligned probe is

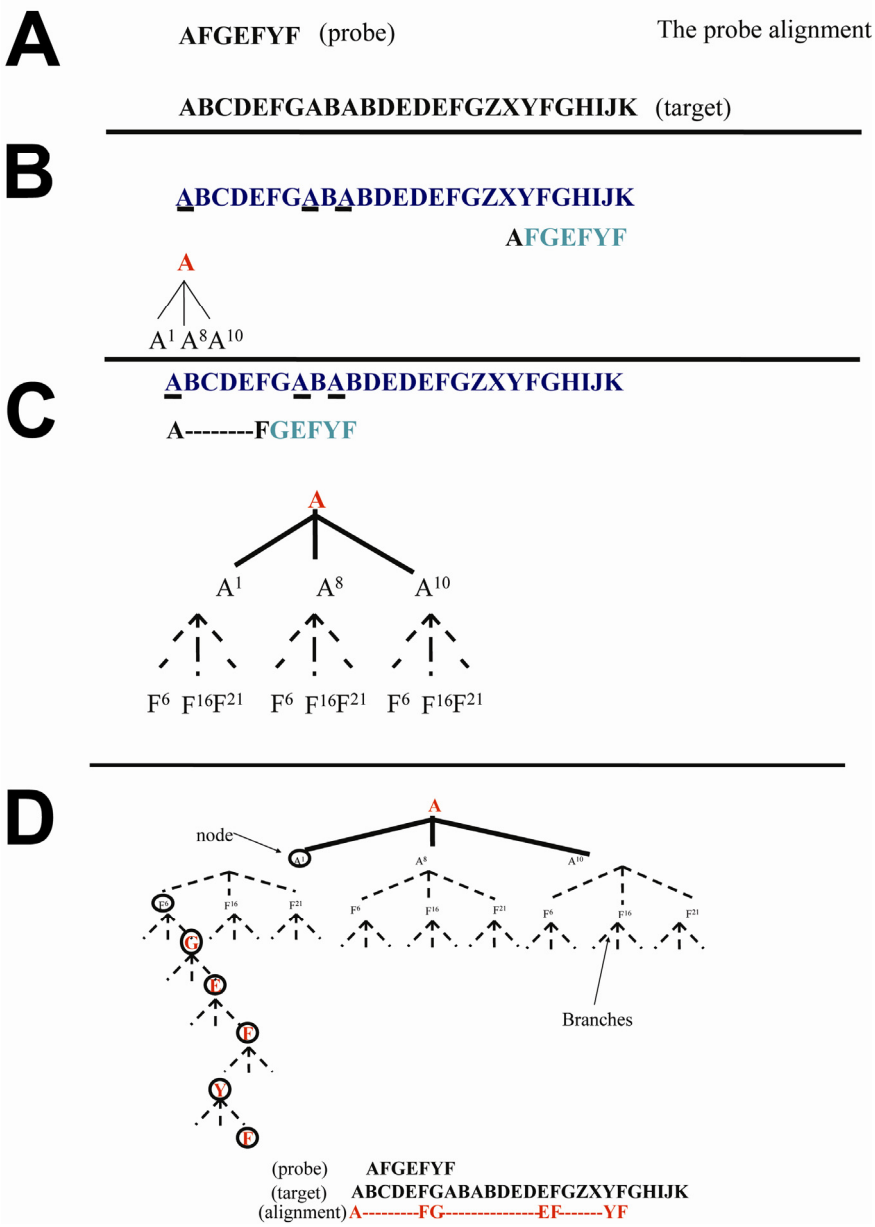


Figure 6.3 Schematic for alignment of peptide probe to antigen primary sequence with FINDMAP and EpiAlign. A) Epitope mimetic peptides selected by phage display (probe) are aligned with the primary sequence of an antigen (target). The top scoring alignments of a probe sequence to a target sequence are found employing a branch and bound search algorithm, there are many possible solutions for the alignment of any probe to any target as shown in B, where the first probe residue (A) of the probe AFGEFYF can be aligned to 3 locations in the target. Alignment of the second residue of the probe as shown in C demonstrates the large number of possible solutions when aligning only two positions of the probe to the target. Ultimately a small subset of top scoring alignments are elucidated as depicted in D.

penalized for each incidence where the probe residues are not aligned to consecutive residues in the target primary sequence. If the gap cost slope is 0.25 and there are two gaps inserted in a probe alignment then this alignment would be penalized -0.5. The maximum gap cost sets the limit for the penalty when inserting a discontinuity in the alignment of a probe to the target, if the gap cost slope is set at 0.25 and the maximum gap cost is set to 1 then a probe alignment with a gap equal to or greater than 4 residues will be penalized a maximum of -1.

Each mimetic peptide selected by phage display is aligned to the primary sequence of the antigen by EpiAlign and the top scoring alignments are reported, often there are many equally scoring alignments. The resultant alignments of a group of probes to the primary sequence of the target establish the putative epitope of the antibody. We have mapped the epitopes of four antibodies, three anti-lysozyme antibodies and an anti-interleukin-10 antibody where the structures of the complexes of antibody and antigen have been determined by x-ray crystallography. Employing these model systems we demonstrate the utility of the program EpiAlign.

Substitution Matrices

Allowing amino acid substitution in the alignment of two sequences greatly increases the number of possible solutions for the alignment of the probe (mimetic peptide) with the target sequence (antigen). Allowing amino acid substitution requires the use of a set of weighted values describing amino acid similarities which imply their substitutability. Previously developed substitution matrixes such as PAM (point accepted mutation) and Blosum developed by Dayhoff et al., (reviewed in [240]). and Henikoff et

al., [241] respectively have been derived from observed changes in amino acid identity for proteins that are related, leading to the development of models for evolutionary change over time. However, amino acid substitutions present in the mimetic peptides selected from random peptide libraries displayed on phage may not exhibit the same exchange frequencies as observed over evolutionary time among homologous proteins. Peptides selected my contain residues that are identical to the genuine epitope or a mixture of chemically equivalent mimetic residues and residues with compensatory changes allowing for divergent peptide variants to bind to the antibody of interest.

Initially we used a substitution matrix derived from matrices presented by Bordo and Argos shown in table 6.1 [242]. Bordo and Argos developed a substitution matrix based on an existing data set of crystal structures. The structures and sequences of related proteins were aligned, the locations and nature of amino acid changes were tabulated, leading to the generation of three substitution matrices, surface exposed substitutions, buried substitutions, and all substitution exposed and buried. The matrix constructed provided very reasonable substitutions, however the resultant substitution scores were approximations and as such rather coarse.

We created a quantitative amino acid substitution matrix by comparing the frequency of the amino acid side chain interactions between residues in folded proteins and antibody antigen interactions. Our assumption is that the substitutability of one amino acid for another with respect to epitope mimicry may be implicitly accounted for when considering similarity of patterns of interaction of amino acid side chains within the native fold of a protein.

Amino acid side chain interaction frequencies reported by Thornton et al., [243] and published on line (http://www.biochem.ucl.ac.uk/bsm/sidechains/) were used to construct a substitution matrix to apply to amino acid substitutions that take place at the interface between antibodies and mimetic peptides. We tabulated and normalized to percentage values the reported frequencies of interactions for all 20 amino acids. The side chain interaction percentages were then used to fill a 20x20 amino acid similarity matrix. To convert the similarity matrix to a substitution probability matrix the Pearson correlation coefficient was calculated for each residue relative to all other residues. The Pearson correlation coefficient values were then used directly as the weighted values of the substitution matrix (table 6.2). Additionally presented is an identity matrix where any substitution of one residue for another employing EpiAlign is penalized (table 6.3). A cluster analysis of the values in the Pearson matrix was performed with the goal of demonstrating grouping of like residues (Figure 6.4).

The clustering analysis demonstrates that for the most part residues that are typically thought to be exchangeable based on analysis of homologous proteins are grouped together. For example lysine and arginine interact with similar frequency with the 20 amino acids as do aspartic acid and glutamic acid. The results from the clustering of amino acids led to groupings that are very similar to what is seen in a typical amino acid Venn diagram [244]. The clustering results are depicted in the Venn diagram in Figure 6.5. Novel groupings occur when considering side chain interaction frequency

	A	R	N	D	C	Q	E	G	H	I	L	K	M	F	P	S	T	W	Y	V	-
A	1	0	0	0	0	0.5	0	0	0	0	0	0	0.25	0	0	0.75	0	0.25	0	0	0
R		1	0	0	0	0	0	0	0	0	0	0	0	0	0	0	0	0	0	0	0
N			1	1	0	0	0	0	0	0	0	0.75	0	0.5	0	0.25	0.25	0	0	0	0
D				1	0	0	0	0	0	0	0	0.5	0	0.75	0	0.25	0.25	0	0	0	0
C					1	0	0	0.25	0	0.25	0	0	0	0	0	0	0	0	0.75	1	0
Q						1	0	0	0	0	0	0	0	0	0	0.5	0	0	0	0	0
E							1	0	0.75	0	0	0	0	0	0.75	0	0	0	0	0	0
G								1	0	1	0.5	0	0.25	0	0	0	0	0.75	0	0	0
H									1	0	0	0.25	0	0.5	1	0	0	0	0	0	0
I										1	0.5	0	0.25	0	0	0	0	0.75	0	0	0
L											1	0	0	0	0	0	0	0.25	0	0	0
K												1	0	1	0	0.5	0.5	0	0	0	0
M													1	0	0	0	0.25	0.25	0	0	0
F														1	0.5	0.25	0.25	0	0	0	0
P															1	0	0	0	0	0	0
S																1	0.75	0	0	0	0
T																	1	0	0	0	0
W																		1	0	0	0
Y																			1	0.75	0
V																				1	0
-																					1

Table 6.1 Substitution matrix Derived from Argos and Bordo et al., [242].

	A	R	N	D	C	Q	E	G	H	I	L	K	M	F	P	S	T	W	Y	V	-
A	1.00	-0.45	-0.52	-0.37	-0.07	-0.59	-0.35	-0.40	-0.42	0.65	0.62	-0.31	0.48	0.48	-0.28	-0.56	-0.41	-0.34	-0.81	0.59	-0.50
R		1.00	0.61	-0.61	-0.21	0.54	-0.07	0.39	0.62	-0.65	-0.68	0.97	-0.68	-0.71	0.14	0.74	0.67	-0.20	0.22	-0.69	-0.50
N			1.00	0.61	-0.26	0.94	0.46	0.88	0.47	-0.89	-0.91	0.53	-0.82	-0.87	0.31	0.96	0.92	-0.13	0.34	-0.88	-0.50
D				1.00	-0.21	0.68	0.96	0.51	0.27	-0.67	-0.66	-0.05	-0.65	-0.65	0.11	0.51	0.48	-0.19	0.33	-0.64	-0.50
C					1.00	-0.35	-0.25	-0.10	-0.08	0.02	0.03	-0.24	0.13	0.16	-0.10	-0.20	-0.36	-0.21	-0.27	0.05	-0.50
Q						1.00	0.60	0.84	0.32	-0.85	-0.84	0.47	-0.80	-0.84	0.34	0.86	0.83	-0.03	0.42	-0.84	-0.50
E							1.00	0.38	0.09	-0.52	-0.50	-0.14	-0.54	-0.54	0.03	0.32	0.32	-0.15	0.34	-0.50	-0.50
G								1.00	0.30	-0.76	-0.78	0.32	-0.68	-0.70	0.40	0.81	0.74	-0.08	0.19	-0.73	-0.50
H									1.00	-0.64	-0.64	0.53	-0.49	-0.52	0.25	0.64	0.53	-0.08	0.34	-0.64	-0.50
I										1.00	0.98	-0.55	0.85	0.88	-0.34	-0.91	-0.77	0.17	-0.40	0.97	-0.50
L											1.00	-0.58	0.89	0.93	-0.28	-0.93	-0.82	0.25	-0.34	0.96	-0.50
K												1.00	-0.62	-0.65	0.07	0.65	0.61	-0.29	0.08	-0.60	-0.50
M													1.00	0.97	-0.04	-0.83	-0.80	0.44	-0.14	0.84	-0.50
F														1.00	-0.10	-0.87	-0.84	0.41	-0.18	0.89	-0.50
P															1.00	0.26	0.16	0.54	0.33	-0.35	-0.50
S																1.00	0.94	-0.15	0.35	-0.88	-0.50
T																	1.00	-0.20	0.23	-0.75	-0.50
W																		1.00	0.66	0.23	-0.50
Y																			1.00	-0.34	-0.50
V																				1.00	-0.50
-																					-0.50

Table 6.2 Atlas of amino acid side chain interactions substitution matrix.

	A	R	N	D	C	Q	E	G	H	I	L	K	M	F	P	S	T	W	Y	V	-
A	1	0	0	0	0	0	0	0	0	0	0	0	0	0	0	0	0	0	0	0	0
R		1	0	0	0	0	0	0	0	0	0	0	0	0	0	0	0	0	0	0	0
N			1	0	0	0	0	0	0	0	0	0	0	0	0	0	0	0	0	0	0
D				1	0	0	0	0	0	0	0	0	0	0	0	0	0	0	0	0	0
C					1	0	0	0	0	0	0	0	0	0	0	0	0	0	0	1	0
Q						1	0	0	0	0	0	0	0	0	0	0	0	0	0	0	0
E							1	0	0	0	0	0	0	0	0	0	0	0	0	0	0
G								1	0	0	0	0	0	0	0	0	0	0	0	0	0
H									1	0	0	0	0	0	0	0	0	0	0	0	0
I										1	0	0	0	0	0	0	0	0	0	0	0
L											1	0	0	0	0	0	0	0	0	0	0
K												1	0	0	0	0	0	0	0	0	0
M													1	0	0	0	0	0	0	0	0
F														1	0	0	0	0	0	0	0
P															1	0	0	0	0	0	0
S																1	0	0	0	0	0
T																	1	0	0	0	0
W																		1	0	0	0
Y																			1	0	0
V																				1	0
-																					1

Table 6.3 Identity Matrix substitution matrix

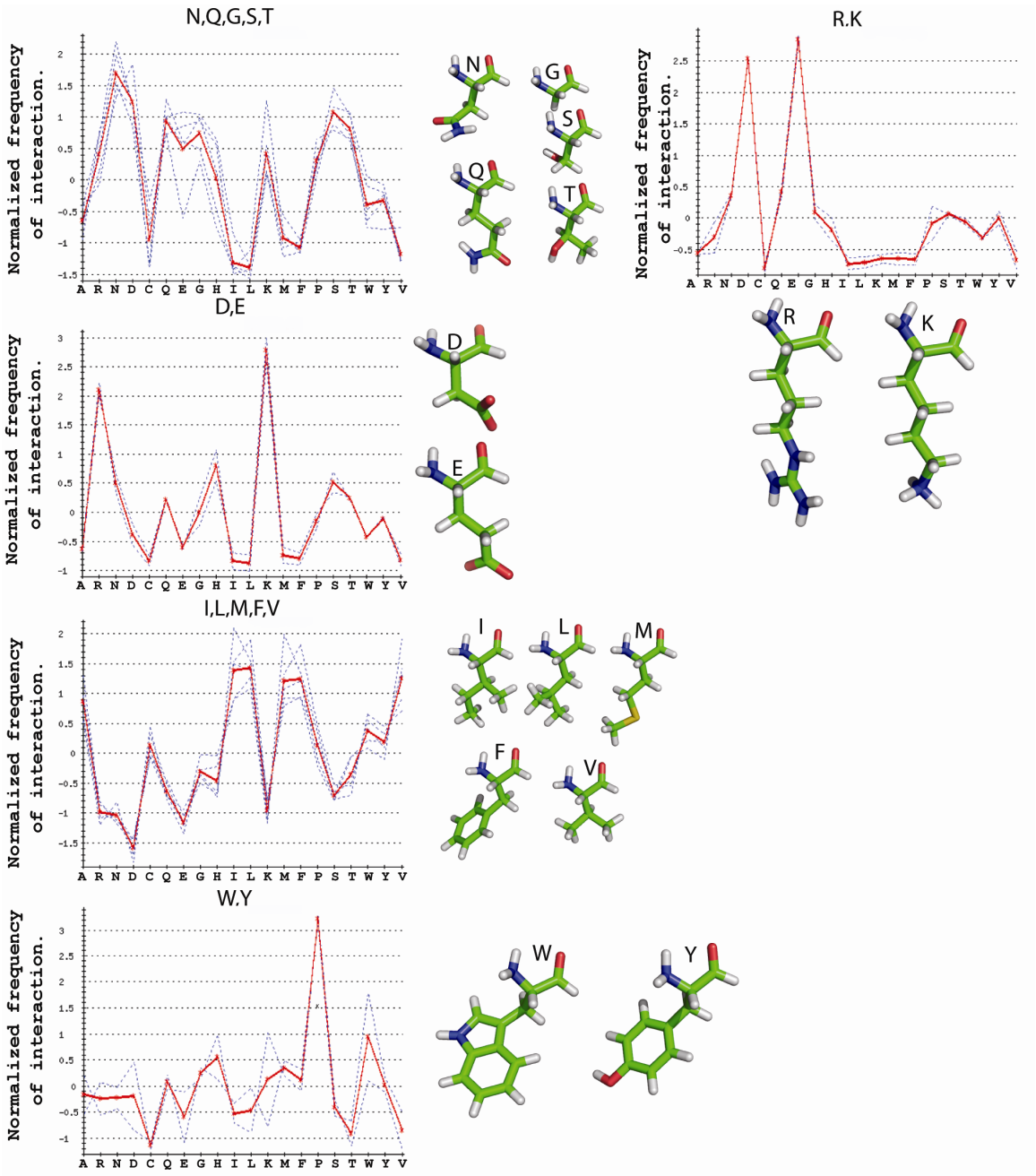


Figure 6.4. Cluster analysis of the Pearson correlation coefficients derived from the amino acid side chain interactions. Plots showing the normalized values of interaction frequencies are depicted in the graphs, the averaged interaction frequencies for a cluster of amino acids is shown in red and the dotted lines are interaction values for each member of a cluster. The deviations from the average for members of a cluster are quantitatively represented in the values in the Atlas of amino acid interactions matrix shown in table 6.2.

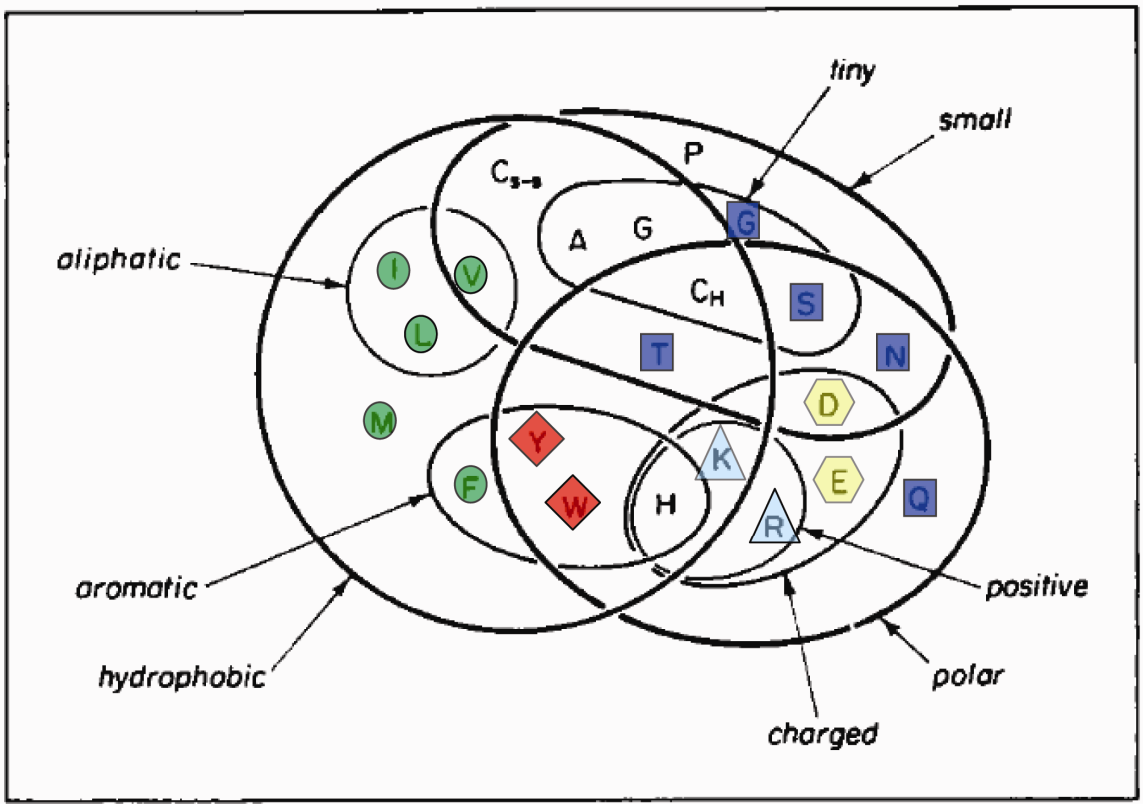


Figure 6.5. Venn diagram showing "typical" grouping of similar amino acids. The colored shapes highlight the clustering results from measuring amino acid similarity based on side chain interaction frequency.

that are not expected, such as phenylalanine and methionine clustering with the aliphatic residues as well as the grouping of glycine, serine, and threonine with asparagines and glutamine. Interestingly residues A, C, H, and P do not cluster with any other residues indicating these residues show very different and unique patterns in interaction relative to the other 16 amino acids. The matrix created from the observed frequency of amino acid side chain interaction is used below as a quantitative description of the acceptability of amino acid substitution of based on the structural, and biophysical properties that govern amino acid interactions within the native fold of a protein, thus we feel that this is the

most appropriate and relevant matrix to be applied in our mimetic peptide alignment and analysis.

Epitope Mapping Anti-Lysozyme Antibodies

Validation of the computational methods embodied in the computer programs FINDMAP and EpiAlign require the mapping of an epitope of an antibody on an antigen, where the epitope is known without ambiguity. We chose to epitope map a panel of anti-lysozyme antibodies where the structural epitopes are known due to the availability of the structural models of the complex of antibody and antigen. Given an antibody antigen co-crystal structure the residues that comprise the epitope can be determined by direct visual observation or by employing structural analysis programs such as CCP4 [245]. To establish if the program Findmap and the most recent Java version EpiAlign were capable of mapping a discontinuous epitope, a set of synthetic probes were derived from analysis of the co-crystal complex of hen egg lysozyme and a monoclonal antibody. The set of synthetic probes were aligned onto the primary amino acid sequence of hen egg lysozyme and the antibody epitope was recovered as previously reported by Mumey et al., [211]. To validate our epitope mapping methods we acquired a panel of anti-lysozyme antibodies consisting of antibodies D1.3, D11.15, and F9.13.7 [246-248]. These antibodies recognize discontinuous epitopes on lysozyme as shown in Figure 6.6. The epitope for antibody F9.13.7 was derived from the analysis of crystal structure 1FBI.pdb and consists of residues H15, R73, L75, N93, K96, K97, S100, and D101. The epitope for antibody D1.3 was derived from analysis of the crystal structure 1KIP.pdb [246] and

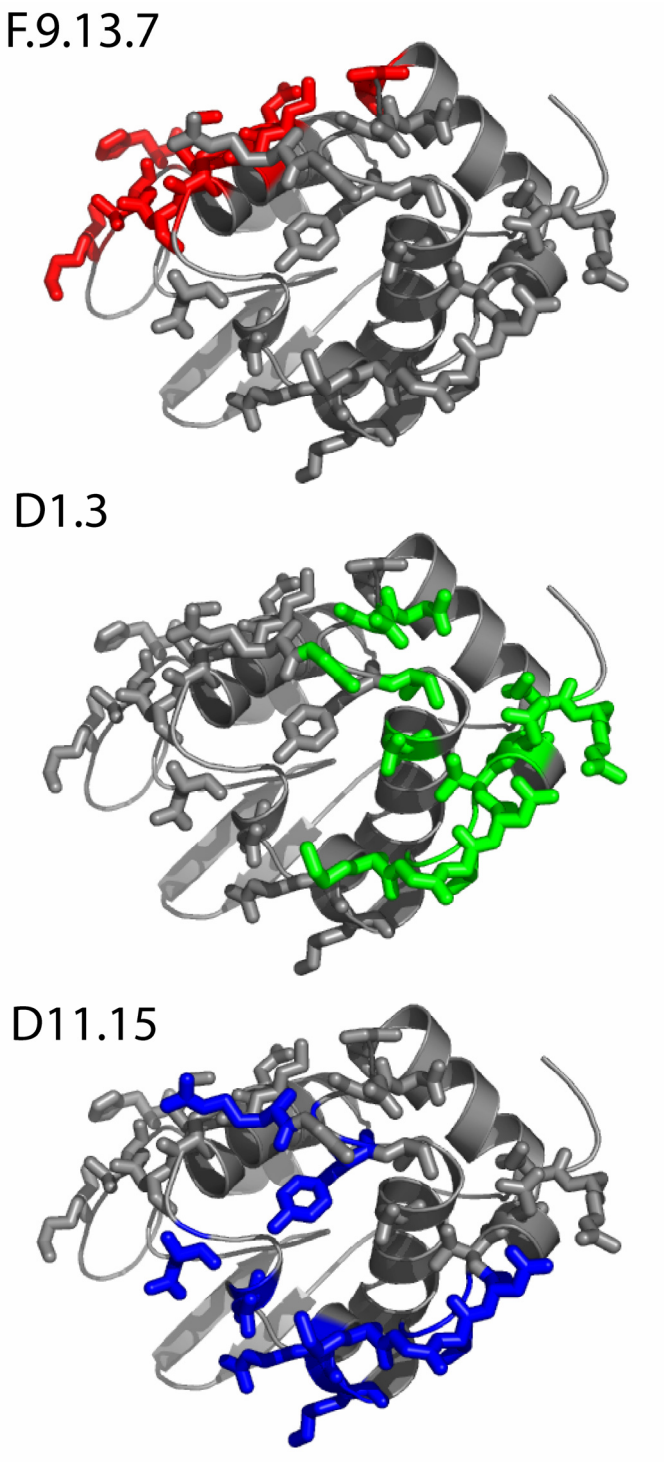


Figure 6.6. Crystal structures of lysozyme with three different antibodies, F9.13.7, D1.3, and D11.15. The epitopes contain have few residues in common, D1.3 and F.9.13.7 do not bind common residues but do bind to locations that are near one another. D1.3 and D11.15 bind overlapping regions, binding shared positions.

consists of residues D18,N19,G22,S24,N27,G117,T118,D119,V120,Q121,I124,R125. The epitope for antibody D11.15 was derived from analysis of the crystal structure 1JHL.pdb and consists of residues Y23, R24, N103, N106, R112, K113, K116, G117, T118, D119. The epitope for antibody F.9.13.7 (**HLRNNKKSD**) shows a great resemblance to that of antibody D11.15 (**YRNNRKKGTD**) however structurally there is little overlap between the epitopes of the two antibodies. The epitope for antibody D1.3 (**DNRGYSLNKGTDVQIR**) differs somewhat in amino acid composition compared to the other two antibodies, containing fewer positively charged residues and being somewhat larger.

Prior to the selection of phage display peptides with antibody D11.15, D1.3 and F9.13.7 antibody activities were assayed by ELISA and western blot. Both assays showed that the purified antibodies were active, and capable of binding lysozyme, and appeared to be suitable for mimetic peptide selection. Following 3 rounds of affinity selection of peptides on phage, an increase in phage titer was observed, indicating that amplification of selected phage resulted in a greater number of phage displaying mimetic peptides following successive rounds of selection and amplification as one would expect. The plaque lift assay was employed to screen phage clones post selection for high affinity peptide mimetics. The plaque lift assay requires the transfer of phage present on an agar plate to a nitrocellulose membrane which is then probed with the antibody used in the selection process, allowing for the screening of a large number of phage for binding to the antibody used in the selection process. Following selection of phage against the panel of anti-lysozyme antibodies the plaque lift assays performed were negative in all cases, indicating phage selected exhibit modest affinity for antibody binding. Phage clones

selected with each of the three antibodies were isolated and the DNA encoding the displayed peptide on the phage was sequenced.

The amino acid sequences of peptides displayed on phage present after three rounds of affinity selection with antibodies D11.15, D1.3 and F9.13.7 are shown in table 6.4. A striking feature of the sequences of the phage selected is several common largely basic peptide sequences were selected with the different antibodies. The same phage sequence being selected with different antibodies presumably indicate a common selective pressure. Consensus sequences of AKK and KKPK are found in common in all three population of peptides selected. Peptides IHAKKPKKP, and IEAYAKKRK are found to in common for all three antibodies. Peptides VIAKIKKPK, IHAKKPKKP, IEAYAKKRK, AYAKHKVKK, and VEAKGHKKK are found in common for selected peptides for antibodies F.9.13.7 and D1.3.

Peptides that were not found in common between each antibody were used as probes for epitope mapping the anti-lysozyme antibodies, employing the computer program EpiAlign. Three different substitution matrices were used when aligning the peptide probes to the primary sequence of lysozyme. Following the alignment of peptide probes onto the primary sequence of lysozyme a histogram showing the results of mapping of the epitopes is shown in Figure 6.7A for antibody F.9.13.7, the mapping employing the atlas of side chain interactions is also shown superimposed on the structure in Figure 6.7B. There is agreement between the genuine epitope residues and the mapped results from the EpiAlign sequence alignments for this antibody. Residues H15, K96, and K97 were mapped on lysozyme with a frequency above that of a

Anti-lysozyme antibodies		
F.9.13.7	**D1.3**	**D11.15**
HLRNNKKSD	**DNRGYSLNKGTDVQIR**	**YRNNRKKGTD**
VHGKKPKNG	VIANIKKPK	VMAKKPLKK(X17)
KPLKVKKPL	VAAKQKKPK	VMAKKVRK
KGSKLKKPM	GKVNVKKPK	VHAKKKPRV
VAAKQKKPK	S*AYEKKRK	AMAKKPLKK
VEAKKKKLK	LYAKKLKPK	VYAKKAPRK
VMAKKKVIK	IHAKNPKKP	LWAKKMKKP (X4)
LHAKKPKRS	IEAYVNKRK	FPVEAKKRR
LHAKKPKRM	IEAKGHKKK	GKVKKEKPI
VYAKKMKRQ	AVAKSKKPA	GKKPHGLLQ
VEAKGKARR	GKLHNKDKQ	VLAKKSKIG
AWAGKHKHK	GWTTGGVRW	GHKKPHRPH
GKHVKRPKS	GHKPKPAKG	GHKKPHRPH
GKHHRMNKV		KKPPRVPRL
GKMAKKPKA		GHKSKLPKR (X2)
GKGKLKVPK		CWGKKQRHV
GHKHHKFHK		KHGHPKVPK
Identical peptides selected with each antibody.		
IHAKKPKKP (X4)	IHAKKPKKP (X2)	IHAKKPKKP (X3)
IEAYAKKRK (X4)	IEAYAKKRK (X5)	IEAYAKKRK (X3)
AYAKHKVKK (X6)	AYAKHKVKK (X2)	
VEAKGHKKK (X7	VEAKGHKKK (X3)	
VIAKIKKPK (X4)	VIAKIKKPK (X3)	

Table 6.4 Peptide selected with three different anti-lysozyme antibodies.

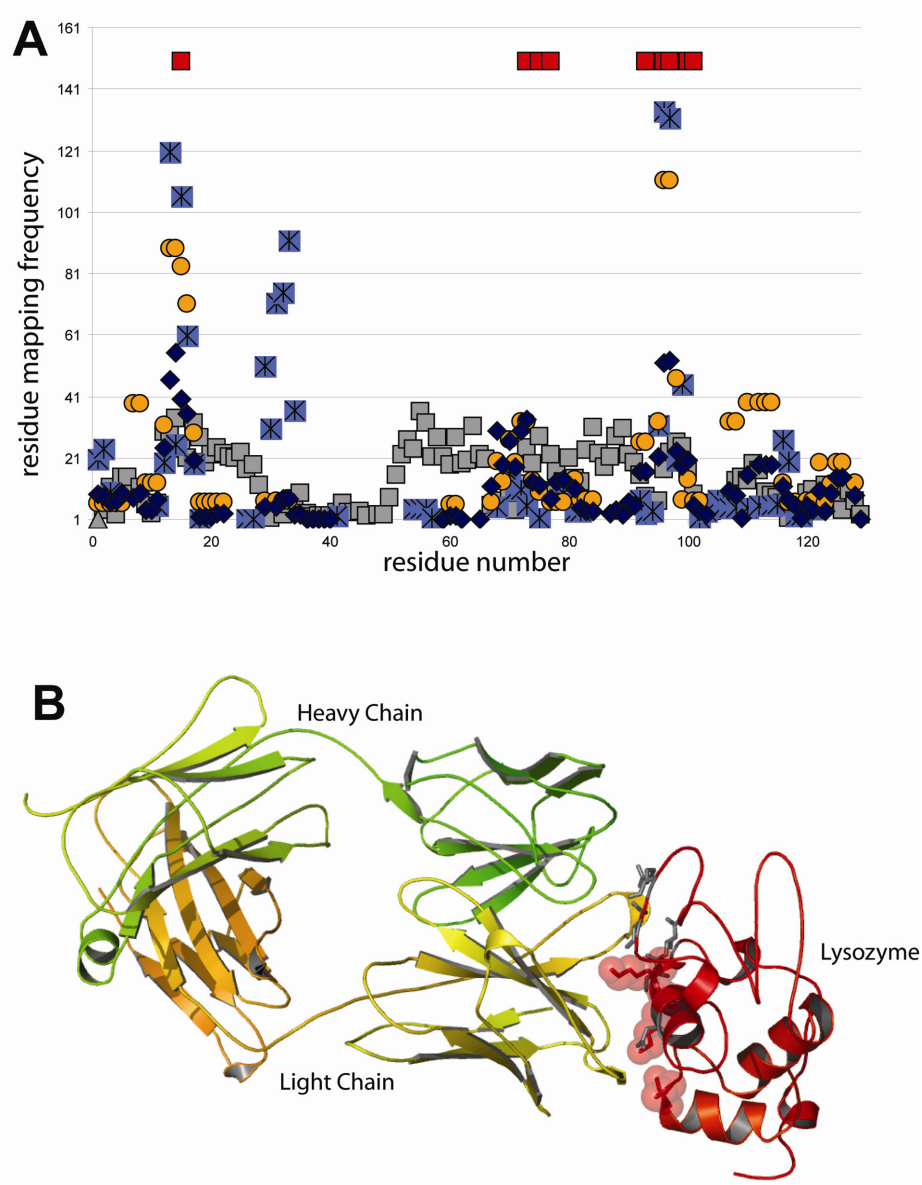


Figure 6.7. A) Epitope mapping results from EpiAlign following aligning of probes that are not shared between antibodies. The known epitope is shown at the top of the histogram (red squares), the mapping of a random set of probes establishes the baseline frequency of peptide alignment (grey squares), the alignment of a set of peptides employing the substitution matrix derived from amino acid side chain interactions (table 6.2) is shown as gold circles, shown as navy blue diamonds is the alignment of peptides employing the Argos and Bordos substitution matrix (table 6.1), and lastly the light blue squares show the alignment of the set of peptides to lysozyme employing the identity matrix shown in table 6.3 B) Structural epitope of antibody F.9.13.7 on lysozyme rendered as sticks and the residues that are mapped with high frequency by EpiAlign are rendered as space filled on the model.

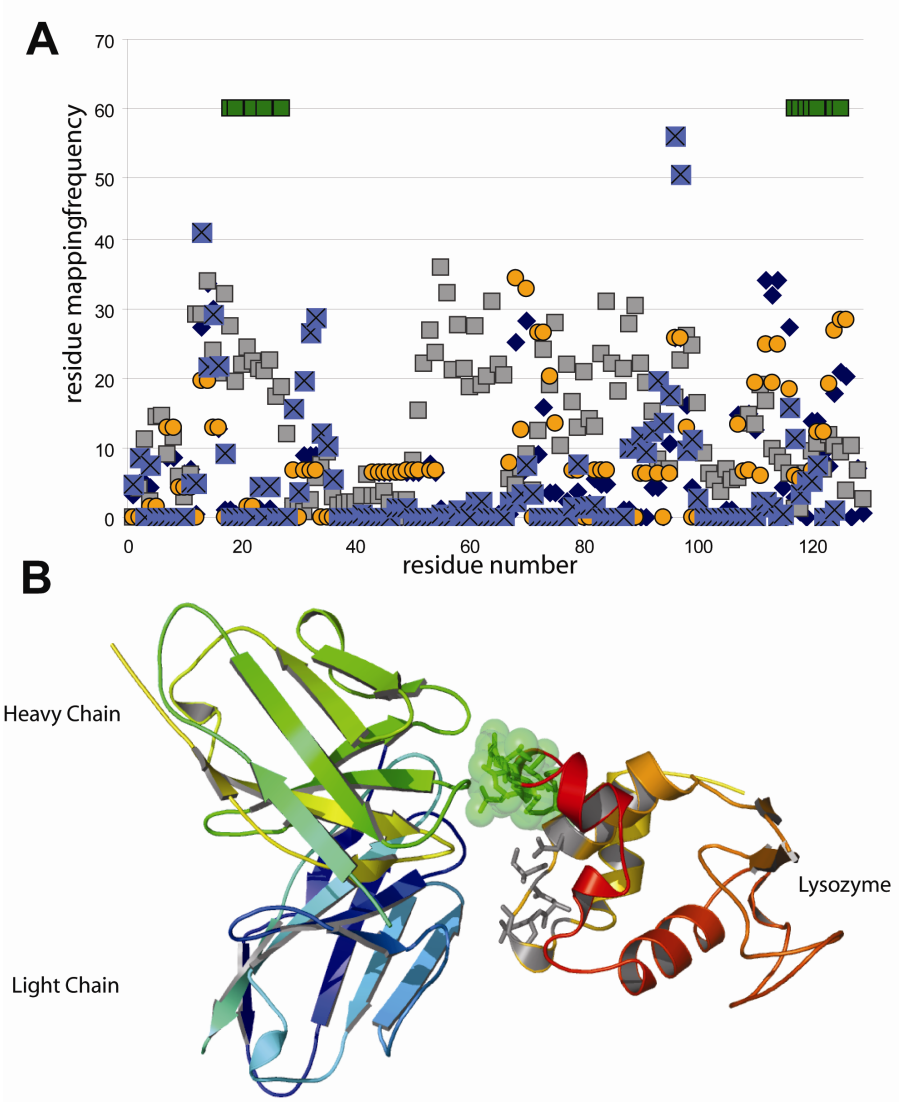


Figure 6.8. A) Epitope mapping results from EpiAlign following aligning of probes that are not shared between antibodies. The known epitope is shown at the top of the histogram (red squares), the mapping of a random set of probes establishes the baseline frequency of peptide alignment(grey squares), the alignment of a set of peptides employing the substitution matrix derived from amino acid side chain interactions (table 6.2) is shown as gold circles, shown as navy blue diamonds is the alignment of peptides employing the Argos and Bordos substitution matrix (table 6.1), and lastly the light blue squares show the alignment of the set of peptides to lysozyme employing the identity matrix shown in table 6.3. B) Structural epitope of antibody D1.3 on lysozyme displayed in grey sticks and the residues that are mapped with high frequency by EpiAlign are rendered as green space filled on the model.

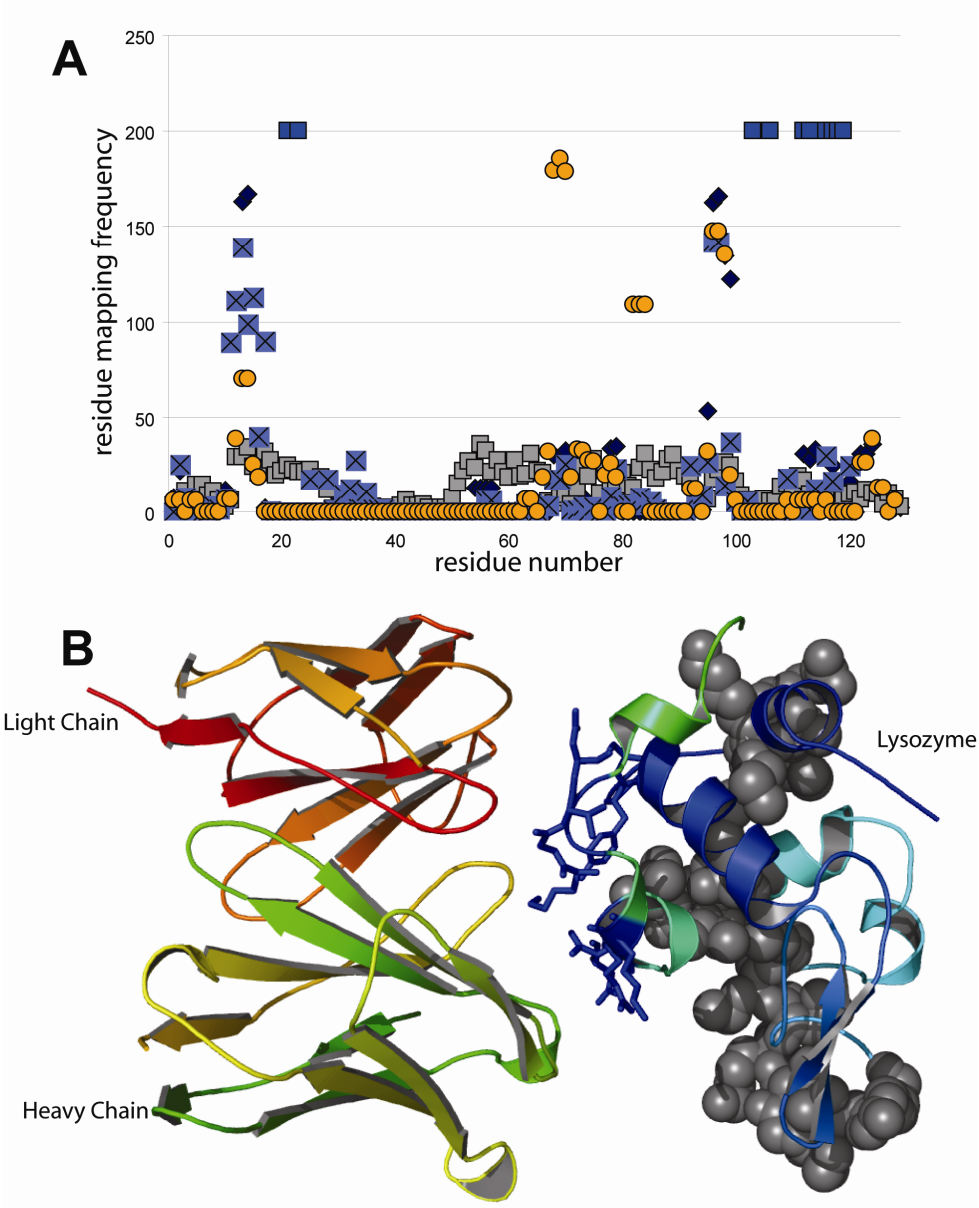


Figure 6.9. A) Epitope mapping results from EpiAlign following aligning of probes that are not shared between antibodies. The known epitope is shown at the top of the histogram (red squares), the mapping of a random set of probes establishes the baseline frequency of peptide alignment (grey squares), the alignment of a set of peptides employing the substitution matrix derived from amino acid side chain interactions (table 6.2) is shown as gold circles, shown as navy blue diamonds is the alignment of peptides employing the Argos and Bordos substitution matrix (table 6.1), and lastly the light blue squares show the alignment of the set of peptides to lysozyme employing the identity matrix shown in table 6.3 B) Structural epitope of antibody D11.15 on lysozyme displayed in blue sticks and the residues that are mapped with high frequency by EpiAlign are rendered as space filled on the model.

the mapped results from the EpiAlign sequence alignments for this antibody. Residues H15, K96, and K97 were mapped on lysozyme with a frequency above that of a random set of probes. The histogram for the alignment of antibody D1.3 is shown in Figure 6.8A, and the mapping employing the atlas of side chain interactions is shown superimposed on the structure in Figure 6.8B. The frequency of mapping positions on antibody D1.3 shows peptide alignments to one region of the known epitope, residues G117, T118, D119, V120, Q121, I124, and R125. The histogram showing the mapping compared to the genuine epitope shows that the quality of the mapping and the selected probes appear much less specific with one region of the discontinuous epitope being strongly identified in the mapping and a second epitope giving a weak signal. The mapping of antibody D11.15 epitope is shown in Figure 6.9, the alignment of the peptide probe sequences on lysozyme failed to coincide with any region of the known epitope as can be seen in Figure 6.9A and 6.9B.

Comparing the alignment results for the three anti-lysozyme antibodies with respect to which substitution matrix was used reveals that the Atlas of side chain interaction matrix provided the best results. The use of the identity matrix led to alignment frequencies that were often the largest, which is not unexpected given there are inherently few solutions for any given alignment; however these alignments were more often incorrect. The substitution matrix derived from side chain interactions out performed the Argos and Bordo derived matrix when mapping the epitopes for antibodies F9.13.7 and D1.3 as can be seen in the histograms in Figures 6.7 and 6.8. The functional and structural epitopes have been previously characterized for antibody D1.3 and hen egg lysozyme (hel), as well as an anti-idiotype antibody E5.2 [249]. The epitope on the anti-



Figure 6.10 Comparison of D1.3 epitope on lysozyme and anti-idotope antibody E5.2. A comparison of the structural nature of the mimetic epitope on antibody E5.2 with epitope on lysozyme recognized by antibody D1.3 shows the potential for plasticity in epitope mimicry.

idiotype antibody E5.2 shares 7/13 of the contact residues found on the D1.3 epitope of lysozyme. There are some structural differences between epitopes on hel and E5.2 indicating that the anti-idiotype antibody may not contain a very high fidelity internal image of the antigen as seen in Figure 6.10, however when considering the pI of the epitope on hel and E5.2 they are both similarly basic, electrostatic complementarity appears to be maintained in this instance of successful mimicry.

The selection of the same peptides with three separate antibodies was unexpected. We believe that the drastic electrostatic difference between the pIII protein on the phage, where the mimetic peptides are displayed, and the antibodies epitopes on lysozyme may account for selection of the same peptides for several different antibodies. The pIII protein domain where the random peptide is displayed in the phage library J404 is very acidic having a pI of ~4 where as the pI of lysozyme is ~9. The paratope for all three antibodies have pI values around 5. We hypothesize that the electrostatic interaction between antibody and phage displayed mimetic peptides results in a biased selection of peptides that neutralize the abundant negative charge residues of the pIII protein instead of predominantly selecting peptides for their ability to mimic the epitope on lysozyme. The charge interaction may add an undesirable selective pressure that may play a more defining role in the selection of peptides from the random peptide libraries then epitope mimicry, thus selected peptides from different antibodies contain similar sequences.

Epitope Mapping of Interleukin-10

A second model system was identified where the isoelectric point of the antigen is acidic, and thus potentially more compatible with epitope mimicry on the acidic pIII



MSENSCTHFPGNLPNMLRDLRDAFSRVKTFFQMKDQLDNLLLKESLLEDFKGYLGCQALS

EMIQ[71]FYLEEVMPQAENQ[83]DPDIKAHVNSLGENLKTLRLRLRRCHRFLPCENGGGSGGKSKA

VEQV [125]KNAFNKLQEKGIY[137]KAMSEFDIFINYIEAYMTMKIRN

Figure 6.11. Epitope of antibody 9D7 rendered in yellow on the structure of IL-10. The primary sequence of recombinant IL-10 is shown below with the epitope regions colored yellow. Boxed residues are found to be involved in extensive interactions between antibody and antigen, with the greatest number of interactions occurring K130, Q131 and E132.

protein of M13 phage. The interleukin-10 9D7 antigen-antibody complex was developed as a model system given the acidic pI of IL-10, and the availability of the antibody and antigen. The x-ray crystal structure of recombinant human interleukin 10 and antibody 9D7 complex was solved by Josephson et al., [250]. The epitope for antibody 9D7 on IL-10 is discontinuous; the rat antibody 9D7 binds to two regions on IL-10 (Figure 6.11). The isoelectric point of IL-10 is acidic; having a pI of 6 that we predict may increase the

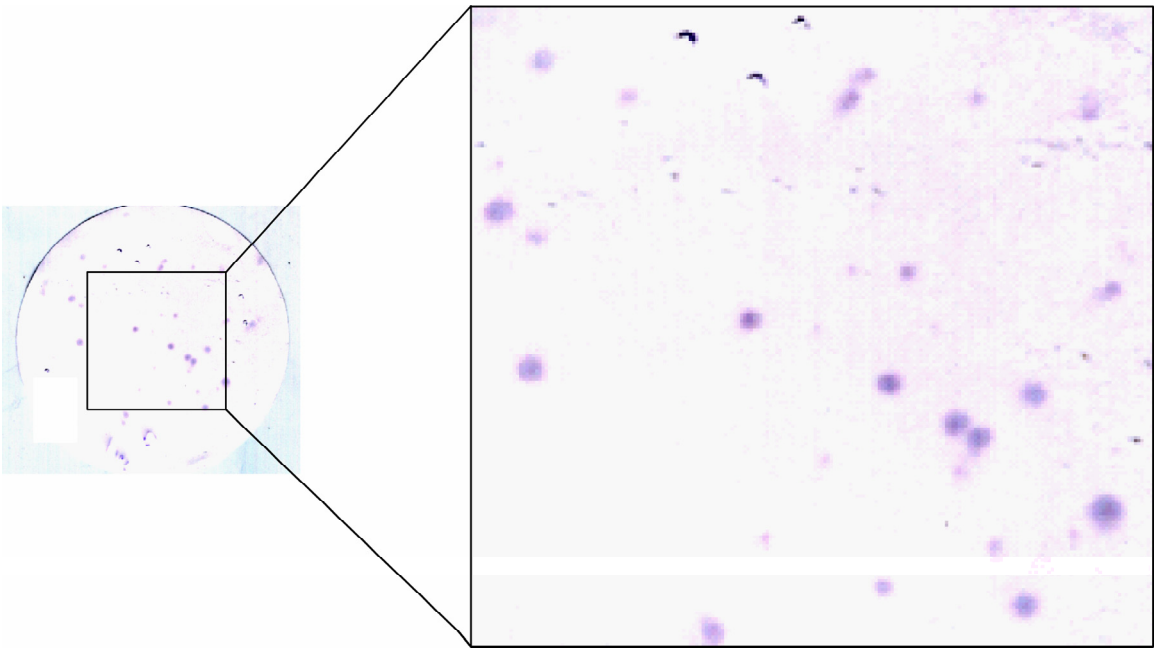


Figure 6.12. Plaque lift of phage clones present in the sub library derived from three rounds of affinity selection and enrichment. Phage clones from present after three rounds of affinity selection and enrichment were cultured and transferred onto nitrocellulose and probed with antibody 9D7 to assay for the presence of phage clones that have been selected and exhibit the ability to bind antibody 9D7.

likelihood that peptides displayed on the pIII protein of the M13 phage will be capable of epitope mimicry, given the net electrostatic similarity between IL-10 and the pIII protein.

Peptides mimetics were selected with antibody 9D7 by performing three rounds of affinity enrichment, where the phage titer increased follow each round of selection. Plaque lifts were performed on phage after 3 rounds of selection and were positive as seen in Figure 6.12. Selected clones from selection round 2 and round 3 were isolated and selected members were sequenced, as shown in table 6.5. The dominant clone, present after 2 and 3 rounds of selection had the peptide sequence GIRNDPIRW; this clone was assayed for activity by enzyme linked immunosorbent assay (ELISA).

Round 2 Clones	Round 3 Clones
GIRNDPIRW (X19)	**GIRNDPIRW (X30)**
GNGNDPIRW	**GMGNDPIRW**
GRVNRSTFR	**TASRDTQRW**
SWFNSRGAS	**FGLRLTSGD**
EKEYWRIQW	**KVIRNSHHE**
TLSLWWH	**AGASGRELR**
SFLAAFSKS	
NLHRLWGIS	
DQRMARLTL	
SVTGW	
KAWN	
AGASGRELP	
LQNTARARL	
LNKISIVNS	
ISTNLGFSQ	
QIQGKQ	
YNLHPLGKV	
RQIEWMTAL	
RGETAENTG	
WRRSDQQKP	

Table 6.5. Phage sequences from second and third rounds of affinity selection for IL-10 mimetic peptides.

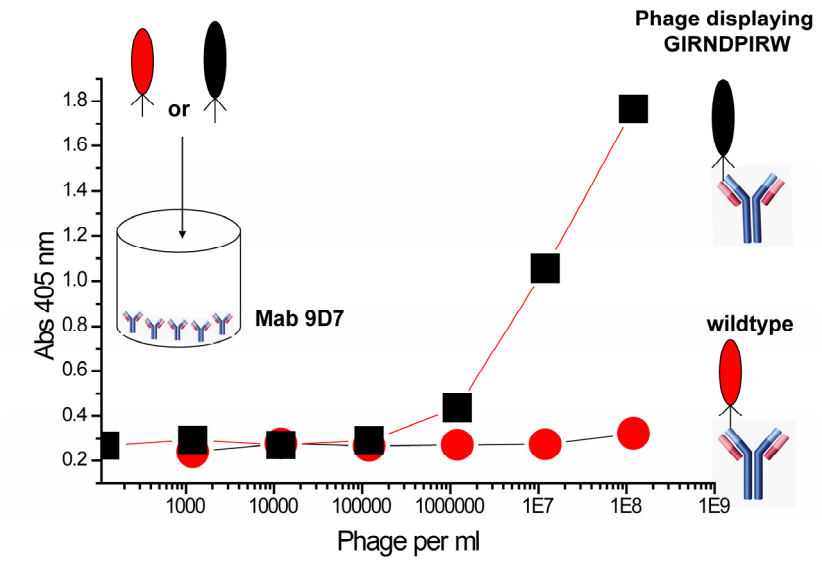


Figure 6.13. ELISA assay demonstrating that the phage displaying sequence GIRNDPIRW is capable of binding to antibody 9D7 with specificity relative to wild-type phage demonstrating the binding of phage to antibody is due to the displayed peptide rather than non specific binding due to other features of the phage.

Antibody 9D7 was adsorbed to the wells of a 96 well plate and then exposed to either the wild type phage or phage displaying GIRNDPIRW peptide, bound phage were detected by rabbit anti phage polyclonal antibody. ELISA showed that antibody 9D7 bound phage displaying peptide GIRNDPIRW where wild-type phage bound to antibody 9D7 weakly as shown in Figure 6.13. Next the binding of antibody 9D7 or an irrelevant antibody (K42-41L) to a phage clone displaying peptide GIRNDPIRW was measured.

Either 9D7 or irrelevant antibody K42-41L were absorbed to the well of a 96 well ELISA plate and the binding of phage displaying peptide GIRNDPIRW was found to be specific for antibody 9D7 showing almost no non-specific binding with irrelevant antibody (Figure 6.14). We assayed the ability of the antigen IL-10 to displace the phage clone displaying peptide GIRNDPIRW in a competitive ELISA assay (Figure 6.15). Antibody 9D7 once again was immobilized on the ELISA plate and a constant number of

phage were added to each well and on increasing amount of IL-10 was added to the wells in triplicate series on the plate. Unbound phage were removed and bound phage were detected. The phage displaying peptide sequence GIRNDPIRW is thus found to bind to the antibody paratope in a fashion that is similar to the binding of the antigen. The selected peptides were then aligned onto the primary sequence of IL-10 employing EpiAlign. The probes were aligned to the primary sequence of IL-10, resulting in the mapping of part of the epitope of IL-10, as shown in Figure 6.16.

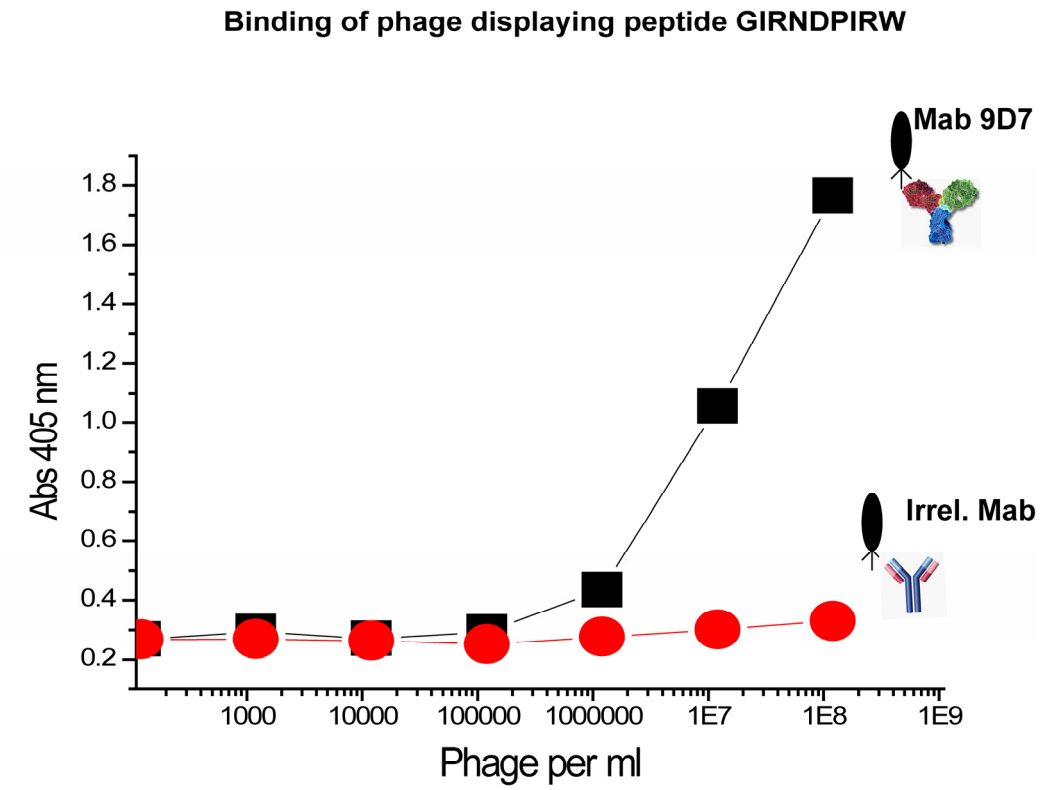


Figure 6.14. Binding of phage displaying peptide GIRNDPIRW to antibody 9D7 relative to an irrelevant antibody, demonstrating specificity of antibody-mimetic peptide specificity.

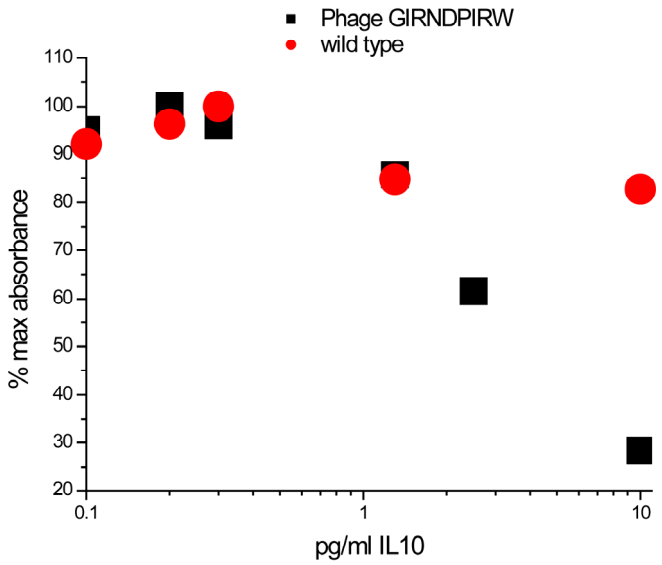


Figure 6.15. Phage displaying peptide GIRNDPIRW can be competed off of antibody 9D7 with IL-10, demonstrating the mimetic peptide is binding to a similar epitope on antibody 9D7

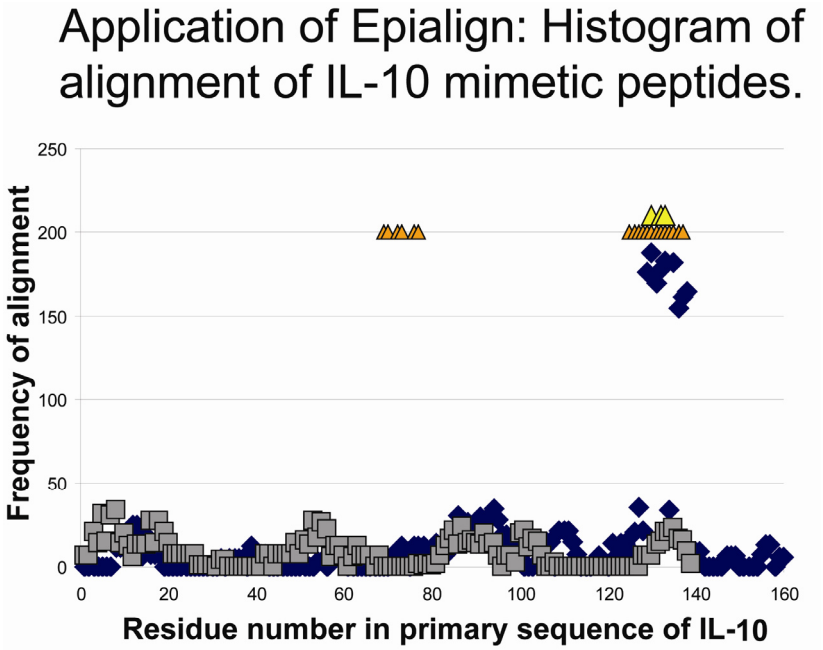


Figure 6.16. Histogram of EpiAlign results for the alignment of peptides following three rounds of selection (shown in table 6.5). The grey squares are the alignment of a random set of peptides employing the substitution matrix shown in table 6.2. The gold triangles are the genuine epitope and the large yellow triangles are key residues mediating binding of antibody to antigen.

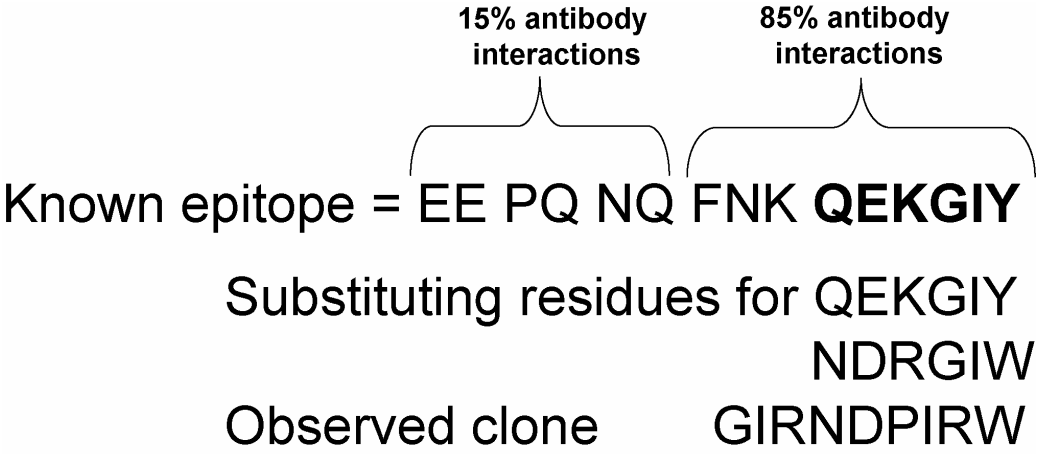


Figure 6.17 Conservative amino acid substitution for residues that make up the epitope for antibody 9D7. The structural epitope of antibody 9D7 is bipartite and residues FNK QEKGIY contribute the majority of interaction between antibody and antigen. Allowing for substitution of the last six residues QEKGIY to chemically similar residues NDRGIW allows for a demonstration where the dominant peptide display by phage can be readily aligned to the primary sequence of IL10.

Phage displaying peptides selected following 2 and 3 rounds of affinity enrichment on immobilized antibody 9D7 were positive by plaque lift (Figure 6.12). The peptide sequence GIRNDPIRW was present in over 50% of the phage clones sequences following two rounds of affinity selection and 80% after 3 rounds of selection (table 6.5). The activity assays of phage displaying peptide GIRNDPIRW demonstrate that the peptide binds with specificity to antibody 9D7 (Figure 6.16) and can be displaced by the genuine antigen IL-10, again demonstrating the specificity of the dominant phage clone for binding to the antibody 9D7. The structural epitope of antibody 9D7 shown in Figure 6.11 is bipartite however each of the two components does not contribute equally to the binding of the antibody to the epitope. 85% of the contacts, salt bridge and hydrogen bonds are formed between the sequence ^{128}FNK_QEKGIY^{137}.and antibody 9D7 therefore selection of peptides that mimic this region specifically may be expected. The dominant

clone sequence selected is GIRNDPIRW, bearing little resemblance to the dominant epitope region on IL-10. Allowing for chemically equivalent residues to be substituted on IL-10 results in an epitope region containing the residues ^{128}WNR_NDRGIW^{137}, which is surprisingly similar to the dominant clone selected from phage display. The lack of conservation between the genuine epitope and the selected mimetic peptide is surprising however the biochemical activity of the phage displayed peptide GIRNDPIRW strongly suggests that this clone is mimicking the genuine epitope. Our selection of a dominant peptide clone containing high levels of substitution is consistent with reported results for the mapping of epitopes on gp120 by Enshell-Seijffers et al., and may be a common feature when selecting mimetic peptides to discontinuous antibody epitopes [231]. Interestingly programs such as Pepsurf, 3DEX and MIMOX, fail to map the dominant peptide sequence GIRNDPIRW to the known epitope of 9D7 on IL-10, and programs MIMOP and Mapitope failed to run completely with the data provided.

Discussion and Conclusion

Phage displayed random peptide libraries have been used to map the epitope of may antibodies [235], however there are few examples where a discontinuous epitope, that is known by x-ray crystallography, have been mapped by the application of phage display [231, 251]. Here we have described the mapping of several antibody epitopes for which there are high resolution structural models of the antibody antigen complexes. We have described the creation and usage of a quantitative amino acid substitution matrix based on the observed frequency of amino acid side chain interactions, which we believe makes the substitution scores more applicable to substitutions that may occur at sites of

protein-protein interactions. The matrix created has been used in sequence alignment of mimetic peptides onto the primary sequence of a target protein, allowing for mapping of known antibody epitopes on hen egg lysozyme and recombinant interleukin 10.

When mapping the epitopes of several anti-lysozyme antibodies the peptides selected contain an abundance of positively charged residues and several identical antibodies were selected using different antibodies. If an identical peptide sequence is selected from a random peptide library using different antibodies this indicates that there is some shared selective pressure between antibodies used in the selection. An obvious shared feature among all of the anti-lysozyme antibodies is that they recognize epitopes on lysozyme which is a very basic protein. Our hypothesis is that peptides were selected such that the positive charges on the peptides neutralized the negative charges on the pIII of the phage reducing an electrostatic incompatibility between the phage pIII and the anti-lysozyme antibody.

Electrostatic compatibility between antigen and mimetope has been observed in many published cases. Two monoclonal antibodies, 3A9 and 5C7, to the chemokine receptor CCR5 were mapped employing pVIII peptide phage display resulting in the assignment of two overlapping putative discontinuous epitopes [252]. The epitopes for antibodies 3A9 and 5C7 have theoretical pI values of 3.8(3A9) and 7.17(5C7). The dominant phage displayed peptides selected mimicking the epitope on antibody 3A9 have a theoretical pI of 5 and the peptides selected mimicking the epitope on antibody 5C7 have a theoretical pI of 8. When screening clones for binding to antibody 3A9, 23 of 26 clones (88%) reacted strongly, 18 of 19 sequenced clones contained the same insert which was acidic in nature. In contrast, 64 clones to antibody 5C7 were screened for

binding,19 of the clones or 30% where found to be active and of those 15 were sequenced and used to map the epitope [252]. The observation that peptide selection by antibody 3A9 resulted in a stronger consensus and a greater number of active clones is possibly due to electrostatic compatibility between antibody epitope being acidic and mimetic selection by phage display.

Residues of the putative epitope of anti-von Willebrand Factor (VWF) antibody 82D6A3 have been mapped by alanine scanning and mimetic peptide selection employing phage display [253]. The residues that make up this putative epitope are PWHMSAD and have a theoretical pI of 4.9. Five peptide sequences selected by phage display are reported and these peptides have theoretical pI values ranging from 5.8 to 10. All selected peptides contain a conserved PW, acidic peptide sequences displayed on phage exhibited greatest binding activity as measured by ELISA. The difference in capacity for antibody binding between selected VWF mimetic peptides that share the same PW residues identified as mimicking the VWF epitope may be attributed to more favorable electrostatic properties of the more acidic peptides.

The experimental evidence gathered in the epitope mapping of the panel of anti-lysozyme antibodies suggests that the electrostatic nature of the epitope and paratope contributes to the outcome of the selection of mimetic peptides from random peptide libraries displayed on phage. The results described above for epitope mapping of lysozyme, CCR5 and VWF all indicate that the electrostatic nature of the epitope and selected mimetic peptide seem to correlate, suggesting the importance of electrostatic mimicry as a component of epitope mimicry. Successful application of phage display for

the mapping of discontinuous epitopes may require electrostatic similarity between antigen and phage allowing for electrostatic mimicry of antibody epitopes.

Our epitope mapping results for the panel of anti-lysozyme antibodies as well as published data supports the notion that current phage display technology based on the negatively charged pIII or PVIII display format may not allow for adequate mimicry for many antibody-antigen pairs. Given the isoelectric distribution of the theoretical proteomes for all domains of life appear strikingly bimodal [254], half basic and half acidic it is likely that current phage display technology only allows for a robust mimicry of approximately half of all antibody epitope. The creation of a charge neutralized pIII variant may improve phage display technology and increase the scope of successful application of this technique.

The new method for mapping discontinuous epitopes that can accommodate for the complexity of the task and is implemented in the computer program EpiAlign was demonstrated. The alignment of the probes to a target sequence, finding a set of top scoring alignments that are used to map the epitope on an antigen is a computationally intensive task however we have developed software that allows for this type of alignment problem to be solved on a typical desktop computer in a manageable amount of time.

We have presented evidence suggesting that successful application of random library display and affinity enrichment of selected mimetics is sensitive to the biological context of display as seen in studies mapping the epitopes of anti-lysozyme antibodies. The successful mapping of part of the epitope of antibody 9D7 on IL-10 and F9.13.7 on lysozyme illustrates that all region and residues involved in antibody binding are not equally represented when selecting mimetopes. This observation is consistent with the

notion that very few residues may contribute the bulk of the required favorable energetic contributions leading to high affinity binding as can be seen in mutagenesis studies.

Material and Methods

Biopanning and Mimetic Peptide Selection

Peptide mimetics for the epitope recognized by antibody 9D7 were selected from the J404 random peptide library [204]. Briefly, antibody 9D7 (Southernbiotech, 10100-01) was immobilized onto CNBr activated sepharose beads (Pharmacia, 17-0430-01) following the manufacturers instructions. Phage displaying mimetic peptides were selected and enriched over three rounds of affinity selection. Each round of affinity enrichment of phage displaying mimetic peptides was performed as follows, 75 ul of naive phage library J404 or amplified phage from the 1^{st} or 2^{nd} rounds for each successive round of selection were added to 250 ul of 9D7 sepharose. The slurry volume was adjusted to a final volume of 1.5 ml with phage buffer (50 mM TBS pH 7.5, 1mg/ml bovine serum albumin, 0.5% Tween 20) and incubated for 48 hours at 4ºC. Unbound phage were removed by washing the antibody sepharose with 100 ml of ice cold phage buffer. Phage bound to antibody immobilized on resin were eluted by addition of 2 ml low pH elution buffer (0.1 M sodium acetate, 0.5 M NaCl, pH 4.0) which was immediately neutralized by addition of 40 ul 2M Tris base pH 8. Selected phage were amplified by infecting 5 ml of starved K91 *e. coli* cells which were then cultured over night in soft agar at 37º C. Amplified phage were then recovered from soft agar lawn by adding 50 ml of 50 mM TRIS-HCl pH7.5 to overnight culture and rocking for 2 hours at room temperature. The tris buffer containing phage from plaques on the soft agar lawn

recovered from the plaque lawn and centrifuged to remove large particles. Amplfied phage from the selection and amplification were then precipitated from the Tris by addition of PEG/NaCl (16.7% PEG 8000, 3.3 M NaCl) and pelleted by centrifugation. Following each round of selection 15 ul of phage eluted from antibody bound to sepharose was used to determine the titer for the selection.

DNA Sequencing of Selected Phage

Phage were diluted and K91 cells infected for 10 minutes then mixed with soft agar and poured on top of hard agar and cultured over night allowing for the isolation of phage clones. Phage clone single stranded DNA was isolated and used for sequencing employing QIAGEN M13 DNA isolation kit (GIAGEN, 27704). DNA sequencing reactions were run at Nevada State genomics facility.

Plaque Lift Assay

Viral plaques were grown by infecting starved K91 *e. coli* cells. 300 ul of starved k91 cells were infected by adding 100 ul of phage containing a sufficient number of virion to generate 50-200 plaques per agar plate. The infected k91 cells were added to 3 ml of soft agar at 45-50 ºC, mix well by inversion and then pour on top of hard agar plate. The agar plate was then incubated overnight at 37ºC. A nitrocellulose disk (S&S) was then placed on top of the plaques and left for several hours to allow for the transfer of the plaques. The nitrocellulose was then blocked with 50 mM Tris pH 7.4 containing 3% bovine serum albumin, 0.2% tween-20 overnight at 4ºC. The plaques were exposed to the primary antibody 9D7, D1.3, D11.15 or F.9.13.7 in 50 mM Tris (pH 7.4) at a concentration of 2 ug/ml overnight at 4ºC, then washed with wash buffer (50 mM Tris

(pH 7.4) containing 0.2% tween-20), 3 times to remove unbound antibody and then exposed to the secondary goat anti rat IGG Alkaline phosphatase conjugate (sigma-aldrich A8438) for 9D7 or goat anti mouse IgG alkaline phosphatase conjugate (maker) for the anti lysozyme antibodies, diluted 1:5000 in 50 mM Tris (pH 7.4) and incubated overnight at 4ºC or 4 hours at room temperature. The nitrocellulose disks were then washed 3 times with wash buffer to remove excess secondary antibody the secondary was developed with NBT-BCIP (source) until spots were visible and stopped by rinsing with water and allowing to air dry.

ELISA

Enzyme-linked immunosorbent assays (ELISA) were performed using polyvinyl chloride microtiter plates coated antibody 9D7 and K4241L by incubating plates with 100 ul of 1 ug/ml of antibody in 50 mM Tris pH7.4 overnight at 4ºC, washed 3 times with PBS and then blocked with 5% (w/v) milk protein, 0.02% NaN_3 in PBS. A serial dilution of phage clone displaying peptide GIRNDPIRW or wild type phage was added to the coated and blocked microtiter plate to measure antibody binding to phage displaying peptide or phage only and binding of phage to antibody 9D7 or irrelevant antibody K4241L. For competition ELISA, microtiter plates were prepared as described above with addition of antibody, blocked and 100 ul containing 10^8 phage, either wild-type or phage displaying GIRNDPIRW, were added to each well. A dilution series of IL-10 was then added to the titer plate and the titer plate was incubated overnight at 4ºC. Unbound phage were removed by washing 3 times with wash buffer prior to exposure to primary and secondary antibodies. Binding of phage to immobilized antibody was detected by the

addition primary rabbit anti phage polyclonal serum diluted 1:10,000, removing unbound antibody by washing with wash buffer 3 times and then adding alkaline phosphatase conjugated goat anti-rabbit antibody (GAR-AP) (Biorad) diluted 1:10,000 in PBS. Following the addition of GAR-AP, plates were incubated for 4 hours at room temperature on an orbital shaker and washed 3 times with PBS. Following the addition of NBT/BCIP substrate, bound GAM-AP was detected by measuring absorbance at 405 nm.

REFERENCES

1. Wald, G., *The molecular basis of visual excitation.* Nature, 1968. **219**(156): p. 800-7.

2. Wald, G., *The Biochemistry of Vision doi:10.1146/annurev.bi.22.070153.002433.* Annual Review of Biochemistry, 1953. **22**(1): p. 497-526.

3. Godchaux, W., 3rd and W.F. Zimmerman, *Soluble proteins of intact bovine rod cell outer segments.* Exp Eye Res, 1979. **28**(4): p. 483-500.

4. Hargrave, P.A., et al., *The structure of bovine rhodopsin.* Biophys Struct Mech, 1983. **9**(4): p. 235-44.

5. Ovchinnikov Yu, A., *Rhodopsin and bacteriorhodopsin: structure-function relationships.* FEBS Lett, 1982. **148**(2): p. 179-91.

6. Nathans, J. and D.S. Hogness, *Isolation, sequence analysis, and intron-exon arrangement of the gene encoding bovine rhodopsin.* Cell, 1983. **34**(3): p. 807-14.

7. Palczewski, K., et al., *Crystal structure of rhodopsin: A G protein-coupled receptor.* Science, 2000. **289**(5480): p. 739-45.

8. Okada, T., et al., *Functional role of internal water molecules in rhodopsin revealed by X-ray crystallography.* Proc Natl Acad Sci U S A, 2002. **99**(9): p. 5982-7.

9. Okada, T., et al., *The retinal conformation and its environment in rhodopsin in light of a new 2.2 A crystal structure.* J Mol Biol, 2004. **342**(2): p. 571-83.

10. Teller, D.C., et al., *Advances in determination of a high-resolution three-dimensional structure of rhodopsin, a model of G-protein-coupled receptors (GPCRs).* Biochemistry, 2001. **40**(26): p. 7761-72.

11. Li, J., et al., *Structure of bovine rhodopsin in a trigonal crystal form.* J Mol Biol, 2004. **343**(5): p. 1409-38.

12. Nakamichi, H. and T. Okada, *Crystallographic analysis of primary visual photochemistry.* Angew Chem Int Ed Engl, 2006. **45**(26): p. 4270-3.

13. Nakamichi, H. and T. Okada, *Local peptide movement in the photoreaction intermediate of rhodopsin.* Proc Natl Acad Sci U S A, 2006. **103**(34): p. 12729-34.

14. Takeda, S., et al., *Identification of G protein-coupled receptor genes from the human genome sequence.* FEBS Lett, 2002. **520**(1-3): p. 97-101.

15. Fredriksson, R., et al., *The G-protein-coupled receptors in the human genome form five main families. Phylogenetic analysis, paralogon groups, and fingerprints.* Mol Pharmacol, 2003. **63**(6): p. 1256-72.

16. Lefkowitz, R.J., *Historical review: a brief history and personal retrospective of seven-transmembrane receptors.* Trends Pharmacol Sci, 2004. **25**(8): p. 413-22.

17. Pierce, K.L., R.T. Premont, and R.J. Lefkowitz, *SEVEN-TRANSMEMBRANE RECEPTORS.* Nature Reviews Molecular Cell Biology
Nat Rev Mol Cell Biol, 2002. **3**(9): p. 639-650.

18. Venter, J.C., et al., *The sequence of the human genome.* Science, 2001. **291**(5507): p. 1304-51.

19. Hill, C.A., et al., *G protein-coupled receptors in Anopheles gambiae.* Science, 2002. **298**(5591): p. 176-8.

20. Josefsson, L.G., *Evidence for kinship between diverse G-protein coupled receptors.* Gene, 1999. **239**(2): p. 333-40.

21. Spudich, J.L., et al., *Retinylidene proteins: structures and functions from archaea to humans.* Annu Rev Cell Dev Biol, 2000. **16**: p. 365-92.

22. Pardo, L., et al., *On the use of the transmembrane domain of bacteriorhodopsin as a template for modeling the three-dimensional structure of guanine nucleotide-binding regulatory protein-coupled receptors.* Proc Natl Acad Sci U S A, 1992. **89**(9): p. 4009-12.

23. Birge, R.R. and B.W. Vought, *Energetics of rhodopsin photobleaching: photocalorimetric studies of energy storage in early and later intermediates.* Methods Enzymol, 2000. **315**: p. 143-63.

24. Okada, T. and K. Palczewski, *Crystal structure of rhodopsin: implications for vision and beyond.* Curr Opin Struct Biol, 2001. **11**(4): p. 420-6.

25. Kolakowski, L.F., Jr., *GCRDb: a G-protein-coupled receptor database.* Receptors Channels, 1994. **2**(1): p. 1-7.

26. Fredriksson, R. and H.B. Schioth, *The repertoire of G-protein-coupled receptors in fully sequenced genomes.* Mol Pharmacol, 2005. **67**(5): p. 1414-25.

27. Arnis, S., et al., *A conserved carboxylic acid group mediates light-dependent proton uptake and signaling by rhodopsin.* J Biol Chem, 1994. **269**(39): p. 23879-81.

28. Cohen, G.B., et al., *Constitutive activation of opsin: influence of charge at position 134 and size at position 296.* Biochemistry, 1993. **32**(23): p. 6111-5.

29. Fahmy, K. and T.P. Sakmar, *Regulation of the rhodopsin-transducin interaction by a highly conserved carboxylic acid group.* Biochemistry, 1993. **32**(28): p. 7229-36.

30. Mirzadegan, T., et al., *Sequence analyses of G-protein-coupled receptors: similarities to rhodopsin.* Biochemistry, 2003. **42**(10): p. 2759-67.

31. Madabushi, S., et al., *Evolutionary trace of G protein-coupled receptors reveals clusters of residues that determine global and class-specific functions.* J Biol Chem, 2004. **279**(9): p. 8126-32.

32. George, S.R., B.F. O'Dowd, and S.P. Lee, *G-protein-coupled receptor oligomerization and its potential for drug discovery.* Nat Rev Drug Discov, 2002. **1**(10): p. 808-20.

33. Whitelegge, J.P., C.B. Gundersen, and K.F. Faull, *Electrospray-ionization mass spectrometry of intact intrinsic membrane proteins.* Protein Sci, 1998. **7**(6): p. 1423-30.

34. Sakmar, T.P., et al., *Rhodopsin: insights from recent structural studies.* Annu Rev Biophys Biomol Struct, 2002. **31**: p. 443-84.

35. Dartnall, H.J., *The photosensitivities of visual pigments in the presence of hydroxylamine.* Vision Res, 1968. **8**(4): p. 339-58.

36. Dratz, E.A. and P.A. Hargrave, *The structure of rhodopsin and the rod outer segment disk membrane.* Trends in Biochemical Sciences, 1983. **8**(4): p. 128-131.

37. Palczewski, K., *G protein-coupled receptor rhodopsin.* Annu Rev Biochem, 2006. **75**: p. 743-67.

38. Fotiadis, D., et al., *Structure of the rhodopsin dimer: a working model for G-protein-coupled receptors.* Curr Opin Struct Biol, 2006. **16**(2): p. 252-9.

39. Cooper, A., *Energy uptake in the first step of visual excitation.* Nature, 1979. **282**(5738): p. 531-3.

40. Rieke, F. and D.A. Baylor, *Molecular origin of continuous dark noise in rod photoreceptors.* Biophys J, 1996. **71**(5): p. 2553-72.

41. Sakmar, T.P., *Structure of rhodopsin and the superfamily of seven-helical receptors: the same and not the same.* Curr Opin Cell Biol, 2002. **14**(2): p. 189-95.

42. Longstaff, C., R.D. Calhoon, and R.R. Rando, *Deprotonation of the Schiff base of rhodopsin is obligate in the activation of the G protein.* Proc Natl Acad Sci U S A, 1986. **83**(12): p. 4209-13.

43. Jager, F., et al., *Identification of glutamic acid 113 as the Schiff base proton acceptor in the metarhodopsin II photointermediate of rhodopsin.* Biochemistry, 1994. **33**(36): p. 10878-82.

44. Sakmar, T.P., R.R. Franke, and H.G. Khorana, *Glutamic acid-113 serves as the retinylidene Schiff base counterion in bovine rhodopsin.* Proc Natl Acad Sci U S A, 1989. **86**(21): p. 8309-13.

45. Arnis, S. and K.P. Hofmann, *Two different forms of metarhodopsin II: Schiff base deprotonation precedes proton uptake and signaling state.* Proc Natl Acad Sci U S A, 1993. **90**(16): p. 7849-53.

46. Steinberg, G., M. Ottolenghi, and M. Sheves, *pKa of the protonated Schiff base of bovine rhodopsin. A study with artificial pigments.* Biophys J, 1993. **64**(5): p. 1499-502.

47. Janz, J.M. and D.L. Farrens, *Assessing structural elements that influence Schiff base stability: mutants E113Q and D190N destabilize rhodopsin through different mechanisms.* Vision Res, 2003. **43**(28): p. 2991-3002.

48. Yan, E.C., et al., *Retinal counterion switch in the photoactivation of the G protein-coupled receptor rhodopsin.* Proc Natl Acad Sci U S A, 2003. **100**(16): p. 9262-7.

49. Vogel, R., et al., *Modulating rhodopsin receptor activation by altering the pKa of the retinal Schiff base.* J Am Chem Soc, 2006. **128**(32): p. 10503-12.

50. Arshavsky, V.Y., T.D. Lamb, and E.N. Pugh, Jr., *G proteins and phototransduction.* Annu Rev Physiol, 2002. **64**: p. 153-87.

51. Palczewski, K., et al., *Mechanism of rhodopsin kinase activation.* J. Biol. Chem., 1991. **266**(20): p. 12949-12955.

52. Kuhn, H., *Light-regulated binding of rhodopsin kinase and other proteins to cattle photoreceptor membranes.* Biochemistry, 1978. **17**(21): p. 4389-95.

53. Maeda, T., Y. Imanishi, and K. Palczewski, *Rhodopsin phosphorylation: 30 years later.* Prog Retin Eye Res, 2003. **22**(4): p. 417-34.

54. Paulsen, R. and J. Bentrop, *Activation of rhodopsin phosphorylation is triggered by the lumirhodopsin-metarhodopsin I transition.* Nature, 1983. **302**(5907): p. 417-9.

55. Miller, J.L. and E.A. Dratz, *Phosphorylation at sites near rhodopsin's carboxyl-terminus regulates light initiated cGMP hydrolysis.* Vision Res, 1984. **24**(11): p. 1509-21.

56. Kuhn, H., S.W. Hall, and U. Wilden, *Light-induced binding of 48-kDa protein to photoreceptor membranes is highly enhanced by phosphorylation of rhodopsin.* FEBS Lett, 1984. **176**(2): p. 473-8.

57. Sommer, M.E., W.C. Smith, and D.L. Farrens, *Dynamics of arrestin-rhodopsin interactions: arrestin and retinal release are directly linked events.* J Biol Chem, 2005. **280**(8): p. 6861-71.

58. Gainetdinov, R.R., et al., *Desensitization of G protein-coupled receptors and neuronal functions.* Annu Rev Neurosci, 2004. **27**: p. 107-44.

59. Wu, C.W. and L. Stryer, *Proximity relationships in rhodopsin.* Proc Natl Acad Sci U S A, 1972. **69**(5): p. 1104-8.

60. Hargrave, P.A., et al., *The partial primary structure of bovine rhodopsin and its topography in the retinal rod cell disc membrane.* Neurochemistry International, 1980. **1**: p. 231-244.

61. Hargrave, P.A. and S.L. Fong, *The amino- and carboxyl-terminal sequence of bovine rhodopsin.* J Supramol Struct, 1977. **6**(4): p. 559-70.

62. Fukuda, M.N., D.S. Papermaster, and P.A. Hargrave, *Structural analysis of carbohydrate moiety of bovine rhodopsin.* Methods Enzymol, 1982. **81**: p. 214-23.

63. Bownds, D., *Site of attachment of retinal in rhodopsin.* Nature, 1967. **216**(121): p. 1178-81.

64. Wang, J.K., J.H. McDowell, and P.A. Hargrave, *Site of attachment of 11-cis-retinal in bovine rhodopsin.* Biochemistry, 1980. **19**(22): p. 5111-7.

65. Ovchinnikov Yu, A., N.G. Abdulaev, and A.S. Bogachuk, *Two adjacent cysteine residues in the C-terminal cytoplasmic fragment of bovine rhodopsin are palmitylated.* FEBS Lett, 1988. **230**(1-2): p. 1-5.

66. Deretic, D., *A role for rhodopsin in a signal transduction cascade that regulates membrane trafficking and photoreceptor polarity.* Vision Res, 2006. **46**(27): p. 4427-33.

67. Piscitelli, C.L., et al., *The equilibrium between metarhodopsin-I and metarhodopsin-II is dependent on the conformation of the 3rd cytoplasmic loop.* J Biol Chem, 2005.

68. Bailey, B.W., et al., *Constraints on the conformation of the cytoplasmic face of dark-adapted and light-excited rhodopsin inferred from antirhodopsin antibody imprints.* Protein Sci, 2003. **12**(11): p. 2453-75.

69. Hubbell, W.L., et al., *Rhodopsin structure, dynamics, and activation: a perspective from crystallography, site-directed spin labeling, sulfhydryl reactivity, and disulfide cross-linking.* Adv Protein Chem, 2003. **63**: p. 243-90.

70. Yang, K., et al., *Structure and function in rhodopsin. Single cysteine substitution mutants in the cytoplasmic interhelical E-F loop region show position-specific effects in transducin activation.* Biochemistry, 1996. **35**(38): p. 12464-9.

71. Farahbakhsh, Z.T., K. Hideg, and W.L. Hubbell, *Photoactivated conformational changes in rhodopsin: a time-resolved spin label study.* Science, 1993. **262**(5138): p. 1416-9.

72. Farrens, D.L., et al., *Requirement of rigid-body motion of transmembrane helices for light activation of rhodopsin.* Science, 1996. **274**(5288): p. 768-70.

73. Gether, U., et al., *Agonists induce conformational changes in transmembrane domains III and VI of the beta2 adrenoceptor.* Embo J, 1997. **16**(22): p. 6737-47.

74. Jensen, A.D., et al., *Agonist-induced conformational changes at the cytoplasmic side of transmembrane segment 6 in the beta 2 adrenergic receptor mapped by site-selective fluorescent labeling.* J Biol Chem, 2001. **276**(12): p. 9279-90.

75. Sheikh, S.P., et al., *Similar structures and shared switch mechanisms of the beta2-adrenoceptor and the parathyroid hormone receptor. Zn(II) bridges between helices III and VI block activation.* J Biol Chem, 1999. **274**(24): p. 17033-41.

76. Shapiro, D.A., et al., *Evidence for a model of agonist-induced activation of 5-hydroxytryptamine 2A serotonin receptors that involves the disruption of a strong ionic interaction between helices 3 and 6.* J Biol Chem, 2002. **277**(13): p. 11441-9.

77. Yu, H. and D.D. Oprian, *Tertiary interactions between transmembrane segments 3 and 5 near the cytoplasmic side of rhodopsin.* Biochemistry, 1999. **38**(37): p. 12033-40.

78. Fritze, O., et al., *Role of the conserved NPxxY(x)5,6F motif in the rhodopsin ground state and during activation.* Proc Natl Acad Sci U S A, 2003. **100**(5): p. 2290-5.

79. Blomgren, F. and S. Larsson, *Primary photoprocess in vision: minimal motion to reach the photo- and bathorhodopsin intermediates.* J Phys Chem B Condens Matter Mater Surf Interfaces Biophys, 2005. **109**(18): p. 9104-10.

80. Rao, V.R. and D.D. Oprian, *Activating mutations of rhodopsin and other G protein-coupled receptors.* Annu Rev Biophys Biomol Struct, 1996. **25**: p. 287-314.

81. Lewis, J.W., et al., *Proton movement and photointermediate kinetics in rhodopsin mutants.* Biochemistry, 2006. **45**(17): p. 5430-9.

82. Borhan, B., et al., *Movement of retinal along the visual transduction path.* Science, 2000. **288**(5474): p. 2209-12.

83. Szundi, I., et al., *Bleaching kinetics of artificial visual pigments with modifications near the ring-polyene chain connection.* Biochemistry, 2002. **41**(6): p. 2028-35.

84. Marr, K. and K.S. Peters, *Photoacoustic calorimetric study of the conversion of rhodopsin and isorhodopsin to lumirhodopsin.* Biochemistry, 1991. **30**(5): p. 1254-8.

85. Furutani, Y., H. Kandori, and Y. Shichida, *Structural changes in lumirhodopsin and metarhodopsin I studied by their photoreactions at 77 K.* Biochemistry, 2003. **42**(28): p. 8494-500.

86. Ishiguro, M., Y. Oyama, and T. Hirano, *Structural models of the photointermediates in the rhodopsin photocascade, lumirhodopsin, metarhodopsin I, and metarhodopsin II.* Chembiochem, 2004. **5**(3): p. 298-310.

87. Pan, D. and R.A. Mathies, *Chromophore structure in lumirhodopsin and metarhodopsin I by time-resolved resonance Raman microchip spectroscopy.* Biochemistry, 2001. **40**(26): p. 7929-36.

88. Matthews, R.G., et al., *Tautomeric Forms of Metarhodopsin 10.1085/jgp.47.2.215.* J. Gen. Physiol., 1963. **47**(2): p. 215-240.

89. Szundi, I., et al., *Proton transfer reactions linked to rhodopsin activation.* Biochemistry, 1998. **37**(40): p. 14237-44.

90. Altenbach, C., et al., *Structural features and light-dependent changes in the cytoplasmic interhelical E-F loop region of rhodopsin: a site-directed spin-labeling study.* Biochemistry, 1996. **35**(38): p. 12470-8.

91. Cooper, A., *Rhodopsin photoenergetics: lumirhodopsin and the complete energy profile.* FEBS Lett, 1981. **123**(2): p. 324-6.

92. Kim, J.M., et al., *Structure and function in rhodopsin: rhodopsin mutants with a neutral amino acid at E134 have a partially activated conformation in the dark state.* Proc Natl Acad Sci U S A, 1997. **94**(26): p. 14273-8.

93. Vogel, R., et al., *Photoreactions of metarhodopsin III.* Biochemistry, 2004. **43**(31): p. 10255-64.

94. Vogel, R., et al., *Formation of Meta III during the decay of activated rhodopsin proceeds via Meta I and not via Meta II.* Biochemistry, 2004. **43**(29): p. 9457-66.

95. Heck, M., et al., *Signaling states of rhodopsin. Formation of the storage form, metarhodopsin III, from active metarhodopsin II.* J Biol Chem, 2003. **278**(5): p. 3162-9.

96. Salom, D., et al., *Crystal structure of a photoactivated deprotonated intermediate of rhodopsin.* Proc Natl Acad Sci U S A, 2006. **103**(44): p. 16123-8.

97. Vogel, R., et al., *Rhodopsin photoproducts in 2D crystals.* J Mol Biol, 2004. **338**(3): p. 597-609.

98. Szundi, I., et al., *Rhodopsin photointermediates in two-dimensional crystals at physiological temperatures.* Biochemistry, 2006. **45**(15): p. 4974-82.

99. Emeis, D. and K.P. Hofmann, *Shift in the relation between flash-induced metarhodopsin I and metarhodpsin II within the first 10% rhodopsin bleaching in bovine disc membranes.* FEBS Lett got, 1981. **136**(2): p. 201-7.

100. Parkes, J.H., S.K. Gibson, and P.A. Liebman, *Temperature and pH dependence of the metarhodopsin I-metarhodopsin II equilibrium and the binding of metarhodopsin II to G protein in rod disk membranes.* Biochemistry, 1999. **38**(21): p. 6862-78.

101. Applebury, M.L., *Dynamic processes of visual transduction.* Vision Res, 1984. **24**(11): p. 1445-54.

102. Parkes, J.H. and P.A. Liebman, *Temperature and pH dependence of the metarhodopsin I-metarhodopsin II kinetics and equilibria in bovine rod disk membrane suspensions.* Biochemistry, 1984. **23**(21): p. 5054-61.

103. Emeis, D., et al., *Complex formation between metarhodopsin II and GTP-binding protein in bovine photoreceptor membranes leads to a shift of the photoproduct equilibrium.* FEBS Lett, 1982. **143**(1): p. 29-34.

104. Angel, T.E., P.C. Kraft, and E.A. Dratz, *Metarhodopsin-II stabilization by crosslinked Gt(alpha) C-terminal peptides and implications for the mechanism of GPCR-G protein coupling.* Vision Res, 2006.

105. Arnis, S. and K.P. Hofmann, *Photoregeneration of bovine rhodopsin from its signaling state.* Biochemistry, 1995. **34**(29): p. 9333-40.

106. Ernst, O.P., et al., *Mutation of the fourth cytoplasmic loop of rhodopsin affects binding of transducin and peptides derived from the carboxyl-terminal sequences of transducin alpha and gamma subunits.* J Biol Chem, 2000. **275**(3): p. 1937-43.

107. Heck, M. and K.P. Hofmann, *Maximal rate and nucleotide dependence of rhodopsin-catalyzed transducin activation: initial rate analysis based on a double displacement mechanism.* J Biol Chem, 2001. **276**(13): p. 10000-9.

108. Hamm, H.E., et al., *Site of G protein binding to rhodopsin mapped with synthetic peptides from the alpha subunit.* Science, 1988. **241**(4867): p. 832-5.

109. Koenig, B.W., et al., *Structure and orientation of a G protein fragment in the receptor bound state from residual dipolar couplings.* J Mol Biol, 2002. **322**(2): p. 441-61.

110. Dratz, E.A., et al., *NMR structure of a receptor-bound G-protein peptide.* Nature, 1993. **363**(6426): p. 276-81.

111. Kisselev, O.G., M.V. Ermolaeva, and N. Gautam, *A farnesylated domain in the G protein gamma subunit is a specific determinant of receptor coupling.* J Biol Chem, 1994. **269**(34): p. 21399-402.

112. Aris, L., et al., *Structural requirements for the stabilization of metarhodopsin II by the C terminus of the alpha subunit of transducin.* J Biol Chem, 2001. **276**(4): p. 2333-9.

113. Pulvermuller, A., et al., *Interactions of metarhodopsin II. Arrestin peptides compete with arrestin and transducin.* J Biol Chem, 2000. **275**(48): p. 37679-85.

114. Wess, J., *Molecular basis of receptor/G-protein-coupling selectivity.* Pharmacol Ther, 1998. **80**(3): p. 231-64.

115. Cai, K., Y. Itoh, and H.G. Khorana, *Mapping of contact sites in complex formation between transducin and light-activated rhodopsin by covalent crosslinking: use of a photoactivatable reagent.* Proc Natl Acad Sci U S A, 2001. **98**(9): p. 4877-82.

116. Wang, X., et al., *Probing rhodopsin-transducin interactions by surface modification and mass spectrometry.* Biochemistry, 2004. **43**(35): p. 11153-62.

117. Acharya, S., Y. Saad, and S.S. Karnik, *Transducin-alpha C-terminal peptide binding site consists of C-D and E-F loops of rhodopsin.* J Biol Chem, 1997. **272**(10): p. 6519-24.

118. Janz, J.M. and D.L. Farrens, *Rhodopsin activation exposes a key hydrophobic binding site for the transducin alpha-subunit C terminus.* J Biol Chem, 2004. **279**(28): p. 29767-73.

119. Kuhn, H., et al., *Interactions between photoexcited rhodopsin and GTP-binding protein: kinetic and stoichiometric analyses from light-scattering changes.* Proc Natl Acad Sci U S A, 1981. **78**(11): p. 6873-7.

120. Vogel, R., et al., *Anions stabilize a metarhodopsin II-like photoproduct with a protonated Schiff base.* Biochemistry, 2001. **40**(44): p. 13342-52.

121. Vogel, R., et al., *Salt dependence of the formation and stability of the signaling state in G protein-coupled receptors: evidence for the involvement of the Hofmeister effect.* Biochemistry, 2001. **40**(2): p. 483-93.

122. Lamola, A.A. and T. Yamane, *The metarhodopsin I--metarhodopsin II equilibrium: effects of detergents and pressure.* Exp Eye Res, 1974. **18**(1): p. 19-27.

123. Konig, B., W. Welte, and K.P. Hofmann, *Photoactivation of rhodopsin and interaction with transducin in detergent micelles. Effect of 'doping' with steroid molecules.* FEBS Lett, 1989. **257**(1): p. 163-6.

124. Lamola, A.A., T. Yamane, and A. Zipp, *Effects of detergents and high pressures upon the metarhodopsin I--metarhodopsin II equilibrium.* Biochemistry, 1974. **13**(4): p. 738-45.

125. Willardson, B.M., et al., *Cooperative binding of the retinal rod G-protein, transducin, to light-activated rhodopsin.* J Biol Chem, 1993. **268**(9): p. 6371-82.

126. Wessling-Resnick, M. and G.L. Johnson, *Transducin interactions with rhodopsin. Evidence for positive cooperative behavior.* J Biol Chem, 1987. **262**(26): p. 12444-7.

127. Kota, P., et al., *Opsin is present as dimers in COS1 cells: identification of amino acids at the dimeric interface.* Proc Natl Acad Sci U S A, 2006. **103**(9): p. 3054-9.

128. Filipek, S., et al., *A concept for G protein activation by G protein-coupled receptor dimers: the transducin/rhodopsin interface.* Photochem Photobiol Sci, 2004. **3**(6): p. 628-38.

129. Suda, K., et al., *The supramolecular structure of the GPCR rhodopsin in solution and native disc membranes.* Mol Membr Biol, 2004. **21**(6): p. 435-46.

130. Conklin, B.R., et al., *Substitution of three amino acids switches receptor specificity of Gq alpha to that of Gi alpha.* Nature, 1993. **363**(6426): p. 274-6.

131. Bourne, H.R., *How receptors talk to trimeric G proteins.* Curr Opin Cell Biol, 1997. **9**(2): p. 134-42.

132. Morizumi, T., H. Imai, and Y. Shichida, *Two-step mechanism of interaction of rhodopsin intermediates with the C-terminal region of the transducin alpha-subunit.* J Biochem (Tokyo), 2003. **134**(2): p. 259-67.

133. Schertler, G.F., *Structure of rhodopsin and the metarhodopsin I photointermediate.* Curr Opin Struct Biol, 2005. **15**(4): p. 408-15.

134. Bartl, F., E. Ritter, and K.P. Hofmann, *FTIR spectroscopy of complexes formed between metarhodopsin II and C-terminal peptides from the G-protein alpha- and gamma-subunits.* FEBS Lett, 2000. **473**(2): p. 259-64.

135. Kisselev, O.G. and M.A. Downs, *Rhodopsin controls a conformational switch on the transducin gamma subunit.* Structure, 2003. **11**(4): p. 367-73.

136. Herrmann, R., et al., *Sequence of interactions in receptor-G protein coupling.* J Biol Chem, 2004. **279**(23): p. 24283-90.

137. Itoh, Y., K. Cai, and H.G. Khorana, *Mapping of contact sites in complex formation between light-activated rhodopsin and transducin by covalent crosslinking: use of a chemically preactivated reagent.* Proc Natl Acad Sci U S A, 2001. **98**(9): p. 4883-7.

138. Kisselev, O.G., et al., *Light-activated rhodopsin induces structural binding motif in G protein alpha subunit.* Proc Natl Acad Sci U S A, 1998. **95**(8): p. 4270-5.

139. Lambright, D.G., et al., *Structural determinants for activation of the alpha-subunit of a heterotrimeric G protein.* Nature, 1994. **369**(6482): p. 621-8.

140. Noel, J.P., H.E. Hamm, and P.B. Sigler, *The 2.2 A crystal structure of transducin-alpha complexed with GTP gamma S.* Nature, 1993. **366**(6456): p. 654-63.

141. Sondek, J., et al., *GTPase mechanism of Gproteins from the 1.7-A crystal structure of transducin alpha-GDP-AIF-4.* Nature, 1994. **372**(6503): p. 276-9.

142. Slep, K.C., et al., *Structural determinants for regulation of phosphodiesterase by a G protein at 2.0 A.* Nature, 2001. **409**(6823): p. 1071-7.

143. Kisselev, O.G., et al., *Signal transfer from rhodopsin to the G-protein: evidence for a two-site sequential fit mechanism.* Proc Natl Acad Sci U S A, 1999. **96**(9): p. 4898-903.

144. Herrmann, R., et al., *Rhodopsin-transducin coupling: Role of the Galpha C-terminus in nucleotide exchange catalysis.* Vision Res, 2006. **46**(27): p. 4582-93.

145. Stone, W.L., C.C. Farnsworth, and E.A. Dratz, *A reinvestigation of the fatty acid content of bovine, rat and frog retinal rod outer segments.* Exp Eye Res, 1979. **28**(4): p. 387-97.

146. Fenn, J.B., *Electrospray wings for molecular elephants (Nobel lecture).* Angew Chem Int Ed Engl, 2003. **42**(33): p. 3871-94.

147. Benesch, J.L. and C.V. Robinson, *Mass spectrometry of macromolecular assemblies: preservation and dissociation.* Curr Opin Struct Biol, 2006. **16**(2): p. 245-51.

148. Bothner, B. and G. Siuzdak, *Electrospray ionization of a whole virus: analyzing mass, structure, and viability.* Chembiochem, 2004. **5**(3): p. 258-60.

149. Suder, P., et al., *Acid-labile surfactant assists in-solution digestion of proteins resistant to enzymatic attack.* Rapid Commun Mass Spectrom, 2004. **18**(7): p. 822-4.

150. Schey, K.L., et al., *Matrix-assisted laser desorption mass spectrometry of rhodopsin and bacteriorhodopsin.* Biophys J, 1992. **63**(5): p. 1240-3.

151. Papac, D.I., et al., *Palmitylation of a G-protein coupled receptor. Direct analysis by tandem mass spectrometry.* J Biol Chem, 1992. **267**(24): p. 16889-94.

152. Ohguro, H., et al., *Sequential phosphorylation of rhodopsin at multiple sites.* Biochemistry, 1993. **32**(21): p. 5718-24.

153. Papac, D.I., et al., *Mass spectrometric identification of phosphorylation sites in bleached bovine rhodopsin.* Biochemistry, 1993. **32**(23): p. 5930-4.

154. Barnidge, D.R., et al., *Identification of transmembrane tryptic peptides of rhodopsin using matrix-assisted laser desorption/ionization time-of-flight mass spectrometry.* Protein Sci, 1997. **6**(4): p. 816-24.

155. Ball, L.E., et al., *Mass spectrometric analysis of integral membrane proteins: application to complete mapping of bacteriorhodopsins and rhodopsin.* Protein Sci, 1998. **7**(3): p. 758-64.

156. Kraft, P., J. Mills, and E. Dratz, *Mass spectrometric analysis of cyanogen bromide fragments of integral membrane proteins at the picomole level: application to rhodopsin.* Anal Biochem, 2001. **292**(1): p. 76-86.

157. Ablonczy, Z., et al., *Mass spectrometric analysis of integral membrane proteins at the subnanomolar level: application to recombinant photopigments.* Anal Chem, 2001. **73**(20): p. 4774-9.

158. Ablonczy, Z., R.K. Crouch, and D.R. Knapp, *Mass spectrometric analysis of integral membrane proteins at the subpicomolar level: application to rhodopsin.* J Chromatogr B Analyt Technol Biomed Life Sci, 2005. **825**(2): p. 169-75.

159. Jacobsen, R.B., et al., *Structure and dynamics of dark-state bovine rhodopsin revealed by chemical cross-linking and high-resolution mass spectrometry.* Protein Sci, 2006. **15**(6): p. 1303-17.

160. Leite, J.F., A.A. Amoscato, and M. Cascio, *Coupled proteolytic and mass spectrometry studies indicate a novel topology for the glycine receptor.* J Biol Chem, 2000. **275**(18): p. 13683-9.

161. Cascio, M., *Glycine receptors: lessons on topology and structural effects of the lipid bilayer.* Biopolymers, 2002. **66**(5): p. 359-68.

162. Han, J. and K.L. Schey, *Proteolysis and mass spectrometric analysis of an integral membrane: aquaporin 0.* J Proteome Res, 2004. **3**(4): p. 807-12.

163. Taylor, R.M., et al., *Analysis of human phagocyte flavocytochrome B by mass spectrometry.* J Biol Chem, 2006.

164. Annesley, T.M., *Ion suppression in mass spectrometry.* Clin Chem, 2003. **49**(7): p. 1041-4.

165. Lim, C.K. and G. Lord, *Current developments in LC-MS for pharmaceutical analysis.* Biol Pharm Bull, 2002. **25**(5): p. 547-57.

166. Browne, C.A., H.P. Bennett, and S. Solomon, *The isolation of peptides by high-performance liquid chromatography using predicted elution positions.* Anal Biochem, 1982. **124**(1): p. 201-8.

167. Matsushita, H., V.G. Lelianova, and Y.A. Ushkaryov, *The latrophilin family: multiply spliced G protein-coupled receptors with differential tissue distribution.* FEBS Lett, 1999. **443**(3): p. 348-52.

168. Shi, G.W., et al., *Light causes phosphorylation of nonactivated visual pigments in intact mouse rod photoreceptor cells.* J Biol Chem, 2005. **280**(50): p. 41184-91.

169. Lee, K.A., et al., *Mass spectrometric analysis of the kinetics of in vivo rhodopsin phosphorylation.* Protein Sci, 2002. **11**(4): p. 862-74.

170. Novak, P., et al., *Unambiguous assignment of intramolecular chemical cross-links in modified mammalian membrane proteins by fourier transform-tandem mass spectrometry.* Anal Chem, 2005. **77**(16): p. 5101-6.

171. Mirzabekov, T., et al., *Enhanced expression, native purification, and characterization of CCR5, a principal HIV-1 coreceptor.* J Biol Chem, 1999. **274**(40): p. 28745-50.

172. Meller, J. and R. Elber, *Linear programming optimization and a double statistical filter for protein threading protocols.* Proteins, 2001. **45**(3): p. 241-61.

173. Farzan, M., et al., *Tyrosine sulfation of the amino terminus of CCR5 facilitates HIV-1 entry.* Cell, 1999. **96**(5): p. 667-76.

174. Klein-Seetharaman, J., *Dynamics in rhodopsin.* Chembiochem, 2002. **3**(10): p. 981-6.

175. Imamoto, Y., et al., *Light-induced conformational changes of rhodopsin probed by fluorescent alexa594 immobilized on the cytoplasmic surface.* Biochemistry, 2000. **39**(49): p. 15225-33.

176. Piscitelli, C.L., et al., *Equilibrium between metarhodopsin-I and metarhodopsin-II is dependent on the conformation of the third cytoplasmic loop.* J Biol Chem, 2006. **281**(10): p. 6813-25.

177. McDowell, J.H., et al., *The reactivity of the sulfhydryl groups of rhodopsin in rod outer segment membranes.* Vision Res, 1979. **19**(10): p. 1143-5.

178. Sale, G.J., P. Towner, and M. Akhtar, *Functional rhodopsin complex consisting of three noncovalently linked fragments.* Biochemistry, 1977. **16**(25): p. 5641-9.

179. De Grip, W.J., S.L. Bonting, and F.J. Daemen, *Biochemical aspects of the visual process. XXVIII. Classification of sulfhydryl groups in phodopsin and other photoreceptor membrane proteins.* Biochim Biophys Acta, 1975. **396**(1): p. 104-15.

180. Albert, A.D., et al., *A distance measurement between specific sites on the cytoplasmic surface of bovine rhodopsin in rod outer segment disk membranes.* Biochim Biophys Acta, 1997. **1328**(1): p. 74-82.

181. Mielke, T., et al., *Light-induced changes in the structure and accessibility of the cytoplasmic loops of rhodopsin in the activated MII state.* Biochemistry, 2002. **41**(25): p. 7875-84.

182. Martin, E.L., et al., *Potent peptide analogues of a G protein receptor-binding region obtained with a combinatorial library.* J Biol Chem, 1996. **271**(1): p. 361-6.

183. Ernst, O.P. and F.J. Bartl, *Active states of rhodopsin.* Chembiochem, 2002. **3**(10): p. 968-74.

184. Natochin, M., et al., *Rhodopsin determinants for transducin activation: a gain-of-function approach.* J Biol Chem, 2003. **278**(39): p. 37574-81.

185. Koenig, B.W., et al., *Measurement of dipolar couplings in a transducin peptide fragment weakly bound to oriented photo-activated rhodopsin.* J Biomol NMR, 2000. **16**(2): p. 121-5.

186. Koenig, B.W., *Structure and orientation of ligands bound to membrane proteins are reflected by residual dipolar couplings in solution NMR measurements.* Chembiochem, 2002. **3**(10): p. 975-80.

187. Struthers, M., et al., *Tertiary interactions between the fifth and sixth transmembrane segments of rhodopsin.* Biochemistry, 1999. **38**(20): p. 6597-603.

188. Yu, H., M. Kono, and D.D. Oprian, *State-dependent disulfide cross-linking in rhodopsin.* Biochemistry, 1999. **38**(37): p. 12028-32.

189. Cai, K., et al., *Structure and function in rhodopsin: effects of disulfide cross-links in the cytoplasmic face of rhodopsin on transducin activation and phosphorylation by rhodopsin kinase.* Biochemistry, 1999. **38**(39): p. 12893-8.

190. Struthers, M., H. Yu, and D.D. Oprian, *G protein-coupled receptor activation: analysis of a highly constrained, "straitjacketed" rhodopsin.* Biochemistry, 2000. **39**(27): p. 7938-42.

191. Altenbach, C., et al., *Structure and function in rhodopsin: mapping light-dependent changes in distance between residue 65 in helix TM1 and residues in the sequence 306-319 at the cytoplasmic end of helix TM7 and in helix H8.* Biochemistry, 2001. **40**(51): p. 15483-92.

192. Jager, S., et al., *Effects of pH on rhodopsin photointermediates from lumirhodopsin to metarhodopsin II.* Biochemistry, 1998. **37**(19): p. 6998-7005.

193. Gouldson, P.R., et al., *Toward the active conformations of rhodopsin and the beta2-adrenergic receptor.* Proteins, 2004. **56**(1): p. 67-84.

194. Hofmann, K.P., *Signalling states of photoactivated rhodopsin.* Novartis Found Symp, 1999. **224**: p. 158-75; discussion 175-80.

195. De Grip, W.J. and F.J. Daemen, *Sulfhydryl chemistry of rhodopsin.* Methods Enzymol, 1982. **81**: p. 223-36.

196. Chen, Y.S. and W.L. Hubbell, *Reactions of the sulfhydryl groups of membrane-bound bovine rhodopsin.* Membr Biochem, 1978. **1**(1-2): p. 107-30.

197. de Grip, W.J., et al., *Biochemical aspects of the visual process. 23. Sulfhydryl groups and rhodopsin photolysis.* Biochim Biophys Acta, 1973. **325**(2): p. 315-22.

198. Regan, C.M., et al., *Biochemical aspects of the visual process. XXXIX. Sulfhydryl group reactivity as a probe of transient protein conformational changes during rhodopsin photolysis.* Biochim Biophys Acta, 1978. **537**(1): p. 145-52.

199. Girault, S., et al., *Coupling of MALDI-TOF mass analysis to the separation of biotinylated peptides by magnetic streptavidin beads.* Anal Chem, 1996. **68**(13): p. 2122-6.

200. Burritt, J.B., et al., *Antibody imprint of a membrane protein surface. Phagocyte flavocytochrome b.* J Biol Chem, 1998. **273**(38): p. 24847-52.

201. Jesaitis, A.J., et al., *Actin surface structure revealed by antibody imprints: evaluation of phage-display analysis of anti-actin antibodies.* Protein Sci, 1999. **8**(4): p. 760-70.

202. Burritt, J.B., et al., *Epitope identification for human neutrophil flavocytochrome b monoclonals 48 and 449.* Eur J Haematol, 2000. **65**(6): p. 407-13.

203. Adamus, G., et al., *Use of peptides to select for anti-rhodopsin antibodies with desired amino acid sequence specificities.* Pept Res, 1988. **1**(1): p. 42-7.

204. Burritt, J.B., et al., *Filamentous phage display of oligopeptide libraries.* Anal Biochem, 1996. **238**(1): p. 1-13.

205. Pini, A., et al., *Design and use of a phage display library. Human antibodies with subnanomolar affinity against a marker of angiogenesis eluted from a two-dimensional gel.* J Biol Chem, 1998. **273**(34): p. 21769-76.

206. Tomlinson, I.M., et al., *The imprint of somatic hypermutation on the repertoire of human germline V genes.* J Mol Biol, 1996. **256**(5): p. 813-17.

207. Iakoucheva, L.M., et al., *Intrinsic disorder in cell-signaling and cancer-associated proteins.* J Mol Biol, 2002. **323**(3): p. 573-84.

208. Dunker, A.K., et al., *Intrinsic disorder and protein function.* Biochemistry, 2002. **41**(21): p. 6573-82.

209. Ruprecht, J.J., et al., *Electron crystallography reveals the structure of metarhodopsin I.* Embo J, 2004. **23**(18): p. 3609-3620.

210. Nikiforovich, G.V. and G.R. Marshall, *Three-dimensional model for meta-II rhodopsin, an activated G-protein-coupled receptor.* Biochemistry, 2003. **42**(30): p. 9110-20.

211. Mumey, B.M., et al., *A new method for mapping discontinuous antibody epitopes to reveal structural features of proteins.* J Comput Biol, 2003. **10**(3-4): p. 555-67.

212. Collis, A.V., A.P. Brouwer, and A.C. Martin, *Analysis of the antigen combining site: correlations between length and sequence composition of the hypervariable loops and the nature of the antigen.* J Mol Biol, 2003. **325**(2): p. 337-54.

213. Fotiadis, D., et al., *The G protein-coupled receptor rhodopsin in the native membrane.* FEBS Lett, 2004. **564**(3): p. 281-8.

214. Wessling-Resnick, M. and G.L. Johnson, *Allosteric behavior in transducin activation mediated by rhodopsin. Initial rate analysis of guanine nucleotide exchange.* J Biol Chem, 1987. **262**(8): p. 3697-705.

215. Breit, A., M. Lagace, and M. Bouvier, *Hetero-oligomerization between beta2- and beta3-adrenergic receptors generates a beta-adrenergic signaling unit with distinct functional properties.* J Biol Chem, 2004. **279**(27): p. 28756-65.

216. Medina, R., D. Perdomo, and J. Bubis, *The hydrodynamic properties of dark- and light-activated states of n-dodecyl beta-D-maltoside-solubilized bovine rhodopsin support the dimeric structure of both conformations.* J Biol Chem, 2004. **279**(38): p. 39565-73.

217. Jastrzebska, B., et al., *Functional characterization of rhodopsin monomers and dimers in detergents.* J Biol Chem, 2004. **279**(52): p. 54663-75.

218. Chabre, M. and M. le Maire, *Monomeric G-protein-coupled receptor as a functional unit.* Biochemistry, 2005. **44**(27): p. 9395-403.

219. Seifert, R. and K. Wenzel-Seifert, *Constitutive activity of G-protein-coupled receptors: cause of disease and common property of wild-type receptors.* Naunyn Schmiedebergs Arch Pharmacol, 2002. **366**(5): p. 381-416.

220. Adamus, G., et al., *Anti-rhodopsin monoclonal antibodies of defined specificity: characterization and application.* Vision Res, 1991. **31**(1): p. 17-31.

221. Barbas, C.F.I., et al., *Phage display, a laboratory manual*. 2001, New York: Cold Spring Harbor Laboratory Press.

222. Burritt, J.B., et al., *Topological mapping of neutrophil cytochrome b epitopes with phage-display libraries.* J Biol Chem, 1995. **270**(28): p. 16974-80.

223. Harrison, P.M., et al., *A question of size: the eukaryotic proteome and the problems in defining it.* Nucleic Acids Res, 2002. **30**(5): p. 1083-90.

224. Smith, G.P., *Filamentous fusion phage: novel expression vectors that display cloned antigens on the virion surface.* Science, 1985. **228**(4705): p. 1315-7.

225. Scott, J.K. and G.P. Smith, *Searching for peptide ligands with an epitope library.* Science, 1990. **249**(4967): p. 386-90.

226. Szardenings, M., *Phage display of random peptide libraries: applications, limits, and potential.* J Recept Signal Transduct Res, 2003. **23**(4): p. 307-49.

227. Lubkowski, J., et al., *The structural basis of phage display elucidated by the crystal structure of the N-terminal domains of g3p.* Nat Struct Biol, 1998. **5**(2): p. 140-7.

228. Nayal, M., B.C. Hitz, and B. Honig, *GRASS: a server for the graphical representation and analysis of structures.* Protein Sci, 1999. **8**(3): p. 676-9.

229. Marvin, D.A., et al., *Molecular models and structural comparisons of native and mutant class I filamentous bacteriophages Ff (fd, f1, M13), If1 and IKe.* J Mol Biol, 1994. **235**(1): p. 260-86.

230. Halperin, I., H. Wolfson, and R. Nussinov, *SiteLight: binding-site prediction using phage display libraries.* Protein Sci, 2003. **12**(7): p. 1344-59.

231. Enshell-Seijffers, D., et al., *The mapping and reconstitution of a conformational discontinuous B-cell epitope of HIV-1.* J Mol Biol, 2003. **334**(1): p. 87-101.

232. Schreiber, A., et al., *3D-Epitope-Explorer (3DEX): localization of conformational epitopes within three-dimensional structures of proteins.* J Comput Chem, 2005. **26**(9): p. 879-87.

233. Huang, J., et al., *MIMOX: a web tool for phage display based epitope mapping.* BMC Bioinformatics, 2006. **7**: p. 451.

234. Bublil, E.M., S. Yeger-Azuz, and J.M. Gershoni, *Computational prediction of the cross-reactive neutralizing epitope corresponding to the monoclonal antibody b12 specific for HIV-1 gp120.* Faseb J, 2006. **20**(11): p. 1762-74.

235. Mayrose, I., et al., *Epitope mapping using combinatorial phage-display libraries: a graph-based algorithm.* Nucleic Acids Res, 2006.

236. Moreau, V., et al., *Discontinuous epitope prediction based on mimotope analysis.* Bioinformatics, 2006. **22**(9): p. 1088-95.

237. Tarnovitski, N., et al., *Mapping a neutralizing epitope on the SARS coronavirus spike protein: computational prediction based on affinity-selected peptides.* J Mol Biol, 2006. **359**(1): p. 190-201.

238. Burritt, J.B., et al., *Functional epitope on human neutrophil flavocytochrome b558.* J Immunol, 2003. **170**(12): p. 6082-9.

239. Coley, A.M., et al., *Rapid and precise epitope mapping of monoclonal antibodies against Plasmodium falciparum AMA1 by combined phage display of fragments and random peptides.* Protein Eng, 2001. **14**(9): p. 691-8.

240. Henikoff, S. and J.G. Henikoff, *Amino acid substitution matrices.* Adv Protein Chem, 2000. **54**: p. 73-97.

241. Henikoff, S. and J.G. Henikoff, *Amino acid substitution matrices from protein blocks.* Proc Natl Acad Sci U S A, 1992. **89**(22): p. 10915-9.

242. Bordo, D. and P. Argos, *Suggestions for "safe" residue substitutions in site-directed mutagenesis.* J Mol Biol, 1991. **217**(4): p. 721-9.

243. M, S.J.T.J., *Atlas of Amino Acid side chain interactions.* Vol. 1. 1992, Oxford: IRL press.

244. Taylor, W.R., *The classification of amino acid conservation.* J Theor Biol, 1986. **119**(2): p. 205-18.

245. *The CCP4 suite: programs for protein crystallography.* Acta Crystallogr D Biol Crystallogr, 1994. **50**(Pt 5): p. 760-3.

246. Fields, B.A., et al., *Hydrogen bonding and solvent structure in an antigen-antibody interface. Crystal structures and thermodynamic characterization of three Fv mutants complexed with lysozyme.* Biochemistry, 1996. **35**(48): p. 15494-503.

247. Chitarra, V., et al., *Three-dimensional structure of a heteroclitic antigen-antibody cross-reaction complex.* Proc Natl Acad Sci U S A, 1993. **90**(16): p. 7711-5.

248. Lescar, J., et al., *Crystal structure of a cross-reaction complex between Fab F9.13.7 and guinea fowl lysozyme.* J Biol Chem, 1995. **270**(30): p. 18067-76.

249. Braden, B.C., et al., *Crystal structure of an Fv-Fv idiotope-anti-idiotope complex at 1.9 A resolution.* J Mol Biol, 1996. **264**(1): p. 137-51.

250. Josephson, K., et al., *Noncompetitive antibody neutralization of IL-10 revealed by protein engineering and x-ray crystallography.* Structure, 2002. **10**(7): p. 981-7.

251. Mayrose, I., et al., *Epitope mapping using combinatorial phage-display libraries: a graph-based algorithm.* Nucleic Acids Res, 2007. **35**(1): p. 69-78.

252. Konigs, C., et al., *Monoclonal antibody screening of a phage-displayed random peptide library reveals mimotopes of chemokine receptor CCR5: implications for the tertiary structure of the receptor and for an N-terminal binding site for HIV-1 gp120.* Eur J Immunol, 2000. **30**(4): p. 1162-71.

253. Vanhoorelbeke, K., et al., *A consensus tetrapeptide selected by phage display adopts the conformation of a dominant discontinuous epitope of a monoclonal anti-VWF antibody that inhibits the von Willebrand factor-collagen interaction.* J Biol Chem, 2003. **278**(39): p. 37815-21.

254. Weiller, G.F., G. Caraux, and N. Sylvester, *The modal distribution of protein isoelectric points reflects amino acid properties rather than sequence evolution.* Proteomics, 2004. **4**(4): p. 943-9.